Synthesis and Characterization of Drug-Containing, Polysaccharide-Based Nanoparticles for Applications in Oral Drug Delivery

Sonal Mazumder

Dissertation submitted to the faculty of the Virginia Polytechnic Institute and State University in partial fulfillment of the requirements for the degree of

Doctor of Philosophy
In
Macromolecular Science and Engineering

Richey M. Davis, Chairman
Kevin J. Edgar
Judy S. Riffle
Nammalwar Sriranganathan
Eugene Joseph

June 27, 2013
Blacksburg, Virginia

Keywords:

polysaccharides, mixing, nanoprecipitation, cellulose derivatives, antibacterial, antiviral, nanoparticle, self-assembly, particle size distribution, crystallization, composition, drug delivery, release kinetics, oral systems

Synthesis and Characterization of Drug-Containing, Polysaccharide-Based Nanoparticles for Applications in Oral Drug Delivery

Sonal Mazumder

ABSTRACT

Amorphous solid dispersions of polysaccharide-drug nanoparticles were produced by a rapid precipitation process known as flash nanoprecipitation and the formulation process and properties of nanoparticles were investigated. In this thesis, several novel cellulose derivatives and a pullulan derivative were studied. Among these polymers, carboxymethyl cellulose acetate butyrate (CMCAB)-drug nanoparticles were investigated in detail. Previous work has shown that the presence of different chemical groups in CMCAB could aid in complexation with hydrophobic drugs with low solubility, forming an amorphous matrix which can increase the effective solubility and, hence, bioavailability of the drug in physiological conditions. An antibacterial drug and two less soluble anti-viral drugs were selected as model drugs for this study. A separate study was conducted with several other cellulose derivatives like cellulose acetate propionate adipates with two different degree of substitution 0.33 and 0.85 (CAP-Adp 0.33 and CAP-Adp 0.85), cellulose acetate sebacate (CA-320S Se) and butyl pullulan-6-carboxylate (BPC) polymers. The effect of polymer interaction with drug molecule on release of antiviral drugs was studied with these latter polymers.

The purpose of this research was two-fold. First, the methodology for producing drug-polymer nanoparticles with well-defined particle size distributions was developed. Second, the factors affecting drug loading and release properties of these nanoparticles were investigated. The nanoparticles were processed using two methods of solvent removal and drying to investigate their effects on drug loading and particle size: (a) various combinations of rotary

vacuum evaporation (rotavap) and acid-induced flocculation were used and (b), dialysis followed by freeze drying. Dynamic light scattering showed particle sizes were between 150-400 nm with polydispersity index values as low as 0.12. The antibiotic drug loading efficiencies ranged from 14-40%, whereas drug loading efficiency as high as 85 % was attained with the antiviral drug. The dissolution studies showed an increase in the solution concentration and release of the amorphous drug nanoparticles. The high glass transition temperature helped to stabilize the drug in an amorphous form, thus increasing the effective solution concentration of the drug in an aqueous medium.

For my late grandfather:
Shri Chittaranjan Majumder

The beginning of knowledge is the discovery of something we do not understand.
- Frank Herbert

Acknowledgements

My Ph.D. program experience was the most challenging, yet enjoyable and rewarding, academic experience of my life, because I like to learn. It was an overwhelming experience as it opened my world throughout the years. I have met a lot of wonderful people. I have had the privilege of working with **Dr. Richey Davis**, who was instrumental in helping me to complete my doctoral work. I sincerely thank him for his unending support and invaluable guidance throughout the period of my PhD.

I am also indebted to **Dr. Judy Riffle** whose help, stimulating suggestions and encouragement helped me in all the time of research. I take the opportunity to express my deepest sense of gratitude to **Dr. Kevin J. Edgar** for his constructive criticism, endless help, and guidance during my period of my PhD work. It was a great pleasure to get input and advice from **Dr. Eugene Joseph**. I am very much grateful to **Dr. Nammalwar Sriranganathan** for his generous support and constant encouragement.

I consider myself very fortunate to have been able to work with **Dr. Ishwar K. Puri** on several other projects and publications during my PhD. He has always encouraged me and given me confidence. While working with him I also got the privilege to work with **Dr. Joseph Falkinham**. He has my deepest gratitude for his extreme encouragement and guidance. I am also very thankful to **Dr. Chris Cornelius** for his input.

I am also very thankful to my colleagues, particularly in Dr. Edgar's group, for synthesizing some of the polymers and helping with release studies. They include **Haoyu Liu, Junia Pereira and Hale Cigdem Arca**. It was also a pleasure to work with **Samantha Casterlow** who executed cell and animal experiments with my nanoparticles. I acknowledge the help rendered by **Bruce Orler**, **Rick Caudill**, **Stephen McCartney**, **Weinan Leng,** in learning and operating several instruments. I am grateful to **Mr. Jason Schroedl** for helping with computer related problems. Thanks to **Raquel Mejia Ariza and Sharavanan Balasubramaniam** for incorporating me into the research group and for introducing me to many laboratory and experimental techniques. I am particularly indebted to **Sharavanan** for his endless help and support during my defense. I would like to thank my labmate **Seyyed Mohammad Hossein Abtahi** and my colleagues from Dr. Edgar and Dr. Riffle group for their help and keeping things interesting.

I would like to thank **Riley Chan** for his ability to fix just about anything and **Angie Flynn**, **Nora Bentley, Tina Kirk, Mary Smith Jane, Cyndy Graham, Tammy Hiner Jo**, **Leslie Thornton- O'Brien**, **Shelley Johnson**, **Lois Hall**, **Dawn Maxey**, **Lisa Smith** ,**Ennis McCrery, Ruth Athanson, Graduate School and Cranwell International Center** for their assistance with countless matters.

A special thanks to **Anne-Marie Bracken**: your friendship and advice has touched me from the day I arrived at Virginia Tech.

I also thank the following for financial support: National Science Foundation (DMR #0909065), Macromolecular Interfaces Institute Graduate Student Fellowship, Institute for Critical Technology and Applied Science (ICTAS), DuPont Chemical Company and Department of Engineering Science and Mechanics.

My life at Virginia Tech is priceless and I am really fortunate to know wonderful people here. I would like to thank **Naresh,** who has supported me through thick and thin- he had been a great friend, philosopher and guide. I thank **Monrudee,** whose care and support always motivated me. I am extremely thankful to my colleagues of my dance group-**Dancilla** and entire Blacksburg Indian community. I would like to thank my committee (2010-2011) and members of **Indian Students Association** in Virginia Tech. I am also very thankful to the members of **Graduate Student Assembly** (GSA), **College of Engineering Graduate Student Committee** (COEGSC) and **ASHA for Education**. I have gained immense experience and learnt various leadership and teamwork qualities while working with them.

Sincerest thanks to my father, **Dhananjoy Mazumder,** and mother, **Jayashri Mazumder,** for being such wonderful parents providing constant support and encouragement. Thanks to my brother, **Joydeep Mazumder**, for everything. I must thank **Anish Kumar Pramanik,** for all his support and encouragement. Thanks for respecting my dreams and helping me to fulfill them. I thank **Rajib Dey** for his immense support and constant guidance as a teacher, a colleague and a friend. Thanks to my friends in India for all their support and love.

Finally, I would like to thank my professors from Jadavpur Univeristy in India, who helped me to follow my dream and pursue my doctoral studies at Virginia Tech.

Sonal Mazumder
Blacksburg, Virginia-USA

June, 2013

Attribution

Professor Richey M. Davis is my research advisor and committee chair. He provided guidance, help, and support throughout the work in this PhD dissertation. Also he significantly contributed to the written communication of the research.

Ms. Samantha Casterlow executed the cell toxicity and MIC experiments with the nanoparticles (Chapter 3).

Ms. Junia Pereira provided training with HPLC technique and learn about drug release studies from particles. She prepared the CMCAB drug microparticles (Chapter 4). She also synthesized the BPC polymer (Chapter 5).

Mr. Haoyu Liu synthesized the cellulose adipates and sebacate, discussed in Chapter 5. He also prepared microparticles with the adipates for the same study.

Dr. Bruce Orler helped with the Differential Calorimetry Scans and also provided guidance and reasoning to the results obtained (Chapter 4 and Chapter 5).

Mr. Rick Caudill helped with the XRD measurements (Chapter 3, 4 and 5)

Ms. Hale Cigdem Arca prepared microparticles and executed dissolution experiments, discussed in Chapter 3.

TABLE OF CONTENTS

Chapter 1: Introduction ***1***

1.1. Significance and Motivation 1

1.2. Specific Research Objectives 3

1.3. Overview of Chapters 6

1.4. References 8

Chapter 2: Literature Review ***12***

2.1. Introduction to Oral Drug Delivery 12

2.1.1. Oral Drug Delivery Route 12

2.1.2. Barriers to Oral Drug Delivery 15

2.1.3. Critical Factors Affecting Oral Drug Delivery 15

2.2. Nanoparticle and Microparticles in Drug Delivery 19

2.3. Amorphous Solid Dispersions 25

2.3.1. Polysaccharides in Drug Delivery 38

2.4. Synthesis of Solid Drug Nanoparticles 45

2.5. Drug Delivery for Tuberculosis (TB) 54

2.5.1. Tuberculosis-The disease 54

2.5.2. TB Drugs in this Study 54

2.5.3. Polymer Nanoparticles in Treating TB 57

2.6. Drug Delivery for Human Immunodeficiency Virus (HIV) 62

2.6.1. Human Immunodeficiency Virus-The disease 62

2.6.2. HIV Drugs in this Study 63

2.6.3. Polymer Nanoparticles in Treating HIV 64

2.7. References 68

Chapter 3: Nanoparticles of Rifampicin and Carboxymethyl Cellulose Acetate Butyrate Prepared by Rapid Precipitation **90**

3.1. Introduction 92

3.2. Materials and methods 98

3.2.1. Materials for particle preparation 98

3.2.2. Materials for cell culture experiments 99

3.3. Particle preparation and characterization ____ 100
3.3.1. General procedure for rapid precipitation in Multi Inlet Vortex Mixer ____ 100
3.3.2. Particle purification and recovery ____ 101
3.3.3. Microparticle preparation and characterization ____ 103
3.3.4. Re-dispersion of dried nanoparticles ____ 103
3.3.5. Particle size – dynamic light scattering ____ 103
3.3.6. Particle morphology – X ray diffraction ____ 104
3.3.7. Drug loading ____ 104
3.3.8. Drug release studies ____ 105
3.3.9. Cell culture experiments ____ 106
3.4. Results and discussion ____ 107
3.4.1. Determination of optimal CMCAB polymer concentration ____ 108
3.4.2. Particle size analysis ____ 109
3.4.3. Rifampicin drug loading ____ 113
3.4.4. Particle morphology ____ 116
3.4.5. Dissolution studies ____ 118
3.4.6. Minimum inhibitory concentrations for *M.Smegmatis* ____ 120
3.4.7. Cell toxicity ____ 120
3.5. Conclusions ____ 122
3.6. References ____ 124
3.7. Supporting Information ____ 129

Chapter 4: Preparation and characterization of nanoparticles of carboxymethyl cellulose acetate butyrate containing anti-viral drugs for oral drug delivery ____ **140**

4.1. Introduction ____ 141
4.2. Materials and methods ____ 145
4.2.1. Materials ____ 145
4.2.2. Nanoparticle preparation by rapid precipitation in Multi Inlet Vortex Mixer ____ 147
4.2.3. Mcroparticle formation ____ 147
4.2.4. Nanoparticles recovery, solvent removal and drying ____ 148

4.2.5. Drug composition by high performance liquid chromatography 148
4.2.6. Particle size – dynamic light scattering and scanning electron microscopy 149
4.2.7. Characterization of crystallinity 149
4.2.8. Dissolution studies 150
4.3. Results and discussion 151
4.3.1. Drug incorporation in particles 151
4.3.2. Particle size analysis 153
4.3.3. Crystallinity studies of nanoparticles and microparticles 155
4.3.4. Differential scanning calorimetry 158
4.3.5. Dissolution studies 162
4.4. Conclusions 169
4.5. References 171
4.6. Supporting Information 179

Chapter 5: Preparation and Properties of Nanoparticles of Complexes of Polysaccharides and Antiviral Drugs: Effect of Polysaccharide Chemistry **186**
5.1. Introduction 188
5.2. Materials and methods 192
5.2.1. Materials 192
5.2.2. Nanoparticle preparation by rapid precipitation in Multi Inlet Vortex Mixer 195
5.2.3. Mcroparticle formation 196
5.2.4. Nanoparticles recovery, solvent removal and drying 196
5.2.5. Drug composition by high performance liquid chromatography 196
5.2.6. Particle size – dynamic light scattering and scanning electron microscopy 197
5.2.7. Characterization of crystallinity 198
5.2.8. Dissolution studies 199
5.3. Results and discussion 199
5.3.1. Drug incorporation in particles 200
5.3.2. Particle size analysis 201

5.3.3. Crystallinity studies of nanoparticles and microparticles_204
5.3.4. Differential scanning calorimetry _____205
5.3.5. Dissolution studies_____210
5.4. Conclusions _____217
5.5. References _____219
5.6. Supporting Information _____225
Chapter 6: Conclusion and Future Work _____ **227**
6.1. Conclusions _____227
6.2. Future Work_____231
6.3. References _____231

List of Figures

Chapter 1: Introduction

Figure 1. Evaluation steps of various factors that affect the oral bioavailability of drug candidates _____2

Chapter 2: Literature Review

Figure 1. Oral drug delivery through GI tract _____13

Figure 2. Spherical particle of radius r _____20

Figure 3. Tacrolimus solid dispersions with HPMC, PVP and PEG 6000 show enhanced solubility initially compared to crystalline Tacrolimus. Only HPMC was able to maintain supersaturation by inhibiting recrystallization in solution _____31

Figure 4a. In-vitro dissolution of a physical mixture (PM) of crystalline ritonavir and PEG (10:90), amorphous solid dispersions (ASD) of ritonavir in PEG at different drug : polymer ratios. There is an increase in release of amorphous drug compared to the crystalline drug. The lowest amorphous drug:PEG ration (10:90) shows the highest release _____33

Figure 4b. Plasma concentration of amorphous ritonavir (in PEG) at different drug: polymer ratios compared to crystalline ritonavir. The lowest amorphous drug : polymer = 10:90 shows highest plasma concentration 34

Figure 5. Structure of Carboxymethyl cellulose acetate butyrate (CMCAB) _____42

Figure 6. Molecular structure of the novel synthesized cellulose derivatives and the in substituent groups. These cellulose derivatives are not regioselectively substituted _____43

Figure 7. Butyl pullulan -6-carboxylate _____44

Figure 8. Schematic representation of MIVM producing polymer-drug nanocomplexes adapted from the work by Mustafa et al. _____48

Figure 9. The surface area increases when solids are fractured from the micron-size range (microparticles) to the nanometer-size particles used in

the various nanoparticle formulations to improve the performance of poorly water-soluble compounds 49

Figure 10. Structure of rifampicin 55

Figure 11. Structure of Isoniazid 56

Figure 12. Structure of Pyrazinamide 57

Figure 13a. Structure of Ritonavir 63

Figure 13b. Structure of Efavirenz 63

Chapter 3: Nanoparticles of Rifampicin and Carboxymethyl Cellulose Acetate Butyrate Prepared by Rapid Precipitation

Figure 1. Structure of Carboxymethyl cellulose acetate butyrate (CMCAB) 99

Figure 2. Structure of rifampicin. Arrow represent hydroxyl group at position C8 99

Figure 3. Intensity-average hydrodynamic diameters of CMCAB and rifampicin-CMCAB particles at pH 7 after acid flocculation followed by vacuum drying and then redispersion. +RV: rotary evaporation used; -RV rotary evaporation not used; CA = citric acid; HCl = hydrochloric acid. n = 3. Targeted rifampicin loading 25 wt% 111

Figure 4. Particle sizes of 3 batches (I-III) of CMCAB and rifampicin-CMCAB particles after fabrication in the multi-inlet vortex mixer and after processing by dialysis and freeze drying followed by redispersion in water at pH 7. The targeted rifampicin composition was 25 wt% 112

Figure 5. Scanning electron microscope images for microparticles at 5Kx magnification. The bar in each image corresponds to 10 μm 113

Figure 6. Rifampicin weight% in nanoparticles prepared by the flocculation method at different conditions as measured by UV-Visible spectrophotometry. +RV means rotary evaporation was used and -RV means rotary evaporation was not used. CA = citric acid, HCl = hydrochloric acid. Results for 2 batches are shown 114

Figure 7. X-ray diffractograms of (a) Rifampicin, (b) CMCAB, (c) Rifampicin-CMCAB physical mixture, (d) Rifampicin-CMCAB nanoparticles (actual drug loading is 10 wt%), (e) Rifampicin-CMCAB microparticles 117

Figure 8a. Drug release profile of rifampicin from nanoparticles and microparticles compared to free rifampicin as received at pH 6.8 119

Figure 8b. Drug release profile of rifampicin from nanoparticles and microparticles compared to free rifampicin as received at pH 1.2 119

Figure 9. Cytotoxicity of rifampicin-CMCAB nanoparticle formulations (average of batch A and batch B) vs. free rifampicin. 500 µg/ml rifampicin, J774A.1 cell line. 121

Figure S1. Calibration curve of rifampicin dissolved in acetonitrile at 475 nm to quantitate the rifampicin compositions in the nanoparticles 131

Figure S2. Calibration curve of rifampicin dissolved in acetonitrile at 254 nm used to quantitate the rifampicin concentration in the dissolution experiments 134

Chapter 4: Preparation and characterization of nanoparticles of carboxymethyl cellulose acetate butyrate containing anti-viral drugs for oral drug delivery

Figure 1. Structure of Carboxymethyl cellulose acetate butyrate (CMCAB) 146

Figure 2a. Structure of ritonavir 146

Figure 2b. Structure of efavirenz 146

Figure 3. RTV and EFV composition in CMCAB nanoparticles measured by HPLC at 240 nm. Average results from three batches are shown 152

Figure 4. Particle sizes (Dynamic light scattering) of CMCAB, CMCAB-RTV and CMCAB- EFV nanoparticles after mixing, dialysis and freeze drying. The targeted drug composition was 25 wt% and the actual compositions of the freeze-dried particles are shown in Figure 3 153

Figure 5. Scanning electron microscope images for microparticles at 50Kx magnification. The bar in each image corresponds to 200 nm 154

Figure 6. X-ray diffractograms of (a) Crystalline RTV (as received), (b) Crystalline EFV (as received), (c) Physical mixture of CMCAB-25 wt% RTV, (d) Physical mixture of CMCAB-25 wt% EFV, (e) CMCAB-RTV (actual drug loading is 19 wt%), (f) CMCAB-EFV (actual drug loading is 19 wt%), (g) CMCAB-RTV microparticles with 25 wt% of RTV, (h) CMCAB-EFV microparticles with 25 wt % of EFV _____157

Figure 7. First DSC scan showing melting peak of RTV at 126° C. A similar peak is observed in the physical mixtures but no such peak is observed in the any of the CMCAB-drug particles. Here NPs = nanoparticles, MPs = microparticles. _____158

Figure 8. Comparison between experimental T_g and theoretical predictions (Fox ideal T_g), (a) RTV containing particles, (b) EFV containing particles at different drug composition _____161

Figure 9a. Dissolution profile of CMCAB-RTV nanoparticles from 3 batches _____162

Figure 9b. Dissolution profile of CMCAB-EFV nanoparticles from 3 batches _____163

Figure 10a. Drug release profile of RTV. Approximately 70% (for drug composition 19 wt %), 60% (for drug composition of 29 wt %) and 55% (for drug composition 40 wt %) of RTV present in the amorphous matrix of CMCAB was dissolved in 5 hours _____164

Figure 10b. Drug release profile of EFV/CMCAB nanoparticles vs pure EFV _____165

Figure 11a. . Solution concentration of RTV from nanoparticle and microparticle ASDs vs pure RTV (potassium phosphate buffer, pH 6.8) _____167

Figure 11b. Solution concentration of EFV from nanoparticle and microparticle ASDs vs pure EFV (potassium phosphate buffer, pH 6.8) _____167

Figure 12a. . Comparison of percentage drug release from CMCAB-RTV microparticles and nanoparticles (results from 3 batches) _____168

Figure 12b. Comparison of percentage drug release from CMCAB-EFV microparticles and nanoparticles (results from 3 batches) _____169

Figure S1. Calibration curve of ritonavir dissolved in acetonitrile at 240 nm_____179

Figure S2. Calibration curve of Efavirenz dissolved in acetonitrile at 240 nm_____180

Figure S3. Particle Size Analysis of CMCAB, CMCAB-RTV and CMCAB-EFV nanoparticles after mixing, dialysis and freeze drying __183

Figure S4. X-ray diffractograms of pure CMCAB as received _____184

Figure S5. X-ray diffractograms of (A) CMCAB-RTV (actual drug loading is 29 wt%), (B) CMCAB-RTV (actual drug loading is 40 wt%), (C) CMCAB-EFV (actual drug loading is 18 wt%), (D) CMCAB-EFV (actual drug loading is 43 wt%) _____184

Figure S6. First DSC scan showing melting peak of EFV at 140° C. No such peak is observed in the any of the CMCAB-EFV nanoparticles __185

Chapter 5: Preparation and Properties of Nanoparticles of Complexes of Polysaccharides and Antiviral Drugs: Effect of Polysaccharide Chemistry

Figure 1a. Structure of ritonavir_____193

Figure 1b. Structure of efavirenz _____193

Figure 2. (a) Molecular structures of the novel cellulose derivatives. These cellulose derivatives are not regioselectively substituted, (b) Butyl pullulan-6-carboxylate (BPC) _____194

Figure 3. Particle sizes of polysaccharide-drug (RTV and EFV) nanoparticles after mixing, dialysis and freeze drying. The freeze dried powders except BPC were mixed with trehalose before freeze drying. The targeted drug composition was 25 wt% and the actual compositions of the freeze-dried particles are shown in Table 2. The error bars shows standard deviation from 3 different batches of particles. A = CAP Adp 0.33, B = CAP Adp 0.85, C= CA 320S Seb, D = BPC nanoparticles _____202

Figure 4. Scanning electron microscope images for (a) CAP Adp 0.33-RTV microparticles at 15Kx magnification , (b) CAP Adp 0.85-RTV microparticles at 7Kx magnification. The bar in each image corresponds to 2 μm 203

Figure 5. X-ray diffractograms of (a) Crystalline RTV (as received), (b) Crystalline EFV (as received) and polyssacharide nanoparticles (c) ascending order: CAP Adp 0.33-RTV, CAP Adp 0.85-RTV, CA 320S Seb-RTV, BPC-RTV, (d) ascending order : CAP Adp 0.33-EFV, CAP Adp 0.85-EFV, CA 320S Seb-EFV, BPC-EFV showed no diffraction peaks implying the drugs were mostly amorphous 205

Figure 6. First DSC scan showing melting peak of RTV at 126° C. No such peak is observed in any of the polymer-drug nanoparticles 206

Figure 7. Comparison between experimental T_g and theoretical predictions (Fox ideal T_g) of nanoparticles 209

Figure 8a. Concentration profile of RTV (A) as received, (B) from CAP Adp 0.33, (C) from CA 320S Seb, (D) from CAP Adp 0.85, (E) from BPC. The error bars represents standard deviation of results from 3 batches 211

Figure 8b. Concentration profile of EFV (A) as received, (B) from CAP Adp 0.33, (C) from CAP Adp 0.85, (D) from CA 320S Seb, (E) from BPC. The error bars represent standard deviation from 3 batches 211

Figure 9a. Release profile of RTV (A) as received, (B) from CAP Adp 0.33, (C) from CAP Adp 0.85, (D) from CA 320S Seb, (E) from BPC. The error bars represent standard deviation of results from 3 batches 213

Figure 9b. Release profile of EFV (A) as received, (B) from CAP Adp 0.33, (C) from CAP Adp 0.85, (D) from CA 320S Seb, (E) from BPC. The error bars represent standard deviation of results from 3 batches 214

Figure 10a. Comparison of solubility of RTV from CAP Adp 0.33 and CAP Adp 0.85 microparticles (MP) and nanoparticles (NP) and crystalline RTV as received (result from 1 batch). RTV compositions are listed in Table 2 216

Figure 10b. Comparison of RTV release from CAP Adp 0.33 and CAP Adp 0.85 microparticles (MP) and nanoparticles (NP), vs crystalline RTV (result from 1 batch). RTV compositions are listed in Table 2 _____216

Figure S1. X-ray diffractograms of (A) polymers as received (B) CAP adipates 0.33 and 0.85 microparticles containing RTV _____225

Figure S2. First DSC scan showing melting peak of EFV at 140° C. No such peak is observed in the any of the polymer-EFV nanoparticles ___226

Figure S3. DSC scan of RTV containing CAP Adp 0.33 and CAP Adp 0.85_____226

Chapter 6: Conclusion and Future Work

Figure 1. Drug concentration using different separation based approaches _____233

List of Tables

Chapter 2: Literature Review

Table 1. Physiological charateristics in the GI tract 14

Table 2. Properties of Nanoparticles and Microparticles in Drug Delivery 20

Table 3. Properties of Polymers commonly used as ASDs 28

Table 4. Polysaccharides in Pharmaceutical use 40

Table 5. Abbreviation and properties of Novel Synthesized Cellulose and Pullulan Derivatives 45

Table 6. Comparative studies of the methods used to synthesize nanoparticles 51

Chapter 3: Nanoparticles of Rifampicin and Carboxymethyl Cellulose Acetate Butyrate Prepared by Rapid Precipitation

Table 1. Effect of CMCAB concentration on particle size at mixer conditions - THF:water ratio 1:9 v/v , 25ºC, and Re = 15,000 109

Table 2. Rifampicin formulations and MIC ranges for susceptibility of *M. Smegmatis* 120

Table S.1. Particle Size Analysis of CMCAB particles after recovering them by vacuum filtration and drying in vacuum oven for 5-6 hours at room temperature by DLS – at different rotary evaporation conditions and addition of different excipients. The average results from 3 batches are shown 135

Table S.2. Particle Size Analysis of Rifampicin-CMCAB particles after recovering them by vacuum filtration and drying in vacuum oven for 5-6 hours at room temperature by DLS - at different rotary evaporation conditions and addition of different excipients. The average results from 3 batches are shown 136

Table S.3. Drug loading of complexes prepared by the acid flocculation method at different conditions 137

Table S.4. Particle size and drug loading comparison of complexes from a single batch that were processed by flocculation with citric acid with no rotary evaporation step and by dialysis followed by freeze drying ____138

Chapter 4: Preparation and characterization of nanoparticles of carboxymethyl cellulose acetate butyrate containing anti-viral drugs for oral drug delivery

Table 1. The glass transitions of CMCAB, drugs and complexes calculated from the second DSC scan and Fox ideal mixing equations _____159

Chapter 5: Preparation and Properties of Nanoparticles of Complexes of Polysaccharides and Antiviral Drugs: Effect of Polysaccharide Chemistry

Table 1. Abbreviation and properties of Novel Synthesized Cellulose and Pullulan Derivatives _____193

Table 2. RTV and EFV composition in polysaccharide nanoparticles measured by HPLC at 240 nm. Averages from three batches are shown _____200

Table 3. Effect of trehalose on particle sizes of freeze dried nanoparticles _____203

Table 4. Glass transitions of polymer, drugs and polymer-drug nanoparticles (2^{nd} DSC scans) and Fox ideal mixing equation_____207

Chapter 1. Introduction

1.1 Significance and Motivation

Drug discovery is a time consuming, onerous and expensive process. The average cost of bringing every new drug from laboratory to patients is approximately $1-2 billion and the process takes up to 14-15 years [1,2]. Due to the high cost, there is tremendous pressure to maximize efficiency and minimize the time it takes to discover and bring a drug to the market. In order to do this, it is necessary to analyze the entire drug discovery and development process and make necessary changes to increase efficiency and minimize time. The goals to be met to commercialize a drug candidate are:

1. Therapeutic strategy
2. Structure-activity relationship
3. Dose form and regimen
4. Best possible safety profile
5. Novelty of the compounds
6. Scalability
7. Cost of the starting materials
8. Toxicity issues
9. Successful drug delivery in animal models
10. Clinical trials and approvals

Oral administration is one of the most important methods of drug delivery. However, it is challenging to design delivery systems optimizing drug stability (chemical, morphological and physiological stability) in the gastrointestinal (GI) tract and liver to achieve a desirable pharmacokinetic profile[3]. Dissolution of drugs is quite often the rate-limiting step which controls the bioavailability of the drug[4]. A flow chart describing sequentially the factors that can impact drug delivery is illustrated in Figure 1.

Polymer encapsulated drug nanoparticles have been investigated for many applications due to the improved material properties that result from a reduction in particle dimensions. They have the potential to provide personalized drug delivery vehicles[5]. Sustained or extended release dosage forms may lead to a constant pharmacological availability and also reduce toxic side effects[6].

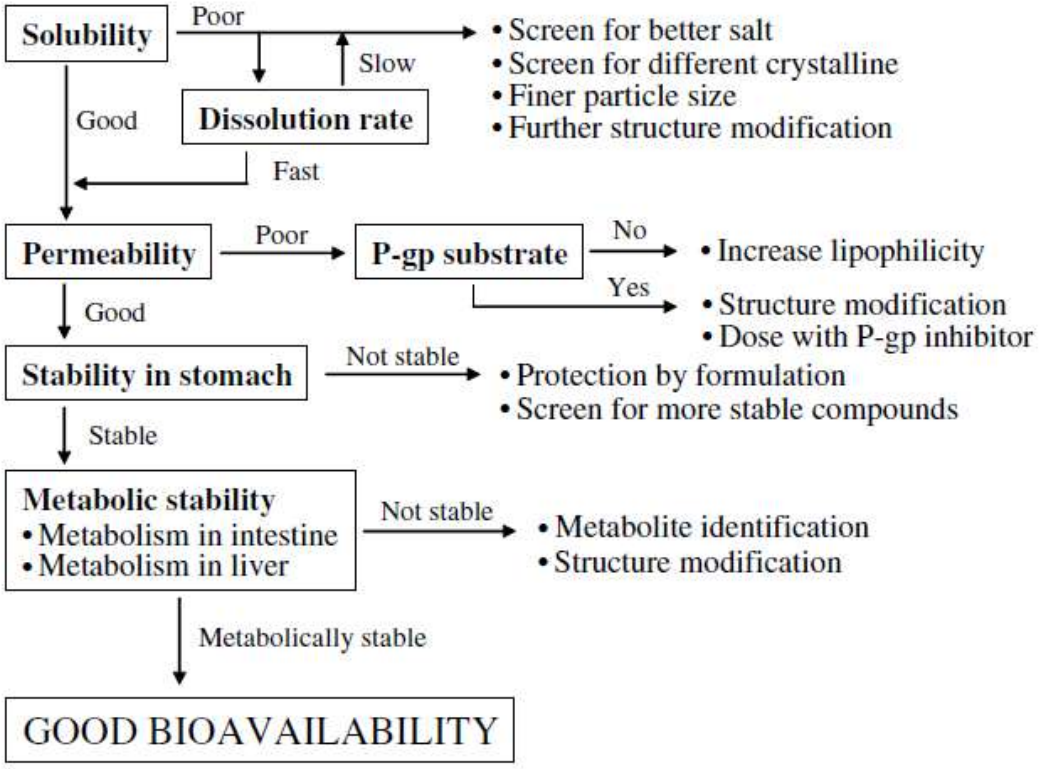

Figure 1. Evaluation steps of various factors that affect the oral bioavailability of drug candidates [7].

The motivation of the research in this thesis is to convert poorly soluble crystalline drugs to amorphous drugs, thus enhancing their solubility in the GI tract which can further enhance their absorption through the GI epithelium. Prior work has also shown the potential applications of amorphous solid dispersions containing amorphous drugs[8,9,9c,10]. However, there is relatively little literature which focuses on the preparation of and drug release characteristics from

amorphous solid dispersions of polymer-drug nanoparticles. This work aimed to make well-defined nanoparticles where a drug was molecularly dispersed in an amorphous polysaccharide matrix. Polymers with pH sensitive chemical groups are used to protect the drug from degradation in the stomach (at lower pH of 1.2) and release most of the drug in the small intestine (absorption site, pH ~ 6.8). Methods were developed to produce nanoparticles rapidly and under conditions that could be scalable. The particle size and drug loading of the particles were controlled and the morphology was characterized to confirm presence of amorphous drugs. The release mechanism of the drug from polymers is also investigated. The nanoparticles and microparticles of same polymer-drug compositions were studied side-by-side to calculate the enhancement of dissolution of drugs from the particles due to surface area effects. This work does not include any studies associated with absorption of drugs through the epithelium or in-vivo studies. In this work, poorly soluble antiviral drugs and a comparatively soluble antibacterial drug are investigated.

1.2 Specific Research Objectives

The overall objective of this research was to investigate the preparation and drug dissolution properties of amorphous solid dispersions of drugs in polysaccharide nanoparticles for oral drug delivery. In order to accomplish this general objective, several specific research objectives were necessary:

1. <u>Investigate a method to prepare well defined polymer-drug nanoparticles in a rapid and scalable manner</u>

The preparation of well-defined nanoparticles has several challenges such as solvent selection, concentration of polymer and drugs, nanoparticle isolation, purification and drying. Some of the common methods of producing polymer-drug nanoparticles are solvent evaporation[11,12] , milling[13], high pressure homogenization[24a, 165b] , electrospraying and

precipitation[14]. Flash nanoprecipitation is a nanoparticle fabrication method that is rapid and scalable [15,16,17] in which an organic solution of a polymer (typically an amphiphilic block copolymer) and organic species (typically poorly water-soluble drugs and hydrophobically-modified particles) are rapidly mixed with a non-solvent such as water under highly turbulent conditions in a confined mixing chamber. This turbulent mixing forms a highly supersaturated solution which undergoes particle nucleation and growth. Particle growth stops due to the formation of a repulsive barrier on the particle surface. When amphiphilic copolymers are used, that barrier typically consists of poly(ethylene oxide) chains that form a brush-like structure on the nanoparticle surfaces. The supersaturation depends on the water/organic solvent ratio injected into the mixer, the concentrations of the drugs and polymers, and temperature. This process is attractive in that the particle size distributions can be controlled [18, 19] and high concentrations of hydrophobic organic species can be incorporated due to kinetic entrapment in the polymers [20,21,22]. Flash nanoprecipitation has been used with a four-jet multi-inlet vortex mixer (MIVM) to produce nanoparticles with high loadings of drugs and imaging agents and with controlled surface chemistries [23,24, 25,26,27].

Drug nanoparticles have many advantages over micro/macro particles. The increase in surface area to mass ratio for nanoparticles is dramatic, sometimes covering several orders of magnitude[28,29]. However, nanoparticles must be stabilized to prevent aggregation. It is also important to note that not all drug candidates have physicochemical properties suitable for effective particle size reduction, and nanoparticulate drugs may be susceptible to polymorphic transition on manufacture or storage[30,31]. The increase in surface area generated due to the reduction in particle size increases the dissolution rate and, therefore, an increase in

bioavailability for drugs where exposure after oral administration is limited by the dissolution rate [32].

In this objective, amorphous solid dispersions of polysaccharide nanoparticles were made using flash nanoprecipitation for the first time. This is important since there are few studies on nanoparticles of amorphous solid dispersions in the literature. Due to the particular features of flash nanoprecipitation, namely the need to remove an organic solvent from the mixture after the particles were made, several methods of particle separation and drying were also investigated. The main objective was to examine the effect of processing conditions on particle size and use excipients to control aggregation when and where required**.**

2. <u>Study formation of amorphous solid dispersions of polymer nanoparticles</u>

Amorphous solid dispersions (ASDs) are formed when the drug is evenly and molecularly dispersed in an amorphous polymer matrix. The drug is in the amorphous form in the matrix and thus there is no heat of fusion barrier that a drug molecule has to overcome in order to dissolve. Therefore, the amorphous form requires less energy for dissolution and thus exhibits higher solution concentrations than the crystalline form. For poorly water soluble drugs, ASDs are particularly useful in producing higher drug concentrations and faster release in the GI tract than those from conventional formulations[33]. The higher dissolution rates leads to significant improvements in drug absorption (mainly BCS II and BCS IV drugs)[8,32,34,35,36,37]. The aim of this objective is to make amorphous dispersions of comparatively novel polysaccharides and antibacterial and antiviral drugs.

Prior studies[38] have shown that the enhancement of solubility and stability are largely due to: (1) a moderate level of polymer hydrophobicity; (2) rigidity of polymer structure - semirigid cellulose polymers have been more effective than the semiflexible synthetic polymers of similar

hydrophobicity; and (3) amphiphilicity which, in the case of the novel cellulose-based polymers studied in this work, can be finely tuned. For example, increasing the degree of carboxylic acid substitution in cellulose derivatives can inhibit drug crystallization. The purpose of this study was to understand the behavior of nanoparticles made of polymers with different chemistries and compare the drug release properties from these nanoparticle systems.

3. Compare drug release from nanoparticles and microparticles

The increase in surface area is considered responsible for increased dissolution for microparticles and nanoparticles. Nanocrystals of ibuprofen and indomethacin showed fast dissolution (around >80% release within 2 min)[39,40,41] . There was a 2-3 fold increase in dissolution rate of itraconazole whose particle size was reduced to 5.5 μm. It was also shown that further reducing the particle size to prepare nanoscale particles of the size between 350-700 nm leads to additional 3- to 5-fold increases in dissolution rate compared with the micronized product[42]. The aim of this study is to compare the enhancement in the dissolution rates of the drug in micron-sized particles (prepared by coprecipitation or spray drying) and nanoparticles (prepared by flash nanoprecipitation in the MIVM) compared to the free crystalline drugs. This is also to understand the effect of particle size on drug release and determine whether synergy between high surface area and suppression of crystallinity is observed.

1.3 Overview of Chapters

Chapter 2 is a literature review providing an overview of relevant topics including basic theoretical background and a review of current research. The five primary topics covered in the review are: (1) The oral drug delivery method, (2) Role of nanoparticles and microparticles in drug delivery, (3) Polymers for oral drug delivery with emphasis on amorphous solid

dispersions, (4) Synthesis of polymer-drug nanoparticles, (5) Prior studies with antibacterial and antiviral drugs.

Chapter 3 is the study of preparation of carboxymethyl cellulose acetate butyrate (CMCAB) nanoparticles containing rifampicin (an antibacterial drug). The nanoparticles were prepared by a rapid, scalable flash nanoprecipitation process using a multi inlet vortex mixer. Two different processing methods were used to recover and dry these particles such as (a) flocculation by acids and vacuum drying, and (b) dialysis and freeze drying. The main goal of the work was to investigate a suitable method to prepare nanoparticles with well-defined particle size and drug loading rapidly. The release of drug from the nanoparticles and microparticles of the same polymer-drug composition were compared.

Chapter 4 is the study of preparation of CMCAB nanoparticles containing two poorly soluble antiviral drugs by flash nanoprecipitation. The main goal of the study was to enhance the solubility of the poorly soluble drugs by forming amorphous solid dispersion with CMCAB. The particle size and release studies were done for three different drug loadings to investigate the role of polymer in stability of drug loaded particles from recrystallization in solution.

Chapter 5 is the study of novel cellulose derivative and a pullulan derivative in enhancing solubility and stability of poorly soluble antiviral drugs. Here, the effects of structure property relationship of the polymers were studied on drug release kinetics.

Chapter 6 describes the conclusions drawn from the preceding chapters and the future direction of this research. Overall conclusions are presented, as well as conclusions for each individual chapter.

1.4 References

1. Adams, C. P.; Brantner, V. V., Spending on new drug development1. *Health Economics* **2010,** *19* (2), 130-141.

2. Pharma 2005--an industrial revolution in R&D. In *Pharma 2005*, Price, Waterhouse, Coopers: Newyork, **1998**; pp 1-20.

3. Lavelle, E. C.; Sharif, S.; Thomas, N. W.; Holland, J.; Davis, S. S., The importance of gastrointestinal uptake of particles in the design of oral delivery systems. *Advanced Drug Delivery Reviews* **1995,** *18* (1), 5-22.

4. Daugherty, A. L.; Mrsny, R. J., Regulation of the intestinal epithelial paracellular barrier. *Pharmaceutical Science & Technology Today* **1999,** *2* (7), 281-287.

5. Petros, R. A.; Desimone, J. M., Strategies in the design of nanoparticles for therapeutic applications. *Nat Rev Drug Discov* **2010,** *9* (8), 615-627.

6. Löbenberg, R.; Kim, J. S.; Amidon, G. L., Pharmacokinetics of an immediate release, a controlled release and a two pulse dosage form in dogs. *European Journal of Pharmaceutics and Biopharmaceutics* **2005,** *60* (1), 17-23.

7. Han, C.; Wang, B., Factors That Impact the Developability of Drug Candidates: An Overview. In *Drug Delivery*, John Wiley & Sons, Inc.: **2005**; pp 1-14.

8. Law, D.; Schmitt, E. A.; Marsh, K. C.; Everitt, E. A.; Wang, W.; Fort, J. J.; Krill, S. L.; Qiu, Y., Ritonavir–PEG 8000 amorphous solid dispersions: In vitro and in vivo evaluations. *Journal of Pharmaceutical Sciences* **2004,** *93* (3), 563-570.

9. (a) Sinha, S.; Ali, M.; Baboota, S.; Ahuja, A.; Kumar, A.; Ali, J., Solid Dispersion as an Approach for Bioavailability Enhancement of Poorly Water-Soluble Drug Ritonavir. *AAPS PharmSciTech* **2010,** *11* (2), 518-527; (b) Li, B.; Konecke, S.; Harich, K.; Wegiel, L.; Taylor, L. S.; Edgar, K. J., Solid dispersion of quercetin in cellulose derivative matrices influences both solubility and stability. *Carbohydrate Polymers* **2013,** *92* (2), 2033-2040; (c) Murdande, S. B.; Pikal, M. J.; Shanker, R. M.; Bogner, R. H., Solubility advantage of amorphous pharmaceuticals: I. A thermodynamic analysis. *Journal of Pharmaceutical Sciences* **2010,** *99* (3), 1254-1264.

10. Posey-Dowty, J.; Watterson, T.; Wilson, A.; Edgar, K.; Shelton, M.; Lingerfelt, L., Zero-order release formulations using a novel cellulose ester. *Cellulose* **2007,** *14* (1), 73-83-83.

11. Bn V Hari, K. D. a. N. N., Development of Efavirenz nanoparticle for enhanced efficiency of anti-retroviral therapy against HIV and AIDS. *BMC Infectious Diseases* **2012,** (12*)*, 7.

12. Christopher J Destache, T. B., Keith Christensen, Annemarie Shibata, Akhilesh Sharma and Alekha Dash, Combination antiretroviral drugs in PLGA nanoparticle for HIV-1. *BMC Infectious Diseases* **2009,** (9*)*, 198.

13. Schwitzer, J. M.; Müller, R. H., Drug Nanocrystals—The Universal Formulation Approach for Poorly Soluble Drugs. In *Nanoparticulate Drug Delivery Systems* **2007**, pp 71-88.

14. Keck, C. M.; Müller, R. H., Drug nanocrystals of poorly soluble drugs produced by high pressure homogenisation. *European Journal of Pharmaceutics and Biopharmaceutics* **2006,** *62* (1), 3-16.

15. Johnson, B. K.; PrudHomme, R. K., Flash NanoPrecipitation of Organic Actives and Block Copolymers using a Confined Impinging Jets Mixer. *Australian Journal of Chemistry* **2003,** *56* (10), 1021-1024.

16. Johnson, B. K.; Prud'homme, R. K., Chemical processing and micromixing in confined impinging jets. *AIChE Journal* **2003,** *49* (9), 2264-2282.

17. Johnson, B. K.; Prud'homme, R. K., Mechanism for Rapid Self-Assembly of Block Copolymer Nanoparticles. *Physical Review Letters* **2003,** *91* (11), 118302.

18. Liu, Y.; Kathan, K.; Saad, W.; Prud'homme, R. K., Ostwald Ripening of β-Carotene Nanoparticles. *Physical Review Letters* **2007,** *98* (3), 036102.

19. Liu, Y.; Cheng, C.; Prud'homme, R. K.; Fox, R. O., Mixing in a multi-inlet vortex mixer (MIVM) for flash nano-precipitation. *Chemical Engineering Science* **2008,** *63* (11), 2829-2842.

20. Gindy, M. E.; Ji, S.; Hoye, T. R.; Panagiotopoulos, A. Z.; Prud'homme, R. K., Preparation of Poly(ethylene glycol) Protected Nanoparticles with Variable Bioconjugate Ligand Density. *Biomacromolecules* **2008,** *9* (10), 2705-2711.

21. Gindy, M. E.; Panagiotopoulos, A. Z.; Prud'homme, R. K., Composite Block Copolymer Stabilized Nanoparticles: Simultaneous Encapsulation of Organic Actives and Inorganic Nanostructures. *Langmuir* **2007,** *24* (1), 83-90.

22. Ji, S.; Zhu, Z.; Hoye, T. R.; Macosko, C. W., Maleimide Functionalized Poly(ε-caprolactone)-block-poly(ethylene glycol) (PCL-PEG-MAL): Synthesis, Nanoparticle Formation, and Thiol Conjugation. *Macromolecular Chemistry and Physics* **2009,** *210* (10), 823-831.

23. Ungun, B.; Prud'homme, R. K.; Budijon, S. J.; Shan, J.; Lim, S. F.; Ju, Y.; Austin, R., Nanofabricated upconversion nanoparticles for photodynamic therapy. *Opt. Express* **2009,** *17* (1), 80-86.

24. Kumar, V.; Hong, S. Y.; Maciag, A. E.; Saavedra, J. E.; Adamson, D. H.; Prud'homme, R. K.; Keefer, L. K.; Chakrapani, H., Stabilization of the Nitric Oxide (NO) Prodrugs and Anticancer Leads, PABA/NO and Double JS-K, through Incorporation into PEG-Protected Nanoparticles. *Molecular Pharmaceutics* **2009,** *7* (1), 291-298.

25. Chen, T.; D'addio, S. M.; Kennedy, M. T.; Swietlow, A.; Kevrekidis, I. G.; Panagiotopoulos, A. Z.; Prud'homme, R. K., Protected Peptide Nanoparticles: Experiments and Brownian Dynamics Simulations of the Energetics of Assembly. *Nano Letters* **2009,** *9* (6), 2218-2222.

26. Ansell, S. M.; Johnstone, S. A.; Tardi, P. G.; Lo, L.; Xie, S.; Shu, Y.; Harasym, T. O.; Harasym, N. L.; Williams, L.; Bermudes, D.; Liboiron, B. D.; Saad, W.; Prud'homme, R. K.; Mayer, L. D., Modulating the Therapeutic Activity of Nanoparticle Delivered Paclitaxel by Manipulating the Hydrophobicity of Prodrug Conjugates. *Journal of Medicinal Chemistry* **2008,** *51* (11), 3288-3296.

27. D'addio, S. M.; Prud'homme, R. K., Controlling drug nanoparticle formation by rapid precipitation. *Advanced Drug Delivery Reviews* **2011,** *63* (6), 417-426.

28. Rh, J. J. a. M., Nanocrystal technology, drug delivery and clinical applications. *Int J Nanomedicine* **2008,** *3*, 295-309.

29. Merisko-Liversidge, E. M.; Liversidge, G. G., Drug Nanoparticles: Formulating Poorly Water-Soluble Compounds. *Toxicologic Pathology* **2008,** *36* (1), 43-48.

30. Van Eerdenbrugh, B.; Van Den Mooter, G.; Augustijns, P., Top-down production of drug nanocrystals: Nanosuspension stabilization, miniaturization and transformation into solid products. *International Journal of Pharmaceutics* **2008,** *364* (1), 64-75.

31. Wu, L.; Zhang, J.; Watanabe, W., Physical and chemical stability of drug nanoparticles. *Advanced Drug Delivery Reviews* **2011,** *63* (6), 456-469.

32. Williams, H. D.; Trevaskis, N. L.; Charman, S. A.; Shanker, R. M.; Charman, W. N.; Pouton, C. W.; Porter, C. J. H., Strategies to Address Low Drug Solubility in Discovery and Development. *Pharmacological Reviews* **2013,** *65* (1), 315-499.

33. Gao, Y.; Carr, R. A.; Spence, J. K.; Wang, W. W.; Turner, T. M.; Lipari, J. M.; Miller, J. M., A pH-Dilution Method for Estimation of Biorelevant Drug Solubility along the Gastrointestinal

Tract: Application to Physiologically Based Pharmacokinetic Modeling. *Molecular Pharmaceutics* **2010,** *7* (5), 1516-1526.

34. Kennedy, M.; Hu, J.; Gao, P.; Li, L.; Ali-Reynolds, A.; Chal, B.; Gupta, V.; Ma, C.; Mahajan, N.; Akrami, A.; Surapaneni, S., Enhanced Bioavailability of a Poorly Soluble VR1 Antagonist Using an Amorphous Solid Dispersion Approach: A Case Study. *Molecular Pharmaceutics* **2008,** *5* (6), 981-993.

35. Van Eerdenbrugh, B.; Van Speybroeck, M.; Mols, R.; Houthoofd, K.; Martens, J. A.; Froyen, L.; Van Humbeeck, J.; Augustijns, P.; Van Den Mooter, G., Itraconazole/TPGS/Aerosil®200 solid dispersions: Characterization, physical stability and in vivo performance. *European Journal of Pharmaceutical Sciences* **2009,** *38* (3), 270-278.

36. Li, S.; Liu, Y.; Liu, T.; Zhao, L.; Zhao, J.; Feng, N., Development and in-vivo assessment of the bioavailability of oridonin solid dispersions by the gas anti-solvent technique. *International Journal of Pharmaceutics* **2011,** *411* (1–2), 172-177.

37. Newman, A.; Knipp, G.; Zografi, G., Assessing the performance of amorphous solid dispersions. *Journal of Pharmaceutical Sciences* **2012,** *101* (4), 1355-1377.

38. Ilevbare, G. A.; Liu, H.; Edgar, K. J.; Taylor, L. S., Understanding Polymer Properties Important for Crystal Growth Inhibition—Impact of Chemically Diverse Polymers on Solution Crystal Growth of Ritonavir. *Crystal Growth & Design* **2012,** *12* (6), 3133-3143.

39. Plakkot, S.; De Matas, M.; York, P.; Saunders, M.; Sulaiman, B., Comminution of ibuprofen to produce nano-particles for rapid dissolution. *International Journal of Pharmaceutics* **2011,** *415* (1–2), 307-314.

40. Liu, P.; Rong, X.; Laru, J.; Van Veen, B.; Kiesvaara, J.; Hirvonen, J.; Laaksonen, T.; Peltonen, L., Nanosuspensions of poorly soluble drugs: Preparation and development by wet milling. *International Journal of Pharmaceutics* **2011,** *411* (1–2), 215-222.

41. Niwa, T.; Miura, S.; Danjo, K., Design of Dry Nanosuspension with Highly Spontaneous Dispersible Characteristics to Develop Solubilized Formulation for Poorly Water-Soluble Drugs. *Pharmaceutical Research* **2011,** *28* (9), 2339-2349.

42. Sun, W.; Mao, S.; Shi, Y.; Li, L. C.; Fang, L., Nanonization of itraconazole by high pressure homogenization: Stabilizer optimization and effect of particle size on oral absorption. *Journal of Pharmaceutical Sciences* **2011,** *100* (8), 3365-3373.

Chapter 2: Literature Review

2.1. Introduction to Oral Drug Delivery

Oral administration is the most simple and convenient mode of drug delivery. It is painless compared to injections; convenient compared to enemas, easy to use, and can be managed by the patient.

Almost 90% of all medicines are oral formulations. However, it is challenging to design delivery systems optimizing drug stability (chemical, morphological and physiological stability in the GI tract) in the gastrointestinal (GI) tract, such that a desirable pharmacokinetic profile may be attained for a given drug[1]. In order to improve oral drug delivery it is important to recognize solubility, permeability and residence time in the gastrointestinal milieu as well as different characteristics of drugs and their delivery systems such as size, pH, density, diffusion, swelling, adhesion, degradation and permeability[2].

2.1.1. Oral Drug Delivery Route - Physicochemical and Physiological Conditions in the GI Tract

The physiological characteristics of the gastrointestinal tract (Figure 2) are described in Table 1. The oral dosage forms comes in contact with saliva. Most drugs are not absorbed to any significant extent in the mouth. The oral dosage form once swallowed rapidly goes to the esophagus. The drug is barely dissolved here before going to the stomach. When it reaches the stomach (fluid volume ≈1.5 L) the acidic milieu dissolves drugs (mainly the ones which dissolves at low pH), for the first step to absorption or acid-labile drugs can be denatured or proteolytically degraded losing efficacy. The pH and gastric retention time affects the dissolution of the drugs in stomach.

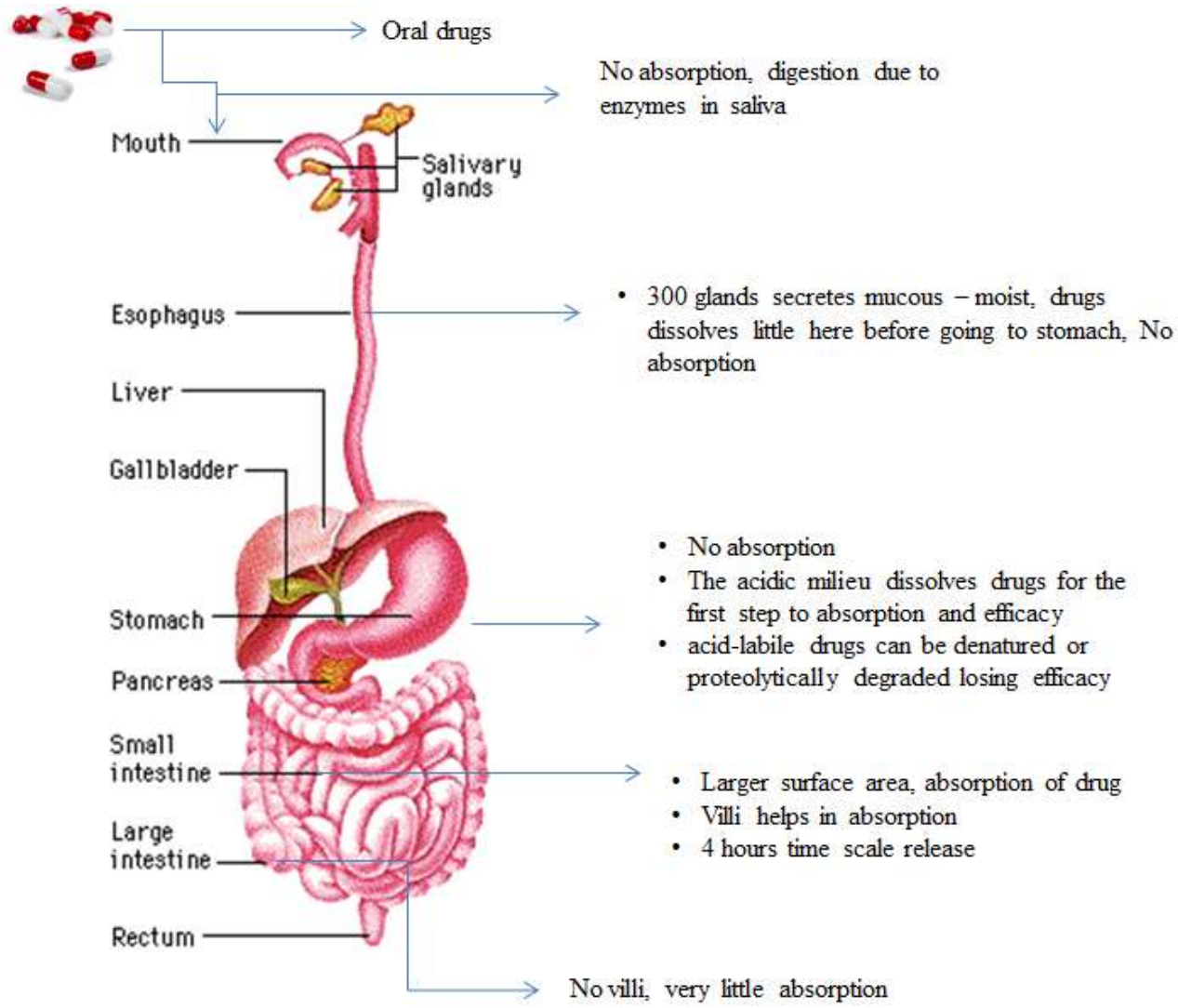

Figure 1. Oral drug delivery route through GI tract [3]

More or less disaggregated dosage forms enter the small intestine. The small intestine contains villi and microvilli increasing the absorptive surface area (250 m^2), which helps in absorption. In addition, the high permeability of the epithelium to small molecules decreases down the small intestine. The duodenum has excellent absorptive capacity. In the large intestine with a pH between 5.5 – 7 the absorptive area is only 0.25 % that of the small intestine, leading to greatly reduced absorption for most drugs. Also, the harmless, native colonic bacteria which

reside in this region may be killed when exposed to antibacterial drugs leading to gastrointestinal side effects.

Table 1. Physiological charateristics in the GI tract [4] .

Section	**Length (m^2)**	**Absorptive area (m^2)**	**Diameter (cm)**	**Max. filling volume (ml)**	**Fasted pH**	**Residence time of single oral dose**	**Enzymes**
Oral Cavity	0.15-0.2	-	10	-	7.0	-	Amylase
Esophagus	0.2-0.3	0.02	2.5	-	6.0-7.0	3.5s	-
Stomach	0.2	0.1	15	1,500	2.1 (men), 2.8 (women)	Up to 2h fasted 2-8 h fed	Pepsin, Lipase
Small intestine	7.0	200	-	8,500	5.5-8.0	3-4 h	Bile Peptidases, Lipases, Amylase
Duodenum	0.2-0.3	0.1	5	500	5.5-6.5	>5mins	-
Jejunum	2.5	60	5	5,000	6.1-7.1	1-2 h	-
Ileum	3.5	60	2.5-5	3,000	7.0-8.0	2-3 h	-
Large intestine	1.5	0.3	-	-	-	15-48 h	Diverse bacterial enzymes
Caecum	-	0.05	7.0	-	-	-	-
Colon	-	0.25	5.0	3,000	8.0	-	-
Rectum	0.15	-	2.5	500	7.0	-	-

[a]Mean and extremes in parenthesis, [b]Represents filling volume, not only fluid

2.1.2. Barriers to Oral Drug Delivery - Bioavailability

The Food and Drug Administration defines bioavailability [5] as ‘‘the rate and extent to which the active ingredient or active moiety is absorbed from a drug product and becomes available at the site of action. For drug products that are not intended to be absorbed into the bloodstream, bioavailability may be assessed by measurements intended to reflect the rate and extent to which the active ingredient or active moiety becomes available at the site of action.’’ Typically one modifies this definition to limit the delivery path from the site of administration to the bloodstream. That is, bioavailability is defined as ‘‘the fraction of the oral dose that actually reaches the systemic circulation intact,’’[6] and is ‘‘commonly applied to both the rate and extent of drug input into the systemic circulation”[7].

It is important for the oral drug to overcome several different obstacles during the delivery through the gastrointestinal tract, as well as through intestinal mucosa or the blood-brain barrier. The barriers can be physiological and biochemical.[8] These various barriers have to be taken into account when designing drugs with improved absorption characteristics. However, the focus of the thesis is to achieve maximum solution concentration in the small intestine to enhance absorption of drug across the intestinal epithelium. The drug, while passing through the stomach, can dissolve in the acidic environment. Some acid labile drugs can be denatured or degraded and therefore lose their efficacy. Drugs which are poorly soluble, have poor bioavailability from the small intestine, thereby decreasing the overall drug bioavailability.

2.1.3. Critical Factors Affecting Oral Drug Delivery

It is challenging to design delivery systems optimizing drug stability in the gastrointestinal (GI) tract, such that a desirable pharmacokinetic profile may be attained for a given drug [9]. There are several factors in the GI tract which may limit the absorption and

solubility of drug in the intestine, like the morphological barriers (mucus layer, microvilli, etc.) and some physiological factors (a wide range of pH, enzymatic activities, specific transport mechanisms). The bioavailability of the drug is dependent on its dissolution which is usually the rate-limiting step[10]. Patient compliance problems can also be reduced by reducing the dosing frequency to one dose per day [11].

Drug Chemistry and Crystallinity

High water-solubility of the drug is required for rapid dissolution in the body fluids. In order to permeate across the phospholipid bilayer of the cellular membrane, it must possess a minimal lipophilicity.

The Lipinski "rule of five" is used to predict certain drug properties such as absorption or permeation from the drug's structure. For example, poor absorption or permeation is more likely when there are more than five H-bond donors (–OH and –NH groups), 10 H-bond acceptors, the molecular weight is greater than 500 and the calculated partition coefficient (log P) is greater than 5 [2].

The presence of different kinds of salts also affects the drug absorption. The presence of excess chloride ions in gastric fluid can depress drug solubility resulting in salting out of the drug[12] . Potassium can irritate the GI, magnesium can be a laxative, and calcium can cause constipation.

The crystallinity of the drug plays a major role in drug dissolution. The extent of solubility and absorption depends on the polymorphic form of the drug. For example a metastable polymorph would show higher solubility and absorption compared to a stable polymorph. A study with beagles showed that the bioavailability of a monoclinic polymorph was 2.5 times higher than that of the more stable orthorhombic form [13]. The amorphous form requires

less energy for dissolution due to lack of crystalline lattices and thus exhibits higher bioavailability than the crystalline form. The storage temperature of the drug formulation should be 50ºC lower than the glass transition temperature to avoid spontaneous crystallization of amorphous drugs [14].

Particle Size

There has been considerable research about the preparation of microparticles and nanoparticles with controlled features. For oral dosage forms, nanoparticles have shown great promise for two reasons

(a) Most of the drugs, especially those which belong to Biopharmaceutics Classification System (BCS) class II (high permeability, low solubility) and IV (low permeability, low solubility), show insufficient bioavailability due to low solubility. Nanoparticles can clearly improve the dissolution profile of the compound, thereby increasing the solubility[15].

(b) Research on the oral absorbability of nanoparticles has shown that drug-loaded systems could effectively transport to systemic circulation[16]. Undisputedly, this route of drug delivery is highly complex.

Nanoparticles show faster and more uniform distribution in the GI tract compared to any other dosage forms due to their small sizes[17]. The larger surface area enhances the interaction of the nanoparticles with the epithelial lining and mucus, prolonging retention time and thereby enhancing bioavailability.[18] Nanoparticle formulations exhibit enhance dissolution, safety, patient compliance and improved drug efficacy.

The efficiency of a drug depends on its ability to dissolve, absorb, distribute and interact with biological environment in the body. Drugs which show poor aqueous solubility are dissolution-rate limited. The reduction in particle size of drug to nanometers improved

bioavailability significantly by enhancing dissolution rate[19,20]. Therefore the amount of poorly water-soluble drug that is free to be absorbed in the gastrointestinal tract and the chemical potential across the membrane is maximized.

The enhancement of the dissolution rate can be shown by the classical convective mass transfer rate equation[21]

$$\mathbf{W_d = KA_{sp}[C_s - C_\infty]} \qquad \mathbf{(1)}$$

where,

W_d = (mass of drug released/time)/unit mass of particle

K = convective mass transfer coefficient

A_{sp} = specific surface area of the particle

C_s = concentration of drug in liquid phase at surface of particle

C_∞ = desired concentration of drug in the physiological environment

and

K = convective mass transfer coefficient ~ 2*D*/d

D = diffusion coefficient of drug in liquid phase

A_{sp} = 6/(ρd) [units = area/particle mass]

Putting the values of K and A_{sp} in equation (1),

$$\mathbf{W_d \sim (12}\boldsymbol{D}\mathbf{[C_s - C_\infty])/(\rho d^2)} \qquad \mathbf{(2)}$$

Reducing particle diameter from 1 micron to 50 nanometers (nm) increases the specific area and, hence, the drug mass transfer rate W_d by 400-fold.

pH Dependent Drug Delivery

Polymers with different backbone modifications and side-chain conjugates have received special attention in pH-controlled delivery of oral drugs. The group of methacrylate acid

copolymers or Eudragit® is widely used for the preparation of pH-sensitive coatings or hydrogels. The dissolution of the polymer or extent of swelling depends on the ratio of free acid to ester groups and also the quantity and type of charged groups (anionic or cationic) [22]. According to the type of charged group, they will either dissolve completely in the stomach or, in the case of quaternary amino groups, show swelling without complete disintegration. For polymers containing polycarboxylic acid groups which are ionized at a pH > 5, release occurs under alkaline conditions but not in acidic gastric fluids.

This pH-sensitive swelling of the polymers prevents exposure of the encapsulated compound to harsh conditions in the stomach and enables unhindered delivery to the preferential site of uptake. The fine-tuning of polymer composition, as well as type and extent of derivatization, allows for a relatively precise controlling of the threshold pH. Some other polymers show similar characteristics like chitosan or carboxymethylcellulose [23,23b]. The above two characteristics of improving oral drug delivery (size and pH sensitive response) using polymers has been used in this thesis to make novel polysaccharide drug nanoparticles of cellulose derivate which has not been explored before.

2.2. Nanoparticles and Microparticles in Drug Delivery

In particulate drug delivery, the distinction is often made between micro- and nanoparticles. Particle diameters between 50-300 nm can be called nanoparticles and diameters above 500 nm are more likely to behave as microparticles... The difference in size between micro- and nanoparticles has several effects. For example, the surface-to-volume ratio for a spherical particle (Figure 2) with a radius r is given by:

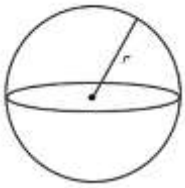

Figure 2. Spherical particle of radius r

$$\text{Surface area/ volume} = \frac{3}{r} \qquad \textbf{(3)}$$

Hence the surface area to volume ratio is inversely proportional to the radius and this has an important effect on mass transfer rate from the particle surface. A comparison of the properties of micro-particles and nanoparticles is presented in Table 2 [24].

Table 2. Properties of Nanoparticles and Microparticles in Drug Delivery[25]

Properties	**Microparticles**	**Nanoparticles**
[a]Particle size distribution	Broad particle size distribution	Narrow particle size distribution
[b]Dissolution rate	Somewhat enhanced	Greatly enhanced
[c]Release kinetics	Slower	Rapid/burst
[d]Drug loading	More loading	Less loading
[e]Elimination	Difficult to eliminate, side effects	Easier to eliminate
Functionalization	Less adaptation	Better binding to specific receptor
Fate after injection	Tend to stay-block organs, arteries	Longer circulation time – clear off
Crossing Barriers	Do not cross biological barriers	Can cross barriers
Entering Cell	Only delivered to phagocytic cell	Delivery in all types of cells
Systemic Delivery	Intravenous delivery not likely	Preferable

a,b,c,d,e properties are more relevant to the work in this thesis

The rate of dissolution for solid drug products can be enhanced by particle size reduction and thereby increasing the surface area available for solvation. Particle size reduction technologies are therefore routinely used to improve the oral bioavailability of poorly water soluble drugs[26,18, 27,27] .

Several top down, dry-impact processes like hammer mills, ball mills, and air-jet mills are used to reduce the particle size of a coarse drug powder (a process called micronization). This results in the formation of drug particles in the micron size range with particle sizes commonly between 2-5 μm[28,28b]. Recent technological developments have led to the ability to produce much smaller (nano) particulates with sizes in the 200-500 nm range using polymeric and surfactant stabilizers. While drug nanoparticles have a much larger surface area-to-volume ratio than micron-scale particles, they can be highly cohesive and must be stabilized to prevent aggregation[29,30].

The increase in surface area generated due to reduction in particle size increases the dissolution and, therefore, an increase in bioavailability for drugs where exposure after oral administration is limited by dissolution rate [31]. For example, there was an improvement in the oral bioavailability of many poorly water-soluble drugs, including cilostazol[32], fenofibrate[33], progesterone[34], proquazone[35], and nitrofurantoin[36] after micronization, all of which are believed to exhibit dissolution rate limited absorption. However, micron-sized drug particles are often unable to overcome the challenges to absorption presented by compounds with very low aqueous solubility (<1 μg/ml)[18, 37]. Therefore a number of methods have been developed to reduce particle sizes to nanometer-scale dimensions.t is not a new concept to use nanoparticles as a drug-delivery approach for various difficult-to-formulate reagents [38,39,40,41]. The nanometer size

increases the surface area which enhances the interaction of the particles with the epithelial lining and mucus.

During past three decades, the pharmaceutical industry has developed and marketed several nanoparticle formulations for intravenous administration such as intravenous nutritional fat emulsion (Intralipid®) and liposomal products (Doxil®, AmBisome®)[30]. However, poor drug loading, high processing cost and limited availability of suitable excipients reduced the use of these formulations. Many of these concerns have been approached by Elan's NanoCrystal® Technology. They successfully demonstrated the advantages of using nanoparticulates or nanosuspension in several different modes of drug delivery [42].

It has been estimated that more than 40% of pharmaceutically active substances have poor bioavailability due to lack of significant solubility in water [43,44]. A molecule which needs to penetrate a biological membrane to be absorbed must possess some hydrophobic or lipophilic characteristics. Salts of such molecule which can retain biological activity have the potential to improve solubility. However, these salt forms have several disadvantages such as poor stability, poor bioavailability poor patient compliance. Nanoparticle formulation has proven to be very useful technique to address the above mentioned issues.

The dissolution rate of a drug from a solid dosage form surrounded by a quiescent diffusion layer is defined by the Noyes Whitney Equation which is analogous to a simple diffusion equation[45]. It is given as

$$\frac{dc_x}{dt} = \frac{D.A}{h}(C_s - C) \qquad \textbf{(4)}$$

D= diffusion rate of the drug

A = surface area of contact of the solid with the dissolution fluid

H = width of the diffusion layer

The increase in surface area is considered responsible for increased dissolution for microparticles and nanoparticles. However, it is also apparent that the improvements in dissolution velocity may exceed that predicted simply on the basis of available surface area. There can be increase in the dissolution rate due to changes to drug solubility (Cs), to the thickness of the diffusional layer (h), and to particle shape. According to traditional solubility theory, the particle size has no effect on solid-state properties nor the efficiency of solvation. Thus, a decrease in particle size is expected to have little impact on equilibrium solubility. However, new technologies that support the isolation of particles with submicron particle sizes require that this view be modified.

The Ostwald-Freundlich equation can be applied to show that a reduction in particle size below 1 μm increases solvation pressure, subsequently giving rise to an increase in solubility[29]. It is difficult to measure the saturated solubility of a nanoparticle accurately, as it is complicated by the potential for very small particles to remain suspended in solution after conventional centrifugation (or even ultracentrifugation in some cases) and to pass through many of the membrane filters used to separate drug in solution from solid drug[46]. Given the low intrinsic solubility of many of the drugs to which this technology is applied, only trace quantities of particle contamination are required to generate large errors in solubility assessment.

The microparticle and nanoparticle systems previously shown to enhance itraconazole dissolution in vitro were also subsequently examined in vivo after oral administration to rats, and the differences in dissolution were shown to translate to differences in bioavailability. Thus, micronization (to 5.5 mm) resulted in a 6-fold increase in oral bioavailability compared with a non-micronized product, and further particle size reduction to yield nanoparticles with diameters

of 350 or 700 nm (by high-pressure homogenization) elicited further (6.8-fold) increases in exposure compared with the micronized product (>40-fold compared with non-micronized drug)[47]. In this case, the additional benefits of a reduction in particle size from 700 to 350 nm were relatively small.

Drug nanosuspensions can be used in capsule and tablet formulation to study pharmacokinetic, efficacy and toxicity for oral delivery[20d,30]. When a formulation of a high permeability and low solubility (<1 mg/ml) was administered as oral nanosuspension to rats, the drug exposure in rats was significantly increased compared with both nonmicronized material and a lipid-surfactant mixture[15].

Polymer nanoparticles in Oral Drug Delivery

Nanocarriers such as polymeric nanoparticles or micelles have provided a promising approach to obtain desirable biopharmaceutical and pharmacokinetic properties for medicines. Different methods can be selected to prepare nanoparticles depending on the nature of the polymer, as well as on the drug to be encapsulated[48]. Some of the methods may be harmful to biopharmaceuticals due to usage of organic solvents, heat, sonication or vigorous agitation. Nanoparticles formation can be also based on electrostatic interactions which do not require aggressive conditions during preparation, therefore minimizing possible damage to the drug during formation [49].

A large number of natural and synthetic biodegradable polymers are available to form nanoparticles[50]. Natural materials used for oral delivered nanoparticles include chitosan, dextran, gelatine, alginate, agar [51]. The synthetic polymers which are used for oral drug delivery are poly (lactide)(PLA), poly(glycolide) (PGA), poly(lactide-co-glycolide) (PLGA), poly(cyanoacrylates) (PCA), polyethylenimine (PEI) or polycaprolactone (PCL)[49, 52] .

2.3 Amorphous Solid Dispersions

Solid dispersions have been explored for enhancing dissolution and oral bioavailability for poorly water-soluble drugs for over 50 years [53,53b,54,55,56]. There are several mechanisms by which solid dispersions can increase drug dissolution such as by reduction in effective particle size, improved wetting, enhanced solubilization, as well as suppressing the lattice energy barrier by stabilizing the drug in the amorphous state.

The desirable properties of a polymer for oral drug delivery are as follows:

a) The polymer and its degradation products should be biocompatible.

b) The polymer must have a high glass transition temperature, so that the drug-polymer formulation can stored for months.

c) A hydrophobic/hydrophilic balance and presence of groups such as charged groups that maximize drug interaction and result in drug-polymer miscibility.

d) It must also prevent or retard drug recrystallization after release and a pH-controlled release is most suitable for oral drug delivery (refer to section 1.3).

Many polymeric materials have been used for this purpose such as poly(lactic acid), poly(glycolic acid), polycaprolactone, polysaccharides, poly(acrylic acid) family, proteins and polypeptides (e.g., gelatin). Among them, polysaccharides are the most popular for making nanoparticles for drug delivery. As stated before, the amorphous form of the drug requires less energy for dissolution and thus exhibits higher bioavailability than the crystalline form. This results in an amorphous solid dispersion (ASD) which is formed when the drug is evenly and molecularly dispersed in an amorphous polymer matrix. ASDs have been proven to increase dissolution rate and drug concentration in the gastrointestinal medium. [57] Higher dissolution rates in some cases led to significant improvements in drug absorption[58,31,59,60,61,56]. ASDs are also

well tolerated *in vivo* due to the presence of non-toxic excipients. Therefore, ASDs are often a preferred method of increasing solubility and bioavailability of poorly soluble drugs.

An example of a commercially available ASD is that of Sporanox capsules (Janssen Pharmaceuticals), an antifungal product containing the poorly water-soluble drug itraconazole molecularly dispersed in HPMC and coated onto inert sugar beads. When Sporanox was administered orally, there was significant enhancement of oral bioavailability compared with the more slowly dissolving crystalline itraconazole [62,60]. Despite several advantages, there are only few ASDs available commercially due to the thermodynamic instability of drug in the amorphous form. For example Norvir (a capsule formulation of the antiviral drug ritonavir; Abbott Laboratories) was withdrawn due to thermodynamic instability and replaced by a more stable and less soluble crystalline polymorph[63].

Previous studies showed that high-molecular-weight polymers such as HPMC (and derivatives), PVP, and the methacrylates are able to inhibit drug crystallization[64,65,66], and, therefore, enhance physical stability. The mechanisms by which an amorphous drug is stabilized include a reduction in molecular mobility by increasing local viscosity in the solid dispersion matrix[53b,67,68], restriction of molecular movement due to intermolecular interactions between polymer and drug[69], and the inhibition of crystal nucleation[70,71,72,73]. The factors which effect the inhibition of crystallization are crystallization tendencies of the drug, the properties of the carrier (hydrophobicity, chain conformation), and the ratio of drug-to-carrier. Increasing the drug load decreases the quantity of carrier available to stabilize the drug in the high energy form. Also, high drug loading will promote phase separation within the solid dispersion thus increasing the risk of instability[74,75].

Table 3 shows most common polymers used as ASDs. Also the polymer must not itself have a tendency to crystallize[70, 76]. It is preferable that all crystallinity of the drug substance be suppressed by the polymer carrier since small pockets of crystallinity can act as seeds, resulting in additional crystal growth which reduces the shelf-life of the drug formulation[77]. To date, polymers used in pharmaceutical formulations, such as polyethylene glycol (PEG) and poly(vinylpyrollidinone) PVP are used to enhance drug solubility. However these polymers are both highly water solubility and have a tendency to crystallize and an inability to stabilize some actives in the solid phase, respectively[78]. Recently, another interesting polysaccharide hydroxypropylmethyl cellulose acetate succinate (HPMCAS) was found to have interesting properties to form amorphous matrix formulations[79].

Most of the methods illustrated in Table 3 produce microparticles. In our work for the first time amorphous solid dispersions of polymer-drug nanoparticles were prepared by a rapid precipitation process. There have been several polysaccharides studied for producing amorphous nanoparticles. However the following showed well defined characteristics suitable for oral drug delivery.

Table 3. Properties of Polymers commonly used as ASDs [80]

Polymer	Tg (ºC)	Solvent Solubility	Amenable Methods of Manufacture
Copovidone (copolymer of 1-vinyl-2-pyrrolidone and vinyl acetate)	106	Dichloromethane Ethanol Methanol Water Acetone	Rotary evaporation Spray drying Hot Melt extrution
Polyvinyl Caprolactam-polyvinyl acetate-polyethyleneglycol copolymer	70	Water Ethanol Methanol Acetone	Rotary evaporation Spray drying Hot Melt extrusion
PVP	130 (K17) 168 (K30)	Chloroform Ethanol Methanol Water Acetone	Rotary evaporation Spray drying Hot Melt extrusion
HPMC	170	Cold water Dichloromenthane:Ethanol Dichloromenthane:Ethanol Water: Alcohol	Spray drying
HPMCP	133-137	Acetone: Methanol Acetone: Ethanol Methanol: Dichloromethane	Spray drying
HPMCAS	110-130	Acetone Ethanol: Dichloromethane (clear turbid viscous solution)	Spray drying
Methacrylate/methacrylic acid copolymer	110-150	Ethanol, Methanol, Acetone, acetone with 3% water	Rotary evaporation Spray drying Hot Melt extrusion

The tendency of the drug to recrystallize from the supersaturated solutions that are generated by dissolution of amorphous drug dictates the formulation performance. Without stabilization, recrystallization occurs which destroys an ASD, leading to a decrease in the quantity of drug in solution available for absorption. However, in several cases it was shown that polymers can be included within the formulation matrix to reduce the tendency to crystallize post-dissolution and to provide for significant increases in oral bioavailability[81,82,83] .

When the drug is molecularly dispersed in the polymer matrix, the particle size of drug in the carrier is minimized, theoretically, to the size of a single molecule[84]. The effective surface area for dissolution is increased due to the reduction in particle size. The dissolution of amorphous drug may lead to secondary precipitation from the supersaturated solutions and results in the formation of suspensions with relatively small particle size[82,85,86]. It is often difficult to distinguish between an increase in dissolution that results from a reduction in the particle size of the aggregates present in the original solid dispersion and the size of particles that may be formed in situ via precipitation on dissolution. Nonetheless, in most cases, an increase in the dissolution rate resulting from a decrease in the size of dissolving drug particles is evident.

PEG-based solid dispersions enhance the dissolution of many low solubility compounds[87,88,89]. However, the tendency of PEG to crystallize is a crucial issue. In some formulations like PEG 6000–based solid dispersions, the dissolution rate of diazepam and temazepam increased compared with the crystalline drug but the rate of dissolution was no better than that of equivalent PEG-drug physical mixtures[87]. Similarly, the rates of dissolution of physical mixtures of nifedipine with PEG 4000 and 6000 were equivalent to that of a solid dispersion, even though the manufacturing of solid dispersions of polymer and drug resulted in nifedipine transforming to a metastable and more soluble physical form[90].

The strength of intermolecular solid-state interactions in an amorphous solid is lower than in crystalline solids. From the solubility equations[31], a reduction in intermolecular forces in the solid state contributes to an increase in solubility. It is often found that there is a notable difference in experimentally determined amorphous and crystalline solubilities[91,92]. Therefore, there have been complexities in measuring the "equilibrium" solubility of a thermodynamically unstable amorphous material since spontaneous crystallization results in underestimation of the initial (kinetic) solubility properties of the amorphous form[92,93,94]. Recent work by Murdance et al.[93, 95] suggests that historical predictions of amorphous drug solubility, which were predicted using the difference in heat capacity between crystalline and amorphous drug, may have been overestimates since amorphous solids are often hygroscopic and constantly absorb water. This results in decreasing the drug-water interactions which decreases the free energy difference between amorphous and crystalline drug and reduces the solubility advantage compared with theoretical predictions. However, there are significant drug solubility advantages from ASDs which are demonstrated through increases in dissolution rate and, ultimately, oral bioavailability.

The dissolution of an amorphous drug from an ASD leads to the attainment of drug solutions that are supersaturated with respect to the equilibrium crystalline drug. The supersaturation provides a greater concentration of dissolved drug and generates drug solutions with increased thermodynamic activity. This also provides an advantage with respect to drug absorption, but the supersaturated solutions are unstable and at risk of precipitation. The rate of drug precipitation from supersaturated solutions can be inhibited or retarded by the presence of materials such as polymers that inhibit crystal nucleation or slow crystal growth[96,83,97]. In work by Yamashita et al.[98], it was shown that HPMC prevented recrystallization of tacrolimus more effectively compared with PVP and PEG 6000 (Figure 3), and HPMC-based ASDs have

increased Cmax and the area under the curve (AUC) in dogs by about 10-fold compared with the crystalline form of the drug. HPMC plays a similar role in enhancing the bioavailability of the poorly water-soluble weak base itraconazole after oral administration of the Sporanox formulation [99,100]. It is important to note that while supersaturated solutions inherently are unstable, if the drug is stable for > 6h which is the time of passage through the GI tract, that should be enough for maximum bioavailability.

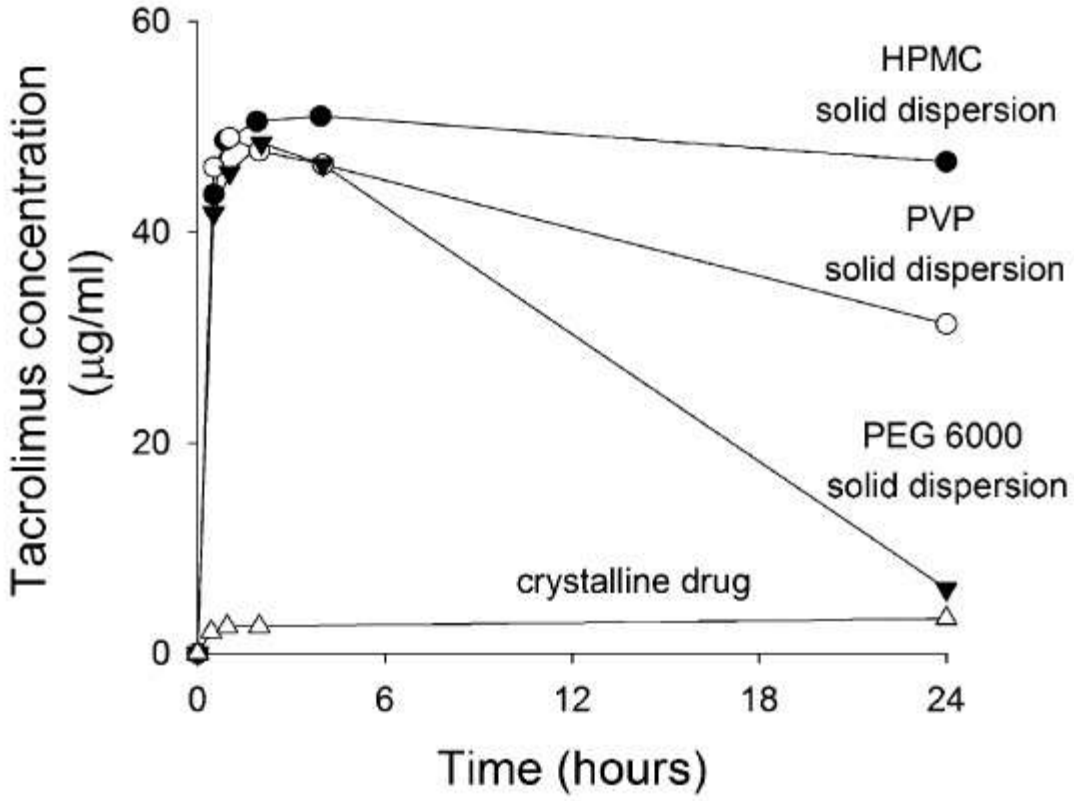

Figure 3. Tacrolimus solid dispersions with HPMC, PVP and PEG 6000 show enhanced solubility initially compared to crystalline Tacrolimus. Only HPMC was able to maintain supersaturation by inhibiting recrystallization in solution[98].

HPMCAS has recently shown promising results in oral formulations [82,59, 101,92, 102]. HPMCAS also has a high glass transition temperature (120°C) and, therefore, can reduce mobility and protect against drug crystallization in the solid state.

The precipitation of the drug from a supersaturated solution consists of the formation of particle nuclei and subsequent particle growth[103,71]. The drivers of phase separation or crystallization are responsible for nucleation and particle/crystal growth in solution. One way of reducing the potential for precipitation from solution is by increasing the drug solubility in solution, as this will reduce the level of supersaturation and the thermodynamic drivers of drug precipitation. Polymeric carriers can enhance stability of supersaturated solutions by increasing drug solubilization. They reduce drug precipitation by slowing the kinetics of drug precipitation or crystallization,[59, 84, 86, 97a, 102, 104] by interacting with the drug in solution and by adsorption to the interface of the emerging particle/crystal nucleus [66,105,106,107]. Therefore the polymer has the ability to reduce crystal growth and to disrupt the manner in which the crystal lattice is formed[71]. For example, a drug released from HPMCAS solid dispersions was stabilized in solution in the form of amorphous drug polymer colloidal assemblies (20 to 300 nm in diameter)[71]. The presence of colloidal drug-polymer aggregates decreases the collision frequency of monomeric , solvated free drug molecules thereby decreasing the kinetic nucleation and providing more sustained periods of supersaturation[71, 93, 108]. The presence of nanoparticles in the dissolution media during release of felodipine from HPMC[85] and ketoconazole from PVP solid dispersions[86] sustain the period of supersaturation. Separation techniques like centrifuge or filtration may not be able to separate small aggregates from free drug in solution. This may complicate analysis. It is difficult to define accurately whether the drug is completely dissolved in solution or dispersed as nanosized aggregates[92]. Another major disadvantage is that these nanoparticles may grow and

stimulate drug crystallization which can be prohibited by presence of carefully selected polymers[96-97].

PEG 8000–based solid dispersions containing amorphous ritonavir show significantly faster dissolution rates (Figure 4a) compared with simple physical mixtures and marked increases in oral bioavailability in beagle dogs compared with the crystalline form of the drug[58] (Figure 4b). Increasing the drug loading, however, led to phase-separation of drug within the crystalline PEG carrier which resulted in decreased dissolution rates and in vivo exposure[58] .

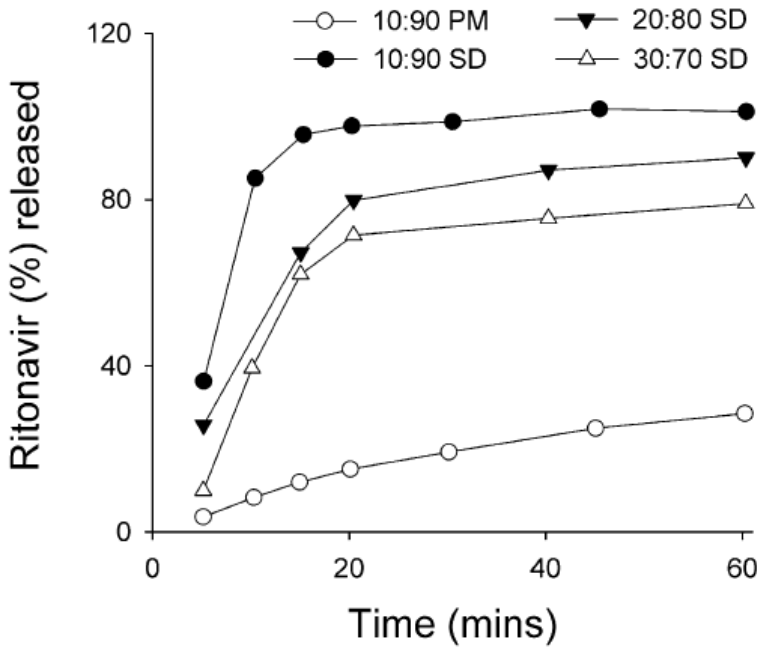

Figure 4a. In-vitro dissolution of a physical mixture (PM) of crystalline ritonavir and PEG (10:90), amorphous solid dispersions (ASD) of ritonavir in PEG at different drug : polymer ratios. There is an increase in release of amorphous drug compared to the crystalline drug. The lowest amorphous drug :PEG ration (10:90) shows the highest release [58].

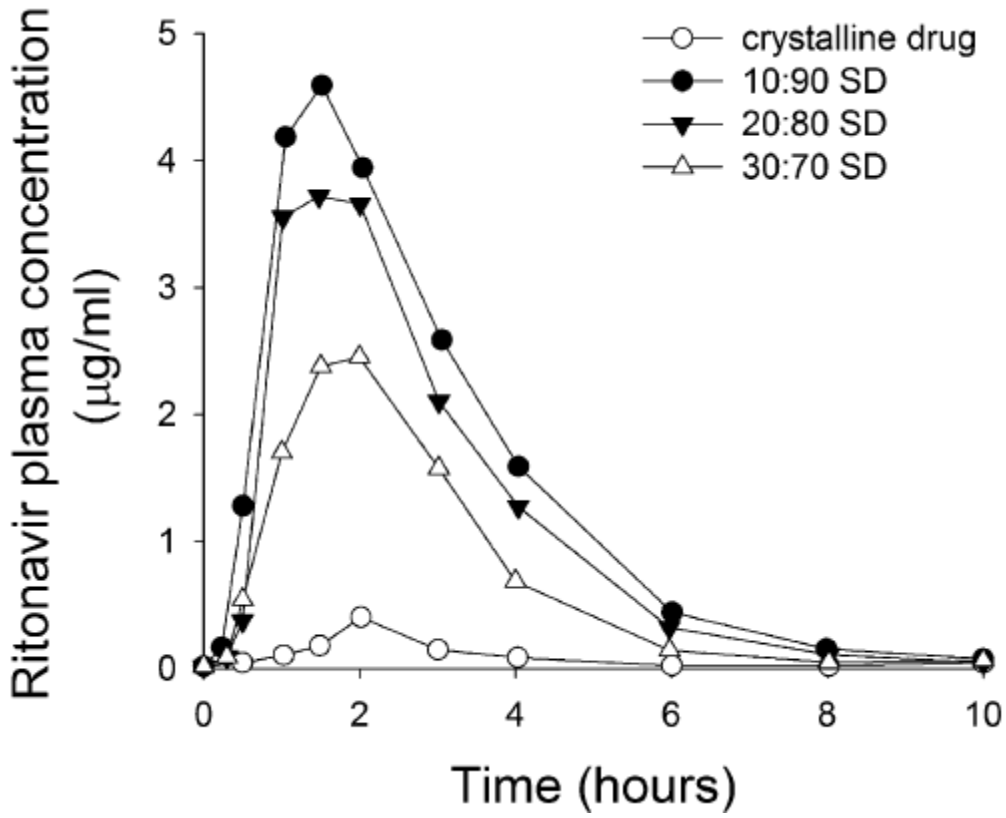

Figure 4b. Plasma concentration of amorphous ritonavir (in PEG) at different drug: polymer ratios compared to crystalline ritonavir. The lowest amorphous drug : polymer = 10:90 shows highest plasma concentration [58] .

Friesen and coworkers[72] summarized studies that use HPMCAS to generate amorphous solid dispersions for a number of investigational Pfizer compounds. HPMCAS solid dispersions of amorphous drugs gave rise to 2- to 40-fold increases in bioavailability compared with the crystalline forms of the drug. Soluplus (BASF Corp.), which is a polyvinyl caprolactam–polyvinyl acetate polyethylene glycol graft copolymer, was used to create solid solutions of BCS class II drugs fenofibrate, danazol, and itraconazole by hot melt extrusion, with each system demonstrating superior *in vivo* performance in beagle dogs compared with the crystalline form of the drug[109]. A significant example of the potential clinical and commercial utility of amorphous solid dispersions is Kaletra (Abbott Laboratories), a combination of two HIV protease inhibitors,

ritonavir (50 mg) and lopinavir (200 mg), in a polyvinylpyrrolidone/ vinylacetate copolymer (PVPVA) solid dispersion prepared by hot-melt extrusion[110,110b]. Sporanox (Janssen Pharmaceuticals) provides a second commercial example of the utility of amorphous solid dispersions.

Molecular dispersion of a drug within a solid polymer is expected to provide the maximum surface area available for hydration and, therefore, faster dissolution rates. Indeed, the dissolution rate of molecularly dispersed drug may be almost instantaneous. However, when drug dissolution is rapid, the dissolution rate of the carrier has the potential to limit drug release[84,111]. Drug dissolution is dependent on carrier hydrophilicity and viscosity. Drug release from solid dispersions is dependent on the relation between the rate of release of drug and the rate of release or dissolution of the polymeric carrier[112]. It is often observed that low drug loading favors the formation of molecular dispersions. Polymer selection is therefore a tradeoff between properties, including release rate and amorphous drug stabilization[113].

Drug-release profiles also change with increasing drug-carrier ratio. It has been shown that increasing the drug load decreases the quantity of carrier available to stabilize the drug in the high energy form. Also, high drug loading will promote phase separation within the solid dispersion, in turn increasing the risk of instability[74,75]. Drug-release profiles also change with increasing drug-carrier ratio. It was shown in several cases that with increasing drug loading, there was a reduction in drug dissolution rate from solid dispersion[114,58,115,116,117,101, 118,64,119,119b]. The decrease in dissolution is due to a reduction in the quantity of molecularly dispersed drug form since increasing drug load reduces the intermolecular distance between drug molecules and the quantity of stabilizing polymer, both of which favor phase separation of amorphous/crystalline particulate drug in the carrier[69,75].

At high drug-polymer ratios, the relative quantity of the polymer present is reduced, thereby leading to a decrease in drug wetting only if the polymer is less hydrophobic than the drug. This leads to a drug-rich solid phase which increases the risk of phase separation or crystallization[120,84,85]. Under these conditions, the rate of drug release is dependent on the physical form of the drug in the drug-rich layer. Where the drug is present as an amorphous suspension, its concentrations that are likely to be achieved during dissolution are expected to be supersaturated relative to the solubility of the crystal form but unlikely (thermodynamically) to exceed the saturated solubility of amorphous drug. In contrast, when the drug is molecularly dispersed, rapid initial dissolution may lead to supersaturation relative to crystal drug solubility.

Most of the polymers which are used in ASDs have high Tg values (such as Tg of PVP K30 is 168°C, and the T_g of HPMC is 170°C) , in excess of that of most drugs[117,121]. The high T_g values of these polymers dictate that homogeneous dispersions of drug and polymer have T_g values that are higher than the drug T_g. Therefore, the polymeric formulations have the potential to stabilize molecular transitions in the amorphous state. Dispersing drugs in a polymer matrix provides a means of kinetic stabilization of the amorphous form of the drug that might not be possible in the absence of polymer, because of rapid molecular relaxation and crystallization[64]. Polymer incorporation usually increases the physical stability of amorphous drug by increasing the Tg of the system and reducing molecular mobility[122,101,123]. The use of high-molecular weight polymers as vehicles for solid dispersion formation, therefore, provides an opportunity to both increase the likelihood of glass formation and promote the stability of the amorphous system formed through increased Tg. The storage temperature of 50°C below the Tg reduces the mobility sufficiently to allow acceptable physical stability[53b,124]. It was shown that, in the absence of polymer, indomethacin recrystallized in less than 6 weeks at storage temperatures

20°C below the Tg. However, when the drug was molecularly dispersed in PVP solid dispersions, the difference between the Tg of indomethacin in the formulations and the storage temperature increased to 40–50°C and recrystallization of indomethacin was suppressed[64].

Amorphous solid dispersions with high Tg values might show evidence of crystallization due to plasticizing effect of moisture adsorption during storage[125,126]. It is shown that sensitivity to moisture was ascribed to the hygroscopic nature of PVP as similar solid dispersions containing the less hygroscopic polymers HPMC and HPMCAS showed reduced instability on exposure to moisture[127] . In this regard one should be cautious about incorporating any hygroscopic excipients or fillers in the tablet formulation which may act as plasticizers[128]. Therefore, it is important to use appropriate storage conditions, barrier packaging, and/or to use less hydrophilic, less hygroscopic polymers to minimize water uptake.

To initiate crystallization, an activation energy barrier must be overcome that reflects the kinetic limitations to crystallization. This is the energy required for molecules to diffuse and appropriately align such that nucleation and the formation of a new solid phase are possible[129]. The stability of an amorphous drug is a function of both the free energy (equivalently, the chemical potential) of the amorphous form and the kinetic barriers to crystallization provided by the viscosity of the glass and supplemented by the addition of excipients, such as polymers[70,72,94].

Differential scanning calorimetry (DSC) is routinely used to determine the miscibility of drug-polymer mixtures. When the T_g of the drug and polymer are different, a single T_g value during a melting DSC cycle is usually considered satisfactory evidence of drug polymer miscibility. In contrast, multiple T_g values suggest incomplete drug-polymer mixing or limited drug-polymer miscibility[114,130]. It is important to note that DSC is not a room temperature

technique; crystallization may occur during heat-up. Solubility parameters (Hildebrand and Hansen) provide an alternative mechanism for estimation of the potential for drug-polymer miscibility, where drug polymer combinations with the most similar solubility parameters are expected to provide the greatest likelihood of miscibility[131,132]. The lack of crystalline peaks and presence of an amorphous halo in X-ray diffraction data also provide additional information about the degree of molecular dispersion of the amorphous drug with the polymer.

The increase in drug loading led to a progressive decrease in the Tg of the drug-polymer mixtures in diazepam-PVP solid dispersions. Above 35% w/w drug, two distinct T_g values were observed (i.e., drug and polymer glass transitions) as the drug-phase separated from the polymer. At higher drug loads, the absolute level of molecularly dispersed drug was largely unchanged. However, the level of the drug arranged as amorphous clusters increased steadily. Solid dispersions greater than the diazepam-PVP miscibility limit (35%), therefore, show characteristics of both an amorphous suspension and an amorphous solid solution[130]

Unlike molecularly dispersed formulations, phase separated drugs present as suspended amorphous particles ars no longer intimately mixed with the carrier. This more heterogeneous molecular rearrangement is more likely to crystallize compared with solid dispersions where drug is present in a molecularly dispersed form that has increased kinetic stability as a result of intimate contact with the polymer[68,133, 134]. Solid dispersions with lower drug-polymer ratios and those with high drug polymer miscibility therefore show better physical stability at ambient temperatures[135,130,82,75].

2.3.1 Polysaccharides in drug delivery

In oral drug delivery, commercial cellulose esters are used as excipients for coating, membranes and promote dissolution of the drug. Cellulose acetate phthalate (Cellacefate, NF) is

used as an enteric coating for pharmaceutical active tablets prevent dissolution of the drug in the stomach by utilizing its pH-mediated solubility .[136] Cellacefate, NF is insoluble below pH~ 3 in the stomach [137] but rapidly dissolves at pH 5 and up, which is typical of the pH range of the gastrointestinal tract from the duodenum through the colon .[138] Other cellulose esters used in drug delivery, cellulose diacetate and cellulose acetate butyrate are water insoluble and pH insensitive.

In oral dosage forms, hydroxypropylcellulose (HPC) is widely used as a binder due to excellent chemical characteristics, water solubility and mucoadhesive properties. Ebube et al. showed that the hydrophilic matrix formulations of HPC during release of acetaminophen were altered due to the presence of pseudoephedrine which generated an additional osmotic gradient resulting in faster polymer swelling and increase in gel thickness[139]. Other applications of HPC were in a preoral, extended-release bioadhesive tablet formulation of verapamil HCl [140], buccoadhesive tablets for insulin and propranolol delivery[141], vaginal bioadhesive tablets of acyclovir[142] and oral drug delivery of poorly soluble cyclosporine[143].

The 2-hydroxylpropyl ether of methyl cellulose (HPMC) is extensively used in oral controlled drug delivery systems [144,144b]. It is derived from alkali-treated cellulose which is reacted with methyl chloride and propylene oxide. HPMC swells and produces a viscous, colloidal solution when dissolved slowly in cold water. It is also soluble in most polar organic solvents. Recently scientists have recognized the interesting properties of hydroxypropylmethylcellulose acetate succinate (HPMCAS) in amorphous matrix formulations[144a]. The most important polysaccharides used in pharmaceuticals are as shown in Table 4.

Table 4. Polysaccharides in Pharmaceutical use[145]

Polymers	Use
Hydrophilic polymers	
Cellulosic Methyl cellulose	Suspending agent, tablet and capsule disintegrant, tablet binder, viscosity increasing agent
Hypromellose (hydroxypropylmethyl Cellulose	Coating agent, film forming agent, rate controlling polymer for sustained release, stabilizing agent, suspending agent, tablet binder, viscosity increasing agent
Hydroxypropyl cellulose	Coating agent, emulsifying agent, suspending agent, stabilizing agent, thickening agent, tablet binder, viscosity-increasing agent
Hydroxyethyl cellulose	Coating agent, suspending agent, thickening agent, tablet binder, viscosity-increasing agent
Sodium carboxymethyl cellulose	Coating agent, suspending agent, tablet and capsule disintegrant, tablet binder, viscosity-increasing agent, stabilizing agent, water absorbing agent
Noncellulosic: gums/ polysaccharides	
Sodium alginate	Stabilizing agent, suspending agent, tablet and capsule disintegrant, tablet binder, viscosity-increasing agent
Xanthan gum	Stabilizing agent, suspending agent, viscosity-increasing agent
Carrageenan	Gel base, suspending agent, sustained release tablet matrix
Cross-linked high amylose starch	Gelling agent, thickening agent
Ceratonia (locust bean gum)	Matrix, binder
Chitosan	Coating agent, disintegrant, film-forming agent, mucoadhesive, tablet binder,

	viscosity increasing agent
Guar gum	Suspending agent, tablet binder, tablet disintegrant, viscosity-increasing agent
Hydrophobic polymers Water-insoluble	
Ethylcellulose	Coating agent, flavoring fixative, tablet binder, tablet filler, viscosity increasing agent
Cellulose acetate	Coating agent, extended release agent, tablet and capsule diluents
Cellulose acetate propionate	Membrane
Cellulose acetate phthalate	Enteric coating agent
Hydroxypropylmethylcellulose phthalate	Enteric coating polymer
Poly(vinyl acetate) phthalate	Viscosity modifying agent with enteric coating
Gantrez1 AN (copolymers of methyl vinyl ether and maleic anhydride)	Mucosal adhesive resins
Methacrylic acid copolymers	Film forming agent, tablet binder, tablet diluents
Eudragit1 acrylate copolymers	The wide range of immediate, enteric and sustained release polymers allow the design of any number of combinations to match targeted release profile

Polysaccharides in this study

A. Carboxymethyl Cellulose Acetate Butyrate

Carboxymethyl cellulose acetate butyrate (CMCAB) is compatible with numerous pharmaceutical actives and has a high glass transition temperature (Tg = 137°C) and thus is useful for forming stable solid blends. It has a combination of chemical groups (shown in Figure 5) suitable for complexing with drugs like

1. Electrostatic → Carboxymethyl group for binding with cationic drugs
2. Hydrogen bonding → Carboxymethyl, Acetyl, Butyryl groups

3. Hydrophobic → Butyryl, Acetyl groups

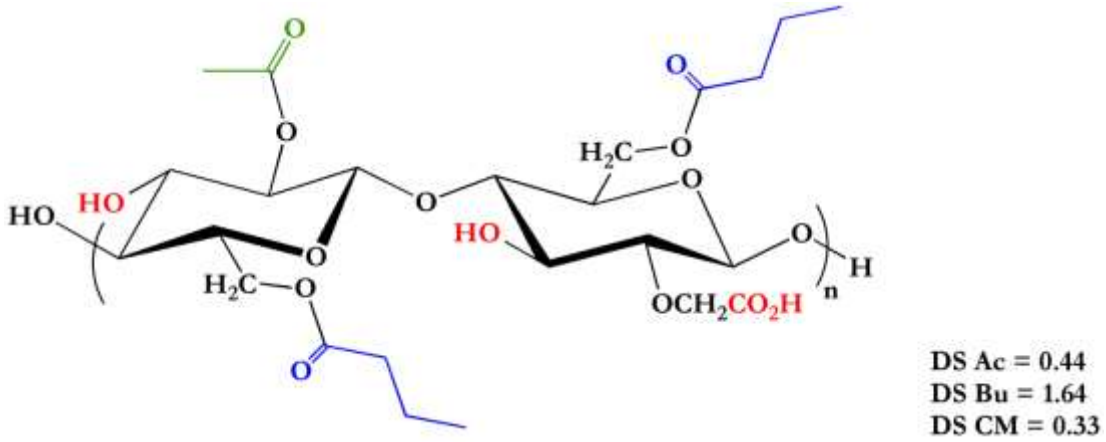

Figure 5. Structure of Carboxymethyl cellulose acetate butyrate (CMCAB)[79]

The properties of CMCAB have been studied extensively [23a]. CMCAB can release encapsulated drugs based on changing pH and it can form an amorphous matrix with many drugs. In addition, it can keep constant drug release over 24 hours, and can be used to increase the solubility, and thus bioavailability of various drugs [23a]. The purpose of this is to produce an oral drug delivery mechanism for common insoluble drugs to enhance their solubility and bioavailability properties. Shelton et al[79] showed that CMCAB can be readily incorporated into pH-controlled, slow release formulations made of the polymer and the drug by techniques like co-precipitation, spray drying and film casting. It was proved that amorphous drugs in solid dispersions of CMCAB had enhanced the solubility and drug release.

Shelton et al[79] showed that CMCAB has a useful hydrophobic/hydrophilic balance, which provides good miscibility with many pharmaceutical actives. It can deliver pH-controlled release to isolate the active from the gastric environment, near zero-order- sustained release, enhanced efficacy, reduced side effects and it provides an amorphous matrix to enhance dissolution of poorly soluble actives.

The structures of other cellulose derivatives and pullulan derivatives are shown in Figure 6 and Figure 7. Some of the important properties are given in Table 5.

B. Other cellulose derivatives used in this thesis

Cellulose Acetate Propionate – Adipate with degree of substitution of the adipate group = 0.33 (CAP-Adp 0.33) or 0.85 (CAP-Adp 0.85) and Cellulose Acetate– Sebacate (CA-320S Seb)[146, 147]

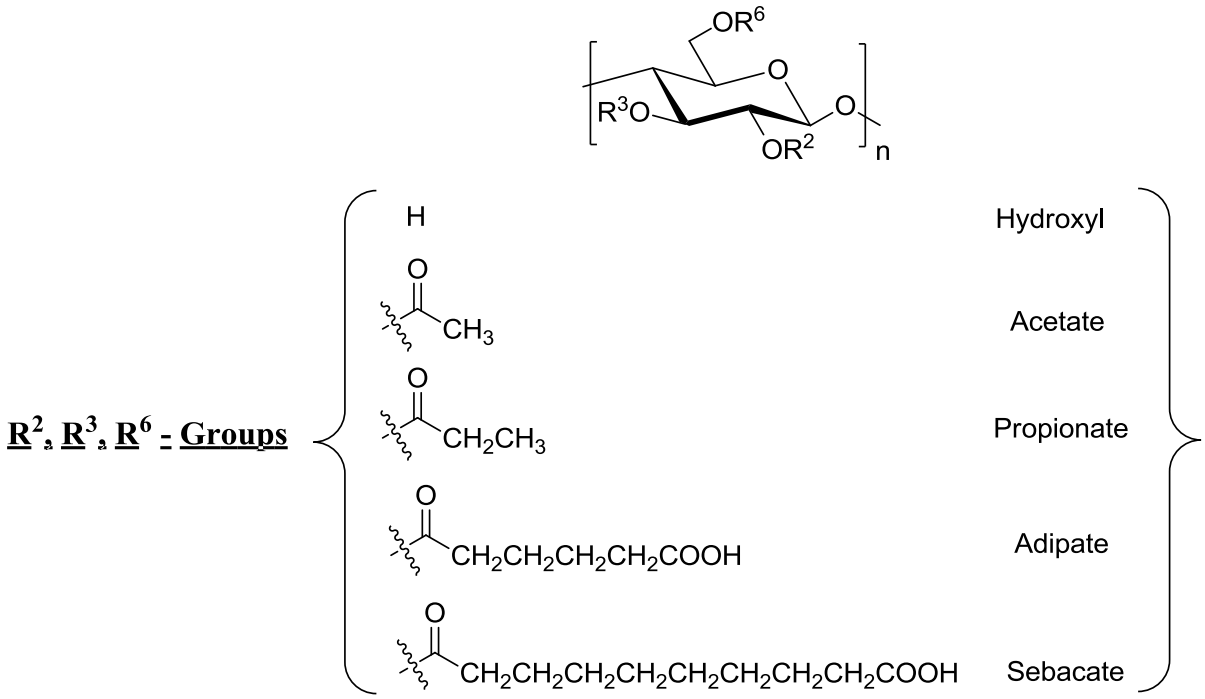

Figure 6. Molecular structure of the novel synthesized cellulose derivatives and the in substituent groups. These cellulose derivatives are not regioselectively substituted.

C. Butyl Pullulan-6- Carboxylate (BPC)

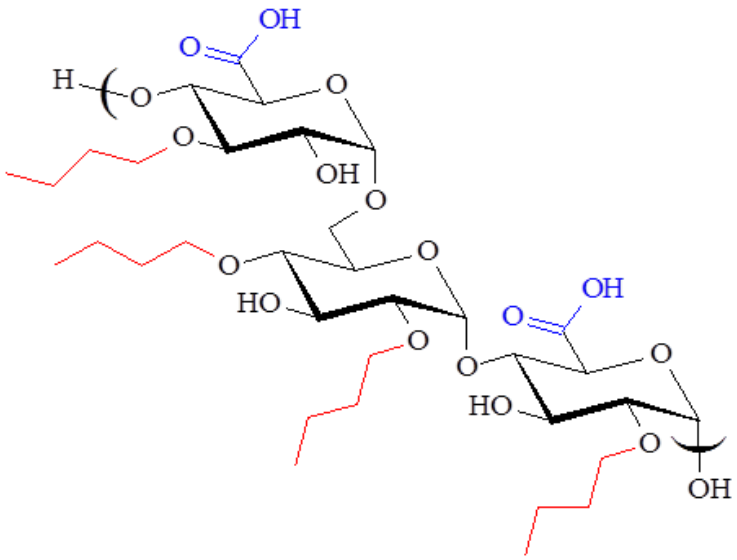

Figure 7. Butyl pullulan -6-carboxylate

Table 5. Abbreviation and properties of Novel Synthesized Cellulose and Pullulan Derivatives

Polymer	Polymer Abbreviation	DS (CO_2H)	DS (Other)	DS (Total)	Solubility Parameter ($MPa^{1/2}$)	Molecular weight ($x10^3$)	T_g (°C)
Cellulose Acetate Propionate 504-0.2 Adipate 0.33	CAP Adp 0.33	0.33	Ac 0.04; Pr 2.09	2.46	20.56	12.0	125
Cellulose Acetate Propionate Adipate 0.85	CAP Adp 0.85	0.85	Ac 0.04; Pr 2.09	2.98	21.27	9.7	110
Cellulose Acetate 320S sebacate	CA 320S Seb	0.57	Ac 1.82	2.39	22.36	25	117
butyl pullulan-6-carboxylate	BPC	0.53			28	Could not be measured due to aggregation	Above 200

2.4. Synthesis of Solid Drug Nanoparticles

There are various ways by which nanoparticles of poorly water-soluble molecules are prepared[20a, b, 42, 148]. Approaches may include the building-up approach through synthesis[149], self-assembly[150] or precipitation of drug molecules[20b]. Some of the common methods used to fabricate nanoparticles are homogenization[151], microfluidation[152] and milling[19]. Some of the methods are briefly described below.

Precipitation

In this method, the substance to be formulated must be soluble in a preferably non-toxic water-miscible solvent. However, there are several new chemical entities which are poorly soluble in aqueous and most organic solvents. This method may not suitable for such

compounds. After mixing the organic solution of the compound with an aqueous solution of stabiliser, the ambient conditions are controlled to trigger precipitation of the desired crystalline or amorphous drug particles in the nano- or micrometer size range (400–2,000 nm)[18] . Then selected polymers like gelatin, chitosan, poloxamer are added to stop the particle growth after a certain stage. The drug nanoparticles are stabilized thereafter by spray-drying with excipients (lactose, mannitol).

External forces

Drug particles can be broken at crystal imperfections by applying external forces[153]. The particle size threshold depends on the drug properties, as well as the energy input. In order to further reduce particle size, the energy input must be exponentially increased after several processing cycles.

Wet-Milling

In this process, a milling chamber is charged with milling media (pearls), dispersion medium (mostly water), drug particles and stabilizer and is subjected to rotary movement as a whole or its contents are stirred by an agitator. The revolving pearls generate a high shear force and leads to interparticle collisions in the mill. Particles in the size range 80-400 nm are generated. The disadvantage of this method is loss of product and higher chance of contamination.

High Pressure Homogenization

In high pressure homogenization, a particulate suspension is driven through a constricted gap of homogenizing valve. The velocity of the fluid in the passage increases immediately when the suspension constantly flows through the narrow gap of ~20 mm. Gas bubbles are formed at room temperature when the fluid's static pressure is dropped below vaporization point. On passing the

gap, the fluid flow velocity decreases leading to loss of the gas bubbles, initiating high-energy micro jet-streams leading to decrease in particle size. In this method, cavitation is very common due to interparticle collisions and high shear forces[20a, 151b, 153]. Also, it is important to reduce the water in the suspension before they can be used as dosage forms. The drying methods (lyophilization, spray drying and fluidized bed drying) are time and energy consuming[153].

Microfluidization

A Microfluidizer processor is used to decrease the size of drug crystals in suspension. A pump forces the particle suspension through microchannels. Due to the narrow diameter of the channels, the streaming velocity results in cavitation and high shear rates. This technique involves high homogenization pressures and higher number of processing cycles to achieve the desired particle size reduction[151b, 153] .

Flash Nanoprecipitation using a Multi- Inlet Vortex Mixer

In this thesis, a Multi-Inlet Vortex Mixer (MIVM) is chosen for its ability to produce nanoparticles of insoluble compounds using a process known as flash nano-precipitation. Most work done with MIVMs involves producing nanoparticles, either of a single molecule or through co-precipitation. [154]. This is due to the MIVM's ability to precipitate particles very rapidly by the controlled nucleation and grown of particles. This allows for the production of nanoparticles in a continuous manner and for the capability to control the size of the nanoparticles. [155] This is achieved by controlling the Reynolds numbers of fluids allowing for rapid and completely mixing. [154c, 155-156] There are two different important time scales to consider, the time of mixing τ_{mix} and the time of aggregation τ_{agg}. The mixing time τ_{mix} concerns how fast materials entering the mixer become well mixed and τ_{agg} concerns how long it takes for the polymers to aggregate (Figure 8). When $\tau_{mix} > \tau_{agg,}$ the particle size resulting from mixing will decrease as τ_{mix}

decreases. [157] This is important because τ_{mix} is dependent on the Reynolds number, which is controllable [155-158]. Work by Gindy et Al. [159] and Yiu et al. [155] explains that intense mixing of the organic solvent stream with water in the MIVM induces supersaturations as high as 1000 in times on the order of milliseconds to initiate rapid precipitation of all hydrophobic components, including the hydrophobic block of the block copolymer. The mixing time is shorter than the time scale for nucleation and growth of dissolved organic solutes. By balancing the nucleation and growth times with the block copolymer assembly time, it is possible to block further particle size growth

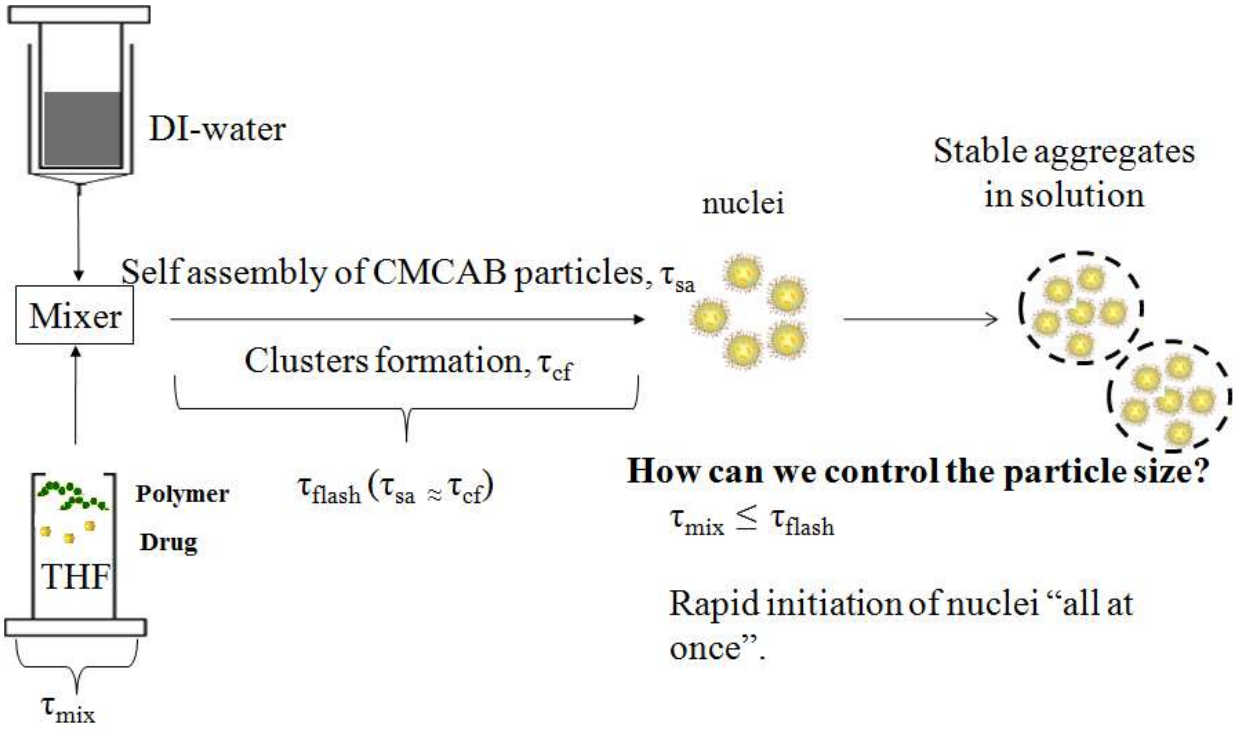

Figure 8. Schematic representation of MIVM producing polymer-drug nanocomplexes adapted from the work by Mustafa et al.[160]

The nanoparticles produced by the above methods shows greater surface area compared to microparticles (size > 1 μm) (Figure 9). Due to higher surface area, there will be greater surface interaction and enhanced dissolution rates. However, these nanoparticles may have tendency to aggregate and also stimulate drug crystallization due to higher surface area.

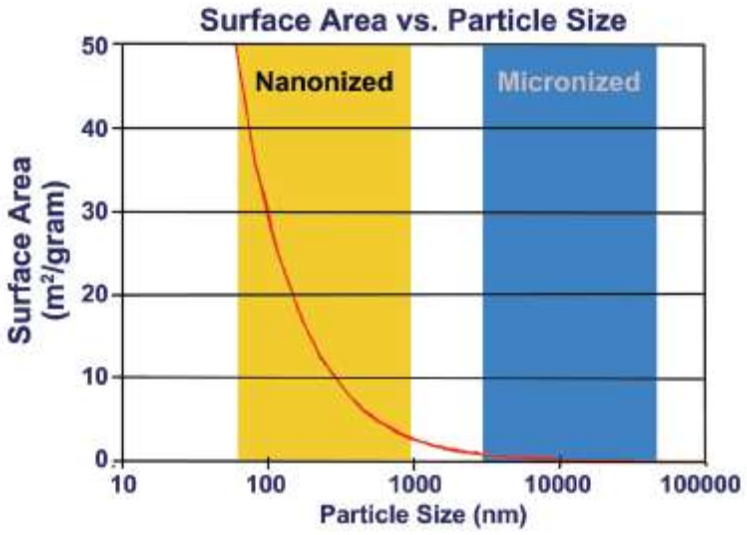

Figure 9. The surface area increases when solids are fractured from the micron-size range (microparticles) to the nanometer-size particles used in the various nanoparticle formulations to improve the performance of poorly water-soluble compounds[30] .

Table 6 shows comparative studies of the methods used to synthesize nanoparticles. The nanoparticles in this work are fabricated by a rapid precipitation process using a multi-inlet vortex mixture (MIVM). The rapid process is especially interesting, because of narrow particle size distributions. The rapid mixing creates high supersaturations of drug leading to nucleation, whereby size is controlled by polymer self-assembly. This process is scalable and has been used

to produce stable nanoparticles that incorporate drugs, imaging agents, peptides, and targeting ligands with controlled particle size distributions.

Table 6. Comparative studies of the methods used to synthesize nanoparticles[161]					
Technique		**Advantages**	**Disadvantages**	**Cost effectiveness**	**Particle size (nm)**
Precipitation	Hydrolysis by antisolvent precipitation	Simple set up	Mostly amorphous nanoparticles, mixing conditions cannot be controlled with laboratory apparatus, anti-solvent must be miscible with water	Fast precipitation, high yield	100-400
	High-gravity controlled precipitation technology	Can produce crystalline particles, suspensions can be recycles for prolonged mixing and reaction	Equipment id highly specialized and not widely available	Variable production time, high yield	100-500
	Confined liquid impinging jets	Effective mixing in a small mixing chamber	Less suitable for hydrophilic drugs, only 2 jets, suspensions cannot be recycled, difficult to scale up	Fast precipitation, high yield	100-1000

	Multi-Inlet Vortex Mixer	Quick; effective mixing, accommodate four jets with variable flow rates	suitable for hydrophilic drugs, only 2 jets, suspensions cannot be recycled, difficult to scale up	Fast precipitation, high yield	75-310
	Supercritical Fluid	Rapid removal of supercritical fluid without lengthy drying	Drug solution must be miscible with supercritical CO_2,potential residual solvent in final form, non-uniform mixing, long production time, clogging of spraying nozzles by precipitates	Slow production time	45-500
	Sonoprecipitation	Simple, reduction of organic solvents	Amorphous particles, immersion depth of horn tip must be established experimentally	Slow, variable yield	80-130
Evaporation	Spray drying	Single step drying from solution,	Amorphous, limited throughput	Fast drying, moderate to high	500-2600

		controlled particle size, scale up		yield	
	Aerosol Flow reactor	Single step drying from solution, controlled particle size, scale up, good morphology	May not be suitable for heat labile compounds	Fast drying, yield depends on nozzle design	80-125
	Electrospraying	Narrow particle size distribution, can be used for atomization in a spray dryer or aerosol flow reactor	Cannot be used for liquid with surface tension > 50 mN/m or conductivity $>10^{-4}$ S/m	Low yield but can be improved using multiple nozzles	4-120

2.5. Drug Delivery for Tuberculosis

2.5.1 Tuberculosis

Every year, almost 2 million deaths and eight million new cases caused by Tuberculosis (TB) are reported. Despite available remedies, TB is a prominent disease in many underdeveloped countries. The major problem in the treatment of TB involves continuous, frequent multiple drug dosing. It is therefore important to formulate drugs which can be introduced for long-duration release of the antimicrobial agents in a slow and sustained manner, therefore reducing frequency and number of doses [162].

2.5.2 TB drugs in this study

The model drugs used in this study were rifampicin, isoniazid and pyrazinamide. The drug loading efficiency of isoniazid and pyrazinamide was very low (8-16 %) and therefore, only rifampicin is discussed here in more detail.

Rifampicin (RIF) is a front line anti-tuberculosis drug usually prescribed in combination with isoniazid, pyrazinamide and streptomycin for a period of six to seven months. Rifampicin exhibits low bioavailability when delivered orally. It is a member of the rifamycin class of antibiotics used for the treatment of tuberculosis, often a component of the prescribed multi-drug fixed dose combination tablet [163].

Rifampicin is a complex semi-synthetic macrocyclic antibiotic derived from *Streptomyces mediterranei.* It was developed in the Dow-Lepetit Laboratories in Milan, Italy as a part of a screening program for new antimicrobial agents [164]. Five compounds named rifamycin A-E were isolated from fermentation cultures of *S. mediterranei* [165]. Rifamycin B was shown to be the most stable, least toxic and most active[164]. In 1965, rifampicin, a hydrazone of rifamycin B, was found to have increased absorption while retaining its parent antimicrobial properties.

Rifampicin was approved by the Food and Drug Administration (FDA) in 1971. Since then, several studies have evaluated its efficacy in tuberculosis treatment [166]. Although it is a first-line drug, several side effects such as hepatoxicity, allergic rashes, lack of appetite, nausea, or immunological disturbances have been reported with the prolonged administration of this drug [167]. The usual dialy dosage of rifampicin in an adult is 10 mg/kg, or 600 mg for a 60 kg person [3].

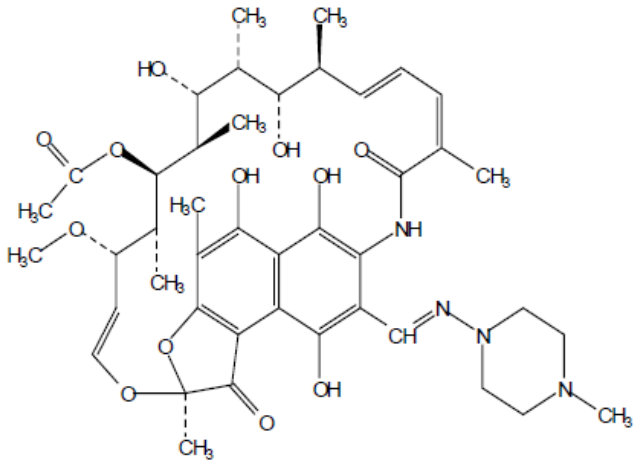

Figure 10. Structure of rifampicin[3]

In humans, orally administered rifampicin reaches peak plasma concentrations 2-4 hours after the dosage is given [168]. Rifampicin is hydrolyzed by the acidic medium in the stomach to form 3-formyl rifamycin which is insoluble and poorly absorbed by the epithelial layer of the intestine [169]. Unaltered rifampicin that makes it though the gastrointestinal tract is metabolized by the liver, eliminated in the bile and then reabsorbed from the intestine thereby entering enterohepatic circulation. It is during this time that rifampicin is deacylated into 25-desacetyl rifampicin [170]. Both 3-formyl rifamycin and 25-desacetyl rifampicin exhibit high antimicrobial activity *in vitro* but have been shown to be inactive *in vivo*.

Rifampicin has variable bioavailability and some of the explanations of decreased bioavailability include changes in the crystalline form of rifampicin, effects of excipients, and degradation in the gastro-intestinal tract, absorption, and metabolism. Rifampicin is categorized by the Biopharmaceutics Classification System as a class II drug because it has characteristics of low solubility and high permeability [170]. Rifampicin exhibits pH-dependent solubility affecting its absorption from the gastro-intestinal tract. Due to its high cost and side effects, it is used mainly in intermittent therapy. Its biological half-life ranges from 1.5-5 hours and thus there is a need for formulations that release rifampicin in a sustained manner that optimizes bioavailability while minimizing side effects. In the last several years, many different types of controlled release formulations of rifampicin have been developed to improve its clinical efficacy [171].

Isoniazid (INH) is an organic compound used for prevention and treatment of tuberculosis[172]. The standard dose of isoniazid in adults 10 mg/kg body weight. The chemical structure of isoniazid is shown in Figure 11.

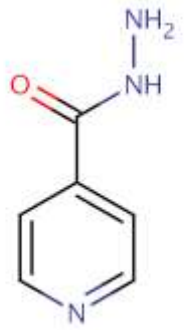

Figure 11. Structure of Isoniazid[3]

Pyrazinamide (PZA) is an antimicrobial agent that is primarily used to treat tuberculosis in combination with rifampicin and isoniazid. However, it demonstrates clinically significant antibacterial activity only against Mycobacterium tuberculosis and M. africanum. PZA appears

to accelerate the sterilizing effect of isoniazid and rifampin when used as a part of combination therapy. The structure is shown in Figure 12.

Figure 12. Structure of pyrazinamide

2.5.3. Polymer Nanoparticles in treating TB

Although there were three drugs used as model in this thesis, the properties and polymer drug nanoparticle studies were done primarily with rifampicin as the drug loading efficiency was extremely low for the other two drugs. Therefore, this section will focus on mainly previous research done on rifampicin.

Although effective therapies have been available for almost fifty years, TB remains a major problem in many developing countries. The treatment of TB requires frequent dosing with multiple drugs and thus it is important to formulate drugs so that they can be released in a sustained manner, reducing the frequency and number of doses [162].

Prior work with rifampicin-polymer particles can be broadly categorized in terms of studies done in vitro [173,174,175,176,177,178,179,] and in vivo, with the latter studies further categorized

in terms of delivery method, i.e. by injection [180], pulmonary delivery [41],[181]and oral delivery [182],[183],[184]. Most studies involved polymer carriers that were either polyesters or polysaccharides. Many of the studies focused on controlling drug loading and characterizing drug release but, in many cases, the method of producing the particles was not rapid and scalable.

In-vitro studies

PLGA (Poly (lactic-co-glycolic) acid) nanoparticles and microparticles have been used for encapsulation of TB drugs [185]. Rifampicin-loaded microspheres of PLGA were made by the solvent evaporation method with particle sizes ranging from 1-10 μm. The drug loading was between 50-67 % independent of microsphere size and it was observed that 80% of the drug was released (measured in-vitro in PBS buffer of pH 7.4 at 37° C) in 24 hours [179]. Poly(3-hydroxybutyrate-co-3-hydroxyvalerate) was used to load rifampicin using an oil-in-water emulsification method. The particles were very large (around 20-60 μm) with only 14 % drug loading and 90% release.

In another study, rifampicin was coated onto starch beads approximately 1 mm in size along with polysaccharides and the subsequent release rates were found to vary inversely with the coating thickness. [171b]. A number of release studies which were done in-vitro polysaccharides like alginate, chitosan and hydroxypropylmethyl cellulose prepared by cation induced gelation, spray drying, and granulation respectively showed prolonged release over 1-3 days with particle sizes of several microns.

Poly(lactic-co-glycolic acid) PLGA was used to prepare rifampcin-polymer nanoparticles (200-260nm). Rifampicin release was studied at pH 5.2 and pH 7.4. An initial burst was observed in the first few hours and then gradually decreased and remained constant after a day

[179]. However, no results were shown regarding protection of the drug from degradation in the stomach acid.

Vitamin E and poly(ε-caprolactone) were used to synthesize 100-200 nm rifampicin-loaded particles by flash nanoprecipitation. However, no drug release studies were done [186]. The rifampicin was conjugated covalently to an "anchoring" species, such as Vitamin E or a biodegradable and biocompatible hydrophobic polymer. This enabled incorporation of active compounds into nanoparticles. The hydrolytic cleavage of the linking group provides sustained release of the active agent [187]. There has been no other work published to our knowledge on preparation of polymer-loaded rifampicin nanoparticles using MIVM.

Pulmonary delivery studies

Anti-TB drugs encapsulated in nanoparticles were studied by pulmonary administration [181]. In guinea pigs, a single aerosol dose of rifampicin-encapsulated nanoparticles resulted in therapeutically useful levels in the circulation for 6-8 days. Pulmonary administration of five doses at 10 day intervals resulted in complete clearance of TB in the lung. Forty six oral doses of the free drug administered daily were required to obtain the same effect. Flexibility of the nanoparticle-based formulations was further demonstrated by effective subcutaneous treatment of mice infected with M. tuberculosis [180]. One subcutaneous dose of poly-(DL lactide-co-glycolide) PLGA nanoparticles containing rifampicin, isoniazid and pyrazinamide resulted in drug levels at therapeutically useful values for 32 and 36 days in the lungs and spleen, resulting in complete clearance of bacteria whereas treatment with the pure drug required 35 daily oral doses.

Cell studies

Anisimova et al. prepared rifampicin, isoniazid and streptomycin loaded PBCA (poly(N-butylcyanoacrylate)) and PIBCA (poly(isobutylcyanoacrylate)) nanoparticles and studied *in-vitro* cellular uptake in human blood monocytes in an effort to develop a drug depot system. The typical particle size was 250 nm. Accumulation of these drugs in human monocytes was studied, as well as their antimicrobial activity against *Mycobacterium tuberculosis* residing in human monocyte-derived macrophages. The nanoparticle formulation led to higher intracellular levels of the drugs and higher antimicrobial activity of isoniazid and streptomycin compared to their free drug analogs but not so for rifampin [175].

Oral delivery studies

Pandey et al. [182] developed sustained release rifampicin, as well as isoniazid and pyrazinamide loaded PLGA nanoparticles for oral delivery. The particles were made by the solvent emulsion technique in which the polymer and rifampicin were dissolved in a mixture of DCM/acetone, and then this solution was slowly poured into an aqueous solution of PVA that was stirred using a high-speed homogenizer. Stirring was continued for 3 hours to allow the evaporation of the internal phase. The NPs were then isolated by centrifuging followed by washing three times with deionized water. The suspension produced was freeze-dried for 48 hours to obtain a fine powder of NPs. This is not a rapid scalable method. The drug loading efficiency of the microparticles was 8-18% and the mean particle size was ~ 2 μm. In animal experiments, microparticles containing rifampicin showed higher therapeutic concentrations in plasma compared to free drug. However, these microparticles suffered from several drawbacks such as a low drug encapsulation, high polymer consumption, and a partial therapeutic benefit. Nanoparticles of size range 186-290 nm (PDI =0.38 ± 0.04) and drug loading efficiency

57-68% showed similar results when tested in guinea pigs with equivalent amount of drug (rifampicin 12 mg/kg + isoniazid 10 mg/kg + pyrazinamide 25 mg/kg body weight) [183]. Also sustained drug release could be achieved in the plasma (5–12 days) with the nanoparticles compared to the microparticles (3–4 days) of equivalent doses. At a 2/3rd therapeutic dosage of nanoparticles, the drug remained in the plasma (at therapeutically useful level, above MIC) for 7, 12 and 11 days for rifampicin, isoniazid and pyrazinamide respectively.

Zahroor et al. prepared alginate nanoparticles (235 nm diameter) of anti-TB drugs (rifampicin, isoniazid, pyrazinamide and ethambutol) using controlled cation-induced gelation of alginate. The drug loading efficiency for rifampicin was 80-90%. When the nanoparticles were administered orally to mice, ethambutol, rifampicin, isoniazid, and pyrazinamide levels were detected in plasma at therapeutic levels above the MIC (minimum inhibitory concentration) up to 7, 9, 11 and 11 days respectively (free drugs were cleared within 12 to 24 h from the blood but were detectable in tissues (e.g. spleen, liver and lung) for more than one day). The drug levels were detectable in tissues above the MIC (minimum inhibitory concentration) up to 15 days [184]. This work is notable in that may be the first detailed study showing that orally-administered nanoparticles can cross the GI-epithelium and enter the circulation in therapeutically useful levels.

Formulations that would reduce dosing frequency and side effects of rifampicin and that would enhance its bioavailability could be extremely valuable in treatment of this disease. Enhancing bioavailability would reduce dosage, cost, and possibly variability and side effects. There have been not many studies done where a polymer carrier was used to inhibit stomach degradation of the drug to increase its bioavailability.

2.6. Drug Delivery for Human Immunodeficiency Virus (HIV)

2.6.1. Human Immunodeficiency Virus – the disease

The Human Immunodeficiency Virus (HIV) affects the immune system, causing acquired immunodeficiency syndrome (AIDS) which results in life-threatening infections and diseases. Currently, more than 33 million people are HIV-positive[188]. Research has been conducted for 25 years regarding the development of prevention methods and treatment strategies. HIV mainly infects cells of the immune system and central nervous systems (CNS). In order to treat HIV, antiretroviral drugs have been developed to interrupt various stages of the HIV life cycle such as:

a) Reverse transcriptase inhibitors which act by blocking the activity of the reverse transcriptase enzyme, thus preventing the construction of viral DNA.
b) Nucleoside analog reverse transcriptase inhibitors, including zidovudine, lamivudine, and others which incorporate into the viral DNA
c) Nonnucleoside analog reverse transcriptase inhibitors, including etravirine, efavirenz, and others
d) Protease inhibitors including ritonavir, atazanavir, and others which inhibit the protease enzyme necessary for cleaving the viral proteins prior to final assembly into new viral particles.
e) Fusion inhibitors that block the fusion of the virus with the cell membrane which is necessary for entry into the cell.
f) Integrase inhibitors (i.e. raltegravir) which block the integration of viral DNA with cellular DNA.
g) Entry inhibitors that bind to CCR5, a receptor on the viral membrane surface used in entry into a cell.

2.6.2. HIV drugs in this study

Ritonavir and Efavirenz are two HIV drugs used in this study. Ritonavir (RTV, Figure 13a) is a selective, competitive and reversible inhibitor of the human immunodeficiency virus (HIV) protease enzyme. It is typically used in dual protease therapy in combination with other antiretroviral drugs such as atazanavir or lopinavir as a booster since it also inhibits the liver enzyme Cytochrome P450 (CYP3A)[189]. This enzymes is responsible for metabolizing a number of protease inhibitors and so inhibiting CYP3A increases their bioavailability. RTV has a low aqueous solubility of 1.2 µg/ml at pH 6.8 in comparison to its high dosage (10 mg/kg, or 600 mg for a 60 kg person). A relatively high dose of the drug is required to maintain therapeutic concentrations for longer periods, which may lead to several side effects (asthenia, malaise, diarrhea, nausea and vomiting, abdominal pain, dizziness, insomnia, sweating, taste abnormality). Its biological half-life varies from 3-5 hours.

The FDA approved drug efavirenz (Figure 13b) is a non-nucleoside reverse transcriptase inhibitor and is a first line drug of choice in Highly Active Anti-Retroviral Therapy (HAART) for treatment of HIV and AIDS. It is a poorly water soluble drug (8.85 µg/ml) with 40-45% bioavailability. Thus, it is typically administered at relatively high doses of 600-800 mg/day. Its biological half-life varies from 40-55 hours.

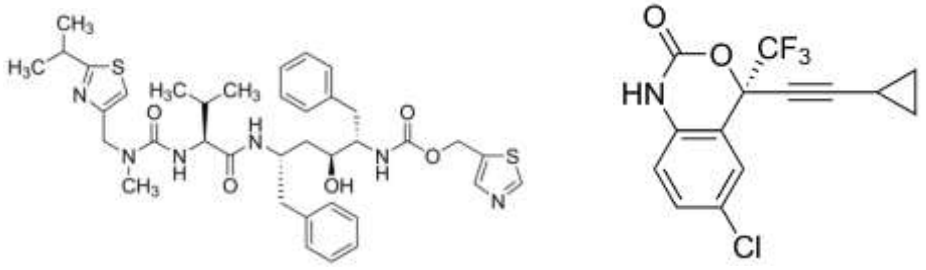

(a) (b)

Figure 13. (a) Structure of ritonavir (RTV)[3], (b) Structure of efavirenz (EFV)[3]

2.6.3. Polymer Nanoparticles in treatment of HIV

Using three or more drugs in combination is known as highly effective antiretroviral therapy (HAART) and is particularly effective in treating drug-resistant HIV strains [190]. HAART has been able to increase the life expectancy of infected individuals from less than one year to 10 years[191,192]. The therapy is limited by the development of multiple resistant strains, by viral reservoir sites that cannot be reached by drugs using current delivery methods, and toxicity as a result of the high and frequent dosing involved which can lead to reduced patient compliance. The high cost associated with HAART is also an important issue, especially in developing nations where HIV prevalence is high[192]. Higher bioavailability would lead to reduced dose which in turn would reduce cost and side effects and result in better compliance.

Drug delivery systems that can raise intracellular drug levels may help in preventing the virus from infecting the cells. Systems that can maintain therapeutic concentrations of the drug in the systemic circulation are useful for reducing the viral load. If systems could be developed that can cross the physiological barriers and deliver their payload to the viral sanctuary sites, such as the CNS, lymphatic system, and macrophages, the virus might ultimately be eradicated in infected individuals.

Examples of nanoparticle delivery systems include liposomes, solid lipid nanoparticles, polymeric nanoparticles, and dendrimers. Nanocarriers offer several advantages, such as the protection of drugs against degradation[193], targeting of drugs to specific sites of action [194], and delivery of biological molecules such as proteins[195], peptides [196], and oligonucleotides[197].
Several *in vitro* and *in vivo* studies are discussed in this section of the review. However, the work in this thesis concerns only *in vitro* studies as most of the polymers are not biodegradable in

plasma. Future studies will emphasize use of biodegradable polymeric nanoparticles and their in-vivo behavior.

The size and morphology of the polymer matrix plays an extremely important role in the drug release and pharmacokinetics. Polymer drug delivery systems must possess the appropriate morphology to produce the required drug release profile [198]. Recently, polymeric nanoparticles (NPs) have been extensively and intensively studied and are considered among the most promising drug delivery systems [199]. Nanoparticles have the ability to improve the half-life of the drug by controlling the release and protecting the loaded drug against degradation [200]. All of these benefits can contribute to the reduction of dose and dosing frequency, thereby reducing the side effects and improving the patient compliance [201]. The next section discusses some of the major studies done with microparticles and nanoparticles to enhance dissolution characteristics of poorly soluble antiviral drugs.

In-vitro studies

Microspheres of polymethacrylate containing ritonavir were prepared using a solvent evaporation method. The particles size of the spheres was 35-45 µm, whereas the drug-loading efficiency was almost 100 %. Drug release was up to 93.4% and release was extended up to 10 hours. The rate of drug release followed zero order kinetics [202].

Microparticles of antiviral drug, acyclovir were prepared for achieving sustained release using cellulose acetate propionate (CAP) and cellulose acetate butyrate (CAB). The particles were made by two different techniques, solvent evaporation-matrix erosion and spray drying. The particle size was between 5-20 µm and the encapsulation efficiency ranged between 50-90 %. The authors recommended spray drying for formulating acyclovir with CAB to obtain a controlled release dosage form with enhanced bioavailability and reduced dose frequency for

improved patient compliance [203]. Ethyl cellulose and Eudragit®RS100 (anionic copolymer based on methacrylic acid and methyl methacrylate) polymeric microspheres containing stavudine were prepared by oil-in-oil emulsion evaporation technique. The size of the particles ranged between 200-420 µm and the drug loading efficiency was between 85-90%. The *in vitro* release rate increased compared to that of the pure drug.

Several nanoparticle formulation systems like micelles, microspheres, liposomes, solid-lipid nanoparticles, dendrimers, cyclodextrins and emulsions are described by Lembo et al.[204]. Efavienz nanoparticles were formulated using methacrylate polymers with the trademark name Eudragit E100 by the solvent evaporation method. The particle sizes ranged from 99-200 nm and the drug loading efficiency ranged from 75-90 %. The in vitro release studies showed that 95-100 % of drug was released compared to 23-58% release of pure drug[205].

In another study, multiple emulsion-solvent evaporation procedure was used to produce nanoparticles of poly-(lactic-co-glycolic acid) (PLGA) containing ritonavir (RTV), lopinavir (LPV), and efavirenz (EFV)[206]. The average nanoparticle size was 262±84 nm and drug loading averaged 4% (w/v). The *in vitro* release of the drugs from nanoparticles using peripheral mononuclear cells (PBMC) was found to be at therapeutically interesting levels over 28 days while the free drug controls were eliminated by 2 days.

The solubility of ritonavir from Gelucire[3] (composed of mixture of glycerides and esters of polyethylene glycol) nanoparticles of 600-800 nm was studied at the ratio of ritonavir: gelucire 1:4 [207]. The in-vitro dissolution studies showed higher release of ritonavir compared to pure drug.

Ritonavir-loaded alginate nanoparticles were prepared by an in situ nano emulsion – polymer cross linking approach [208]. The ritonavir ratio was varied in the nanoparticle at alginate:

ritonavir ratios of 1:1, 1:2 and 1:3. Drug loading efficiencies as high as 92% were reported and the particle size was 77 ± 0.47 nm. Sustained drug release was observed for a period of 16 hours which was better than what was observed with the free drug.

Cellulose acetate butyrate (CAB) and poly(vinyl pyrrolidone) (PVP) polymers were used to make nanoparticles to enhance dissolution profile of an antiviral drug. The particle size was 322 - 434 nm and the drug loading efficiency was 50% - 70%. All the nanoparticles improved the physicochemical properties of the drug [209].

The control of drug release kinetics from the nanocarrier can be difficult. The drug diffuses out of smaller nanocarriers faster, resulting in burst effects, making it difficult to obtain sustained or controlled drug delivery over prolonged periods of time[186, 210]. The drug release kinetics can be improved by increasing the size of the nanocarriers, which results in higher drug loading and prolonged drug release with a lower burst effect[211,211b]. However, larger particle size may hinder their transport across membranes. A significant challenge for nanocarrier drug delivery is the optimization of particle size with desired release characteristics.

The studies above did not conclusively show decrease of crystallinity of RTV, EFV or other HIV drugs for enhancement of solubility. Amorphous solid dispersions (discussed in section 2.3) have demonstrated potential for enhancing solubility and bioavailability of poorly soluble HIV drugs. However, there is a lack of understanding about the structure-property relationship of polymer-drug nanoparticles and crystallization effect on drug solubility. There is also limited literature available on rapid synthesis of nanoparticles with desired properties. This thesis addresses the issues of rapid synthesis of amorphous solid dispersions in the form of nanoparticles and the development of structure-property relationships that affect drug crystallization and its effect on drug solubility.

2.7 References

1. Lavelle, E. C.; Sharif, S.; Thomas, N. W.; Holland, J.; Davis, S. S., The importance of gastrointestinal uptake of particles in the design of oral delivery systems. *Advanced Drug Delivery Reviews* **1995,** *18* (1), 5-22.

2. Lipinski, C. A.; Lombardo, F.; Dominy, B. W.; Feeney, P. J., Experimental and computational approaches to estimate solubility and permeability in drug discovery and development settings. *Advanced Drug Delivery Reviews* **1997,** *23* (1–3), 3-25.

3. Gastroenterology consultants of greater cinncinnati, Your digestive system and how it works **2006**, https://ssl.gcis.net/giconsults/gi-tract.htm.

4. Franz Gabor, C. F., Lukas Neutsch, Improving Oral Delivery. In *Drug Delivery - Principle and Applications*, Wiley, Ed. 2005; pp 345-397.

5. Guidance for Industry, CDER, FDA, Bioavailability and Bioequivalence Studies for Orally Administered Drug Products—General Considerations. *21CFR320.1 Code of Federal Regulations* **1999,** *5* (21), 300-499.

6. Gibaldi, M. P., D. , In *In Pharmacokinetics*,, 2nd ed.; Dekker: **1982**; pp 145.

7. Rowland, M. T., T. , In *In Clinical Pharmacokinetics*, 3rd ed.; &, W.; Wilkins, Eds. **1995**; pp 34.

8. Anna Maria, C. a. T. J. S., Physiological, Biochemical and Chemical Barriers to Oral Drug Delivery. In *Drug Delivery- Principles and Applications*, Wiley: **2005**; pp 345-397.

9. Daugherty, A. L.; Mrsny, R. J., Regulation of the intestinal epithelial paracellular barrier. *Pharmaceutical Science & Technology Today* **1999,** *2* (7), 281-287.

10. Gaucher, G.; Satturwar, P.; Jones, M.-C.; Furtos, A.; Leroux, J.-C., Polymeric micelles for oral drug delivery. *European Journal of Pharmaceutics and Biopharmaceutics* **2010,** *76* (2), 147-158.

11. Srivastava, K., Arora, A., Kataria, A., Cappelleri, C,J., Sadosky, A., Peterson, M, A.,, Impact of reducing dosing frequency on adherence to oral therapies: a literature review and meta-analysis. *Patient Preference and Adherence* **2013,** *7*, 419-434.

12. Thomas, E.; Rubino, J., Solubility, melting point and salting-out relationships in a group of secondary amine hydrochloride salts. *International Journal of Pharmaceutics* **1996,** *130* (2), 179-185.

13. Kimura, K.; Hirayama, F.; Uekama, K., Characterization of tolbutamide polymorphs (burger's forms II and IV) and polymorphic transition behavior. *Journal of Pharmaceutical Sciences* **1999,** *88* (4), 385-391.

14. Yoshioka, M.; Hancock, B. C.; Zografi, G., Crystallization of indomethacin from the amorphous state below and above its glass transition temperature. *Journal of Pharmaceutical Sciences* **1994,** *83* (12), 1700-1705.

15. Kesisoglou, F.; Panmai, S.; Wu, Y., Nanosizing — Oral formulation development and biopharmaceutical evaluation. *Advanced Drug Delivery Reviews* **2007,** *59* (7), 631-644.

16. Borm, W. H. D. J. P. J., Drug delivery and nanoparticles: Applications and hazards. *Int J Nanomedicine* **2008,** *3* (2), 133-149.

17. Asghar, L. F. A.; Chandran, S., *Multiparticulate formulation approach to colon specific drug delivery: current perspectives*. **2006**, 9, 327-38.

18. Keck, C. M.; Müller, R. H., Drug nanocrystals of poorly soluble drugs produced by high pressure homogenisation. *European Journal of Pharmaceutics and Biopharmaceutics* **2006,** *62* (1), 3-16.

19. Liversidge, G. G.; Cundy, K. C., Particle size reduction for improvement of oral bioavailability of hydrophobic drugs: I. Absolute oral bioavailability of nanocrystalline danazol in beagle dogs. *International Journal of Pharmaceutics* **1995,** *125* (1), 91-97.

20. (a) Müller, R. H.; Jacobs, C.; Kayser, O., Nanosuspensions as particulate drug formulations in therapy: Rationale for development and what we can expect for the future. *Advanced Drug Delivery Reviews* 2001, *47* (1), 3-19; (b) Horn, D.; Rieger, J., Organic Nanoparticles in the Aqueous Phase—Theory, Experiment, and Use. *Angewandte Chemie International Edition* 2001, *40* (23), 4330-4361; (c) Wu, Y.; Loper, A.; Landis, E.; Hettrick, L.; Novak, L.; Lynn, K.; Chen, C.; Thompson, K.; Higgins, R.; Batra, U.; Shelukar, S.; Kwei, G.; Storey, D., The role of biopharmaceutics in the development of a clinical nanoparticle formulation of MK-0869: a Beagle dog model predicts improved bioavailability and diminished food effect on absorption in human. *International Journal of Pharmaceutics* 2004, *285* (1–2), 135-146; (d) Langguth, P.; Hanafy, A.; Frenzel, D.; Grenier, P.; Nhamias, A.; Ohlig, T.; Vergnault, G.; Spahn-Langguth, H., Nanosuspension Formulations for Low-Soluble Drugs: Pharmacokinetic Evaluation Using Spironolactone as Model Compound. *Drug Development and Industrial Pharmacy* 2005, *31* (3), 319-329; (e) Jinno, J.-I.; Kamada, N.; Miyake, M.; Yamada, K.; Mukai, T.; Odomi, M.; Toguchi,

H.; Liversidge, G. G.; Higaki, K.; Kimura, T., Effect of particle size reduction on dissolution and oral absorption of a poorly water-soluble drug, cilostazol, in beagle dogs. *Journal of Controlled Release* 2006, *111* (1-2), 56-64.

21. R.B. Bird, E. L., W.E. Stewart, *Transport Phenomena*. 1st ed.; Wiley & Sons: **1960**.

22. Moustafine, R. I.; Kabanova, T. V.; Kemenova, V. A.; Van Den Mooter, G., Characteristics of interpolyelectrolyte complexes of Eudragit E100 with Eudragit L100. *Journal of Controlled Release* **2005,** *103* (1), 191-198.

23. (a) Posey-Dowty, J.; Watterson, T.; Wilson, A.; Edgar, K.; Shelton, M.; Lingerfelt, L., Zero-order release formulations using a novel cellulose ester. *Cellulose* **2007,** *14* (1), 73-83-83; (b) Lorenzo-Lamosa, M. L.; Remuñán-López, C.; Vila-Jato, J. L.; Alonso, M. J., Design of microencapsulated chitosan microspheres for colonic drug delivery. *Journal of Controlled Release* **1998,** *52* (1–2), 109-118.

24. Kohane, D. S., Microparticles and Nanoparticles for Drug Delivery. *Biotechnology and Bioengineering* **2006,** *96* (2), 203-209.

25. Kohane, D. S., Microparticles and nanoparticles for drug delivery. *Biotechnology and Bioengineering* **2007,** *96* (2), 203-209.

26. Rabinow, B. E., Nanosuspensions in drug delivery. *Nature Reviews Drug Discovery* **2004,** *3*, 785-796.

27. Merisko-Liversidge, E.; Liversidge, G. G., Nanosizing for oral and parenteral drug delivery: A perspective on formulating poorly-water soluble compounds using wet media milling technology. *Advanced Drug Delivery Reviews* **2011,** *63* (6), 427-440.

28. (a) Nykamp, G.; Carstensen, U.; Müller, B. W., Jet milling—a new technique for microparticle preparation. *International Journal of Pharmaceutics* **2002,** *242* (1–2), 79-86; (b) Rasenack, N.; Müller, B., Dissolution Rate Enhancement by in Situ Micronization of Poorly Water-Soluble Drugs. *Pharmaceutical Research* **2002,** *19* (12), 1894-1900.

29. Rh, J. J. a. M., Nanocrystal technology, drug delivery and clinical applications. *Int J Nanomedicine* **2008,** *3*, 295-309.

30. Merisko-Liversidge, E. M.; Liversidge, G. G., Drug Nanoparticles: Formulating Poorly Water-Soluble Compounds. *Toxicologic Pathology* **2008,** *36* (1), 43-48.

31. Williams, H. D.; Trevaskis, N. L.; Charman, S. A.; Shanker, R. M.; Charman, W. N.; Pouton, C. W.; Porter, C. J. H., Strategies to Address Low Drug Solubility in Discovery and Development. *Pharmacological Reviews* **2013,** *65* (1), 315-499.

32. Wu, L.; Zhang, J.; Watanabe, W., Physical and chemical stability of drug nanoparticles. *Advanced Drug Delivery Reviews* **2011,** *63* (6), 456-469.

33. Vogt, M.; Kunath, K.; Dressman, J. B., Dissolution enhancement of fenofibrate by micronization, cogrinding and spray-drying: Comparison with commercial preparations. *European Journal of Pharmaceutics and Biopharmaceutics* **2008,** *68* (2), 283-288.

34. Hargrove Jt, M. W., And Wentz Ac, Absorption of oral progesterone is influenced by vehicle and particle size. *Am J Obstet Gynecol* **1989,** *161*, 948-951.

35. J, N. F. a. R., Dependence of area under the curve on proquazone particle size and in vitro dissolution rate. *J Pharm Sci* **1980,** *69*, 605-607.

36. Watari, N.; Funaki, T.; Aizawa, K.; Kaneniwa, N., Nonlinear assessment of nitrofurantoin bioavailability in rabbits. *Journal of Pharmacokinetics and Biopharmaceutics* **1983,** *11* (5), 529-545.

37. Gao, P., Amorphous pharmaceutical solids: Characterization, stabilization, and development of marketable formulations of poorly soluble drugs with improved oral absorption. *Molecular Pharmaceutics* **2008,** *5* (6), 903-904.

38. Poste, G.; Papahadjopoulos, D.; Vail, W. J.; David, M. P., Chapter 4 Lipid vesicles as carriers for introducing biologically active materials into cells. In *Methods in Cell Biology*, Academic Press: **1976,** 14, pp 33-71.

39. Chen, T.; Shukoor, M. I.; Wang, R.; Zhao, Z.; Yuan, Q.; Bamrungsap, S.; Xiong, X.; Tan, W., Smart multifunctional nanostructure for targeted cancer chemotherapy and magnetic resonance imaging. *ACS Nano* **2011,** *5* (10), 7866-7873.

40. Li, Y. Y.; Chen, X. G.; Zhang, J.; Liu, C. S.; Xue, Y. P.; Sun, G. Z.; Zhang, W. F., In vitro release of rifampicin and biocompatibility of oleoylchitosan nanoparticles. *Journal of Applied Polymer Science* **2009,** *111* (5), 2269-2274.

41. Sung, J.; Padilla, D.; Garcia-Contreras, L.; Verberkmoes, J.; Durbin, D.; Peloquin, C.; Elbert, K.; Hickey, A.; Edwards, D., Formulation and pharmacokinetics of self-assembled rifampicin nanoparticle systems for pulmonary delivery. *Pharmaceutical Research* **2009,** *26* (8), 1847-1855.

42. Merisko-Liversidge, E.; Liversidge, G. G.; Cooper, E. R., Nanosizing: a formulation approach for poorly-water-soluble compounds. *European Journal of Pharmaceutical Sciences* **2003,** *18* (2), 113-120.

43. Christopher A, L., Drug-like properties and the causes of poor solubility and poor permeability. *Journal of Pharmacological and Toxicological Methods* **2000,** *44* (1), 235-249.

44. (a) Lipinski, C., Poor aqueous solubility: an industry wide problem in drug discovery. *Am Pharm Rev 5* **2002,** *5*, 82; (b) Lipper, R. A., E pluribus product. *Modern Drug Discovery* **1999**, 55-60.

45. Noyes, A. A.; Whitney, W. R., The rate of solution of solid substances in their own solutions. *Journal of the American Chemical Society* **1897,** *19* (12), 930-934.

46. Van Eerdenbrugh, B.; Vermant, J.; Martens, J. A.; Froyen, L.; Humbeeck, J. V.; Van Den Mooter, G.; Augustijns, P., Solubility Increases Associated with Crystalline Drug Nanoparticles: Methodologies and Significance. *Molecular Pharmaceutics* **2010,** *7* (5), 1858-1870.

47. Sun, W.; Mao, S.; Shi, Y.; Li, L. C.; Fang, L., Nanonization of itraconazole by high pressure homogenization: Stabilizer optimization and effect of particle size on oral absorption. *Journal of Pharmaceutical Sciences* **2011,** *100* (8), 3365-3373.

48. Bawarski,W.E.;Chidlowsky,E.; Bharali, D. J.; Mousa, S. A., Emerging nanopharmaceuticals. *Nanomedicine: Nanotechnology, Biology and Medicine* **2008,** *4* (4), 273-282.

49. Kumari, A.; Yadav, S. K.; Yadav, S. C., Biodegradable polymeric nanoparticles based drug delivery systems. *Colloids and Surfaces B: Biointerfaces* **2010,** *75* (1), 1-18.

50. Hillaireau, H.; Couvreur, P., Nanocarriers' entry into the cell: relevance to drug delivery. *Cellular and Molecular Life Sciences* **2009,** *66* (17), 2873-2896.

51. Prego, C.; Torres, D.; Fernandez-Megia, E.; Novoa-Carballal, R.; Quiñoá, E.; Alonso, M. J., Chitosan–PEG nanocapsules as new carriers for oral peptide delivery: Effect of chitosan pegylation degree. *Journal of Controlled Release* **2006,** *111* (3), 299-308.

52. W.H.D. Jong, P. J. B., Drug delivery and nanoparticles: Applications and hazards. *International Journal of Nanomedicine* **2008** *3*(2), 133-149.

53. (a) Sekiguchi K.; Obi N.; Ueda Y., Studies on absorption of eutectic mixture. II. Absorption of fused conglomerates of chloramphenicol and urea in rabbits. *Chem Pharm Bull (Tokyo)* **1961,** *12*, 134-144; (b) Hancock, B. C.; Zografi, G., Characteristics and significance of the amorphous state in pharmaceutical systems. *Journal of Pharmaceutical Sciences* **1997,** *86* (1), 1-12.

54. Serajuddin, A. T. M., Solid dispersion of poorly water-soluble drugs: Early promises, subsequent problems, and recent breakthroughs. *Journal of Pharmaceutical Sciences* **1999,** *88* (10), 1058-1066.

55. Leuner, C.; Dressman, J., Improving drug solubility for oral delivery using solid dispersions. *European Journal of Pharmaceutics and Biopharmaceutics* **2000,** *50* (1), 47-60.

56. Newman, A.; Knipp, G.; Zografi, G., Assessing the performance of amorphous solid dispersions. *Journal of Pharmaceutical Sciences* **2012,** *101* (4), 1355-1377.

57. Gao, Y.; Carr, R. A.; Spence, J. K.; Wang, W. W.; Turner, T. M.; Lipari, J. M.; Miller, J. M., A pH-dilution method for estimation of biorelevant drug solubility along the gastrointestinal tract: Application to physiologically based pharmacokinetic modeling. *Molecular Pharmaceutics* **2010,** *7* (5), 1516-1526.

58. Law, D.; Schmitt, E. A.; Marsh, K. C.; Everitt, E. A.; Wang, W.; Fort, J. J.; Krill, S. L.; Qiu, Y., Ritonavir–PEG 8000 amorphous solid dispersions: In vitro and in vivo evaluations. *Journal of Pharmaceutical Sciences* **2004,** *93* (3), 563-570.

59. Kennedy, M.; Hu, J.; Gao, P.; Li, L.; Ali-Reynolds, A.; Chal, B.; Gupta, V.; Ma, C.; Mahajan, N.; Akrami, A.; Surapaneni, S., Enhanced bioavailability of a poorly soluble VR1 antagonist using an amorphous solid dispersion approach: A case study. *Molecular Pharmaceutics* **2008,** *5* (6), 981-993.

60. Van Eerdenbrugh, B.; Van Speybroeck, M.; Mols, R.; Houthoofd, K.; Martens, J. A.; Froyen, L.; Van Humbeeck, J.; Augustijns, P.; Van Den Mooter, G., Itraconazole/TPGS/Aerosil®200 solid dispersions: Characterization, physical stability and in vivo performance. *European Journal of Pharmaceutical Sciences* **2009,** *38* (3), 270-278.

61. Li, S.; Liu, Y.; Liu, T.; Zhao, L.; Zhao, J.; Feng, N., Development and in-vivo assessment of the bioavailability of oridonin solid dispersions by the gas anti-solvent technique. *International Journal of Pharmaceutics* **2011,** *411* (1–2), 172-177.

62. Mellaerts, R.; Mols, R.; Jammaer, J. a. G.; Aerts, C. A.; Annaert, P.; Van Humbeeck, J.; Van Den Mooter, G.; Augustijns, P.; Martens, J. A., Increasing the oral bioavailability of the poorly water soluble drug itraconazole with ordered mesoporous silica. *European Journal of Pharmaceutics and Biopharmaceutics* **2008,** *69* (1), 223-230.

63. Bauer, J.; Spanton, S.; Henry, R.; Quick, J.; Dziki, W.; Porter, W.; Morris, J., Ritonavir: An Extraordinary Example of Conformational Polymorphism. *Pharmaceutical Research* **2001,** *18* (6), 859-866.

64. Yoshioka, M.; Hancock, B. C.; Zografi, G., Inhibition of indomethacin crystallization in poly(vinylpyrrolidone) coprecipitates. *Journal of Pharmaceutical Sciences* **1995,** *84* (8), 983-986.

65. Van Den Mooter, G.; Augustijns, P.; Blaton, N.; Kinget, R., Physico-chemical characterization of solid dispersions of temazepam with polyethylene glycol 6000 and PVP K30. *International Journal of Pharmaceutics* **1998,** *164* (1–2), 67-80.

66. Matsumoto, T.; Zografi, G., Physical properties of solid molecular dispersions of indomethacin with poly(vinylpyrrolidone) and poly(vinylpyrrolidone-co-vinyl-acetate) in relation to indomethacin crystallization. *Pharmaceutical Research* **1999,** *16* (11), 1722-1728.

67. Shamblin, S. L.; Hancock, B. C.; Dupuis, Y.; Pikal, M. J., Interpretation of relaxation time constants for amorphous pharmaceutical systems. *Journal of Pharmaceutical Sciences* **2000,** *89* (3), 417-427.

68. Six, K.; Verreck, G.; Peeters, J.; Brewster, M.; Mooter, G. V. D., Increased physical stability and improved dissolution properties of itraconazole, a class II drug, by solid dispersions that combine fast- and slow-dissolving polymers. *Journal of Pharmaceutical Sciences* **2004,** *93* (1), 124-131.

69. Vasanthavada, M.; Tong, W.-Q.; Joshi, Y.; Kislalioglu, M. S., Phase behavior of amorphous molecular dispersions ii: role of hydrogen bonding in solid solubility and phase separation kinetics. *Pharmaceutical Research* **2005,** *22* (3), 440-448.

70. Konno, H.; Taylor, L. S., Influence of different polymers on the crystallization tendency of molecularly dispersed amorphous felodipine. *Journal of Pharmaceutical Sciences* **2006,** *95* (12), 2692-2705.

71. Lindfors, L.; Forssén, S.; Westergren, J.; Olsson, U., Nucleation and crystal growth in supersaturated solutions of a model drug. *Journal of Colloid and Interface Science* **2008,** *325* (2), 404-413.

72. Marsac, P.; Konno, H.; Rumondor, A. F.; Taylor, L., Recrystallization of nifedipine and felodipine from amorphous molecular level solid dispersions containing poly(vinylpyrrolidone) and sorbed water. *Pharmaceutical Research* **2008,** *25* (3), 647-656.

73. Caron, V.; Bhugra, C.; Pikal, M. J., Prediction of onset of crystallization in amorphous pharmaceutical systems: Phenobarbital, nifedipine/PVP, and phenobarbital/PVP. *Journal of Pharmaceutical Sciences* **2010,** *99* (9), 3887-3900.

74. Marsac, P.; Li, T.; Taylor, L., Estimation of Drug–Polymer Miscibility and Solubility in Amorphous Solid Dispersions Using Experimentally Determined Interaction Parameters. *Pharmaceutical Research* **2009,** *26* (1), 139-151.

75. Qian, F.; Huang, J.; Hussain, M. A., Drug–polymer solubility and miscibility: Stability consideration and practical challenges in amorphous solid dispersion development. *Journal of Pharmaceutical Sciences* **2010,** *99* (7), 2941-2947.

76. Hancock, B. C.; Parks, M., What is the True Solubility Advantage for Amorphous Pharmaceuticals? *Pharmaceutical Research* **2000,** *17* (4), 397-404.

77. Florence, A. T., Atwood, D., *Physicochemical Principles of Pharmacy*. 3rd ed ed.; MacMillan Press: London., **1998**.

78. (a) GinãS, J. M.; Arias, M. J.; Moyano, J. R.; Sãnchez-Soto, P. J., Thermal investigation of crystallization of polyethylene glycols in solid dispersions containing oxazepam. *International Journal of Pharmaceutics* **1996,** *143* (2), 247-253; (b) Marsac, P.; Konno, H.; Rumondor, A.; Taylor, L., Recrystallization of Nifedipine and Felodipine from Amorphous Molecular Level Solid Dispersions Containing Poly(vinylpyrrolidone) and Sorbed Water. *Pharmaceutical Research* **2008,** *25* (3), 647-656.

79. Shelton Michael, C.; Posey-Dowty Jessica, D.; Lingerfelt, L.; Kirk Shane, K.; Klein, S.; Edgar Kevin, J., Enhanced dissolution of poorly soluble drugs from solid dispersions in carboxymethylcellulose acetate butyrate matrices. In *Polysaccharide Materials: Performance by Design*, *American Chemical Society*: **2009,** 1017, 93-113.

80. Rowe R.C., S., P.J., and Quinn M.E.,, *Handbook of Pharmaceutical Excipients,*. 6 ed.; Pharmaceutical Press, **2009**.

81. Tanno, F.; Nishiyama, Y.; Kokubo, H.; Obara, S., Evaluation of hypromellose acetate succinate (HPMCAS) as a carrier in solid dispersions. *Drug Development and Industrial Pharmacy* **2004,** *30* (1), 9-17.

82. Friesen, D. T.; Shanker, R.; Crew, M.; Smithey, D. T.; Curatolo, W. J.; Nightingale, J. A. S., Hydroxypropyl methylcellulose acetate succinate-based spray-dried dispersions: An overview. *Molecular Pharmaceutics* **2008,** *5* (6), 1003-1019.

83. Brouwers, J.; Brewster, M. E.; Augustijns, P., Supersaturating drug delivery systems: The answer to solubility-limited oral bioavailability? *Journal of Pharmaceutical Sciences* **2009,** *98* (8), 2549-2572.

84. Craig, D. Q. M., The mechanisms of drug release from solid dispersions in water-soluble polymers. *International Journal of Pharmaceutics* **2002,** *231* (2), 131-144.

85. Alonzo, D. E.; Gao, Y.; Zhou, D.; Mo, H.; Zhang, G. G. Z.; Taylor, L. S., Dissolution and precipitation behavior of amorphous solid dispersions. *Journal of Pharmaceutical Sciences* **2011,** *100* (8), 3316-3331.

86. Kanaujia, P.; Lau, G.; Ng, W. K.; Widjaja, E.; Hanefeld, A.; Fischbach, M.; Maio, M.; Tan, R. B. H., Nanoparticle formation and growth during in vitro dissolution of ketoconazole solid dispersion. *Journal of Pharmaceutical Sciences* **2011,** *100* (7), 2876-2885.

87. Verheyen, S.; Blaton, N.; Kinget, R.; Van Den Mooter, G., Mechanism of increased dissolution of diazepam and temazepam from polyethylene glycol 6000 solid dispersions. *International Journal of Pharmaceutics* **2002,** *249* (1–2), 45-58.

88. Valizadeh, H.; Nokhodchi, A.; Qarakhani, N.; Zakeri-Milani, P.; Azarmi, S.; Hassanzadeh, D.; Löbenberg, R., Physicochemical characterization of solid dispersions of indomethacin with PEG 6000, Myrj 52, Lactose, Sorbitol, Dextrin, and Eudragit® E100. *Drug Development and Industrial Pharmacy* **2004,** *30* (3), 303-317.

89. Baird, J. A.; Taylor, L. S., Evaluation and modeling of the eutectic composition of various drug-polyethylene glycol solid dispersions. *Pharmaceutical Development and Technology* **2011,** *16* (3), 201-211.

90. Save, T.; Venkitachalam, P., Studies on solid dispersions of nifedipine. *Drug Development and Industrial Pharmacy* **1992,** *18* (15), 1663-1679.

91. Hancock, B.; Parks, M., What is the True Solubility Advantage for Amorphous Pharmaceuticals? *Pharmaceutical Research* **2000,** *17* (4), 397-404.

92. Murdande, S. B.; Pikal, M. J.; Shanker, R. M.; Bogner, R. H., Aqueous solubility of crystalline and amorphous drugs: Challenges in measurement. *Pharmaceutical Development and Technology* **2011,** *16* (3), 187-200.

93. Murdande, S. B.; Pikal, M. J.; Shanker, R. M.; Bogner, R. H., Solubility advantage of amorphous pharmaceuticals: I. A thermodynamic analysis. *Journal of Pharmaceutical Sciences* **2010,** *99* (3), 1254-1264.

94. Bhugra, C.; Pikal, M. J., Role of thermodynamic, molecular, and kinetic factors in crystallization from the amorphous state. *Journal of Pharmaceutical Sciences* **2008,** *97* (4), 1329-1349.

95. Murdande, S.; Pikal, M.; Shanker, R.; Bogner, R., Solubility advantage of amorphous pharmaceuticals: II. Application of quantitative thermodynamic relationships for prediction of solubility enhancement in structurally diverse insoluble pharmaceuticals. *Pharmaceutical Research* **2010,** *27* (12), 2704-2714.

96. Vandecruys, R.; Peeters, J.; Verreck, G.; Brewster, M. E., Use of a screening method to determine excipients which optimize the extent and stability of supersaturated drug solutions and application of this system to solid formulation design. *International Journal of Pharmaceutics* **2007,** *342* (1–2), 168-175.

97. (a) Warren, D. B.; Benameur, H.; Porter, C. J. H.; Pouton, C. W., Using polymeric precipitation inhibitors to improve the absorption of poorly water-soluble drugs: A mechanistic basis for utility. *Journal of Drug Targeting* **2010,** *18* (10), 704-731; (b) Guzmán, H. R.; Tawa, M.; Zhang, Z.; Ratanabanangkoon, P.; Shaw, P.; Gardner, C. R.; Chen, H.; Moreau, J.-P.; Almarsson, Ö.; Remenar, J. F., Combined use of crystalline salt forms and precipitation inhibitors to improve oral absorption of celecoxib from solid oral formulations. *Journal of Pharmaceutical Sciences* **2007,** *96* (10), 2686-2702.

98. Yamashita, K.; Nakate, T.; Okimoto, K.; Ohike, A.; Tokunaga, Y.; Ibuki, R.; Higaki, K.; Kimura, T., Establishment of new preparation method for solid dispersion formulation of tacrolimus. *International Journal of Pharmaceutics* **2003,** *267* (1–2), 79-91.

99. Augustijns, P.; Brewster, M. E., Supersaturating drug delivery systems: Fast is not necessarily good enough. *Journal of Pharmaceutical Sciences* **2012,** *101* (1), 7-9.

100. Six, K.; Daems, T.; De Hoon, J.; Van Hecken, A.; Depre, M.; Bouche, M.-P.; Prinsen, P.; Verreck, G.; Peeters, J.; Brewster, M. E.; Van Den Mooter, G., Clinical study of solid dispersions of itraconazole prepared by hot-stage extrusion. *European Journal of Pharmaceutical Sciences* **2005,** *24* (2–3), 179-186.

101. Konno, H.; Handa, T.; Alonzo, D. E.; Taylor, L. S., Effect of polymer type on the dissolution profile of amorphous solid dispersions containing felodipine. *European Journal of Pharmaceutics and Biopharmaceutics* **2008,** *70* (2), 493-499.

102. Curatolo, W.; Nightingale, J.; Herbig, S., Utility of hydroxypropylmethylcellulose acetate succinate (HPMCAS) for initiation and maintenance of drug supersaturation in the GI milieu. *Pharmaceutical Research* **2009,** *26* (6), 1419-1431.

103. Gebauer, D.; Völkel, A.; Cölfen, H., Stable prenucleation calcium carbonate clusters. *Science* **2008,** *322* (5909), 1819-1822.

104. Miller, D. A.; Dinunzio, J. C.; Yang, W.; Mcginity, J. W.; Williams, R. O., Enhanced in vivo absorption of itraconazole via stabilization of supersaturation following acidic-to-neutral ph transition. *Drug Development and Industrial Pharmacy* **2008,** *34* (8), 890-902.

105. Yokoi, Y.; Yonemochi, E.; Terada, K., Effects of sugar ester and hydroxypropyl methylcellulose on the physicochemical stability of amorphous cefditoren pivoxil in aqueous suspension. *International Journal of Pharmaceutics* **2005,** *290* (1–2), 91-99.

106. Gao, F.; Zhang, Z.; Bu, H.; Huang, Y.; Gao, Z.; Shen, J.; Zhao, C.; Li, Y., Nanoemulsion improves the oral absorption of candesartan cilexetil in rats: Performance and mechanism. *Journal of Controlled Release* **2011,** *149* (2), 168-174.

107. Brewster, M. E.; Vandecruys, R.; Peeters, J.; Neeskens, P.; Verreck, G.; Loftsson, T., Comparative interaction of 2-hydroxypropyl-β-cyclodextrin and sulfobutylether-β-cyclodextrin with itraconazole: Phase-solubility behavior and stabilization of supersaturated drug solutions. *European Journal of Pharmaceutical Sciences* **2008,** *34* (2–3), 94-103.

108. Gebauer, D.; Cölfen, H., Prenucleation clusters and non-classical nucleation. *Nano Today* **2011,** *6* (6), 564-584.

109. Linn, M.; Collnot, E.-M.; Djuric, D.; Hempel, K.; Fabian, E.; Kolter, K.; Lehr, C.-M., Soluplus® as an effective absorption enhancer of poorly soluble drugs in vitro and in vivo. *European Journal of Pharmaceutical Sciences* **2012,** *45* (3), 336-343.

110. (a) Breitenbach, J., Melt extrusion: from process to drug delivery technology. *European Journal of Pharmaceutics and Biopharmaceutics* **2002,** *54* (2), 107-117; (b) Lei Gao, D. Z., Minghui Chen, Drug nanocrystals for the formulation of poorly soluble
drugs and its application as a potential drug delivery system. *J Nanopart Res* **2008,** *10*, 845-862.

111. Dinunzio, J. C.; Brough, C.; Miller, D. A.; Williams, R. O.; Mcginity, J. W., Fusion processing of itraconazole solid dispersions by kinetisol® dispersing: A comparative study to hot melt extrusion. *Journal of Pharmaceutical Sciences* **2010,** *99* (3), 1239-1253.

112. Esnaashari, S.; Javadzadeh, Y.; Batchelor, H. K.; Conway, B. R., The use of microviscometry to study polymer dissolution from solid dispersion drug delivery systems. *International Journal of Pharmaceutics* **2005,** *292* (1–2), 227-230.

113. Janssens, S.; Van Den Mooter, G., Review: physical chemistry of solid dispersions. *Journal of Pharmacy and Pharmacology* **2009,** *61* (12), 1571-1586.

114. Six, K.; Berghmans, H.; Leuner, C.; Dressman, J.; Van Werde, K.; Mullens, J.; Benoist, L.; Thimon, M.; Meublat, L.; Verreck, G.; Peeters, J.; Brewster, M.; Van Den Mooter, G., Characterization of solid dispersions of itraconazole and hydroxypropylmethylcellulose prepared by melt extrusion, Part II. *Pharmaceutical Research* **2003,** *20* (7), 1047-1054.

115. Kapsi, S. G.; Ayres, J. W., Processing factors in development of solid solution formulation of itraconazole for enhancement of drug dissolution and bioavailability. *International Journal of Pharmaceutics* **2001,** *229* (1–2), 193-203.

116. Janssens, S.; Nagels, S.; Armas, H. N. D.; D'autry, W.; Van Schepdael, A.; Van Den Mooter, G., Formulation and characterization of ternary solid dispersions made up of Itraconazole and two excipients, TPGS 1000 and PVPVA 64, that were selected based on a supersaturation screening study. *European Journal of Pharmaceutics and Biopharmaceutics* **2008,** *69* (1), 158-166.

117. Lakshman, J. P.; Cao, Y.; Kowalski, J.; Serajuddin, A. T. M., Application of melt extrusion in the development of a physically and chemically stable high-energy amorphous solid dispersion of a poorly water-soluble drug. *Molecular Pharmaceutics* **2008,** *5* (6), 994-1002.

118. Abu-Diak, O. A.; Jones, D. S.; Andrews, G. P., An investigation into the dissolution properties of celecoxib melt extrudates: understanding the role of polymer type and concentration in stabilizing supersaturated drug concentrations. *Molecular Pharmaceutics* **2011,** *8* (4), 1362-1371.

119. (a) Dontireddy, R.; Crean, A. M., A comparative study of spray-dried and freeze-dried hydrocortisone/polyvinyl pyrrolidone solid dispersions. *Drug Development and Industrial Pharmacy* **2011,** *37* (10), 1141-1149; (b) Ghosh, I.; Snyder, J.; Vippagunta, R.; Alvine, M.; Vakil, R.; Tong, W.-Q.; Vippagunta, S., Comparison of HPMC based polymers performance as carriers for manufacture of solid dispersions using the melt extruder. *International Journal of Pharmaceutics* **2011,** *419* (1–2), 12-19.

120. Higuchi, W. I.; Mir, N. A.; Desai, S. J., Dissolution rates of polyphase mixtures. *Journal of Pharmaceutical Sciences* **1965,** *54* (10), 1405-1410.

121. Padden B, M. J., Robbins T, Zocharski Pd, Prasad L, Spence Jk, Lafountaine J, Amorphous solid dispersions as enabling formulations for discovery and early development. *Am Pharm Rev* **2011,** *1*, 66-73.

122. Van Den Mooter, G.; Wuyts, M.; Blaton, N.; Busson, R.; Grobet, P.; Augustijns, P.; Kinget, R., Physical stabilisation of amorphous ketoconazole in solid dispersions with polyvinylpyrrolidone K25. *European Journal of Pharmaceutical Sciences* **2001,** *12* (3), 261-269.

123. Karavas, E.; Ktistis, G.; Xenakis, A.; Georgarakis, E., Miscibility behavior and formation mechanism of stabilized felodipine-polyvinylpyrrolidone amorphous solid dispersions. *Drug Development and Industrial Pharmacy* **2005,** *31* (6), 473-489.

124. Hancock, B.; Shamblin, S.; Zografi, G., Molecular mobility of amorphous pharmaceutical solids below their glass transition temperatures. *Pharmaceutical Research* **1995,** *12* (6), 799-806.

125. Zhou, D.; Zhang, G. G. Z.; Law, D.; Grant, D. J. W.; Schmitt, E. A., Physical stability of amorphous pharmaceuticals: Importance of configurational thermodynamic quantities and molecular mobility. *Journal of Pharmaceutical Sciences* **2002,** *91* (8), 1863-1872.

126. Miyazaki, T.; Yoshioka, S.; Aso, Y.; Kojima, S., Ability of polyvinylpyrrolidone and polyacrylic acid to inhibit the crystallization of amorphous acetaminophen. *Journal of Pharmaceutical Sciences* **2004,** *93* (11), 2710-2717.

127. Konno, H.; Taylor, L., Ability of different polymers to inhibit the crystallization of amorphous felodipine in the presence of moisture. *Pharmaceutical Research* **2008,** *25* (4), 969-978.

128. Bruce, C. D.; Fegely, K. A.; Rajabi-Siahboomi, A. R.; Mcginity, J. W., The influence of heterogeneous nucleation on the surface crystallization of guaifenesin from melt extrudates containing Eudragit® L10055 or Acryl-EZE®. *European Journal of Pharmaceutics and Biopharmaceutics* **2010,** *75* (1), 71-78.

129. James, P. F., Kinetics of crystal nucleation in silicate glasses. *Journal of Non-Crystalline Solids* **1985,** *73* (1–3), 517-540.

130. Van Drooge, D. J.; Hinrichs, W. L. J.; Visser, M. R.; Frijlink, H. W., Characterization of the molecular distribution of drugs in glassy solid dispersions at the nano-meter scale, using

differential scanning calorimetry and gravimetric water vapour sorption techniques. *International Journal of Pharmaceutics* **2006,** *310* (1–2), 220-229.

131. Huang, J.; Li, Y.; Wigent, R. J.; Malick, W. A.; Sandhu, H. K.; Singhal, D.; Shah, N. H., Interplay of formulation and process methodology on the extent of nifedipine molecular dispersion in polymers. *International Journal of Pharmaceutics* **2011,** *420* (1), 59-67.

132. Paudel, A.; Van Humbeeck, J.; Van Den Mooter, G., Theoretical and experimental investigation on the solid solubility and miscibility of naproxen in poly(vinylpyrrolidone). *Molecular Pharmaceutics* **2010,** *7* (4), 1133-1148.

133. Marsac, P.; Shamblin, S.; Taylor, L., Theoretical and practical approaches for prediction of drug–polymer miscibility and solubility. *Pharmaceutical Research* **2006,** *23* (10), 2417-2426.

134. Rumondor, A. C. F.; Taylor, L. S., Effect of polymer hygroscopicity on the phase behavior of amorphous solid dispersions in the presence of moisture. *Molecular Pharmaceutics* **2009,** *7* (2), 477-490.

135. Chan, K. L. A.; Kazarian, S. G., FTIR spectroscopic imaging of dissolution of a solid dispersion of nifedipine in poly(ethylene glycol). *Molecular Pharmaceutics* **2004,** *1* (4), 331-335.

136. Palmieri, G. F.; Michelini, S.; Martino, P. D.; Martelli, S., Polymers with pH-dependent solubility: Possibility of use in the formulation of gastroresistant and controlled-release matrix tablets. *Drug Development and Industrial Pharmacy* **2000,** *26* (8), 837-845.

137. Dressman, J. B.; Berardi, R. R.; Dermentzoglou, L. C.; Russell, T. L.; Schmaltz, S. P.; Barnett, J. L.; Jarvenpaa, K. M., Upper gastrointestinal (GI) pH in young, healthy men and women. *Pharmaceutical Research* **1990,** *7* (7), 756-761.

138. Charman, W. N.; Porter, C. J. H.; Mithani, S.; Dressman, J. B., Physicochemical and physiological mechanisms for the effects of food on drug absorption: The role of lipids and pH. *Journal of Pharmaceutical Sciences* **1997,** *86* (3), 269-282.

139. Ebube, N. K.; Jones, A. B., Sustained release of acetaminophen from a heterogeneous mixture of two hydrophilic non-ionic cellulose ether polymers. *International Journal of Pharmaceutics* **2004,** *272* (1–2), 19-27.

140. Elkheshen S, Y. A., Alkhaled F., Per-oral extended-release bioadhesive tablet formulation of verapamil HCl. *Boll Chim Farm* **2003,** *142* (5), 226-31.

141. Hosny Ea, E. S., Saleh Si., Buccoadhesive tablets for insulin delivery: in-vitro and in-vivo studies. *Boll Chim Farm.* **2002,** *141* (3), 210-7.

142. Genç L, O. C., Güler E., Studies on vaginal bioadhesive tablets of acyclovir. *Pharmazie.* **2000,** *55* (4), 297-9.

143. Francis Mira, F.; Piredda, M.; Winnik Françoise, M., Hydroxypropylcellulose in oral drug delivery. In *Polysaccharides for Drug Delivery and Pharmaceutical Applications*, American Chemical Society: 2006; Vol. 934, pp 57-75.

144. (a) Shelton Michael, C.; Posey-Dowty Jessica, D.; Lingerfelt, L.; Kirk Shane, K.; Klein, S.; Edgar Kevin, J., Enhanced dissolution of poorly soluble drugs from solid dispersions in carboxymethylcellulose acetate butyrate matrices. In *Polysaccharide Materials: Performance by Design*, American Chemical Society: 2009; Vol. 1017, pp 93-113; (b) Guyot, M.; Fawaz, F., Design and in vitro evaluation of adhesive matrix for transdermal delivery of propranolol. *International Journal of Pharmaceutics* **2000,** *204* (1–2), 171-182.

145. Khandare, J.; Haag, R., Pharmaceutically used polymers: Principles, structures, and applications of pharmaceutical delivery systems. *Handb Exp Pharmacol.* **2010,** (197), 221-50.

146. Liu, H.; Kar, N.; Edgar, K., Direct synthesis of cellulose adipate derivatives using adipic anhydride. *Cellulose* **2012,** *19* (4), 1279-1293.

147. Liu, H.; Ilevbare, G. A.; Cherniawski, B. P.; Ritchie, E. T.; Taylor, L. S.; Edgar, K. J., Synthesis and structure-property evaluation of cellulose ω-carboxyesters for amorphous solid dispersions. *Carbohydrate Polymers* **2012**, http://dx.doi.org/10.1016/j.carbpol.2012.11.049

148. (a) Rabinow, B. E., Nanosuspensions in drug delivery. *Nat Rev Drug Discov* **2004,** *3* (9), 785-796; (b) Merisko-Liversidge, E.; Mcgurk, S. L.; Liversidge, G. G., Insulin Nanoparticles: A Novel Formulation Approach for Poorly Water Soluble Zn-Insulin. *Pharmaceutical Research* **2004,** *21* (9), 1545-1553.

149. Liu, M.; Frãchet, J. M. J., Designing dendrimers for drug delivery. *Pharmaceutical Science & Technology Today* **1999,** *2* (10), 393-401.

150. (a) Letchford, K.; Burt, H., A review of the formation and classification of amphiphilic block copolymer nanoparticulate structures: micelles, nanospheres, nanocapsules and polymersomes. *European Journal of Pharmaceutics and Biopharmaceutics* **2007,** *65* (3), 259-269; (b) Kawakami, K.; Yoshikawa, T.; Hayashi, T.; Nishihara, Y.; Masuda, K., Microemulsion formulation for enhanced absorption of poorly soluble drugs: II. In vivo study. *Journal of*

Controlled Release **2002,** *81* (1-2), 75-82; (c) Colin W, P., Lipid formulations for oral administration of drugs: non-emulsifying, self-emulsifying and "self-microemulsifying" drug delivery systems. *European Journal of Pharmaceutical Sciences* **2000,** *11, Supplement 2*, S93-S98.

151. (a) Liedtke, S.; Wissing, S.; Müller, R. H.; Mader, K., Influence of high pressure homogenisation equipment on nanodispersions characteristics. *International Journal of Pharmaceutics* **2000,** *196* (2), 183-185; (b) Keck, C. M.; Müller, R. H., Drug nanocrystals of poorly soluble drugs produced by high pressure homogenisation. *European Journal of Pharmaceutics and Biopharmaceutics* **2006,** *62* (1), 3-16.

152. Pace, S., Pace, G. W., Parikh, I., and Mishra, A., Novel injectable formulationsof insoluble drugs. *Pharm Tech* **1999,** *23*, 116-34.

153. Schwitzer, J. M.; Müller, R. H., Drug Nanocrystals—The Universal Formulation Approach for Poorly Soluble Drugs. *Nanoparticulate Drug Delivery Systems*, **2007,**71-88.

154. (a) Liu, Y.; Tong, Z.; Prud'homme, R. K., Stabilized polymeric nanoparticles for controlled and efficient release of bifenthrin. *Pest Management Science* **2008,** *64* (8), 808-812; (b) Matsumura, Y.; Maeda, H., A new concept for macromolecular therapeutics in cancer chemotherapy: Mechanism of tumoritropic accumulation of proteins and the antitumor agent smancs. *Cancer Research* **1986,** *46* (12 Part 1), 6387-6392; (c) Gindy, M., Composite block copolymer stabilized nanoparticles: Simultaneous encapsulation of organic actives and inorganic nanostructures. *Langumir* **2008,** *24*, 83-90.

155. Liu, Y.; Cheng, C.; Prud'homme, R. K.; Fox, R. O., Mixing in a multi-inlet vortex mixer (MIVM) for flash nano-precipitation. *Chemical Engineering Science* **2008,** *63* (11), 2829-2842.

156. Johnson, B. K.; Prud'homme, R. K., Chemical processing and micromixing in confined impinging jets. *AIChE Journal* **2003,** *49* (9), 2264-2282.

157. Johnson, B. K.; Prud'homme, R. K., Flash NanoPrecipitation of Organic Actives and Block Copolymers using a Confined Impinging Jets Mixer. *Australian Journal of Chemistry* **2003,** *56* (10), 1021-1024.

158. (a) Mahajan, A. J.; Kirwan, D. J., Micromixing effects in a two-impinging-jets precipitator. *AIChE Journal* **1996,** *42* (7), 1801-1814; (b) Gillian, J. M.; Kirwan, D. J., Identification and correlation of mixing times in opposed-jet mixers. *Chemical Engineering Communications* **2008,** *195* (12), 1553 - 1574.

159. Gindy, M. E.; Panagiotopoulos, A. Z.; Prud'homme, R. K., Composite block copolymer stabilized nanoparticles: simultaneous encapsulation of organic actives and inorganic Nanostructures. *Langmuir* **2007,** *24* (1), 83-90.

160. Akbulut, M.; Ginart, P.; Gindy, M. E.; Theriault, C.; Chin, K. H.; Soboyejo, W.; Prud'homme, R. K., Generic Method of Preparing Multifunctional Fluorescent Nanoparticles Using Flash NanoPrecipitation. *Advanced Functional Materials* **2009,** *19* (5), 718-725.

161. Chan, H.-K.; Kwok, P. C. L., Production methods for nanodrug particles using the bottom-up approach. *Advanced Drug Delivery Reviews* **2011,** *63* (6), 406-416.

162. Gelperina, S.; Kisich, K.; Iseman, M. D.; Heifets, L., The Potential Advantages of Nanoparticle Drug Delivery Systems in Chemotherapy of Tuberculosis. *American Journal of Respiratory and Critical Care Medicine* **2005,** *172* (12), 1487-1490.

163. Pählka, R.; Lambert, J.; Ansko, P.; Winstanley, P.; Davies, P. D. O.; Kiivet, R. A., Comparative bioavailability of three different preparations of rifampicin. *Journal of Clinical Pharmacy and Therapeutics* **1999,** *24* (3), 219-225.

164. Sensi, P., History of the development of rifampin. *Reviews of infectious diseases* **1983,** *5* (3), 402-406.

165. Van Ingen, J.; Aarnoutse, R. E.; Donald, P. R.; Diacon, A. H.; Dawson, R.; Plemper Van Balen, G.; Gillespie, S. H.; Boeree, M. J., Why Do We Use 600 mg of Rifampicin in Tuberculosis Treatment? *Clinical Infectious Diseases* **2011,** *52* (9), e194-e199.

166. Lester, W., Rifampin: A Semisynthetic Derivative of Rifamycin-A Prototype for the Future. *Annual Review of Microbiology* **1972,** *26* (1), 85-102.

167. Calleja, I.; Blanco-PríEto, M. a. J.; Ruz, N.; Renedo, M. a. J.; Dios-Viéitez, M. a. C., High-performance liquid–chromatographic determination of rifampicin in plasma and tissues. *Journal of Chromatography A* **2004,** *1031* (1–2), 289-294.

168. Acocella, G., Pharmacokinetics and Metabolism of Rifampin in Humans. *Review of Infectious Diseases* **1983,** *5* (Supplement 3), S428-S432.

169. Shishoo, C. J.; Shah, S. A.; Rathod, I. S.; Savale, S. S.; Kotecha, J. S.; Shah, P. B., Stability of rifampicin in dissolution medium in presence of isoniazid. *International Journal of Pharmaceutics* **1999,** *190* (1), 109-123.

170. Panchagnula, R.; Agrawal, S., Biopharmaceutic and pharmacokinetic aspects of variable bioavailability of rifampicin. *International Journal of Pharmaceutics* **2004,** *271* (1-2), 1-4.

171. (a) Mathur, I. S.; Gupta, H. P.; Srivastava, S. K.; Singh, S.; Madhu, K.; Khanna, N. M., Evaluation of Subdermal Biodegradable Implants Incorporating Rifampicin as a Method of Drug Delivery in Experimental Tuberculosis of Guinea Pigs. *Journal of Medical Microbiology* **1985,** *20* (3), 387-392; (b) Rao, B. S.; Murthy, K. V. R., Studies on rifampicin release from ethylcellulose coated nonpareil beads. *International Journal of Pharmaceutics* **2002,** *231* (1), 97-106; (c) Schierholz, J. M., Physico-chemical properties of a rifampicin-releasing polydimethyl-siloxane shunt. *Biomaterials* **1997,** *18* (8), 635-641; (d) Ammar, H. O.; Khalil, R. M., Preparation and Evaluation of Sustained-Release Solid Dispersions of Drugs with Eudragit Polymers. *Drug Development and Industrial Pharmacy* **1997,** *23* (11), 1043-1054.

172. Meyer, H.; Mally, J., Über Hydrazinderivate der Pyridincarbonsäuren. *Monatshefte für Chemie* **1912,** *33* (4), 393-414.

173. Ito, F.; Makino, K., Preparation and properties of monodispersed rifampicin-loaded poly(lactide-co-glycolide) microspheres. *Colloids and Surfaces B: Biointerfaces* **2004,** *39* (1–2), 17-21.

174. Durán, N.; Alvarenga, M. A.; Silva, E. C.; Melo, P. S.; Marcato, P. D., Microencapsulation of antibiotic rifampicin in poly(3-hydroxybutyrate-co-3-hydroxyvalerate). *Archives of Pharmacal Research* **2008,** *31* (11), 1509-1516.

175. Anisimova, Y. V.; Gelperina, S. I.; Peloquin, C. A.; Heifets, L. B., Nanoparticles as antituberculosis drugs carriers: Effect on activity against mycobacterium tuberculosis in human monocyte-derived macrophages. *Journal of Nanoparticle Research* **2000,** *2* (2), 165-171.

176. Hiremath, P. S.; Saha, R. N., Oral matrix tablet formulations for concomitant controlled release of anti-tubercular drugs: Design and in vitro evaluations. *International Journal of Pharmaceutics* **2008,** *362* (1–2), 118-125.

177. Gupta, K. C.; Fawzi Habeeb, J., Controlled-release formulations for hydroxy urea and rifampicin using polyphosphate-anion-crosslinked chitosan microspheres. *J Appl Polym Sci* **2007,** *104* (3), 1942-1956.

178. Samad, A.; Sultana, Y.; Khar, R. K.; Chuttani, K.; Mishra, A. K., Gelatin microspheres of rifampicin cross-linked with sucrose using thermal gelation method for the treatment of tuberculosis. *Journal of Microencapsulation* **2008,** *26* (1), 83-89.

179. Esmaeili, F.; Hosseini-Nasr, M.; Rad-Malekshahi, M.; Samadi, N.; Atyabi, F.; Dinarvand, R., Preparation and antibacterial activity evaluation of rifampicin-loaded poly

lactide-co-glycolide nanoparticles. *Nanomedicine : nanotechnology, biology, and medicine* **2007,** *3* (2), 161-167.

180. Pandey, R.; Khuller, G. K., Subcutaneous nanoparticle-based antitubercular chemotherapy in an experimental model. *Journal of Antimicrobial Chemotherapy* **2004,** *54* (1), 266-268.

181. Pandey, R.; Khuller, G. K., Antitubercular inhaled therapy: opportunities, progress and challenges. *Journal of Antimicrobial Chemotherapy* **2005,** *55* (4), 430-435.

182. Pandey, R.; Sharma, A.; Zahoor, A.; Sharma, S.; Khuller, G. K.; Prasad, B., Poly (dl-lactide-co-glycolide) nanoparticle-based inhalable sustained drug delivery system for experimental tuberculosis. *Journal of Antimicrobial Chemotherapy* **2003,** *52* (6), 981-986.

183. Sharma, A.; Pandey, R.; Sharma, S.; Khuller, G. K., Chemotherapeutic efficacy of poly (dl-lactide-co-glycolide) nanoparticle encapsulated antitubercular drugs at sub-therapeutic dose against experimental tuberculosis. *International Journal of Antimicrobial Agents* **2004,** *24* (6), 599-604.

184. Ahmad, Z.; Pandey, R.; Sharma, S.; Khuller, G. K., Pharmacokinetic and pharmacodynamic behaviour of antitubercular drugs encapsulated in alginate nanoparticles at two doses. *International Journal of Antimicrobial Agents* **2006,** *27* (5), 409-416.

185. Bala I, H. S., Kumar M.N.V.R., PLGA nanoparticles in drug delivery: The state of the art. *Crit Rev Ther Drug Carrier Syst.* **2004,** *21* (5), 387-422.

186. Gref, R.; Minamitake, Y.; Peracchia, M.; Trubetskoy, V.; Torchilin, V.; Langer, R., Biodegradable long-circulating polymeric nanospheres. *Science* **1994,** *263* (5153), 1600-1603.

187. D'addio, S. M. Tuberculosis Therapeutics: Engineering Of Nanomedicinal Systems For Local Delivery Of Targeted Drug Cocktails. Princeton University, 2012.

188. World Helath Organization, AIDS epidemic update **2009**, Retrieved from http://data.unaids.org/pub/report/2009/jc1700_epi_update_2009_en.pdf

189. Yekkala, R. S.; Ashenafi, D.; Mariën, I.; Xin, H.; Haghedooren, E.; Hoogmartens, J.; Adams, E., Evaluation of an International Pharmacopoeia method for the analysis of ritonavir by liquid chromatography. *Journal of Pharmaceutical and Biomedical Analysis* **2008,** *48* (3), 1050-1054.

190. Rohan, R. M. a. L. C., Progress in antiretroviral drug delivery using nanotechnology. *Int J Nanomedicine* **2010,** *5*, 533-547.

191. Holtgrave, D. R., Causes of the decline in AIDS deaths, United States, 1995–2002: prevention, treatment or both? *Int J STD AIDS* **2005,** *16* (12), 777-781.

192. Vyas, T. K.; Shah, L.; Amiji, M. M., Nanoparticulate drug carriers for delivery of HIV/AIDS therapy to viral reservoir sites. *Expert Opinion on Drug Delivery* **2006,** *3* (5), 613-628.

193. (a) Perera, G.; Greindl, M.; Palmberger, T. F.; Bernkop-Schnürch, A., Insulin-loaded poly(acrylic acid)-cysteine nanoparticles: Stability studies towards digestive enzymes of the intestine. *Drug Delivery* **2009,** *16* (5), 254-260; (b) Mallipeddi, R.; Rohan, L. C., Nanoparticle-based vaginal drug delivery systems for HIV prevention. *Expert Opinion on Drug Delivery* **2010,** *7* (1), 37-48.

194. (a) Sharma, P.; Garg, S., Pure drug and polymer based nanotechnologies for the improved solubility, stability, bioavailability and targeting of anti-HIV drugs. *Advanced Drug Delivery Reviews* **2010,** *62* (4-5), 491-502; (b) Rao, K. S.; Ghorpade, A.; Labhasetwar, V., Targeting anti-HIV drugs to the CNS. *Expert Opinion on Drug Delivery* **2009,** *6* (8), 771-784.

195. Ham, A.; Cost, M.; Sassi, A.; Dezzutti, C.; Rohan, L., Targeted Delivery of PSC-RANTES for HIV-1 Prevention using Biodegradable Nanoparticles. *Pharm Res* **2009,** *26* (3), 502-511.

196. Takeuchi, H.; Yamamoto, H.; Kawashima, Y., Mucoadhesive nanoparticulate systems for peptide drug delivery. *Advanced Drug Delivery Reviews* **2001,** *47* (1), 39-54.

197. (a) Weber, N.; Ortega, P.; Clemente, M. I.; Shcharbin, D.; Bryszewska, M.; De La Mata, F. J.; Gómez, R.; Muñoz-Fernández, M. A., Characterization of carbosilane dendrimers as effective carriers of siRNA to HIV-infected lymphocytes. *Journal of Controlled Release* **2008,** *132* (1), 55-64; (b) Liu, Y.; Franzen, S., Factors Determining the Efficacy of Nuclear Delivery of Antisense Oligonucleotides by Gold Nanoparticles. *Bioconjugate Chemistry* **2008,** *19* (5), 1009-1016.

198. Raval, J. P.; Naik, D. R.; Amin, K. A.; Patel, P. S., Controlled-release and antibacterial studies of doxycycline-loaded poly(ε-caprolactone) microspheres. *Journal of Saudi Chemical Society* **2011,** doi:10.1016/j.jscs.2011.11.004.

199. Duan, J.; Zhang, Y.; Han, S.; Chen, Y.; Li, B.; Liao, M.; Chen, W.; Deng, X.; Zhao, J.; Huang, B., Synthesis and in vitro/in vivo anti-cancer evaluation of curcumin-loaded

chitosan/poly(butyl cyanoacrylate) nanoparticles. *International Journal of Pharmaceutics* **2010,** *400* (1–2), 211-220.

200. Mainardes, R. M.; Evangelista, R. C., PLGA nanoparticles containing praziquantel: effect of formulation variables on size distribution. *International Journal of Pharmaceutics* **2005,** *290* (1–2), 137-144.

201. Siccardi, M.; Martin P.; McDonald T. O.; Liptrott, N.J.; Giardiello, M.; Rannard, S.; Owen, A.; Research Spotlight: Nanomedicines for HIV therapy. *20th Conference on Retroviruses and Opportunistic Infections* **2013,** http://www.natap.org/2013/CROI/croi_187.htm

202. Jenita, J. J. L. N. T., Madhusudhan; Wilson, B.; Vithya, T.; Premakumari, K. B., Formulation and characterization of ritonavir loaded polymethacrylate microspheres for oral delivery. *Journal of Pharmacy Research* **2011,** *4* (7), 2159.

203. Naik, D. R. R., Jignesh P., Characteristic and controlled release of antiviral drug: A comparative study on preparative techniques and polymer affected parameter. *Biointerface Research in Applied Chemistry* **2012,** *2* (5), 409.

204. Lembo D, C. R., Nanoparticulate delivery systems for antiviral drugs. *Antivir Chem Chemother*. **2010,** *21* (2), 53-70.

205. Hari, BN. V.; Dhevendaran, K.; Narayan, N., Development of Efavirenz nanoparticle for enhanced efficiency of anti-retroviral therapy against HIV and AIDS. *BMC Infectious Diseases* **2012,** *12*, 7.

206. Christopher J Destache, T. B., Keith Christensen, Annemarie Shibata, Akhilesh Sharma and Alekha Dash, Combination antiretroviral drugs in PLGA nanoparticle for HIV-1. *BMC Infectious Diseases* **2009,** *9*, 198.

207. Sinha, S.; Ali, M.; Baboota, S.; Ahuja, A.; Kumar, A.; Ali, J., Solid Dispersion as an Approach for Bioavailability Enhancement of Poorly Water-Soluble Drug Ritonavir. *AAPS PharmSciTech* **2010,** *11* (2), 518-527.

208. T.Vetrichelvan , I. S. B., Formulation and in vitro characterization of Sustained release Ritonavir nanoparticles in alginates. *Journal of Pharmacy Research* **2011,** *4* (7), 2152.

209. Naik, D. R.; Raval, J. P., Amorphous polymeric binary blend pH-responsive nanoparticles for dissolution enhancement of antiviral drug. *Journal of Saudi Chemical Society* **2012,** http://dx.doi.org/10.1016/j.jscs.2012.09.020.

210. Fu, K.; Harrell, R.; Zinski, K.; Um, C.; Jaklenec, A.; Frazier, J.; Lotan, N.; Burke, P.; Klibanov, A. M.; Langer, R., A potential approach for decreasing the burst effect of protein from PLGA microspheres. *Journal of Pharmaceutical Sciences* **2003,** *92* (8), 1582-1591.

211. (a) Yoo, H. S.; Oh, J. E.; Lee, K. H.; Park, T. G., Biodegradable Nanoparticles Containing Doxorubicin-PLGA Conjugate for Sustained Release. *Pharm Res* **1999,** *16* (7), 1114-1118; (b) Langer, R., Drug delivery and targeting. *Nature* **1998,** *392* (6679 Suppl), 5-10.

Chapter 3: Nanoparticles of rifampicin and carboxymethyl cellulose acetate butyrate prepared by rapid precipitation

Sonal Mazumder[a], Hale Cigdem Arca[a], Samantha A. Casterlow[b], Nammalwar Sriranganathan[b], Kevin J. Edgar [c] and Richey M Davis[*d]

[a]*Macromolecular Interface Institute*, [b]*Department of Biomedical Sciences and Pathobiology*, [c]*Department of Sustainable Biomaterials*, [d]*Department of Chemical Engineering*

Virginia Polytechnic Institute and State University, Blacksburg, VA 24061, USA

*Corresponding author:

Richey M. Davis

Department of Chemical Engineering, VirginiaTech, Blacksburg, VA - 24061

Tel: 001+ 540-231-4578 ; Fax : 001+ 540-231-5022

E-mail address: rmdavis@vt.edu

ABSTRACT

Nanoparticles made up of antibiotic rifampicin and carboxymethyl cellulose acetate butyrate (CMCAB) were produced by a rapid precipitation process. The particle formation process and particle properties were investigated. Two different particle purification and recovery methods were investigated – flocculation with acids and dialysis followed by freeze drying. Particle diameters as measured by dynamic light scattering were in the range 150-400 nm and depended upon the purification method used. The particles processed by flocculating with acids were larger with diameters ~300-400 nm measured by dynamic light scattering whereas particles processed by dialysis followed by freeze drying were smaller with diameters approximately 150-200 nm with lower polydispersity indices. Rifampicin drug loading ranged

from 3-16 wt% and the corresponding drug loading efficiencies ranged from 12-45% depending on the particle recovery/processing methods. The MTS cytotoxicity assay showed no significant reduction in cell viability by the nanoparticles. The minimum inhibitory concentration results obtained with *M. smegmatis* for the rifampicin-containing nanoparticles indicated that the biological activity of rifampicin was well preserved after CMCAB nanoparticle formation.

Keywords: Rifampicin, carboxymethyl cellulose acetate butyrate, nanoparticles, flash nanoprecipitation, flocculation, multi-inlet vortex mixer, cell viability

3.1. INTRODUCTION

Every year almost 2 million deaths and eight million new cases caused by Tuberculosis (TB) are reported. Despite of available remedies, TB is a prominent disease in many progressive countries. The treatment of TB requires frequent dosing with multiple drugs and thus it is important to formulate drugs so that they can be released in a sustained manner, reducing the frequency and number of doses [2]. Rifampicin is a first-line drug recommended by WHO for the treatment of tuberculosis. It is slightly soluble in water (2.5 mg/ml at pH 7.3) and degrades at low pH [3]. It has suboptimal oral bioavailability, especially for the preferred, multidrug dosage form. The usual dosage of rifampicin in an adult is 10 mg/kg, or 600 mg for a 60 kg person daily orally or intravenously [4]. Due to bioavailability limitations, this relatively high dose of the drug is required to maintain therapeutic concentrations which may lead to several side effects such as hives, facial swelling, and breathing difficulty. Due to its high cost and side effects, rifampicin is used mainly in intermittent therapy. Its biological half-life ranges from 1.5-5 hours. There is a need for formulations that release rifampicin in a sustained manner and enhance bioavailability, thereby creating the potential for enhanced patient convenience and adherence, and reduced drug expense, side effects, and interpatient and chronological variability. Polymer encapsulated drug nanoparticles have been investigated for many applications due to the improved material properties that result from a reduction in particle dimensions and due to the potential for targeted drug delivery [5]. Oral administration of therapeutic agents represents the easiest and most convenient mode of drug delivery, especially in cases of chronic treatment, since there is no requirement for hospitalization, a critical issue in developing countries. In addition, patient compliance in taking oral medications tends to be greater than with injected formulations [6]. However, it is challenging to design delivery systems for the gastrointestinal (GI) tract to obtain

desired pharmacokinetics [7]. Several factors can limit the bioavailability of drugs from the GI tract including aqueous solubility, ability to permeate through the lipid bilayer membranes of the enterocytes that line the GI tract, and active processes such as efflux transport and metabolism. Dissolution of drugs is frequently the rate-limiting step which controls bioavailability [8]. Sustained release formulations can lead to improved bioavailability, less frequent dosing, and reduced undesirable side effects [9].

Prior work with rifampicin-polymer particles can be broadly categorized in terms of studies done in vitro with microparticles [10,11,12,13], in vitro with nanoparticles [14,15], and in vivo, with the latter studies further categorized in terms of delivery method, i.e. by injection [16], pulmonary delivery [17,18] and oral delivery[19,20,21]. Most studies involved polymeric carriers, either polyesters or polysaccharides. Many of the studies focused on controlling drug loading and characterizing drug release but, in many cases, the method of producing the particles was not rapid and scalable.

Flash nanoprecipitation is a nanoparticle fabrication method that is rapid and scalable in which an organic solution of a polymer (typically an amphiphilic block copolymer) and organic species (typically poorly water-soluble drugs and hydrophobically-modified particles) is rapidly mixed with a non-solvent such as water under highly turbulent conditions in a confined mixing chamber [22,23,24]. This turbulent mixing forms a highly supersaturated solution which undergoes particle nucleation and growth. Particle growth stops due to the formation of a repulsive barrier on the particle surface. When amphiphilic copolymers are used, that barrier typically consists of poly(ethylene oxide) chains that form a brush-like structure on the nanoparticle surfaces. The supersaturation depends on the water/organic solvent ratio injected into the mixer, the concentrations of the drugs and polymers, and temperature. This process is attractive in that the

particle size distributions can be controlled [25, 26] and high concentrations of hydrophobic organic species can be incorporated due to kinetic entrapment in the cores [27,28,29]. Flash nanoprecipitation has been used with a four-jet multi-inlet vortex mixer (MIVM) to produce nanoparticles with high loadings of drugs and imaging agents and with controlled surface chemistries [30,31, 32,33,34].

Rifampicin has been incorporated into poly(ε-caprolactone) nanoparticles in the size range 100-200 nm using flash nanoprecipitation. Due to rifampicin's solubility in water, it was necessary to first make an insoluble pro-drug form by conjugating it with Vitamin E succinate and with poly(ε-caprolactone) which is biodegradable. The resulting pro-drugs were then co-precipitated with diblock copolymers of poly(ethylene oxide-b-ε-caprolactone) at loadings of 14.5 wt % of rifampicin. Hydrolytic cleavage of the linking group provided a mechanism for the sustained release of rifampicin[35]. There has been no other work published to our knowledge on preparation of rifampicin-loaded polymer nanoparticles using the MIVM.

Pandey et al.,[19] developed PLGA particles loaded with rifampicin as well as isoniazid and pyrazinamide. The drug loading efficiency of the microparticles was 8-18% and the mean particle size was ~ 2 μm. The microparticles containing rifampicin showed higher therapeutic concentration in plasma compared to free drug. However, these microparticles suffered from several drawbacks such as a low drug encapsulation, high polymer consumption, and a partial therapeutic benefit. When nanoparticles were dosed (5 oral doses every 10^{th} day) compared to 46 daily doses of free drugs, there was complete clearance of TB from the organs of infected mice. Nanoparticles ranging in size from 186-290 nm (PDI =0.38 ± 0.04) and drug loading efficiency 57-68% showed similar results when tested in guinea pigs with equivalent amount of drug (rifampicin 12 mg/kg + isoniazid 10 mg/kg + pyrazinamide 25 mg/kg body weight) [20]. It was also observed that sustained drug release could be achieved in the plasma (5–12 days) with the

nanoparticles compared to the microparticles (3–4 days) of equivalent dose. At a 2/3rd therapeutic dosage of nanoparticles, the drug remained in the plasma (at therapeutically useful levels) for 7, 12 and 11 days for rifampicin, isoniazid and pyrazinamide, respectively.

Zahroor et al. prepared alginate nanoparticles (235 nm diameter) of anti-TB drugs (rifampicin, isoniazid, pyrazinamide and ethambutol) using controlled cation-induced gelation of alginate. The drug loading efficiency for rifampicin was 80-90%. When the nanoparticles were administered orally to mice, ethambutol, rifampicin, isoniazid and pyrazinamide levels were detected in plasma above the MIC and therapeutic level up to 7,9,11 and 11 days, respectively (free drugs were cleared within 12 to 24 h from the blood but were detectable in tissues (e.g. spleen, liver and lung) for more than one day). The drug levels were detectable in tissues above the MIC (minimum inhibitory concentration) up to 15 days [21]. This work is notable as it is one of the first detailed studies showing that orally-administered nanoparticles can cross the GI-epithelium and enter the circulation in therapeutically useful levels.

Amorphous solid dispersions (ASD) are formed when the drug forms a molecular dispersion in an amorphous polymer matrix. Due to the lack of an ordered molecular lattice, the energy required for a molecule to go from the amorphous state to the solvated state is lower than the energy required for the corresponding transition from the crystalline state and this increases the bioavailability of the drug [36]. The most important polymer properties required for amorphous matrix formulations are that they: (1) must be non-toxic and miscible at least in part with the (often hydrophobic) drug, (2) must possess a high glass transition temperature (in order to inhibit drug recrystallization in and migration through the matrix), and (3) must not itself have a tendency to crystallize since it is important for the ASD to be stable during transport and extended storage. There are relatively few ASDs available commercially due to the

thermodynamic instability of drugs in the amorphous form. Several synthetic polymers like polyethylene glycol (PEG) and polyvinyl pyrrolidone (PVP) have been used for preparing amorphous dispersions. PEG has high water solubility and has a tendency to crystallize[37], while PVP is hygroscopic, dissolves fast at low pH, very water soluble and doesn't always prevent solution crystallization[38]. Several polysaccharides (HPMC, HPMCAS, chitosan) have shown promising results in forming amorphous drugs and improving dissolution and stability [39].

There are few studies in the literature regarding nanoparticles of amorphous solid dispersions. Improvement in the oral bioavailability of sirolimus - an immunosuppresent drug used to prevent rejection in organ transplantation - was observed when ASDs of sirolimus-polyvinylpyrrolidone (PVP) K30 nanoparticles (mean particle size 250 nm) were prepared using a supercritical antisolvent (SAS) process [40].

The high surface area of amorphous hydroxypropylmethylcellulose (HPMC) and itraconazole (ITZ) nanoparticles (particle size 200-600 nm) prepared by controlled precipitation showed rapid and higher supersaturation compared to low surface area solid dispersions[41].

A wet milling technique was used to prepare nanosized ASDs of Nobiletin (NOB) [42]. The diameter of the nanoparticles was 270 nm, and there was a significant improvement in the dissolution behavior compared with that of crystalline NOB.

ASDs of indomethacin (IM) and PVP prepared by co-grinding were compared with those between IM and silica nanoparticles. The sizes of the particles were not mentioned. The results showed that the solubility was solely dependent on the state of IM, irrespective of the carrier species and carrier-dependent chemical interactions [43]

In this present work, we made rifampicin-containing nanoparticles using carboxymethyl cellulose acetate butyrate (CMCAB), a cellulose ester that was developed relatively recently.

CMCAB is pH-sensitive and water-swellable when partially ionized at the neutral pH of the small intestine (ca. pH 6.8), but is insoluble at gastric pH (ca. pH 1.2). CMCAB has good solubility in common organic solvents. We hypothesized that the pH-dependent swelling controlled by the carboxyl groups of CMCAB might reduce rifampicin degradation by minimizing release in the stomach, but permitting controlled release in the small intestine. CMCAB is compatible with numerous pharmaceutical actives and has a high glass transition temperature (T_g = 137°C). It has been shown to be useful for forming amorphous solid dispersions. [39a, 44]. Due to its hydrophobic character, CMCAB is a useful polymer for the slow, in some cases zero-order (with respect to time) release of hydrophobic drugs [39b]. This characteristic has also been shown to lead to slow release of more hydrophilic drugs like aspirin and ibuprofen. There have been no previous reports of preparation and testing of CMCAB/drug nanoparticles. Nanometer-scale drug/polymer particles are of interest since they possess very high surface area/volume ratio, which could enhance the interaction of the particles with the epithelial lining and mucus and could result in a desirable drug release profile in the first few hours in the small intestine. We investigated the effect of processing conditions on the particle size and drug loading of rifampicin/CMCAB nanoparticles made using a flash nano-precipitation method in a multi-inlet vortex mixer. Impacts of key process parameters on particle size and drug loading were elucidated in order to test the control and reproducibility of the particle formation process. These studies focus on establishing a methodology for preparing drug-polymer complexes in a relatively rapid, efficient and scalable manner. We further evaluated the morphology of the product nanoparticles and carried out a preliminary, *in vitro* evaluation of toxicity and efficacy. Finally a comparison was made between the CMCAB nanoparticles and corresponding CMCAB microparticles to understand the effect of particle size on the release characteristics of the drug.

3.2. MATERIALS AND METHODS

3.2.1 Materials for particle preparation

Tetrahydrofuran (anhydrous, ACS reagent, ≥ 99.0% inhibitor free) was used for polymer/drug nanoparticle formation. Carboxylmethyl cellulose acetate butyrate (CMCAB; approximate molecular weight 22,000, degree of substitution of butyryl group = 1.64, degree of substitution acetyl group = 0.44, degree of substitution carboxymethyl group = 0.33), was from Eastman Chemical Company) (Figure 1). Citric acid (anhydrous, ACS, 99.5 +%) and hydrochloric acid (ACS grade, 37%). Rifampicin (Figure 2)Sigma Aldrich (≥ 97% by HPLC). All the reagents were used as received. Rifampicin possesses two ionization constants (pKa), respectively at pH 1.7 (proton lost on the hydroxyl group at position C8, arrow mark in figure 2) and 7.9 (proton gained on the piperazine moiety at position N4). In aqueous solution, rifampicin exists as a zwitterion with an isoelectric point at 4.8 [45].

The moisture % present in CMCAB and rifampicin was measured by Thermogravimetric Analysis (TGA, Q-500, TA instruments). The measurements were done under nitrogen atmosphere with the temperature ramped from 28-200ºC at 10ºC/minute; typically 5 mgs of sample were used. Reverse osmosis water (RO water) was used for DLS measurements and in the formation of the nanoparticles. The dialysis tubing (Spectropore, cellulose ester) which was used for solvent removal had a molecular weight cut off (MWCO) of 25K.

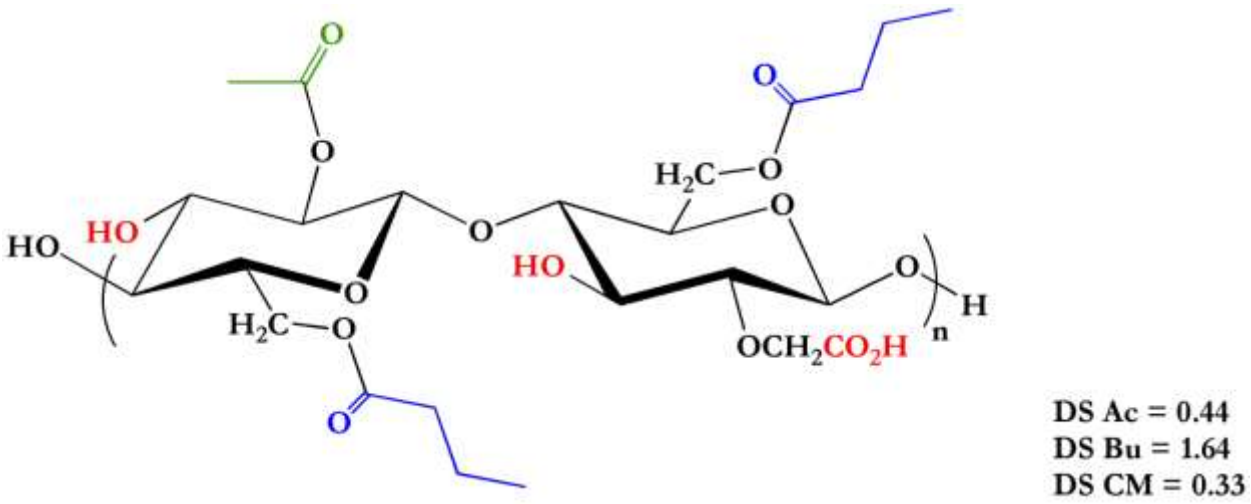

Figure 1. Structure of carboxymethyl cellulose acetate butyrate (CMCAB) [39a]

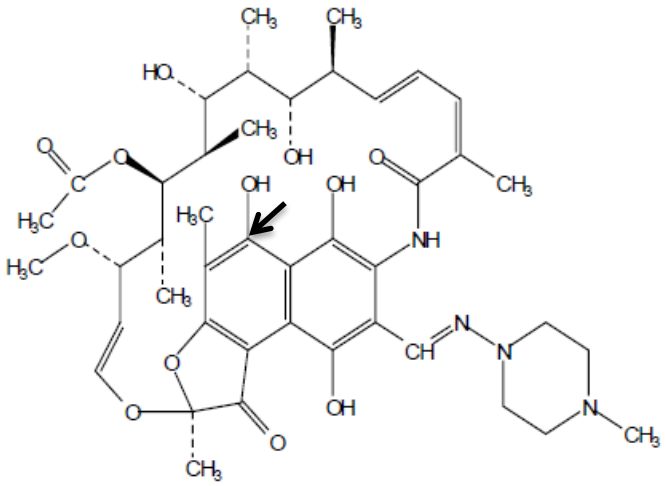

Figure 2. Structure of rifampicin [4] Arrow represent hydroxyl group at position C8

3.2.2 Materials for cell culture experiments

The J774A.1 murine like macrophage cell line used in *in vitro* cell studies was obtained from American Type Culture Collection. J774A.1 cells were maintained using Dulbecco's modified Eagle's medium (DMEM) supplemented with 10% heat- inactivated fetal bovine serum (FBS), L-glutamine, $NaHCO_3$, pyridoxine-HCL, 45,000 mg/L glucose, and 1% penicillin-streptomycin solution at 10,000 µg/ml. The Cell Titer 96® Aqueous Non-Radioactive Cell

Proliferation MTS (3-(4,5-dimethylthiazol-2-yl)-5-(3-carboxymethoxyphenyl)-2-(4-sulfophenyl)-2H-tetrazolium) Assay (Promega Corporation) was used to determine in vitro cell viability. The absorbance values of samples were measured at 490 nm using a 96-well ELISA reader (SoftMax Pro Inc., USA). Minimal inhibitory concentrations were determined following standard operating protocols [46]. *M. smegmatis* ATCC# 700084 **was** obtained from the American Type Culture Collection and was maintained using Middlebrook 7H10 agar (Difacto, Detroit, MI) containing 0.5% glycerol and 10% OADC enrichment. Bacterial cultures were diluted with 1x PBS (Mediatech, Manassas, VA) and the suspension adjusted to equal the McFarland No. 0.5 turbidity standard.

3.3 Particle preparation and characterization

3.3.1 General procedure for rapid precipitation in the Multi Inlet Vortex Mixer

Powdered CMCAB, rifampicin and THF were weighed into a glass vial that was then sealed with a screw cap and mixed with a wrist action shaker overnight. The masses of CMCAB and rifampicin were corrected for the moisture present in the powdered samples which was 1.81 and 0.14 wt%, respectively, as measured by TGA. Flash nanoprecipitation of CMCAB particles and rifampicin-CMCAB complexes was carried out in a Multi-Inlet Vortex Mixer that accommodates four liquid streams [47]. CMCAB (with or without rifampicin) dissolved in THF formed the organic stream whereas the other three streams consisted of reverse osmosis (RO) water. The temperature of each stream was adjusted to 25°C prior to injection into the mixer by immersing the syringes containing the organic solution and the water in a temperature-controlled bath. The four inlet streams are tangential to the mixing chamber and the effluent was collected from the center of the chamber. CMCAB particles were first made to establish appropriate processing conditions for controlling particle size. Next, rifampicin-CMCAB particles were

made based on those processing conditions. The nanoparticles were formed at a Reynolds number of ~ 3900. The Reynolds number is a dimensionless number that is a measure of turbulence and, in this case, of mixing time. It depends upon the inlet stream velocities, viscosities, and densities [47], [23]. The defining equations for the Reynolds number in the mixer are shown in the Supporting Information.

A New Era 4000 double syringe pump (for the organic stream) and a Harvard Apparatus Remote Infuse/Withdraw PHD 4000 Hpsi Programmable syringe pump (for the three water streams) controlled the inlet flow rates. The New Era pump was controlled with the software Syringe Pump Pro version 1.53. The injected volume ratio of THF to RO water was 1:9 v/v. The target composition of rifampicin was 25 wt% of the total solids on a dry basis.

3.3.2 Particle purification and recovery

Since the particles exit from the MIVM in a mixed THF-water phase, it was necessary to remove the solvent and unincorporated drug from the particles before they can be used in biological studies. Two purification methods were investigated to learn how they affected drug loading and particle size. First, acid-induced flocculation followed by vacuum filtration and drying was used. Second, dialysis followed by freeze drying was investigated as an alternative processing route.

Particle flocculation followed by vacuum drying was previously shown to be an effective method for quickly purifying and recovering dry particles that could be redispersed. Citric acid was used to flocculate nanoparticles coated with steric stabilizing layers of poly(ethylene oxide) and multivalent citric acid [48]. The resulting precipitate was recovered by vacuum filtration. We investigated the use of both citric acid and HCl as flocculating agents. Suspensions of pure CMCAB particles as well as rifampicin-CMCAB particles prepared in the mixer were divided

into two parts. The first part was used in the flocculation step without removing THF, while in the second part, some of the THF was removed by rotary evaporation in a Buchi Rotavaporator 210/215 at 40°C under vacuum for 45 minutes before the flocculation step. Rotary evaporation was done to inhibit drug leaching out from the particles due to the presence of THF. In a typical experiment, the mass of the suspension collected from the mixer was measured and then powdered citric acid was added to the suspension at a concentration of ~ 1 wt%. The suspension was stirred for 10 mins by a magnetic stirrer and the pH was measured as ~2.0 using a pH meter. The time required for significant flocculation to occur was noted by visual inspection. The nanoparticle suspensions with citric acid and HCl were passed through a Nalgene vacuum filter with a polycarbonate membrane (Millipore, 1.2 μm) followed by washing with 1% citric acid solution and 1% dilute HCl solution, respectively. The wet cake collected on the membrane was placed in aluminum drying pans and dried under vacuum at room temperature for 5-6 hours. The dried samples were stored in sealed, screw cap glass vials and stored in the dark at room temperature. The % moisture of the dry powder was measured using TGA. The above experiment was done three times to quantitate the reproducibility in particle size and drug loading. Similar precipitation experiments were done with dilute hydrochloric acid also at pH~2.

Particle purification and recovery was also studied using dialysis followed by freeze drying. Pure CMCAB and rifampicin-CMCAB suspensions were dialyzed to remove THF, free drug, and dissolved polymer. The dialysis was done with 35 mL of the suspension using dialysis tubing with a molecular weight cutoff (MWCO) of 25K. In a typical experiment, 3.5 L of DI water was used in a beaker and the water was changed 4 times over a period of 24 hours. The dialyzed particles were dried in a LABCONCO freeze dryer at 0.018 mbar for 2 days.

3.3.3 Microparticle preparation and characterization

Since particle size could have significant effects on drug release, we compared the drug release properties of the nanoparticles with microparticles made using a spray drying process. CMCAB totaling 0.5 g was suspended in 50 ml of THF and mixed by magnetic stir bar for 16 - 18 hours at room temperature. After mixing, 0.05 g of rifampicin were added to the polymer solution and was mixed for 10 minutes. The mixture was then pumped into a Buchi B-290 spray dryer (Buchi, Newcastle, Delaware). The spray dryer conditions were programmed with an inlet and outlet temperature of 90°C (to insure solvent evaporation), aspirator chamber at 100% efficiency and pump pressure at 40% for optimal drying and isolation of homogeneous particles. Dried powders were obtained and used for further analysis.

3.3.4 Re-dispersion of dried nanoparticles

The dried powders of the nanoparticles from the flocculation step were re-dispersed in DI water and 50 µl of 0.1 N sodium hydroxide was added to adjust the solution to pH ~ 7.0, thus ionizing the carboxylic acid groups which would disrupt any hydrogen bonding between NPs and acids and also increase repulsive electrostatic forces. These particles were sonicated with a probe tip sonicator for 3 minutes. The freeze dried powders purified by dialysis were dispersed in DI water and mixed in a wrist action shaker for 15 minutes.

3.3.5 Particle size – Dynamic light scattering

Dynamic light scattering (DLS) measurements were performed before and after the rotary evaporation and dialysis steps using a Malvern Zetasizer Nano-ZS (Malvern Instruments Ltd, Malvern, UK) at a wavelength of 633 nm and with a scattering angle of 173˚ at 25 ± 0.1 ºC. Typically 200 µl of the nanoparticle suspension diluted with 2 mL of deionized water The suspensions were sonicated with a Tekmar TM 300 probe tip sonicator equipped with a microtip

at a power setting = 4 and duty cycle = 60% for 30 seconds and then filtered with a 1 μm PTFE filter (Whatman, USA). Intensity average diameters were obtained by calculations using Malvern's Zetasizer Nano-ZS V 6.12, software that utilizes an algorithm based upon Mie theory with the assumption that the scattering particles are hard spheres [49].

Field emission scanning electron microscope (FESEM) images of the microparticles were obtained using a LEO (Zeiss) 1550 instrument at a 5 kV accelerating voltage in the conventional high vacuum mode.

The spray dried particles were bath sonicated at 0.1 mg/ml in DI water. About 100 μl of each prepared sample was placed on imaging tape and allowed to dry at room temperature overnight. Samples for SEM were mounted on metal stubs and coated with gold prior to analysis.

3.3.6 Particle morphology – X ray diffraction

The crystallinity properties of nanoparticles and microparticles were evaluated by powder X-ray diffraction (PXRD). PXRD experiments were conducted with samples of the CMCAB (as received), rifampicin (as received), physical mixtures of the as-received CMCAB and rifampicin (mixed by grinding with a mortar and pestle) and the nanoparticles. PXRD patterns were obtained using a Bruker D8 Discover X-ray Diffraction system (Madison, Wisconsin) which emits Kα radiation (λ = 1.54 Aº) at 2200 watts and an accelerating potential of 60 kV. The divergence and scattering slits were set at 1.0° and the receiving slit was set at 0.1 mm. The experiment was conducted with a scan range from 10° - 40° 2θ, while the scanning speed was 4°/min.

3.3.7 Drug loading

In order to measure the drug loading of the nanoparticles and microparticles, a calibration curve for the rifampicin dissolved in acetonitrile was developed using a UV–Visible

spectrophotometer (Thermo Scientific, Evolution 300) at a wavelength of 475 nm where the absorbance was a maximum (Figure S.1 in Supporting Information). The resulting equation for the calibration curve of rifampicin in acetonitrile was:

Absorbance at 475 nm = $0.0153C_{rif} + 0.0096$ [1]

where $R^2 = 0.9999$.

3.3.8 Drug Release studies

Typically, an amount equivalent to 1 mg drug (free drug, nanoparticles or microparticles) was dispersed in 80 mL potassium phosphate buffer, pH 6.8 or pH 1.2 buffer for 6 hours at 37°C. The apparatus used in the release experiments consisted of 250-mL jacketed flasks with circulating ethylene glycol/water (1:1) to control the temperature. The solution was constantly stirred at 350 rpm with a magnetic bar. Aliquots (1 mL) were withdrawn from the suspensions every 0.5 h (during the first 2 h), then every hour for 6 h. Phosphate buffer (1 mL) was added to maintain constant volume after each aliquot was withdrawn. The supernatant was separated from excess solid in solution by ultracentrifugation at 13000 rpm (equivalent of 16060 g's) in an accuSpin Micro (Fisher Scientific) for 10 minutes. The supernatant was recovered, and the solution concentration was determined by a high-performance liquid chromatography (HPLC) system. The solubility studies were done approximately 2 weeks after the preparation of the particles.

Drug release was measured using an Agilent 1200 Series HPLC system which consisted of a quaternary pump, online degasser, manual injector with a 20 μL sample loop and Agilent chemstation LC 3D software. Chromatography was conducted in reverse mode using an 50/50 (v/v) acetonitrile and phosphate buffer 0.01 M pH 2.3. The total analysis time was 8 min. The mobile phase was delivered at a flow rate of 1.5 mL/min and the column temperature was

maintained at 30^{o}C. The sample injection volume was 5 µL. Detection was performed by a diode array detector at a wavelength of 254 nm for rifampicin. A calibration curve for the rifampicin dissolved in acetonitrile was developed using at a wavelength of 254 nm (Figure S.2 in Supporting Information).

3.3.9 Cell Culture Experiments

Initial concentrations of free drug and rifampicin nanoparticle formulations were prepared at 1 mg/mL concentration by weight in PBS. Serial dilutions were done to obtain concentrations ranging from 0.244-500 µg/mL of rifampicin. The amount of biologically active rifampicin loaded in the nanoparticles was determined by comparing the MIC results to those of the free drug.

Murine macrophage like cell line J774A.1 was maintained in Dulbecco's modified Eagle's medium (DMEM) supplemented with 10% heat- inactivated fetal bovine serum (FBS), L-glutamine, $NaHCO_3$, pyridoxine-HCl, 45,000 mg/L glucose, and 1% penicillin-streptomycin solution at 10,000 µg/mL. Approximately 2 x 10^4 cells were incubated for 24-36 hours at 37°C in 5% CO_2 atmosphere until ~90% confluency was achieved. After confluency was achieved, the cell culture medium was removed; the cells were gently washed with phosphate –buffered saline solution (PBS) and fresh medium containing DMEM supplemented with 1% heat- inactivated fetal bovine serum. Cell Titer 96® Aqueous Non-Radioactive Cell Proliferation MTS was performed using procedures described in the Supplemental Information section.

M. smegmatis ATCC# **700084** was grown using Middlebrook 7H10 agar (Difacto, Detroit, MI) containing 0.5% glycerol and 10% OADC enrichment. The bacterial cultures were diluted in 1x PBS (Mediatech, Manassas, VA), the suspension adjusted to equal the McFarland No. 0.5 turbidity standard, and 0.02 mL aliquots were transferred to each well of the 96-well

round bottom plate that contained 0.1 mL of Middlebrook 7H9 broth (Difacto, Detroit, MI) and 0.1 mL of each particle formulations and free drug at 2-fold serial dilutions in PBS ranging from 500 μg/mL to 7.81 μg/mL. The inoculated plates were incubated at 37°C for 48 hrs and the minimum inhibitory concentration (MIC) was defined as the lowest concentration of compound that inhibited visible growth.

3.4. RESULTS AND DISCUSSION

We first investigated the effect of injected CMCAB concentration on particle formation to find the highest concentration at which well-defined particles were formed. This was done to optimize particle processing. We then investigated how different particle processing schemes affected particle properties, notably particle size and rifampicin loading. These processing approaches included (i) particle flocculation and recovery by filtration and vacuum drying, and (ii) particle recovery by dialysis and freeze drying. Next, the effect of the processing conditions on the drug loading was studied. Drug release studies were conducted with rifampicin nanoparticles and were compared to rifampicin microparticles of equivalent drug loading. Finally, the minimum inhibitory concentration (MIC) was investigated and the cell toxicity of the nanoparticles was characterized.

This is the first study for preparing nanoparticles of rifampicin and CMCAB by flash nanoprecipitation. We explored the processing conditions on particle size and size distribution. However, due to the need for using mixtures of solvent and water, this poses a problem for particle isolation and purification because the drug is soluble in both water and THF. Thus we explored two distinct approaches for purifying and recovery of particles to see how they effect particle size and drug loading. We hypothesized that due to the pH sensitivity of CMCAB, there

would be a greater drug release at higher pH compared to the low pH found in the stomach, thus providing protection of rifampicin in stomach.

3.4.1 Determination of optimal CMCAB polymer concentration

The concentration of CMCAB in the mixer was varied to find the highest concentration at which particles with well-defined size distributions were formed. This was done to minimize the amount of solvent removal and the particle purification time. Solutions of CMCAB dissolved in THF at three concentrations - 5, 10, and 15 mg/mL - were injected into the mixer at a constant THF:water ratio of 1:9 v/v and 25ºC. These corresponded to CMCAB concentrations in the mixer of 0.45, 0.91, and 1.36 mg/mL assuming that there was no volume change upon mixing of the THF and water streams. Solutions with a concentration of 5 mg/mL resulted in dispersions with polydispersity index (PDI, measured by dynamic light scattering) ≤ 0.2 (Table 1). Particles made with a CMCAB concentration of 15 mg/ml were very polydisperse and there were multiple peaks in the correlogram. However, particles made with a CMCAB concentration of 10 mg/ml had PDI = 0.2. Thus, particles made in the rest of this study were made with an injected CMCAB concentration of 10 mg/mL. These results demonstrate that, unlike many previous particle systems made by flash nanoprecipitation, nanoparticles of CMCAB with reasonably well-defined particle size distributions can be formed in the multi-inlet vortex mixer without the need for an amphiphilic block copolymer to sterically stabilize them. We hypothesize that the surface of the CMCAB nanoparticles consists at least in part of mobile, hydrated chains that provide a repulsive potential energy that arrests particle growth, probably by a combination of steric and electrostatic interactions.

Table 1. Effect of CMCAB concentration on particle size at mixer conditions - THF:water ratio 1:9 v/v , 25ºC, and Re = 15,000.

Concentration of CMCAB (mg/ml)	Intensity average particle size from DLS (nm)	Polydispersity Index (PDI)
5	115	0.2
10	256	0.2
15	399	very polydisperse

3.4.2 Particle Size Analysis

After processing by flocculation

Immediate flocculation (around 30 seconds) was observed for the samples not subjected to rotary evaporation (non-rotary evaporation) prior to the addition of either citric acid or dilute hydrochloric acid. However, for samples subjected to rotary evaporation to remove some THF prior to the addition of acid, flocculation occurred after 30-45 minutes. Flocculation in the presence of acid may be due to loss of electrostatic stabilization at low pH or by hydrogen bonding and other interactions between CMCAB molecules. After the flocculated powder was dried in a vacuum oven, the typical % moisture of the dry powder was measured using TGA as 1.01 wt %.

We hypothesized that, at low pH, CMCAB carboxyl groups would be protonated, eliminating charge-charge repulsion between particles, allowing hydrogen bond and other interactions between adjacent particles to induce flocculation. In the samples not subjected to rotary evaporation, the color of the supernatant turned reddish orange (the color of rifampicin) due to partial rifampicin dissolution into the THF/water supernatant. By contrast, the supernatant was almost colorless for the samples processed by rotary evaporation, probably due to the lower concentration of THF in the liquid phase. We hypothesize that, during the solvent evaporation

step, rifampicin dissolved in the liquid phase precipitated onto the rifampicin-CMCAB nanoparticles as THF concentration decreased.

Figure 3 shows the particle sizes of the redispersed CMCAB and rifampicin-CMCAB nanoparticles (NPs) processed by acid flocculation with and without rotary evaporation, denoted as +RV and –RV, respectively. In virtually every case, rifampicin-CMCAB particles were larger than the pure CMCAB control particles and the particles flocculated with citric acid were larger than the corresponding particles flocculated with HCl. These sizes were measured after the flocculated particles were dried in a vacuum oven followed by redispersion in water at pH 7. For comparison, sizes are shown for particles that were not subjected to acid flocculation with and without rotary evaporation. For the CMCAB particles subjected to rotary evaporation prior to acid flocculation, the particle size did not depend upon the type of acid used but was slightly higher than the control particles that were not flocculated by acid. For the CMCAB particles not subjected to rotary evaporation prior to acid flocculation, the particles were 60-100% larger than the unflocculated control. In virtually every case, the polydispersity index values measured by dynamic light scattering experiments were 0.2 or less. The values of the particle sizes dispersed in water and PBS buffer along with RSD values are given in the Supporting Information (Tables S.1 and Table S.2).

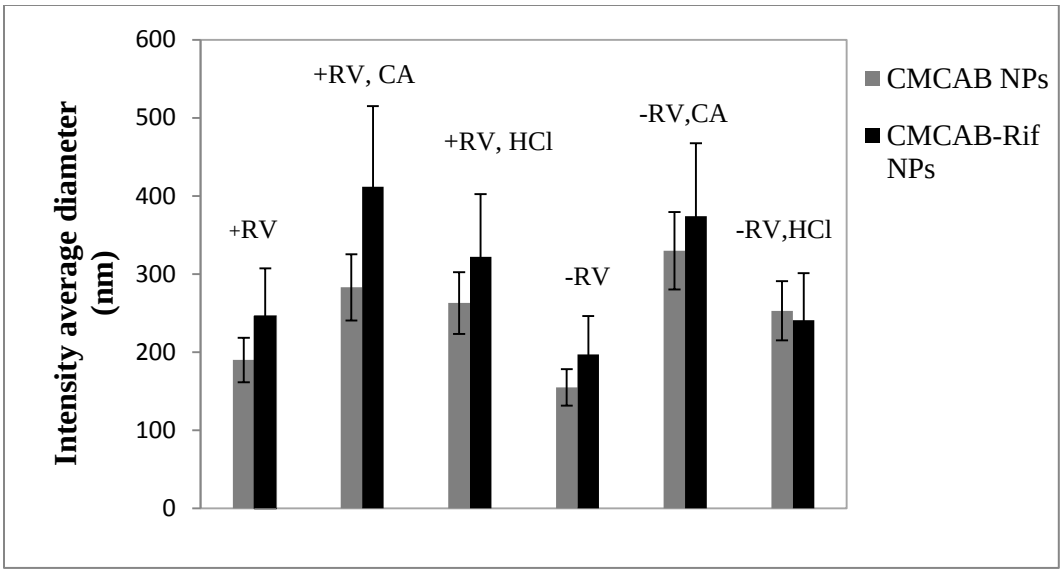

Figure 3. Intensity-average hydrodynamic diameters of CMCAB and rifampicin-CMCAB particles at pH 7 after acid flocculation followed by vacuum drying and then redispersion. +RV: rotary evaporation used; -RV rotary evaporation not used; CA = citric acid; HCl = hydrochloric acid. n = 3. Targeted rifampicin loading 25 wt%.

The acid-flocculated particles processed with rotary evaporation were ~50- 70 % larger than the unflocculated particles, whereas the sizes of the corresponding particles that were not processed with rotary evaporation were ~30-40% larger. For rifampicin-containing particles the relative standard deviation (RSD= standard deviation of particle diameter/particle diameter) was 22 % or less except with HCl, -RV. Some of the CMCAB cases such as rotary evaporated and flocculated with HCl, non-rotary evaporated control and non-rotary evaporated flocculated with HCl had higher RSD. The sizes of particles flocculated with a given acid did not depend greatly on whether rotary evaporation was used or not.

<u>After dialysis and freeze drying</u>

The particle sizes of rifampicin-CMCAB particles processed by dialysis and freeze drying are shown in Figure 4. Also shown are the sizes of the particles just after mixing in the

MIVM but before dialysis to illustrate the effect of this processing step. The batch-to-batch repeatability of the particle size (after freeze-drying and redispersion) was good with the relative standard deviation (= standard deviation/particle size) ~ 7 % established using data from 3 batches.

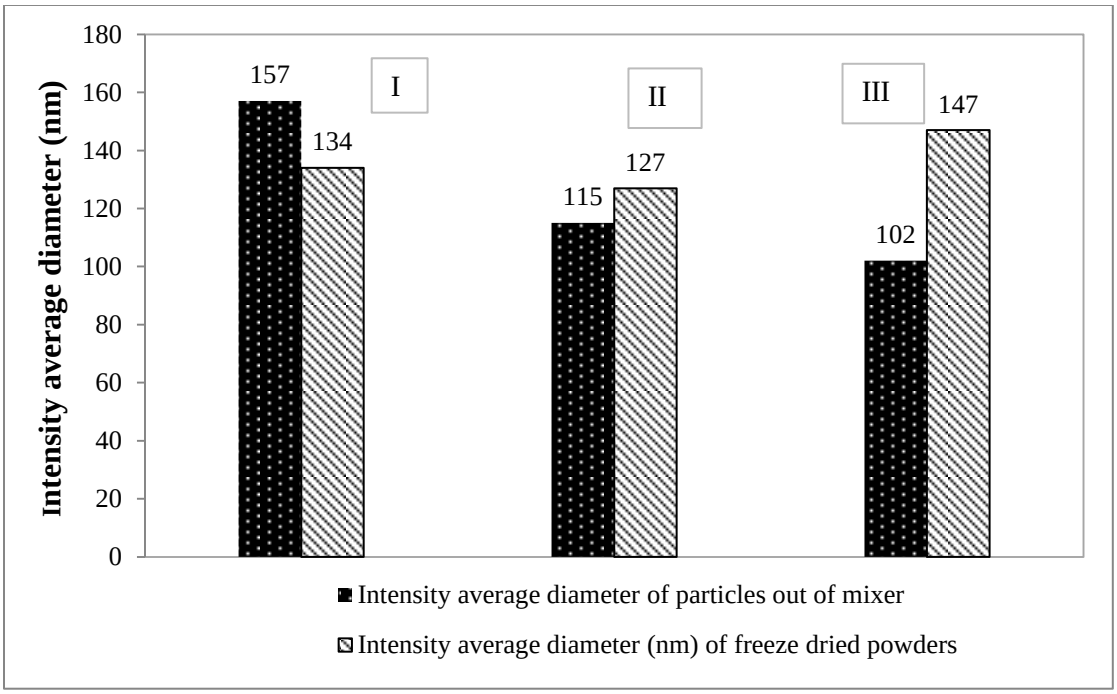

Figure 4. Particle sizes of 3 batches (I-III) of CMCAB and rifampicin-CMCAB particles after fabrication in the multi-inlet vortex mixer and after processing by dialysis and freeze drying followed by redispersion in water at pH 7. The targeted rifampicin composition was 25 wt%.

The microparticles were too large and too aggregated to be measure by dynamic light scattering and so they were characterized by FESEM.

The FESEM for the spray dried formulations demonstrated bowl-shaped collapsed poly-dispersed particles ranging from 2 -10 μm. During spraying and atomization of the liquid, some

droplets may have been larger than the others accounting for the variation in size of the particles seen in these images (Figure 5).

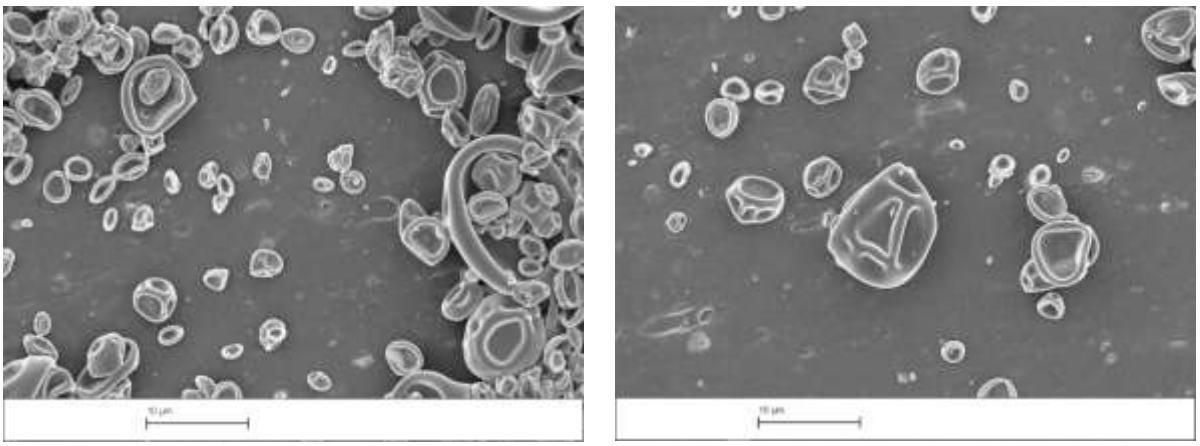

(a) (b)

Figure 5: Scanning electron microscope images for microparticles at 5Kx magnification. The bar in each image corresponds to 10 µm.

3.4.3 Rifampicin Drug Loading

<u>After processing by flocculation</u>

The rifampicin drug loadings of nanoparticles processed by acid flocculation are shown in Figure 6. Two of the 3 batches whose particle sizes were presented in Figure 3 were analyzed to characterize repeatability. The effect of variations of the processing conditions with and without rotary evaporation and acid flocculating agents on rifampicin loading were explored. Calculations of drug loading wt % (W_{rif}) and relative standard deviation of drug loading (σ_{Wrif}) used equations [S.9] and [S.10] (Supplementary Information). Drug loadings of samples subjected to rotary evaporation followed by flocculation with either citric acid or HCl were comparable. Drug loadings (W_{rif} = 16.6 wt% for batch A and = 15.2 wt% for batch B) were highest in the samples which were subjected to rotary evaporation and then flocculated with citric acid (see Table S.3 in Supporting Information for more details) whereas we observed relatively low drug loadings in non-rotary evaporated samples flocculated with HCl. For all of

these samples, the relative standard deviation (RSD) of the rifampicin loading in wt% - defined by RSD_{Wrif} = *100 % - was 3 % for all samples except the [–RV, HCl] case where RSD_{Wrif} = 7 %.

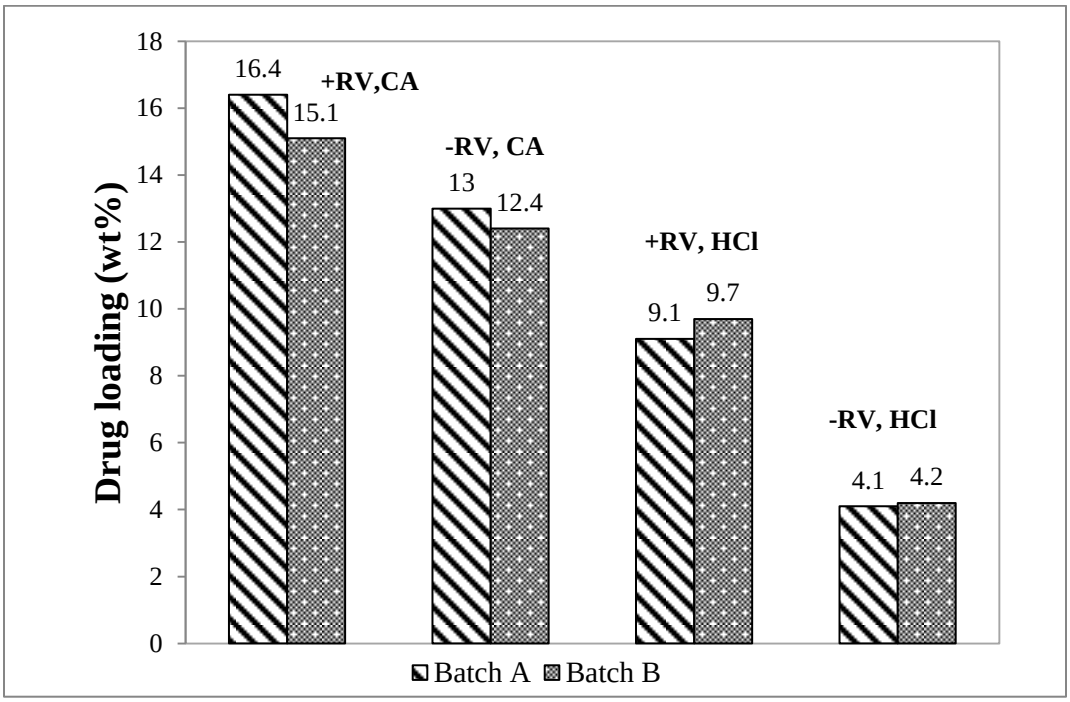

Figure 6. Rifampicin weight% in nanoparticles prepared by the flocculation method at different conditions as measured by UV-Visible spectrophotometry. +RV means rotary evaporation was used and -RV means rotary evaporation was not used. CA = citric acid, HCl = hydrochloric acid. Results for 2 batches are shown.

When the pH is lowered with either acid, it promotes flocculation by reducing the degree of ionization of the carboxylic groups in CMCAB. This reduces the electrostatic repulsion and also promotes hydrogen bonding between hydroxyls and ether oxygens in CMCAB chains on adjacent particles. The multivalent citric acid has an additional effect in that it can serves as a bridging flocculating agent between adjacent CMCAB particles.

At pH 2, citric acid could hydrogen bond with 2-3 positively charged rifampicin molecules. The binding of such a complex with CMCAB could explain the relatively high drug

loading. However, no such complexes of 2 or more rifampicin molecules could readily form with HCl. The higher rifampicin loadings in the particles flocculated with citric acid suggest that the solubility of rifampicin at pH 2 in citric acid may be lower than in HCl.

After dialysis and freeze drying

Drug loading in dialyzed and freeze dried particles was low (Figure 5). The targeted rifampicin loading was 25 wt% while the actual loadings were 10.1 wt%, 9.6 wt%, and 11.7 wt% in batches I, II, and III, respectively. The relative standard deviation RSD_{Wrif} was 7 % for these samples as calculated using equations S.9 and S.10. This is understandable given the solubility of rifampicin in THF and the enhanced water solubility due to these formulations. The drug loading of rifampicin in the microparticles of rifampicin-CMCAB made by spray drying was 9.2 wt%.

Further comparison of processing methods

To further explore the effects of the processing method on rifampicin loading and to minimize batch-to-batch variation, we prepared a batch of rifampicin-CMCAB nanoparticles and processed part by flocculation/vacuum filtration and part by dialysis/freeze drying. The particles processed by flocculation were not subjected to rotary evaporation because these samples flocculated more quickly than did the samples subjected first to rotary evaporation. As noted earlier, the flocculation time of samples processed using rotary evaporation was much shorter than that for samples that were not subjected to rotary evaporation (30 seconds compared to 30-45 minutes). We wanted to minimize the time that the particles were exposed to the THF/water mixture after exiting the multi-inlet vortex mixer in order to minimize the loss of rifampicin due to diffusion from the particles. The rifampicin loading was higher for the particles processed by flocculation/vacuum filtration - W_{rif} = 11.3 wt% corresponding to a drug loading efficiency of 45% - compared to that for the particles processed by dialysis/freeze drying where W_{rif} = 8.5

wt% corresponding to a drug loading efficiency of 34% (Table S.4. in supplementary information).

3.4.4 Particle morphology

The influence of CMCAB in the possible phase transformation in rifampicin-CMCAB nanoparticles and microparticles was investigated through X-ray diffraction. The X-ray diffraction pattern for the as-received rifampicin drug (as shown in Figure 7a) showed numerous strong distinctive peaks at ~ 12º, 14º, 18º, 21º at 2θ indicating high its crystalline nature. The polymer is amorphous in nature (Figure 7b). Some crystalline peaks for rifampicin were detected in the physical mixture, showing that the rifampicin in the physical mixture remains crystalline as expected. Finally, X-ray diffraction patterns of the nanoparticle and microparticle solid dispersions showed no diffraction peaks, indicating that the rifampicin therein was amorphous.

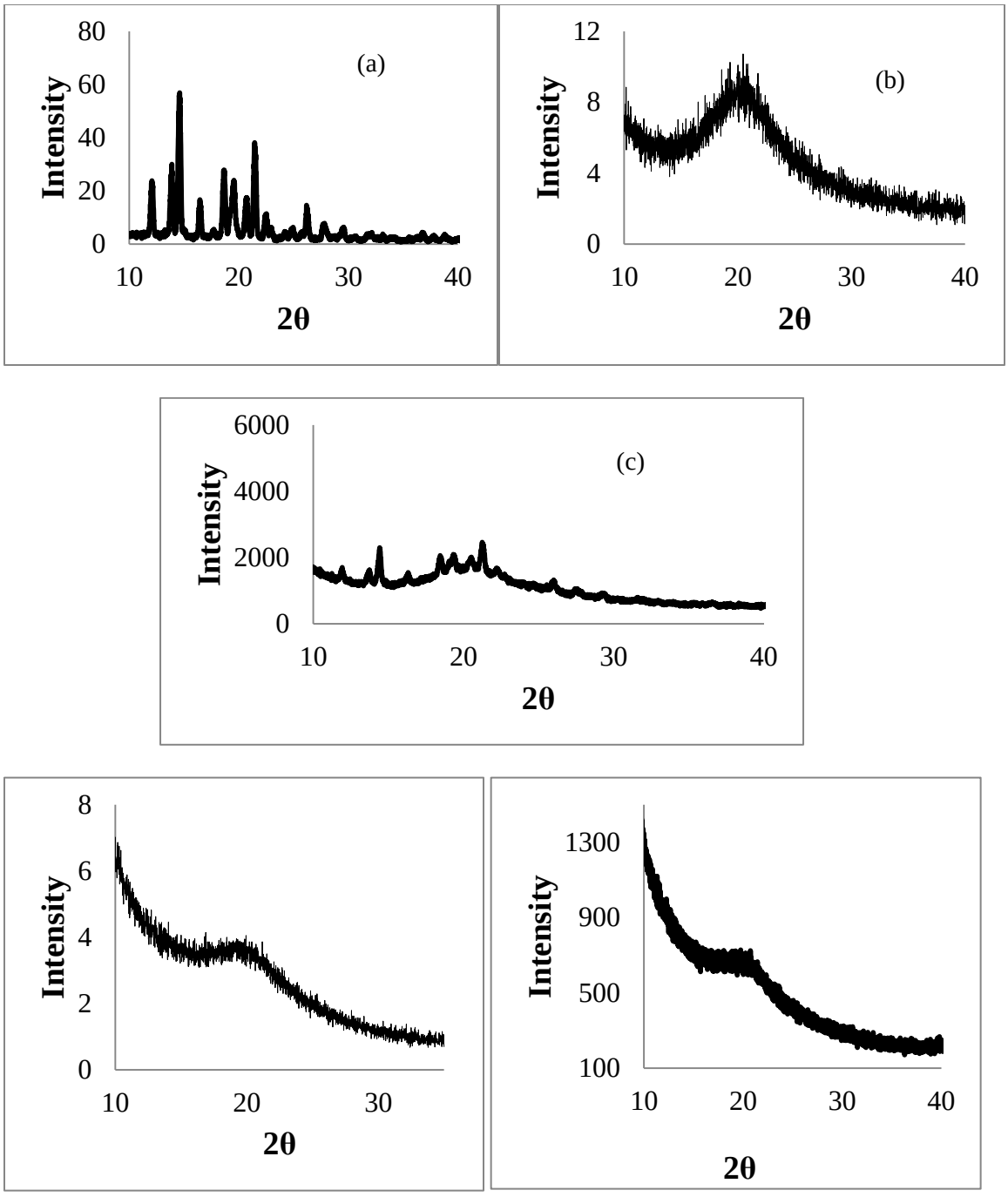

Figure 7. X-ray diffractograms of (a) Rifampicin, (b) CMCAB, (c) Rifampicin-CMCAB physical mixture, (d) Rifampicin-CMCAB nanoparticles (actual drug loading is 10 wt%), (e) Rifampicin-CMCAB microparticles

3.4.5 Dissolution studies

The percent drug release calculated from equation 2 for rifampicin from the nanoparticles is shown in Figure 8a and Figure 8b.

$$\%\, drug\ release\ =\ \frac{C_{experimental}}{C_{theoritical}} \qquad [2]$$

$C_{experimental}$ is calculated from HPLC and $C_{theoretical}$ is calculated from the known values of volume of the buffer solution, amount of particles and drug composition. The results from the dissolution experiment did not show any enhancement of drug release from the amorphous solid dispersion at pH 6.8 compared to the crystalline drug. Approximately, 83 % of the drug from microparticles and 100 % of the drug from nanoparticles was released in 6 hours. At the acidic pH of 1.2, there was no drug release from the microparticles, but there was drug release from the nanoparticles in about 30 minutes. Both the free drug and the drug from the nanoparticles started degrading after 2 hours. This suggests that nanoparticles of CMCAB might not be effective in protecting the drug from stomach acid degradation compared to the microparticles. Please note that the HPLC curve in Figure S.2 in the Supporting Information which was only used to quantitate rifampicin concentration in the dissolution studies.

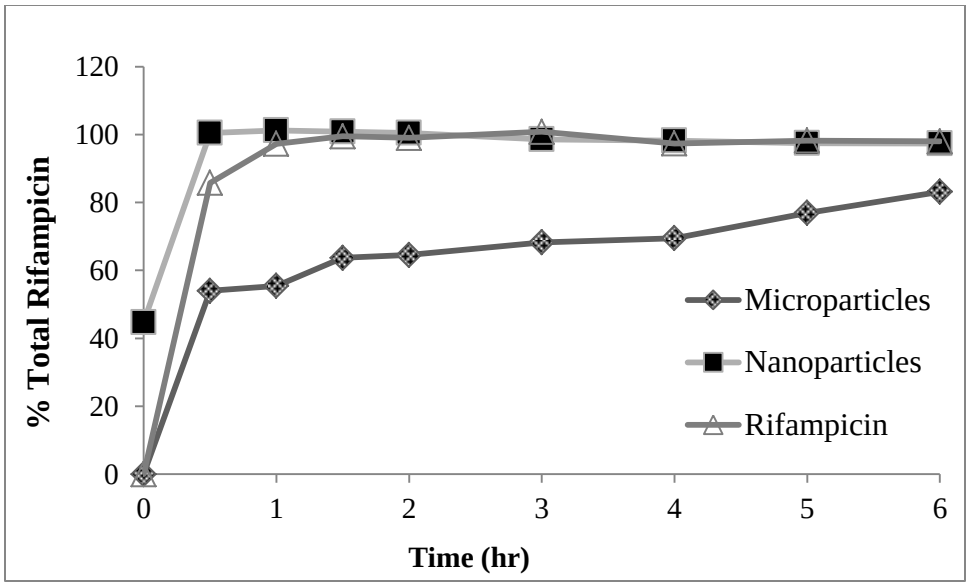

Figure 8a. Drug release profile of rifampicin from nanoparticles and microparticles compared to free rifampicin as received at pH 6.8

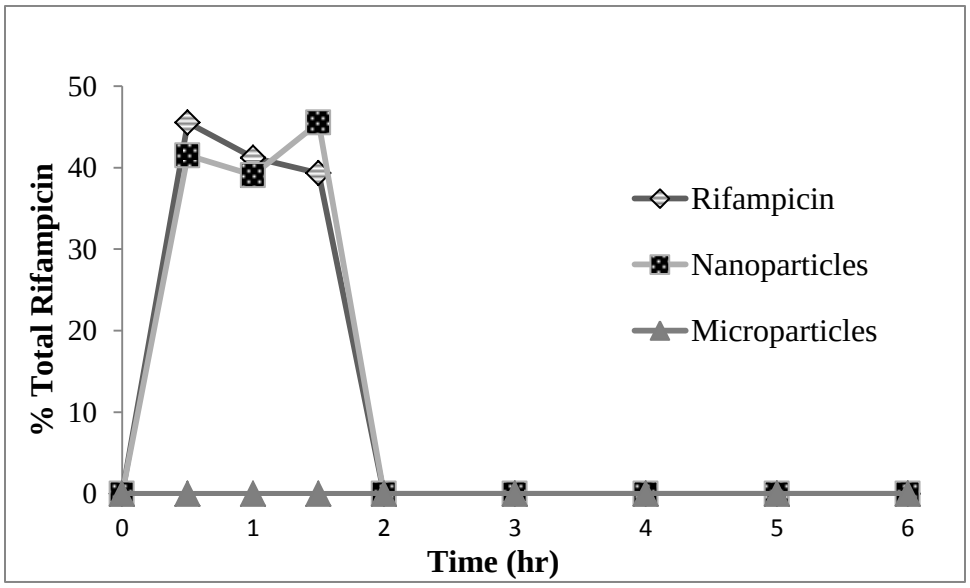

Figure 8b. Drug release profile of rifampicin from nanoparticles and microparticles compared to free rifampicin as received at pH 1.2

3.4.6 Minimum Inhibitory Concentrations for *M. Smegmatis*

It was important to understand how formulation into CMCAB nanoparticles impacts the MIC of rifampicin in these particles. Nanoparticle formulations could impact MIC by altering the amount of available rifampicin, the concentration vs. time profile, or by direct action of the polymer or the nanoparticles upon the bacterium. MIC values of the particles processed using the 4 combinations of rotary evaporation and acid flocculating for batches A and batch B for *M. Smegmatis* varied from 125-500 µg/ml (Table 2).

Table 2: Rifampicin formulations and MIC ranges for susceptibility of *M. Smegmatis

Rifampicin Formulations	**Batch A MIC (µg/ml) (Drug weight %, W_{rif})**	**Batch B MIC (µg/ml) (Drug weight %, W_{rif})**
*Free Rifampicin	15.6 -31.3	15.6-31.3
Rifampicin CMCAB (+RV, CA)	125-250 (16.4)	125-250 (15.1)
Rifampicin CMCAB (-RV, CA)	125-250 (13)	250-500 (12.4)
Rifampicin CMCAB (+RV, HCl)	125-250 (9.1)	250-500 (9.7)
Rifampicin CMCAB (-RV, HCl)	125-250 (4.1)	250-500 (3.2)

* The measured MIC of free rifampicin was 15.6-31.3 µg/ml which is consistent with reported literature value of 32 µg/ml

3.4.7 Cell Toxicity

Cytotoxicity assays are vital steps that provide insight to the cellular response to a toxicant. Also, they provide information regarding cell death, survival, and metabolic activities. MTS cytotoxicity assays were performed on all nanoparticle formulations to assess whether the rifampicin encapsulated CMCAB nanoparticles demonstrated in vitro toxicity (Figure 9). Figure

9 clearly indicates that CMCAB/rifampicin had no cytotoxic activity as the viability of cells after 24 hours of incubation was the same in all of the samples including control (no drug and particles). Cell viability was slightly lower in samples with free drug compared to drug loaded CMCAB irrespective of the method of sample preparation.

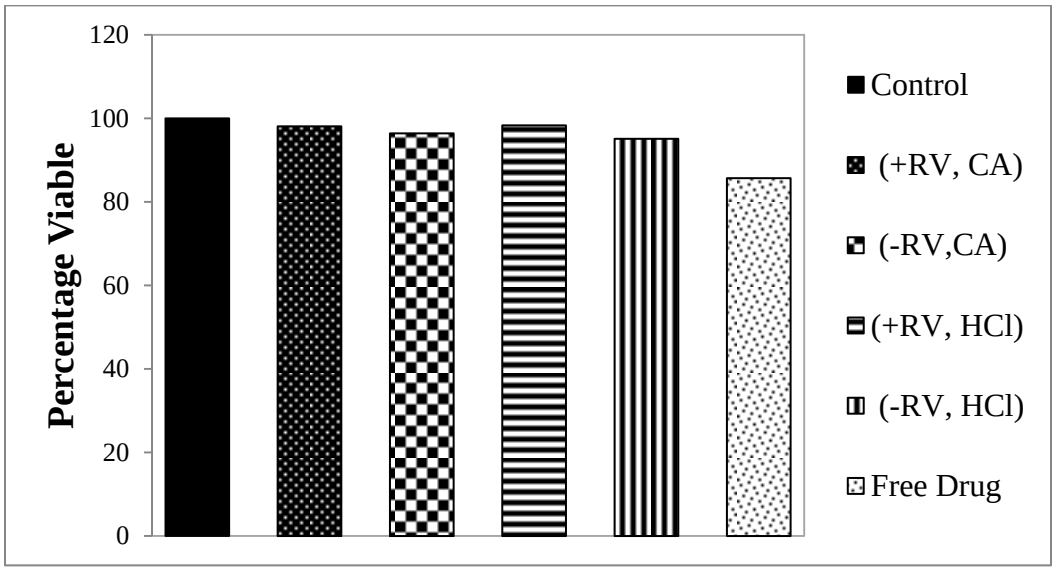

Figure 9. Cytotoxicity of rifampicin-CMCAB nanoparticle formulations (average of batch A and batch B) vs. free rifampicin. 500 µg/ml rifampicin, J774A.1 cell line.

In comparing the viability of cells exposed to rifampicin-containing nanoparticle formulations to that of control cells, the nanoparticles caused no biologically significant reduction in cell viability. Results from this analysis indicate that rifampicin-containing nanoparticles at 500 µg/ml are non-toxic to normal cells *in vitro.*

Results from the free drug rifampicin and particle formulations indicate that the antibacterial activity of rifampicin was preserved after CMCAB nanoparticle formation (Figure 6). The total weights (CMCAB+RIF) in the nanoparticle formulation were used and compared to that of the free rifampicin to more easily distinguish CMCAB particle components from bacterial growth during visual MIC analysis. The differences seen in the MIC values for nanoparticles

formulated under the same conditions in Batch A and B are due to variations in drug encapsulation efficiency between the groups.

3.5. CONCLUSIONS

This study demonstrates a methodology to produce rifampicin-CMCAB nanoparticle suspensions with a multi inlet vortex mixer which is a rapid and scalable method. The amorphous solid dispersions of these nanoparticles were formed for the first time. The intensity-average hydrodynamic diameters ranged from 100 to 400 nm. The flocculation step followed by vacuum filtration served to be a useful separation technique for the particles. Both citric acid and dilute hydrochloric acid gave comparable results, inducing flocculation in almost the same times. There was a significant difference in the flocculation time of rotary evaporated samples (30 seconds) compared to non-rotary evaporated samples (30-45 minutes). The flocculation/vacuum filtration process is significantly faster than the dialysis/freeze drying process in purifying rifampicin-CMCAB nanoparticles.

The particles processed by acid flocculation were not easily dispersible so probe sonication was used to redisperse the particles in DI water. However, particles processed by dialysis/freeze drying were much easily redispersed. Particles processed by the flocculation/vacuum filtration process also had higher rifampicin loadings than did particles processed by dialysis/freeze drying. It was shown that rifampicin-containing nanoparticles at 500 μg/ml were non-toxic *in vitro*. The biological activity of rifampicin was well preserved after CMCAB nanoparticle formation. The nanoparticles were compared to microparticles of Rifampicin-CMCAB (particle size between 2-10 μm). Both the particles consist of amorphous drug. The release studies of the drug showed that the nanoparticles have higher release than that of microparticles and the crystalline rifampicin at pH 6.8. There is also release of rifampicin

from nanoparticles at pH 1.2. The microparticles were shown to protect the drug from releasing in stomach acid conditions.

ACKNOWLEDGEMENT

The authors gratefully acknowledge funding and support from the Macromolecules and Interface Institute and the National Science Foundation, (under Contract # DMR 0909065). The authors thank Eastman Chemical Company for kindly donating the CMCAB polymer. The authors also thank Rick Caudill, Research Specialist, Department of Sustainable Biomaterials, Virginia Tech for his assistance with the PXRD analysis and Mr. Steve McCartney of the Institute for Critical Technology and Applied Science-Nanoscale Characterization and Fabrication Laboratory (ICTAS-NCFL) at Virginia Tech for help with the FESEM images.

3.6 References

1. Organization, W. H. *2010/2011 Tuberculosis Global Facts*; WHO: **2010**.

2. Gelperina, S.; Kisich, K.; Iseman, M. D.; Heifets, L., The potential advantages of nanoparticle drug delivery systems in chemotherapy of tuberculosis. *American Journal of Respiratory and Critical Care Medicine* **2005,** *172* (12), 1487-1490.

3. Panchagnula, R.; Agrawal, S., Biopharmaceutic and pharmacokinetic aspects of variable bioavailability of rifampicin. *International Journal of Pharmaceutics* **2004,** *271* (1-2), 1-4.

4. Sensi P, Margalith P, Timbal MT., Rifomycin, a new antibiotic—preliminary report. *Farmaco Ed Sci* **1959,** 14, 146–147

5. Petros, R. A.; Desimone, J. M., Strategies in the design of nanoparticles for therapeutic applications. *Nat Rev Drug Discov* **2010,** *9* (8), 615-627.

6. Lavelle, E. C.; Sharif, S.; Thomas, N. W.; Holland, J.; Davis, S. S., The importance of gastrointestinal uptake of particles in the design of oral delivery systems. *Advanced Drug Delivery Reviews* **1995,** *18* (1), 5-22.

7. Daugherty, A. L.; Mrsny, R. J., Regulation of the intestinal epithelial paracellular barrier. *Pharmaceutical Science & Technology Today* **1999,** *2* (7), 281-287.

8. Gaucher, G.; Satturwar, P.; Jones, M.-C.; Furtos, A.; Leroux, J.-C., Polymeric micelles for oral drug delivery. *European Journal of Pharmaceutics and Biopharmaceutics* **2010,** *76* (2), 147-158.

9. Löbenberg, R.; Kim, J. S.; Amidon, G. L., Pharmacokinetics of an immediate release, a controlled release and a two pulse dosage form in dogs. *European Journal of Pharmaceutics and Biopharmaceutics* **2005,** *60* (1), 17-23.

10. Ito, F.; Makino, K., Preparation and properties of monodispersed rifampicin-loaded poly(lactide-co-glycolide) microspheres. *Colloids and Surfaces B: Biointerfaces* **2004,** *39* (1–2), 17-21.

11. Durán, N.; Alvarenga, M. A.; Silva, E. C.; Melo, P. S.; Marcato, P. D., Microencapsulation of antibiotic rifampicin in poly(3-hydroxybutyrate-co-3-hydroxyvalerate). *Archives of Pharmacal Research* **2008,** *31* (11), 1509-1516.

12. Gupta, K. C.; Fawzi Habeeb, J., Controlled-release formulations for hydroxy urea and rifampicin using polyphosphate-anion-crosslinked chitosan microspheres. *J Appl Polym Sci* **2007,** *104* (3), 1942-1956.

13. Samad, A.; Sultana, Y.; Khar, R. K.; Chuttani, K.; Mishra, A. K., Gelatin microspheres of rifampicin cross-linked with sucrose using thermal gelation method for the treatment of tuberculosis. *Journal of Microencapsulation* **2008,** *26* (1), 83-89.
14. Anisimova, Y. V.; Gelperina, S. I.; Peloquin, C. A.; Heifets, L. B., Nanoparticles as antituberculosis drugs carriers: effect on activity against mycobacterium tuberculosis in human monocyte-derived macrophages. *Journal of Nanoparticle Research* **2000,** *2* (2), 165-171.
15. Esmaeili, F.; Hosseini-Nasr, M.; Rad-Malekshahi, M.; Samadi, N.; Atyabi, F.; Dinarvand, R., Preparation and antibacterial activity evaluation of rifampicin-loaded poly lactide-co-glycolide nanoparticles. *Nanomedicine : nanotechnology, biology, and medicine* **2007,** *3* (2), 161-167.
16. Pandey, R.; Khuller, G. K., Subcutaneous nanoparticle-based antitubercular chemotherapy in an experimental model. *Journal of Antimicrobial Chemotherapy* **2004,** *54* (1), 266-268.
17. Sung, J.; Padilla, D.; Garcia-Contreras, L.; Verberkmoes, J.; Durbin, D.; Peloquin, C.; Elbert, K.; Hickey, A.; Edwards, D., Formulation and pharmacokinetics of self-assembled rifampicin nanoparticle systems for pulmonary delivery. *Pharmaceutical Research* **2009,** *26* (8), 1847-1855.
18. Pandey, R.; Khuller, G. K., Antitubercular inhaled therapy: opportunities, progress and challenges. *Journal of Antimicrobial Chemotherapy* **2005,** *55* (4), 430-435.
19. Pandey, R.; Sharma, A.; Zahoor, A.; Sharma, S.; Khuller, G. K.; Prasad, B., Poly (dl-lactide-co-glycolide) nanoparticle-based inhalable sustained drug delivery system for experimental tuberculosis. *Journal of Antimicrobial Chemotherapy* **2003,** *52* (6), 981-986.
20. Sharma, A.; Pandey, R.; Sharma, S.; Khuller, G. K., Chemotherapeutic efficacy of poly (dl-lactide-co-glycolide) nanoparticle encapsulated antitubercular drugs at sub-therapeutic dose against experimental tuberculosis. *International Journal of Antimicrobial Agents* **2004,** *24* (6), 599-604.
21. Ahmad, Z.; Pandey, R.; Sharma, S.; Khuller, G. K., Pharmacokinetic and pharmacodynamic behaviour of antitubercular drugs encapsulated in alginate nanoparticles at two doses. *International Journal of Antimicrobial Agents* **2006,** *27* (5), 409-416.
22. Johnson, B. K.; Prud'homme, R. K., Flash NanoPrecipitation of organic actives and block copolymers using a confined impinging jets mixer. *Australian Journal of Chemistry* **2003,** *56* (10), 1021-1024.
23. Johnson, B. K.; Prud'homme, R. K., Chemical processing and micromixing in confined impinging jets. *AIChE Journal* **2003,** *49* (9), 2264-2282.

24. Johnson, B. K.; Prud'homme, R. K., Mechanism for Rapid Self-Assembly of Block Copolymer Nanoparticles. *Physical Review Letters* **2003,** *91* (11), 118302.

25. Liu, Y.; Kathan, K.; Saad, W.; Prud'homme, R. K., Ostwald ripening of β-carotene nanoparticles. *Physical Review Letters* **2007,** *98* (3), 036102.

26. Liu, Y.; Cheng, C.; Prud'homme, R. K.; Fox, R. O., Mixing in a multi-inlet vortex mixer (MIVM) for flash nano-precipitation. *Chemical Engineering Science* **2008,** *63* (11), 2829-2842.

27. Gindy, M. E.; Ji, S.; Hoye, T. R.; Panagiotopoulos, A. Z.; Prud'homme, R. K., Preparation of Poly(ethylene glycol) protected nanoparticles with variable bioconjugate ligand density. *Biomacromolecules* **2008,** *9* (10), 2705-2711.

28. Gindy, M. E.; Panagiotopoulos, A. Z.; Prud'homme, R. K., Composite Block Copolymer Stabilized Nanoparticles: Simultaneous encapsulation of organic actives and inorganic nanostructures. *Langmuir* **2007,** *24* (1), 83-90.

29. Ji, S.; Zhu, Z.; Hoye, T. R.; Macosko, C. W., Maleimide functionalized poly(ε-caprolactone)-block-poly(ethylene glycol) (pcl-peg-mal): synthesis, nanoparticle formation, and thiol conjugation. *Macromolecular Chemistry and Physics* **2009,** *210* (10), 823-831.

30. Ungun, B.; Prud'homme, R. K.; Budijon, S. J.; Shan, J.; Lim, S. F.; Ju, Y.; Austin, R., Nanofabricated upconversion nanoparticles for photodynamic therapy. *Opt. Express* **2009,** *17* (1), 80-86.

31. Kumar, V.; Hong, S. Y.; Maciag, A. E.; Saavedra, J. E.; Adamson, D. H.; Prud'homme, R. K.; Keefer, L. K.; Chakrapani, H., Stabilization of the nitric oxide (no) prodrugs and anticancer leads, PABA/NO and double JS-K, through incorporation into peg-protected nanoparticles. *Molecular Pharmaceutics* **2009,** *7* (1), 291-298.

32. Chen, T.; D'addio, S. M.; Kennedy, M. T.; Swietlow, A.; Kevrekidis, I. G.; Panagiotopoulos, A. Z.; Prud'homme, R. K., Protected peptide nanoparticles: experiments and brownian dynamics simulations of the energetics of assembly. *Nano Letters* **2009,** *9* (6), 2218-2222.

33. Ansell, S. M.; Johnstone, S. A.; Tardi, P. G.; Lo, L.; Xie, S.; Shu, Y.; Harasym, T. O.; Harasym, N. L.; Williams, L.; Bermudes, D.; Liboiron, B. D.; Saad, W.; Prud'homme, R. K.; Mayer, L. D., Modulating the therapeutic activity of nanoparticle delivered paclitaxel by manipulating the hydrophobicity of prodrug conjugates. *Journal of Medicinal Chemistry* **2008,** *51* (11), 3288-3296.

34. D'addio, S. M.; Prud'homme, R. K., Controlling Drug Nanoparticle Formation By Rapid Precipitation. *Advanced Drug Delivery Reviews* **2011,** *63* (6), 417-426.

35. (a) D'addio, S. M. Tuberculosis Therapeutics: Engineering Of Nanomedicinal Systems For Local Delivery Of Targeted Drug Cocktails (Doctoral Dissertation). Princeton University, **2012**; (b) Ying, L. Formulating Nanoparticles By Flash Nanoprecipitation For Drug Delivery And Sustained Release (Doctoral Dissertation). Princeton University, **2007**.

36. Hancock, B.; Parks, M., What is the True Solubility Advantage for Amorphous Pharmaceuticals? *Pharmaceutical Research* **2000,** *17* (4), 397-404.

37. Ginés, J. M.; Arias, M. J.; Moyano, J. R.; Sánchez-Soto, P. J., Thermal investigation of crystallization of polyethylene glycols in solid dispersions containing oxazepam. *International Journal of Pharmaceutics* **1996,** *143* (2), 247-253.

38. Marsac, P.; Konno, H.; Rumondor, A. F.; Taylor, L., Recrystallization of nifedipine and felodipine from amorphous molecular level solid dispersions containing poly(vinylpyrrolidone) and sorbed water. *Pharmaceutical Research* **2008,** *25* (3), 647-656.

39. (a) Shelton Michael, C.; Posey-Dowty Jessica, D.; Lingerfelt, L.; Kirk Shane, K.; Klein, S.; Edgar Kevin, J.; Enhanced dissolution of poorly soluble drugs from solid dispersions in carboxymethylcellulose acetate butyrate matrices. In *Polysaccharide Materials: Performance by Design*, *American Chemical Society* **2009**, 1017, 93-113; (b) Posey-Dowty, J.; Watterson, T.; Wilson, A.; Edgar, K.; Shelton, M.; Lingerfelt, L., Zero-order release formulations using a novel cellulose ester. *Cellulose* **2007,** *14* (1), 73-83.

40. Min-Soo Kim, J.-S. K., Hee Jun Park, Won Kyung Cho, Kwang-Ho Cha, and Sung-Joo Hwang, Enhanced bioavailability of sirolimus via preparation of solid dispersion nanoparticles using a supercritical antisolvent process. *Int J Nanomedicine* **2011,** *6*, 2997-3009.

41. Matteucci, M. E.; Brettmann, B. K.; Rogers, T. L.; Elder, E. J.; Williams, R. O.; Johnston, K. P., Design of potent amorphous drug nanoparticles for rapid generation of highly supersaturated media. *Molecular Pharmaceutics* **2007,** *4* (5), 782-793.

42. Onoue, S.; Uchida, A.; Takahashi, H.; Seto, Y.; Kawabata, Y.; Ogawa, K.; Yuminoki, K.; Hashimoto, N.; Yamada, S., Development of high-energy amorphous solid dispersion of nanosized nobiletin, a citrus polymethoxylated flavone, with improved oral bioavailability. *Journal of Pharmaceutical Sciences* **2011,** *100* (9), 3793-3801.

43. Watanabe, T.; Hasegawa, S.; Wakiyama, N.; Kusai, A.; Senna, M., Comparison between polyvinylpyrrolidone and silica nanoparticles as carriers for indomethacin in a solid state dispersion. *International Journal of Pharmaceutics* **2003,** *250* (1), 283-286.

44. (a) Li, B.; Konecke, S.; Harich, K.; Wegiel, L.; Taylor, L. S.; Edgar, K. J., Solid dispersion of quercetin in cellulose derivative matrices influences both solubility and stability. *Carbohydrate Polymers* **2013,** *92* (2), 2033-2040; (b) Li, B.; Harich, K.; Wegiel, L.; Taylor, L. S.; Edgar, K. J., Stability and solubility enhancement of ellagic acid in cellulose ester solid dispersions. *Carbohydrate Polymers* **2013,** *92* (2), 1443-1450.

45. Malabarba, A., Ferrari, P., Depaoli, A., Gallo, G. G. & Cavalleri, B. , Synthesis and conformation of some acetyl derivatives of rifampicin. *Farmaco Scientifica* **1986,** *41*, 131-50.

46. In *Performance Standards for Antimicrobial Susceptibility Testing; Seventeenth Informational Supplement M100-S17.* , Clinical and laboratory Standards Institute (CLSI): **2007**, 27.

47. Liu, Y., Cheng, C., Prud'homme, R. K., Fox, R. O., Mixing in a multi-inlet vortex mixer (MIVM) for flash nano-precipitation. *Chemical Engineering Science* **2008,** *63* (11), 2829-2842.

48. D'addio, S. M., Kafka, C., Akbulut, M.; Beattie, P., Saad, W., Herrera, M., Kennedy, M. T., Prud'homme, R. K., Novel method for concentrating and drying polymeric nanoparticles: hydrogen bonding coacervate precipitation. *Molecular Pharmaceutics* **2010,** *7* (2), 557-564.

49. Wriedt, T., *Mie Theory: A Review*. *Springer-Verlag Berlin Heidelberg* **2012,** Vol. 169.

3.7. Supporting Information

Calculation of Reynolds number in the multi-inlet vortex mixer

$$R_e = D_{mixer} \sum \frac{u_i}{v_i} = D_{mixer} \left(\frac{u_1}{v_1} + \frac{u_2}{v_2} + \frac{u_3}{v_3} + \frac{u_4}{v_4} \right) \quad [S.1]$$

where u_i is the velocity of each individual inlet stream and v_i is the kinematic viscosity (density over viscosity) of each inlet solvent at the mixer temperature. The volumetric flow rate, Q_i, is determined by the equation:

$$Q_i = u_i A_{is} \quad [S.2]$$

where A_{is} is the cross-sectional area of the inlet streams. When A_{is} is the same for all four streams and it is assumed that the solution formed by mixing is ideal, i.e. there is no volume change upon mixing, the liquid phase volume fractions ϕ_i are calculated from:

$$\emptyset_i = \frac{u_i}{u_1 + u_2 + u_3 + u_4} \quad [S.3].$$

For the drug/polymer nanoparticles, u_1, and for antisolvent, $u_2 = u_3 = u_4$. Substituting these into Equation 3 for the volume fraction and designating stream 1 as the organic stream

$$\emptyset_1 = \frac{u_1}{u_1 + 3u_{2\text{-}4}} \quad [S.4]$$

or

$$u_1 = \frac{3\emptyset_{THF}}{1 - \emptyset_{THF}} u_{2\text{-}4} \quad [S.5]$$

Using the inlet velocities of the different streams as a function of the volume fraction of the drug stream produces a calculation of the Reynolds number using Equation 1:

$$R_e = D_{mixer} \left(\frac{u_1}{v_1} + \frac{u_2}{v_2} + \frac{u_3}{v_3} + \frac{u_4}{v_4} \right) = D_{mixer} \left(\frac{u_1}{v_1} + 3\frac{u_{2\text{-}4}}{v_2} \right) = D_{mixer} \left(\frac{3\emptyset_{THF}}{1 - \emptyset_{THF}} \frac{u_{2\text{-}4}}{v_1} + 3\frac{u_{2\text{-}4}}{v_2} \right)$$

$$R_e = 3u_{2\text{-}4} D_{mixer} \left(\frac{\emptyset_{THF}}{1 - \emptyset_{THF}} \frac{1}{v_1} + \frac{1}{v_2} \right) \quad [S.6]$$

$$x = \left(\frac{\emptyset_{THF}}{1 - \emptyset_{THF}} \frac{1}{v_1} + \frac{1}{v_2} \right)$$

where v_1 – v_4 are the kinematic viscosities of the stream 1-4.

Equation [S.6] simplifies to:

$$R_e = 3u_{2\text{-}4} D_{mixer}\, x$$

and is then used to solve for the volumetric flow rates of inlets 2-4 as a function of the Reynolds number:

$$Q_{2\text{-}4} = \frac{R_e A_{2-4}}{3D_{mixer}\, x} \qquad [S.7]$$

Calculation of Drug Loading

Construction of calibration curve

In order to measure the rifampicin loading of the CMCAB nanoparticles, a calibration curve (**Figure S.1**) for the rifampicin dissolved in acetonitrile was developed using a UV–Visible spectrophotometer (Thermo Scientific, Evolution 300) at a wavelength of 475 nm where the absorbance was a maximum. In a typical experiment, 10 mgs of Rifampicin were dissolved in a 10 ml volumetric flask containing 2 ml acetonitrile. More acetonitrile was added up to the 10 ml mark to prepare the stock solution of rifampicin in acetonitrile. This solution was serially diluted with acetonitrile to make solutions with rifampicin concentrations of 10, 20, 30, 40, 50, 60, and 70 µg/ml. The equation for the calibration curve of rifampicin in acetonitrile is

$$\text{Absorbance at 475 nm} = 0.0153C_{rif} + 0.0096 \qquad [S.8]$$

where $R^2 = 0.9999$

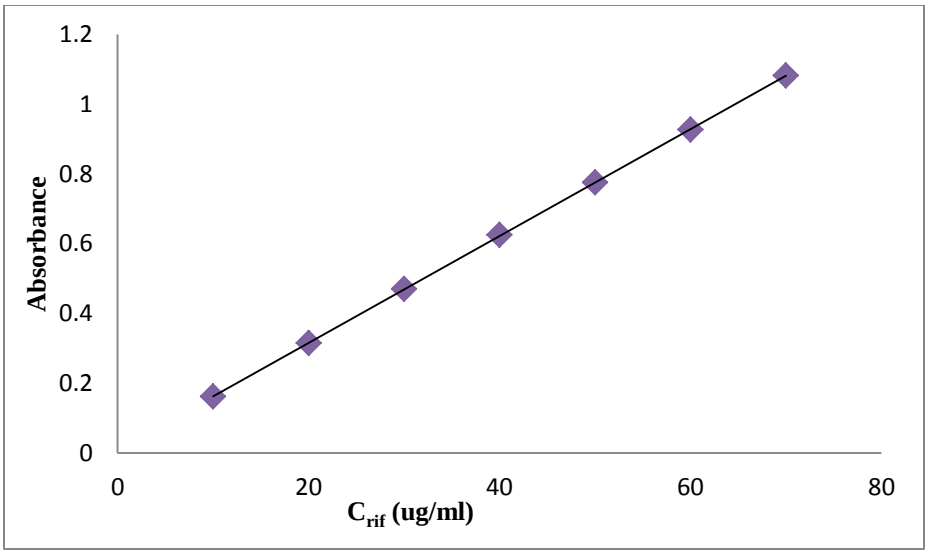

Fig. S.1. Calibration curve of rifampicin dissolved in acetonitrile at 475 nm to quantitate the rifampicin compositions in the nanoparticles

The dry powders (concentration of 1 mg/ml i.e. 15 mgs of powder dissolved in 15 ml of acetonitrile) of Rifampicin-CMCAB were dissolved in acetonitrile and shaken for 15 minutes in a wrist action shaker. The sample was placed in a quartz cuvette that was used for spectrophotometric measurements. The same cuvette was used to do a baseline correction with the pure acetonitrile before analyzing any samples.

The drug loading W_{rif} for the dried particles (after dissolving them in acetonitrile) is given by:

$$W_{rif} = \frac{Final\ concentration\ of\ the\ Rifampicin\ in\ the\ solvent}{Initial\ concentration\ of\ particles\ in\ the\ solvent}\ x\ 100 = \frac{C_{rif}}{C_{part}} \text{ x } 100 \qquad [S.9]$$

C_{rif} = Concentration of the drug calculated from calibration curve equation 1.

C_{part}= Concentration of the particles dissolved in acetonitrile.

The standard deviation of the drug loading σ_{Wrif} of the rifampicin-CMCAB nanoparticles is given by:

$$\sigma_{Xrif}^2 = \sigma_{Crif}^2 \left(\frac{m_{Ace}}{\rho_{Ace}\, m_{comp}}\right)^2 + \sigma_{mAce}^2 \left(\frac{C_{rif}}{\rho_{Ace} m_{comp}}\right)^2 + \sigma_{mcomp}^2 \left(\left(\frac{C_{rif} m_{Ace}}{\rho_{Ace}}\right)\left(\frac{1}{m_{comp}^2}\right)\right)^2$$

$$\sigma_{W_{rif}} = \sigma_{X_{rif}} \times 100 \qquad [S.10]$$

where:

σ_{Xrif} = standard deviation of mass fraction of Rifampicin drug in the particles

σ_{wrif} = standard deviation of weight fraction of Rifampicin drug in the particles

m_{Ace} = mass of acetonitrile which is used to make samples. For example, the mass of 1.5 mls of acetonitrile that were typically used in the experiments would be used here.

m_{comp} = mass of the complex used in the drug loading measurements.

σ_{mAce} = standard deviation of the mass of acetonitrile used to make sample. For example, 1.5 mls of acetonitrile were measured into a pre-weighed bottle and the mass was measured. This was done 5 times and the information was used to calculate σ_{mAce} = 0.1649 grams.

σ_{mcomp} = standard deviation of the mass of the dried complexes. For example, a typical mass of complex was weighed on the balance and the balance readout was observed over a period of 1 minute, recording the magnitude of the fluctuation in the measurement, Δm_{fluct}, (the maximum-to-minimum value of the mass). Here σ_{mcomp} = 0.0001 gms.

σ^2_{crif} = standard deviation of the rifampicin concentration measured with the UV-Visible spectrophotometer and is given by:

$$\sigma_{Crif}^2 = \sigma_{Abs}^2 (\frac{1}{b})^2 + \sigma_a^2 \left(\frac{1}{b}\right)^2 + \sigma_b^2 \left(\frac{Abs - a}{b^2}\right)^2 \qquad [S.11]$$

where:

σ_{Abs} = standard deviation of the absorbance measurement. This can be estimated from information about the typical uncertainty of the instrumental measurement of the absorbance. In this work, $\sigma_{Abs} \approx 0.004$ based on information from the manual of the UV –Visible Spectrophotometer (Thermo Scientific, Evolution 300).

a = y- intercept of the absorbance-calibration curve = 0.018285714

b = slope of the absorbance-calibration curve = 0.015192857

σ_a^2 = variance of the y intercept = 0.000958265

σ_b^2 = variance of the slope = 4.79133×10^{-7}

When the concentration of a sample is 62 µg/ml and the absorbance is 0.953

We can write from equation S.11,

$$\sigma_{Crif}^2 =$$

$$0.004^2 \times \left(\frac{1}{0.015192857}\right)^2 + 0.000958265 \times \left(\frac{1}{0.015192857}\right)^2 +$$

$$(4.79133 * 10^{-7} \left(\frac{0.953 - 0.018285714}{0.015192857^2}\right)^2$$

σ_{Crif}^2 = 12.077

Now putting the value of σ_{Crif}^2 in equation S.10, and substituting the following

σ_{mAce} = 16491 µg

ρ_{Ace} = 787000 µg/ml

m_{comp} = 1500 µg

m_{Ace}/ρ_{Ace} = V_{Ace} = volume of acetonitrile = 1.5 mls

We can write equation S.10 as,

$$\sigma_{Xrif}^2 = (12.077)\left(\frac{1.5}{1500}\right)^2 + (16491)^2\left(\frac{62}{78700 \times 1500}\right)^2 + 100^2\left((62 \times 1.5)\left(\frac{1}{1500^2}\right)\right)^2$$

σ_{Xrif}^2 = $2.97 * 10^{-5}$

$or\ \sigma_{Xrif}$ = 0.005

$\sigma_{wrif} = \sigma_{Xrif} \times 100 = 0.5$

Calculation of Drug Concentration during Dissolution Studies

Construction of calibration curve

In order to measure the rifampicin concentration of the CMCAB nanoparticles and microparticles in potassium phosphate buffer during dissolution studies, a calibration curve (**Figure S.2**) for the rifampicin dissolved in acetonitrile was developed using a High Performance Liquid Chromatograohy (Agilent 1200) at a wavelength of 254 nm. In a typical experiment, 10 mgs of Rifampicin were dissolved in a 10 ml volumetric flask containing 2 ml acetonitrile. More acetonitrile was added up to the 10 ml mark to prepare the stock solution of rifampicin in acetonitrile. This solution was serially diluted with acetonitrile to make solutions with rifampicin concentrations of 10, 20, 30, 40, 50 and 60 µg/ml. The equation for the calibration curve of rifampicin in acetonitrile is:

Area under the curve at 254 nm = $2.446C_{rif} - 8.86$ [S.8]

where $R^2 = 0.999$

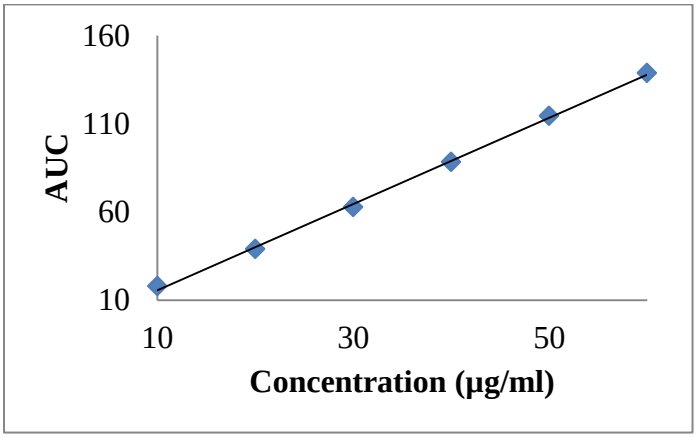

Fig. S.2. Calibration curve of rifampicin dissolved in acetonitrile at 254 nm used to quantitate the rifampicin concentration in the dissolution experiments

Table S.1. Particle Size Analysis of CMCAB particles after recovering them by vacuum filtration and drying in vacuum oven for 5-6 hours at room temperature by DLS – at different rotary evaporation conditions and addition of different excipients. The average results from 3 batches are shown.

CMCAB (Rotary evaporation conditions)	**Excipient (pH ≈2)**	**Intensity average diameter (nm) in DI water (NaOH added) (RSD)**	**PDI**	**Intensity average diameter (nm) in PBS**	**PDI**
Rotary evaporated (control)	None	190±0.19	0.19 ±0.04	-	-
Rotary evaporated	1 wt% citric acid	283± 0.19	0.2 ±0.04	270±0.08	0.14±0.04
Rotary evaporated	1 wt% dil. HCl	263±0.24	±0.04	282±0.04	±0.04
Non-rotary evaporated (control)	None	155±0.28	0.14±0. 04	-	-
Non-rotary evaporated	1wt% citric acid	330±0.27	0.12±0. 04	258±0.27	0.23±0.04
Non-rotary evaporated	1 wt% dil. HCl	253±0.18	0.17±0. 04	282±0.24	±0.04

Table S.2. Particle Size Analysis of Rifampicin-CMCAB particles after recovering them by vacuum filtration and drying in vacuum oven for 5-6 hours at room temperature by DLS - at different rotary evaporation conditions and addition of different excipients. The average results from 3 batches are shown.

CMCAB-Rif (Rotary evaporation conditions)	**Excipient (pH ≈ 2)**	**Intensity average diameter (nm) in DI water (NaOH added) - RSD**	**PDI**	**Intensity average diameter (nm) in PBS**	**PDI**
Rotary evaporated (control)	None	246±0.13	0.17±0.04	-	-
Rotary evaporated	1 wt% citric acid	412±	0.16±0.04	301±0.18	0.23±0.04
Rotary evaporated	1 wt% dil. HCl	322±0.21	0.2±0.04	257±0.20	0.21±0.04
Non-rotary evaporated (control)	None	197±	0.15±0.04	-	-
Non-rotary evaporated	1wt% citric acid	374±0.2	0.18±0.04	238±0.21	0.15±0.04
Non-rotary evaporated	1 wt% dil. HCl	241±0.28	0.18±0.04	229±0.08	0.21±0.04

Table S.3. Drug loading of complexes prepared by the acid flocculation method at different conditions.

Sample	Flocculation time	Wrif[d](%)	σ_{Wrif}[e]	RSD_{Wrif}[f]
A +RV[a],CA[c]	30-45 minutes	16.4	0.5	3 %
B +RV[a],CA[c]	30-45 minutes	15.1	0.4	3 %
A -RV[b],CA[c]	Few seconds	13	0.3	3 %
B -RV[b],CA[c]	Few seconds	12.4	0.2	5 %
A +RV[a], HCl	30-45 minutes	9.1	0.5	3 %
B +RV[a], HCl	30-45 minutes	9.7	0.3	3 %
A -RV[b],HCl	Few seconds	4.1	0.4	3 %
B -RV[b], HCl	Few seconds	3.2	0.2	7 %

[a] +RV = Rotary evaporated

[b] -RV= Non Rotary evaporated

[c] CA = Citric acid

[d] W_{rif} = Weight fraction of the drug, calculated from equation (A.9)

[e] σ_{Wrif}= Standard deviation of theweight fraction of the drug, calculated from equation (A.10)

[f] RSD_{Wrif} = Relative standard deviation of the weight fraction of the drug, given by σ_{Wrif}/ W_{rif}

Table S.4. Particle size and drug loading comparison of complexes from a single batch that were processed by flocculation with citric acid with no rotary evaporation step and by dialysis followed by freeze drying.

Purification Method	Particle Diameter, nm (PDI)	Drug Loading W_{rif}, % (Target drug wt %)	Drug Loading Efficiency (%)	$RSDc_{rif} = \sigma_{crif} / C_{rif}$
Flocculation - RV, CA	330 (0.2)	11.3 (25)	45.2	3 %
Dialysis and freeze dried	147 (0.16)	8.4 (25)	34.2	3 %

MTS Cell Toxicity Assay

The CellTiter 96 AQ_{ueous} Non-Radioactive cell proliferation assay was used to determine the number of viable cells using manufacturer's protocol (Dr. Nathan : please provide a reference). Approximately ~2 x 10^4 J774A.1 macrophage-like cells were suspended in 200 µl of DMEM supplemented with 10% fetal bovine serum (FBS) and 1% penicillin-streptomycin solution. These were then seeded in 96-well plates and then were incubated for 24-36 hours at 37°C in 5% CO_2 atmosphere until ~90% confluency was achieved. After confluency was achieved, the cell culture media was removed and the cells were gently washed with phosphate –buffered saline solution (PBS) to ensure complete removal of culture media. Fresh medium (200 µl) containing either free drug or Rifampicin-CMCAB nanoparticles in a concentration of 62.5-500 µg/ml were added to the cells and were incubated for 24 hours at 37°C in a 5% CO_2 atmosphere. For the control experiment, cells were incubated with only medium. After incubation for 24 hrs, the culture media was discarded and cells were gently washed with PBS and 100 µl of fresh culture media were added to each well sample well along with 20 µl of CellTiter 96® Aqueous reagents solution (Promega). Wells containing cells and culture media only served as a control (negative

for signs of demised viability). After 3 hours of incubation at 37°C in the 5% CO_2 atmosphere, the absorbance of samples in the 96–well plate were measured at 490 nm using a ELISA reader (SoftMax Pro Inc., USA). Results were expressed as a percentage mean absorbance by cell upon incubation with various treatments with respect to the untreated control, considering the absorption of control cells as 100% cell viability.

Chapter 4: Preparation and characterization of nanoparticles of carboxymethyl cellulose acetate butyrate containing anti-viral drugs for oral drug delivery

Sonal Mazumder[1], Junia M. Pereira[2], Jennifer M. Carter[3], E. Bruce Orler[4], Robert B. Moore III[5], Kevin J. Edgar [6] and Richey M Davis[*7]

[1,2,3]Macromolecules and Interfaces Institute, [4,5]Department of Chemistry, [6]Department of Sustainable Biomaterials,[7]Department of Chemical Engineering

Virginia Polytechnic Institute and State University, Blacksburg, VA 24061, USA

*Corresponding author:

Richey M. Davis
Department of Chemical Engineering, VirginiaTech, Blacksburg, VA - 24061
Tel: 001+ 540-231-4578 ; Fax : 001+ 540-231-5022
E-mail address: rmdavis@vt.edu

ABSTRACT

Nanoparticles comprised of carboxymethyl cellulose acetate butyrate (CMCAB) complexed with the poorly soluble antiviral drugs ritonavir and efavirenz were produced by a rapid precipitation process and the formulation process and properties of nanoparticles were investigated. Two poorly soluble anti-viral drugs ritonavir and efavirenz were selected as model drugs for this study. Methodology for producing drug-polymer nanoparticles with well-defined particle size distributions was developed and factors affecting drug loading and release properties of these nanoparticles were investigated. A comparison between drug release from nanoparticles made by nanoprecipitation and microparticles made by a co-precipitation process was made in

order to investigate the effect of particle size on drug release from the polymer. Dynamic light scattering showed particle sizes were between 150-250 nm with polydispersity index values as low as 0.12. Drug loading efficiencies as high as 72-86% were attained. The dissolution studies showed an increase in the solubility and faster release of the amorphous drug nanoparticles compared to the as-received crystalline forms of the drugs and microparticles which were prepared by co-precipitation.

Keywords: cellulose, ritonavir, efavirenz, mixing, nanoparticles, microparticles, drug release, solubility, bioavailability, crystallization

4.1. INTRODUCTION

The Human Immunodeficiency Virus (HIV) attacks the immune system, causing life-threatening secondary infections and diseases. Ritonavir and efavirenz are two important drugs for HIV treatment. Ritonavir inhibits an enzyme which metabolizes other protease inhibitors and Efavirenz is a non-nucleoside reverse transcriptase inhibitor (NNRTI). However, both drugs are highly crystalline and poorly soluble in the gastrointestinal tract leading to poor bioavailability.

Oral drug delivery is commonly used in treating HIV but there are several factors in the GI tract which can limit the bioavailability of drugs such as tissue barriers (mucosa, microvilli) and physiological factors (varying pH, enzymes, transporter mechanisms)[1]. Low drug solubility reduces bioavailability and so microparticles and nanoparticles of amorphous polymer-drug complexes have been used in some cases to enhance the dissolution of poorly soluble drugs in the intestinal tract [2,3,4,5].

Reducing the particle size can improve the material properties of polymer-drug particles as potential drug delivery systems[6]. We hypothesize that amorphous solid dispersions in the form of polymer-drug nanoparticles with well-defined size distributions may release most of the

complexed drug in the ~4-5 hours that they reside in the small intestine. This high solution concentration in the small intestine could lead to increased bioavailability that could enable the use of reduced-dose formulations and reduced costs and side effects.

In this work, amorphous solid dispersions (ASDs) in the form of polysaccharide-drug nanoparticles and microparticles were made in order to study the effect of particle size and amorphous drug content on drug dissolution. Most drugs will crystallize and this creates an energy barrier which must be overcome for the drug to dissolve in the bodily fluid. This can greatly limit bioavailability and so one approach that has been taken is to create an amorphous form of the drug which results in a much smaller energy barrier that must be overcome for dissolution. In an ASD, the drug is dispersed, ideally molecularly, in a polymer matrix which inhibits drug crystallization. ASDs have been reviewed in details in sections 2.3 and 3.1 of this thesis. In addition to suppressing drug crystallization in the solid state, polymeric carriers can also reduce drug precipitation by slowing the kinetics of drug precipitation or crystallization in the solution state [3, 7]. [8].

The drug release from solid dispersions depends on dissolution of the polymeric carrier and properties of the drug [9]. It has been found that low drug loading favors the formation of molecular dispersions. Increasing the drug loading necessarily decreases the quantity of polymer carrier available to stabilize the drug in the high energy form. As a result, high drug loading can promote phase separation within the solid dispersion[10,11] which can affect drug-release profiles. Several studies have shown that the drug dissolution rate from solid dispersions decreases with increasing drug loading [12,13,14,15,16,17,18,19,19b]. This decrease in dissolution rate is due to a reduction in the quantity of molecularly dispersed drug in polymer matrix [20,11]. The phase separated drugs are more likely to crystallize compared with solid dispersions where drug is

present in a molecularly dispersed form that has increased kinetic stability as a result of intimate contact with the polymer [21,22,23]. Solid dispersions with lower drug-polymer ratios and with good miscibility between the drug and polymer and with glass transition temperatures appreciably above room temperature show better physical stability at ambient temperatures[24,25,26,11].

Most of the polymers which are used in ASDs have high glass transition temperatures (Tgs). For example, the Tg of PVP K30 is 168°C while the Tg of HPMC is 170°C[16,27]. Homogeneous dispersions of a drug and a high T_g polymer will have higher T_g values than that of the pure drug. Thus, polymeric formulations can stabilize molecular transitions in the amorphous state.

Considerable work has been done to formulate polymer-antiviral drug nanoparticles with synthetic or semisynthetic polymers[28,29,30,31,32,33]. More recently, studies have shown that polysaccharides are very promising for oral drug delivery due to their affinity for complexing with a variety of drugs which can suppress drug crystallization, their relatively high glass transition temperatures, and their biocompatibility[34,35,36]. The composition and morphology of the polymer matrix plays an extremely important role in the drug release and pharmacokinetics [37]. Nanoparticles have the ability to improve the dissolution rate of the drug [38]. All of these benefits can contribute to the reduction of dose and dosing frequency, thereby reducing the side effects and improving the patient compliance[39]. A detailed review of previous studies on polymer-antiviral drug complexes can be found in literature review section 2.8.3 of this thesis.

In this present work, we made RTV and EFV-containing amorphous nanoparticles using a recently developed cellulose ester, carboxymethyl cellulose acetate butyrate (CMCAB)[35], which is pH-sensitive; water-swellable when partially ionized at pH 6-7, but is insoluble at pH ~ 3-4. There is no previous study reported where these drugs were complexed with CMCAB to

form nanoparticles. We hypothesized that the pH-dependent swelling could lead to less release of and less degradation of the drug incorporated into the particles when in the stomach and controlled release of drug in the small intestine. There is no previous study reported where these drugs were complexed with CMCAB to form nanoparticles. Many studies of nanoparticles made with synthetic polymers have focused on controlling drug loading and characterizing drug release but, in many cases, the method of producing the particles was not rapid and scalable. We investigate the effect of processing conditions on the particle size and drug loading of nanoparticles of RTV and EFV, made with a polysaccharide – CMCAB - using the flash nano-precipitation method[40],[41],[42] in a multi-inlet vortex mixer (MIVM) [43,44, 45,46,47]. In this method, nanoparticles form very rapidly by controlled nucleation and growth of particles, which allows for the production of nanoparticles of controlled size in a continuous manner[48]. This is achieved by controlling the Reynolds numbers and the liquid phase composition, allowing for rapid and complete mixing[41, 48-49].

The work reported in this paper focused on establishing a methodology for preparing well-defined drug-polymer complexes relatively rapidly and in a manner that can produce particles with high drug loadings. The particle sizes and drug loading of the nanoparticles were measured to test control and reproducibility of the particle formation process as quantified by an error analysis. The suppression of crystallinity of the drugs in the amorphous nanoparticles was studied by X-ray diffraction analysis and differential scanning calorimetry. Release of the drugs from the polymer matrix was measured to understand the impact of the inhibition of drug crystallization on release. Finally, we compare CMCAB-drug nanoparticles and the corresponding microparticles to understand the effect of particle size on drug release and

determine whether synergy between high surface area and suppression of crystallinity is observed.

4.2. MATERIALS AND METHODS

4.2.1 Materials

Tetrahydrofuran (anhydrous, ACS reagent, ≥99.0% inhibitor free) was used for polymer/drug nanoparticles formation without further purification. Acetonitrile (HPLC grade, >95 %) was used for HPLC analysis. Carboxylmethyl cellulose acetate butyrate (CMCAB); approximate molecular weight 22000, degree of Substitution (DS) of butyryl group = 1.64, DS of acetyl group = 0.44, DS of Carboxymethyl group = 0.33, Eastman Chemical Company) (Figure 1). CMCAB was provided in its free acid form and used as received. Ritonavir (RTV) and efavirenz (EFV) were from Attix Pharmaceuticals, Canada) (Figure 2a and Figure 2b). The pKa of RTV is 14.23 and that of EFV is 10.2. Millipore water (18.2 MΩ•cm at 25 °C ultrapure water, Synergy Ultrapure Water Systems, USA) was used for DLS measurements and in the formation of polymer/drug nanoparticles. The dialysis tubing (Spectropore, cellulose ester) which was used for solvent removal had a molecular weight cut off (MWCO) of 25K.

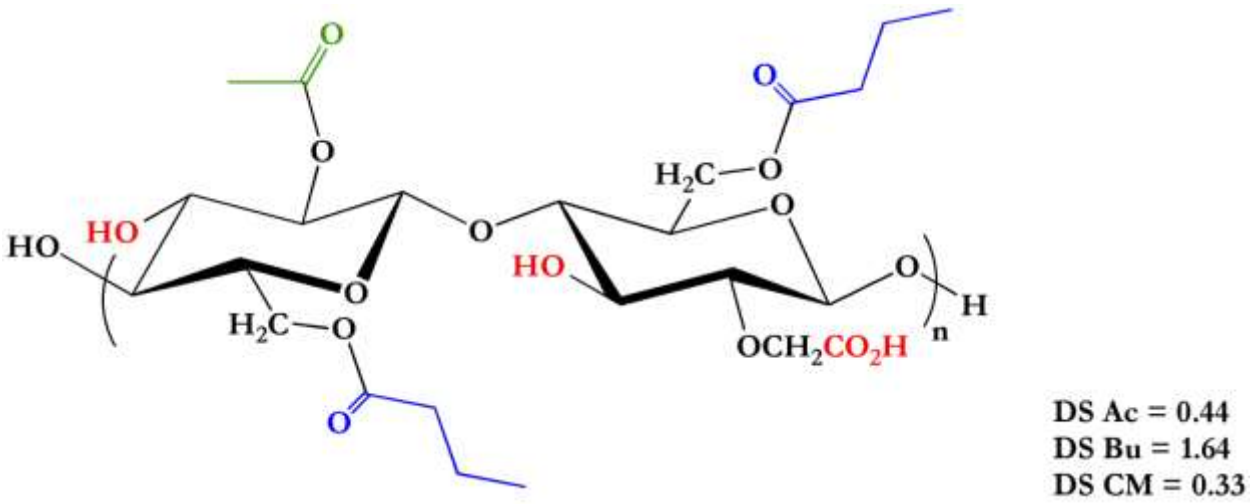

Figure1. Structure of carboxymethyl cellulose acetate butyrate (CMCAB)[35]

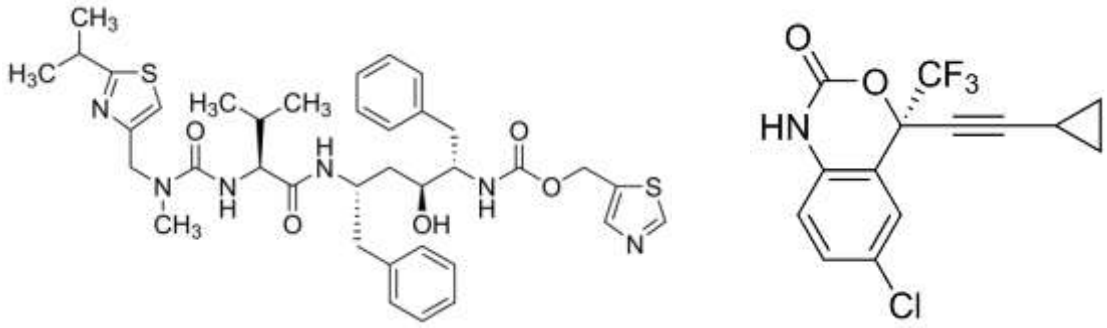

(a) (b)

Figure 2. (a) Structure of ritonavir (RTV)[50] (b) Structure of efavirenz (EFV)[50]

4.2.2 Nanoparticle preparation by rapid precipitation in the Multi Inlet Vortex Mixer

Powdered CMCAB, drugs, and THF were weighed into a glass vial that was then sealed with a screw cap and bath sonicated (Cole Parmer model 8890) for 45 minutes. Flash nanoprecipitation of CMCAB-drug complexes was carried out in a four jet Multi-Inlet Vortex Mixer that accommodates four streams[49a,51]. The THF solution of CMCAB and drug (RTV/EFV) was injected into the mixer along with three other water streams. The temperature of the streams was adjusted to 25°C prior to injection into the mixer by immersing the delivery syringes in a temperature controlled bath. The four inlet streams are tangential to the mixing chamber and exit stream comes from the center of the chamber. The nanoparticles were formed at a nominal Reynolds number of ~ 3900. The Reynolds number is a dimensionless number that is a measure of turbulence and, in this case, of mixing time. It depends upon the inlet stream velocities, viscosities, and densities[49a,41]. The calculations for the Reynolds number are shown in Supporting Information in Chapter 3.

A New Era 4000 double syringe pump (for the organic stream) and a Harvard Apparatus Remote Infuse/Withdraw PHD 4000 Hpsi Programmable syringe pump (for the three water streams) controlled the inlet flow rates. The New Era pump was controlled by the software, Syringe Pump Pro version 1.53. The injected volume ratio of THF to Millipore water was 1:9 v/v. The concentration of CMCAB in THF used to make the particles was 10 mg/mL.

4.2.3 Microparticle formation

CMCAB (450 mg) in 30 mL acetone was stirred at room temperature until the polymer was completely dissolved (approximately 2h). Ritonavir (150 mg) or efavirenz (150 mg) was added to this solution and stirred for 10 min. The acetone solution containing the dissolved polymer and drug was added drop-wise to 90 mL of water. The organic solvent was removed

from the resulting suspension using a rotary evaporator. The aqueous solution was then freeze-dried to yield amorphous solid dispersions of ritonavir or efavirenz in CMCAB.

4.2.4 Nanoparticles recovery, solvent removal and drying

CMCAB-RTV/EFV suspensions were recovered from the MIVM and dialyzed to remove THF, free drug, and dissolved polymer molecules. The dialysis was done with 40 mL of the particles in dialysis tubing placed in a 4 L of DI water. The water was changed 4 times over a period of 24 hours. The dialyzed particles were dried in a LABCONCO freeze dryer at 0.018 mbar for 2 days.

4.2.5 Drug composition by High Performance Liquid Chromatography (HPLC)

The drug contents of ASDs and dissolution samples were measured using an Agilent 1200 Series HPLC system which consisted of a quaternary pump, online degasser, manual injector with a 20-µL sample loop and Agilent chemstation LC 3D software. Chromatography was conducted in reverse mode using acetonitrile and phosphate buffer (0.05M pH 5.65). A concentration gradient with the potassium phosphate buffer and acetonitrile was programmed. The proportion of acetonitrile stayed at 40% for 1 min, was raised to 60% in 14 min, was reduced back to 40% in 1 min and stayed at 40% for 4 min. The total analysis time was 20 min. The mobile phase was delivered at a flow rate of 1.5 mL/min and the column temperature was maintained at 30^{o}C. The sample injection volume was 5 µL. Detection was performed by a diode array detector at a wavelength of 240 nm for ritonavir and efavirenz. Calibration curves for RTV and EFV dissolved in acetonitrile were developed and are shown in Figures S.1 and Figure S.2, respectively, in the Supporting Information.

4.2.6 Particle size – Dynamic light scattering and scanning electron microscopy

Dynamic light scattering (DLS) measurements were performed of the nanoparticle sizes were performed before and after the dialysis steps using a Malvern Zetasizer Nano-ZS (Malvern Instruments Ltd, Malvern, UK) at a wavelength of 633 nm and with a scattering angle of 173˚ at 25 ± 0.1 ºC. Intensity average diameters were obtained by calculations using Malvern's Zetasizer nano 6.12, software that utilizes an algorithm based upon Mie theory with the assumption that the scattering particles are hard spheres. For DLS analysis of the complexes, typically 200 µl of the nanoparticle suspension obtained from the mixer were diluted with 2 mL of deionized water. The dialyzed suspensions (1 mL) were diluted with 3 mL of deionized water and the freeze dried powders were diluted with deionized water to make a concentration of 0.1 mg/mL. The suspensions were sonicated with a bath sonicator (Cole Parmer model 8890) for 10 minutes before measuring the particle size by dynamic light scattering. Field emission scanning electron microscope (FESEM) images of the microparticles were obtained using a LEO (Zeiss) 1550 instrument at a 5 kV accelerating voltage in the conventional high vacuum mode.

4.2.7 Characterization of crystallinity

The crystallinity properties of nanoparticles and microparticles were evaluated by powder X-ray diffraction (PXRD) and differential scanning calorimeter (DSC) experiments within 2-3 weeks from the preparation of the particles. PXRD experiments were conducted with samples of the CMCAB (as received), RTV and EFV (as received), physical mixtures of the as-received CMCAB and the drugs (mixed by grinding with a mortar and pestle) and the nanoparticles. PXRD patterns were obtained using a Bruker D8 Discover X-ray Diffraction system (Madison, Wisconsin) which emits Kα radiation (λ = 1.54 Aº) at 2200 watts and an accelerating potential of 60 kV. The divergence and scattering slits were set at 1.0° and the receiving slit was set at 0.1

mm. The experiment was conducted with a scan range from 10° - 40° 2θ, while the scanning speed was 4°/min.

A differential scanning calorimeter (TA instruments model Q2000) equipped with a RCA90 refrigerated cooling accessory was used to characterize the thermal transitions of the polymer-drug mixtures. About 1.5-3.5 mg of sample (polymer, pure drugs, or nanoparticles) in an aluminum Tzero pan as heated at a scanning rate of 10° C/min from a temperature of -85°C to 180°C, quenched, and then heated again. Dry N_2 was used as the purge gas at 50 mL/min. The instrument was equilibrated at -85°C. Calibration of temperature and the cell constant as carried out with Indium. Glass transition (T_g) values were recorded as the mid-point of the endothermic step transition from 2^{nd} heat scans. Thermal transitions were viewed and analyzed using the analysis software Universal Analysis 2000.

4.2.8 Dissolution studies

Typically, 10 mg of RTV/EFV or 15 mg of nanoparticles were dispersed in 80 mL potassium phosphate buffer, pH 6.8, at 37°C for 5 h. The apparatus used in the release experiments consisted of 250-mL jacketed flasks with circulating ethylene glycol/water (1:1) to control temperature. The solution was constantly stirred at 200 rpm with a magnetic bar. Aliquots (0.8 mL) were withdrawn from the suspensions every 0.5 h (during the first 2 h), then every hour for 5 h. Phosphate buffer (0.8 mL) was added to maintain constant volume after each aliquot was withdrawn. The supernatant was separated from excess solid in solution by ultracentrifugation at 13,000 rpm (equivalent of 16,060 g's) in an accuSpin Micro (Fisher Scientific) for 10 minutes. The supernatant was recovered, and drug concentration was determined by HPLC. Microparticles containing an amount of drug equivalent to that of the

nanoparticles were used to compare the solubility and release of drugs vs particle diameter. Solubility studies were done approximately 2-3 weeks after the preparation of the particles.

4.3. RESULTS AND DISCUSSION

We investigated the drug content, size, crystallinity and solubility of the nanoparticles. We compared our results with microparticles of CMCAB-RTV and CMCAB-EFV formed by the co-precipitation method. The role of CMCAB in enhancing solubility and inhibiting drug crystallinity in the particles is also discussed. The multi-inlet vortex mixer makes it possible to produce nanoparticles with high drug loadings and well-controlled particle size distributions. Increasing the drug concentration in the mixer causes the drug supersaturation to increase which should lead to a higher drug loading in the nanoparticles.

4.3.1 Drug incorporation in particles

Drug incorporation in nanoparticles

The RTV and EFV drug loadings of nanoparticles, shown in Figure 3 as wt % of drug, W_{drug}, were calculated using equation [S.9] in Supplementary Information. The calculations for the relative standard deviation of drug loading (σ_{wdrug}) were made using equation [S.10] in Supplementary Information.

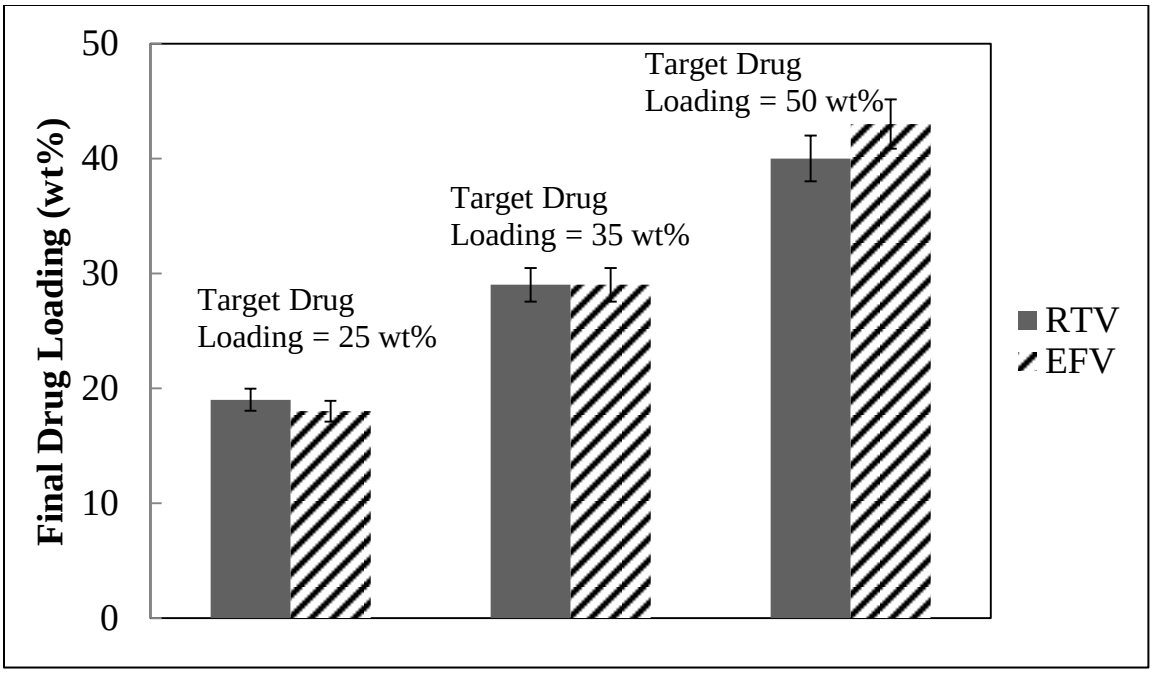

Figure 3. RTV and EFV composition in CMCAB nanoparticles measured by HPLC at 240 nm. Average results from three batches are shown.

For the RTV-CMCAB nanoparticles, the drug loading efficiency ranged from 66%-93% while, for the EFV-CMCAB nanoparticles, the drug loading efficiency ranged from 54%-89%. For both drugs, the drug loading efficiencies increased systematically with the target loading which is consistent with the hypothesis that higher drug supersaturation values in the MIVM result in higher nucleation densities and more efficient drug incorporation into the nanoparticles. For all of these samples, the relative standard deviation of drug loading in percentage, defined by $RSD_{Wdrug} = \sigma_{Wdrug} / W_{drug} \times 100$ % was 3-4 % for all samples. There was some loss of free drug during the processing steps like dialysis.

Drug incorporation in microparticles

The microparticles were not subjected to dialysis (the organic solvent was evaporated by using a rotary evaporator); therefore, the drug concentration in a known amount of particles, evaluated by HPLC was equal to the amount injected into the particles initially.

4.3.2 Particle size analysis

Particle size analysis by dynamic light scattering

In Figure 4, the particle sizes of CMCAB-RTV and CMCAB-EFV nanoparticles with actual drug composition of 19 wt % and 18 wt % respectively are shown after each processing step such as: (a) after mixing in the MIVM and (b) after dialysis and (c) after freeze drying. The particle sizes were compared after each processing step to observe any significant change in the size due to the processing step. For comparison, results of pure CMCAB nanoparticles are also shown.

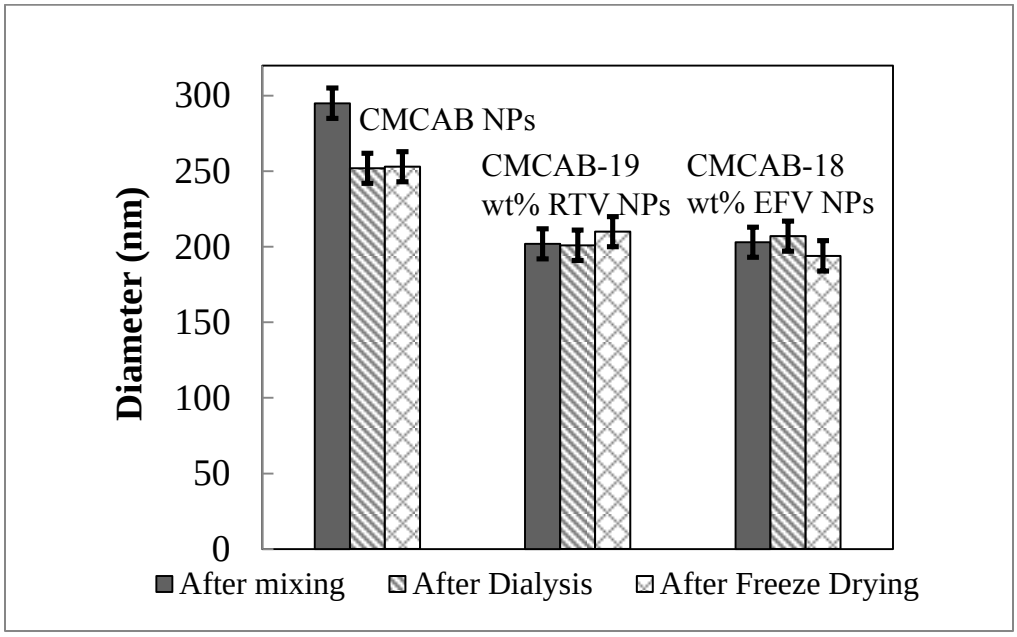

Figure 4. Particle sizes (Dynamic light scattering) of CMCAB, CMCAB- RTV and CMCAB- EFV nanoparticles after mixing, dialysis and freeze drying. The targeted drug composition was 25 wt% and the actual compositions of the freeze-dried particles are shown in Figure 3.

Particle sizes from all three processing steps for all the drug compositions were found to range between 200-300 nm with polydispersity indices (PDIs) ranging from 0.15 -0.2. The

particle sizes of the complexes with higher drug composition are shown in Figure S.3 of Supporting Information. Similar trends were observed for particles with higher drug loading. The particle sizes did not change appreciably after each processing step with a deviation of approximately ±30 nm. Batch-to-batch particle size repeatability (after freeze drying and redispersion) was characterized by the relative standard deviation (=standard deviation/particle size x 100 %) which was typically ~6 %. Particle sizes of drug loaded nanoparticles are smaller than those of pure CMCAB nanoparticles, possibly because the hydrophobic drugs may have served as nucleating agents for CMCAB particle formation. The nanoparticles of CMCAB-drugs in this work could be redispersed in aqueous buffers after freeze-drying and exhibited well-defined particle size distributions with PDIs ≤ 0.2 without the use of any cryoprotectants, unlike many drug nanoparticle systems [52,53] which require cryoprotectants.

Particle size analysis of the microparticles by FESEM

The microparticles were too large and too aggregated to be measure by dynamic light scattering and so they were characterized by FESEM. The microparticles formed agglomerated subunits of nearly spherical particles ranging in size from 500 nm – 2 microns (Figure 5).

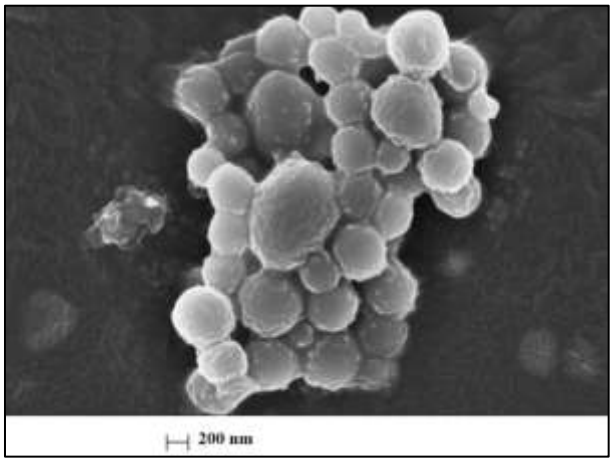

Figure 5. Scanning electron microscope images for microparticles at 50Kx magnification. The bar in each image corresponds to 200 nm.

Control of particle size distribution is very important for controlling the kinetics of drug release. Polydisperse microparticles (various range of particle size) can lead to potential peak/trough fluctuations and undesirable side effects. It is important to note that, for drugs with very low aqueous solubility (<1 μg/ml), polydisperse microparticles may result in poor bioavailability due to the difficulty in their transport across the biological barriers such GI epithelium barrier, blood brain barrier[54]. By contrast, recent studies have shown that nanoparticles may not suffer from the same limitation. Therefore alternative methods were developed to reduce particle size further to nanometer-scale dimensions [55,56,57,58] .

The rate of dissolution for solid drug products can be enhanced by particle size reduction, thereby increasing the surface area per unit mass available for solvation. Particle size reduction techniques are routinely used to improve the oral bioavailability of poorly water soluble drugs[59,4, 60,4,61,62] . The increase in surface area generated due to reduction in particle size increases the dissolution and, therefore, an increase in bioavailability for drugs where exposure after oral administration is limited by dissolution rate [63]. There was an improvement in the oral bioavailability of many poorly water-soluble drugs, including cilostazol[64], fenofibrate[65], progesterone[66], proquazone[67], and nitrofurantoin[68] after micronization, all of which are believed to exhibit dissolution rate limited absorption.

4.3.3 Crystallinity studies of the nanoparticles and microparticles

The X-ray diffraction pattern for RTV (as received) showed numerous strong distinctive peaks at ~ 16°, 18°, 20°, 22° at 2θ indicating its crystalline nature. The X-ray diffraction pattern for EFV (as received) drug also showed numerous strong distinctive peaks at 10°, 12°, 20°, 22°, 25°, 28° at 2θ indicating its crystalline nature. CMCAB is an amorphous polymer; its PXRD pattern is shown in Figure S.4 of the Supporting Information. A comparison of the patterns for

the physical mixtures (Figures 6c and 6d) with those of pure drugs and of pure CMCAB indicates that physical mixtures contain crystalline drug. Finally, the PXRD patterns of the solid dispersions (both microparticles and nanoparticles) showed no diffraction peaks, indicating that the drug in these particles was amorphous.

PXRD patterns of CMCAB-RTV and CMCAB-EFV nanoparticles with higher drug compositions are shown in Figure S.5 of the Supporting Information. Diffraction patterns of these particles with higher drug composition showed amorphous halos with no indication of significant crystallinity, just like the particles shown in Figure 6 (e and f).

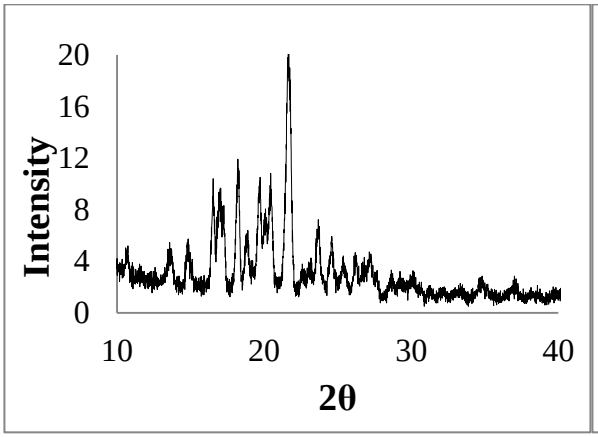

(a)

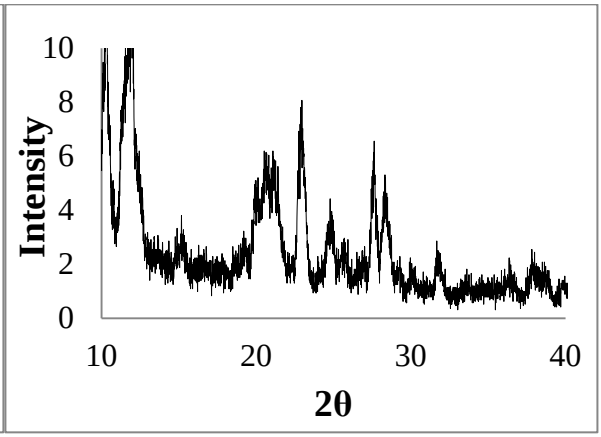

(b)

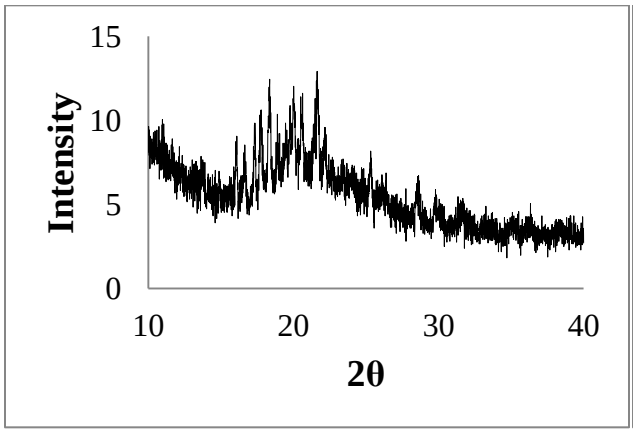

(c)

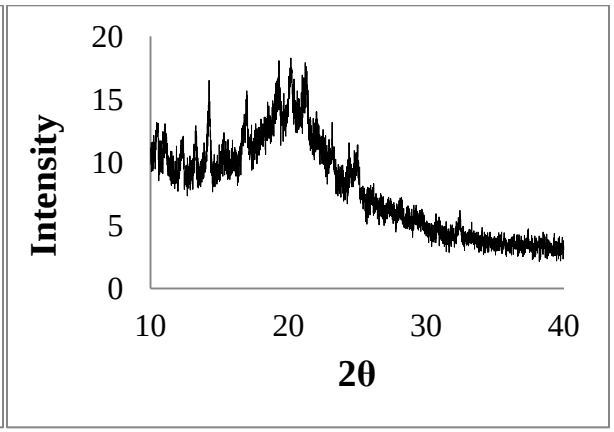

(d)

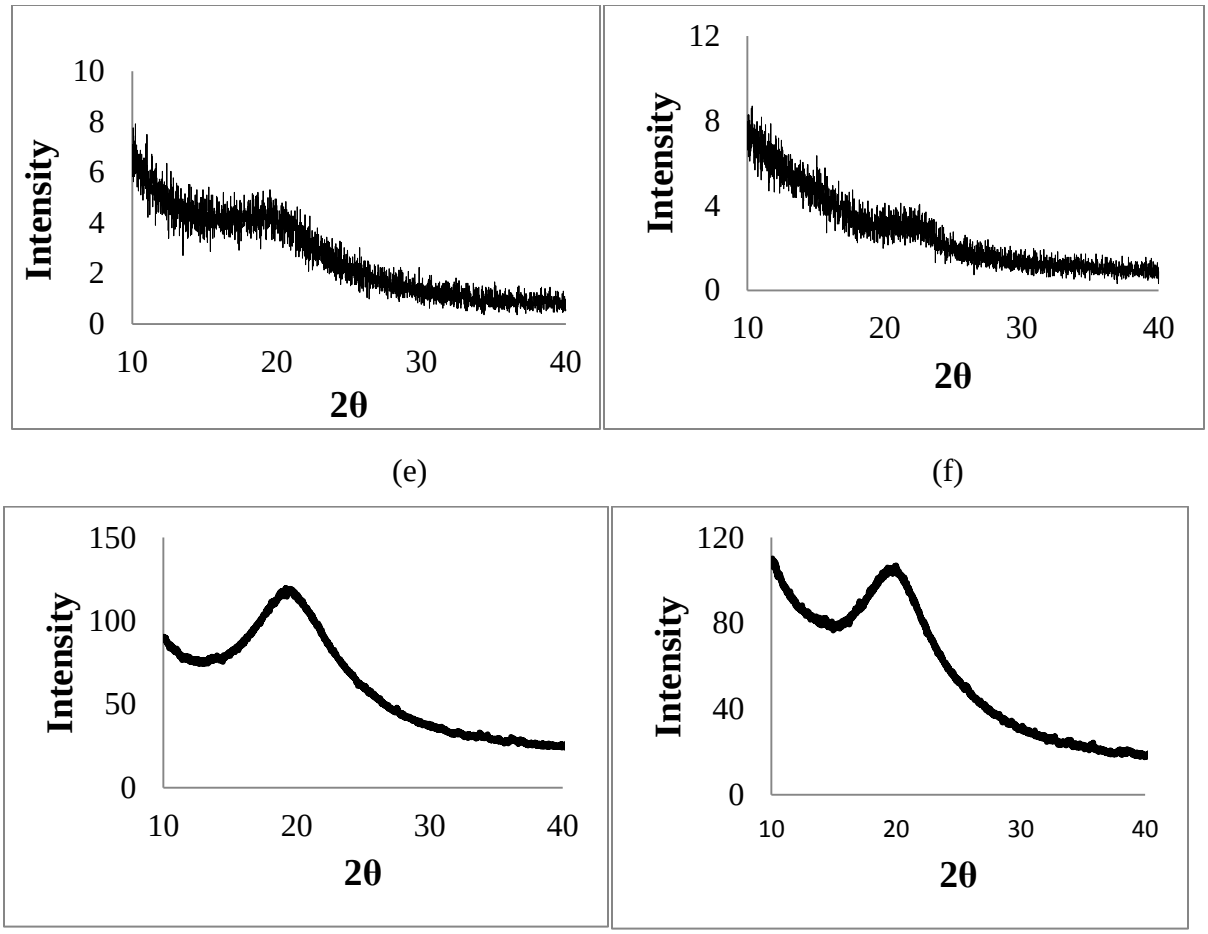

Figure 6. X-ray diffractograms of (a) Crystalline RTV (as received), (b) Crystalline EFV (as received), (c) Physical mixture of CMCAB-25 wt% RTV, (d) Physical mixture of CMCAB-25 wt% EFV, (e) CMCAB-RTV (actual drug loading is 19 wt%), (f) CMCAB-EFV (actual drug loading is 19 wt%), (g) CMCAB-RTV microparticles with 25 wt% of RTV, (h) CMCAB-EFV microparticles with 25 wt % of EFV

4.3.4 Differential Scanning Calorimetry

The initial DSC scan of processed samples is shown in Figure 7 for RTV-loaded particles. Ritonavir showed a sharp endothermic melting peak at 126° C. During the scanning of CMCAB, a broad endotherm at 66° C was observed which could be related to moisture loss[69]. A similar endotherm was observed (at 68° C) in case of CMCAB nanoparticles as well as CMCAB-RTV nanoparticles (containing different wt % of RTV) made by mixing in MIVM, but no endotherm was observed around the melting point of ritonavir indicating that ritonavir was available in its amorphous state. The physical mixture showed an endotherm corresponding to the melting point of ritonavir showing the presence of crystalline drug. Similar results were obtained for CMCAB-EFV particles as shown in Figure S.6 of the Supporting Information.

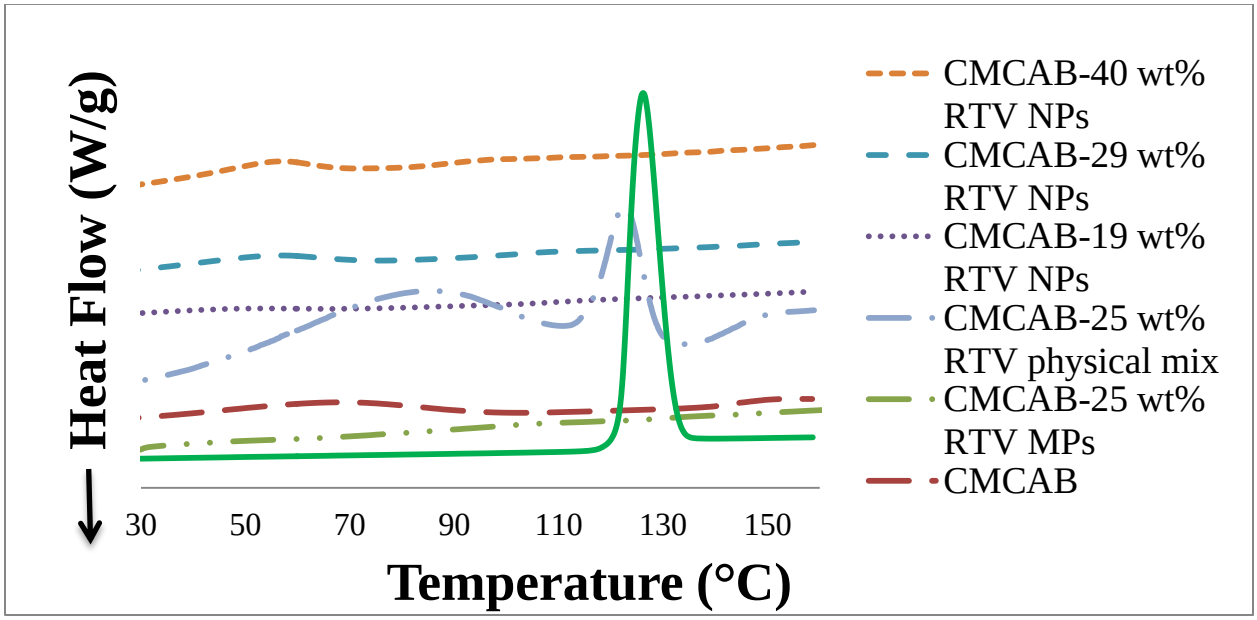

Figure 7. First DSC scan showing melting peak of RTV at 126° C. A similar peak is observed in the physical mixtures but no such peak is observed in the any of the CMCAB-drug particles. Here NPs = nanoparticles, MPs = microparticles.

The glass transitions of the nanoparticles and microparticles were between the glass transitions of CMCAB (142°C) and pure RTV (51° C) and pure EFV (35°C). The intermediate

T_g suggested that the drugs are homogeneously and molecularly dispersed in the amorphous CMCAB matrix. Similar results are observed with EFV nanoparticles. The values of T_gs of RTV and EFV nanoparticles and microparticles and the pure components are shown in Table 1.

Table 1. The glass transitions of CMCAB, drugs and complexes calculated from the second DSC scan and Fox ideal mixing equations.

Samples	T_g (°C) Measured	T_g (°C) Fox ideal
CMCAB	142	142
RTV as received	51	51
EFV as received	35	35
CMCAB-RTV nanoparticles (19 wt% RTV)	91	121
CMCAB-RTV nanoparticles (29 wt% RTV)	87	111
CMCAB-RTV nanoparticles (40 wt% RTV)	63	100
CMCAB-EFV nanoparticles (18 wt% EFV)	99	117
CMCAB-EFV nanoparticles (29 wt% EFV)	76	104
CMCAB-EFV nanoparticles (43 wt% EFV)	45	88
CMCAB-RTV microparticles (25wt% RTV)	100	114
CMCAB-EFV microparticles (25 wt% EFV)	94	109

It is helpful to study the amorphous form of the drugs (RTV and EFV) in the solid dispersions by measuring the glass transition temperatures of the solid dispersions. Such measurements can establish whether or not the drug and the polymer form one miscible phase (i.e. a single T_g value, solid dispersion) or immiscible phases (i.e. multiple T_g values)[2,70]. The results obtained in the present study show the presence of a single glass transition temperature, suggesting that the drug and the polymer formed one miscible amorphous phase. Using the Fox equation, a rule of mixing for an ideal system, the predicted glass transition temperatures for the

CMCAB-RTV and CMCAB-EFV solid dispersions obtained using these methods, were compared with the experimentally determined values obtained from the DSC.

Fox ideal mixing: $\frac{1}{T_g} = \frac{W_{CMCAB}}{T_g^{CMCAB}} + \frac{W_{RTV(or\ EFV)}}{T_g^{RTV\ (or\ EFV)}}$ (1)

where $W_{(\text{RTV or EFV})}$ and $W_{(\text{CMCAB})}$ are the weight fractions of RTV (or EFV) and HPMCAS, respectively, and $T_g^{(\text{RTV or EFV})}$ and $T_g^{(\text{CMCAB})}$ are the glass transition temperatures of RTV (or EFV) (i.e. 51ºC or 35 ºC) and CMCAB (142 ºC), respectively. As these predictions assume that there is a linear extrapolation between the T_g values obtained for drugs (RTV and EFV) and CMCAB, any deviation from the predicted values is taken to indicate the presence of molecular interactions between the molecules. For both the RTV- and EFV-containing nanoparticles, increasing the drug loading resulted in increasing deviations from the Fox-equation prediction, particularly at drug loading of 29 wt% and higher. The microparticles prepared by co-precipitation also showed variations from predicted Fox equation values.

In all cases for both RTV and EFV, both nanoparticles and microparticles the values of T_g fall below the predictions of the Fox equation whereas those of the physical mixtures lie above the predictions. This is consistent with the view that the drug polymer interactions are much the same, regardless of particle size and these particular preparation methods. In view of the limited data for the microparticles, the deviations of these from the Fox equations are similar in magnitude to those of the nanoparticles.

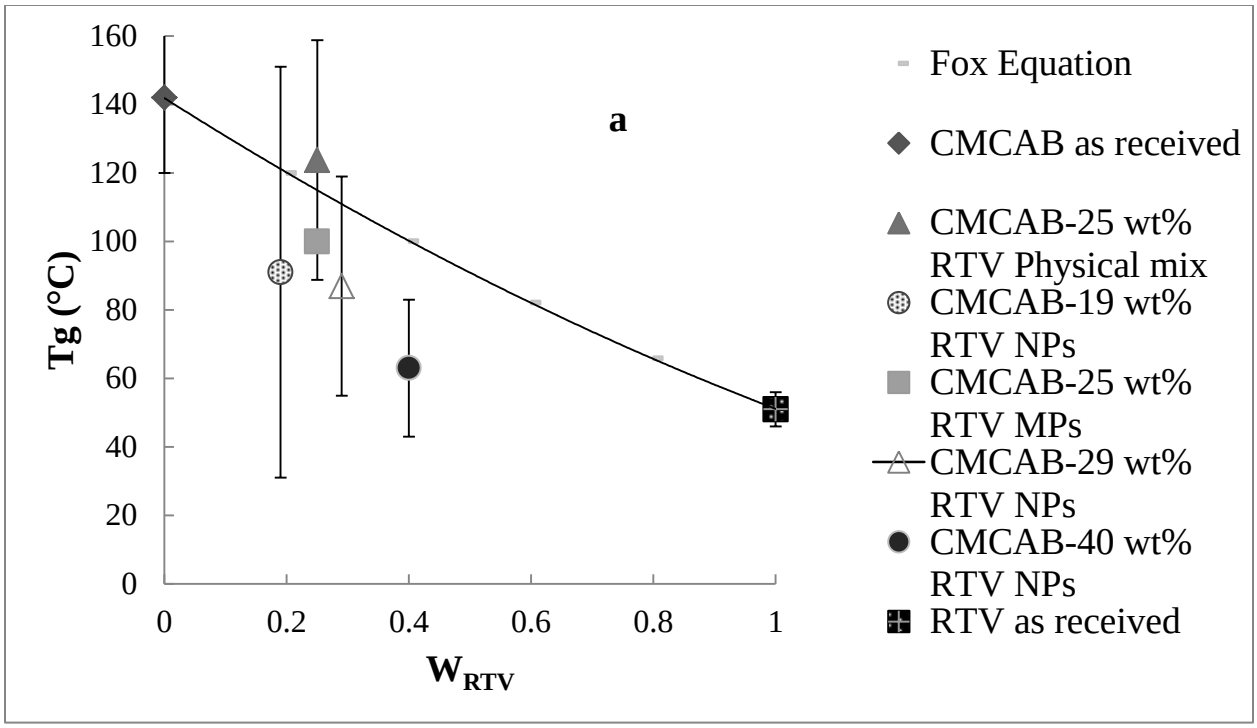

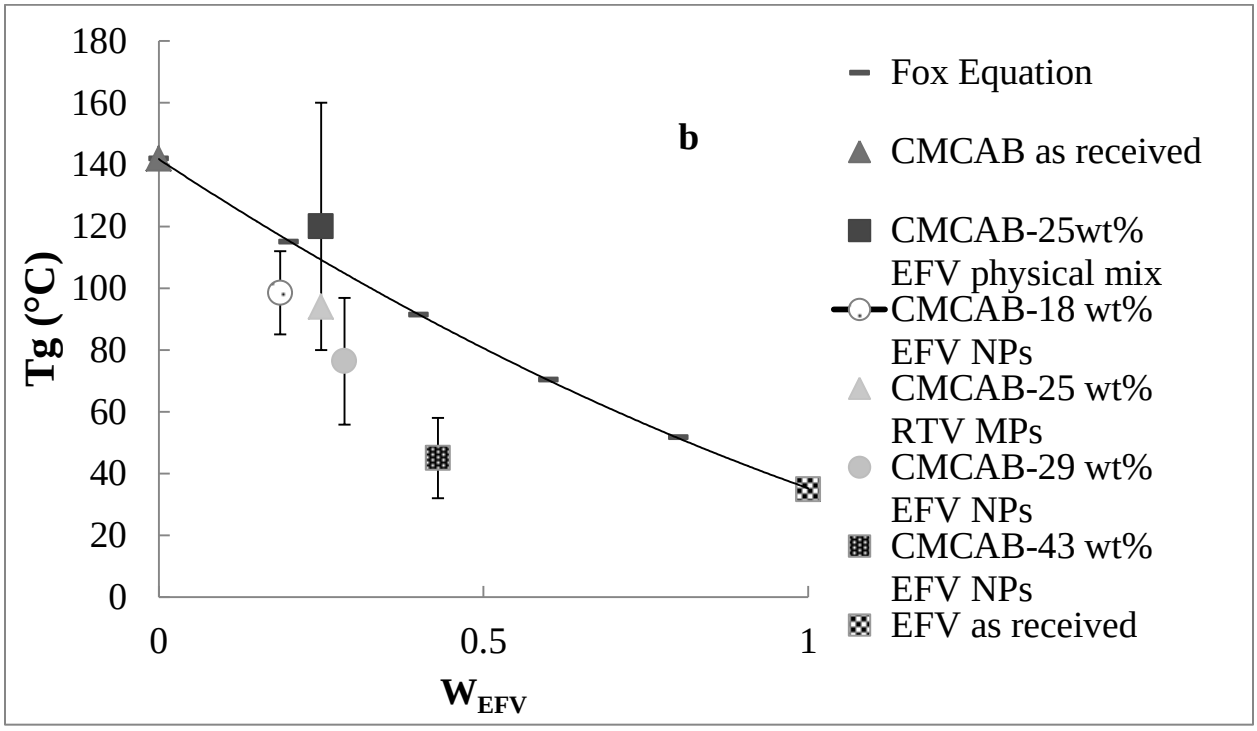

Figure 8. Comparison between experimental T_g and theoretical predictions (Fox ideal T_g), (a) RTV containing particles, (b) EFV containing particles at different drug composition.

4.3.5. Dissolution studies

The concentration profiles of the CMCAB-RTV and CMCAB-EFV nanoparticles with variable drug loading are shown in Figure 9a and Figure 9b, respectively, measured at pH 6.8 at 37 °C for 5 hours. The solution concentration of RTV was increased to 20-, 30-, and 40-fold for particles with final drug content of 19 wt%, 29 wt% and 40 wt%, respectively. The increase in solution concentration of EFV from nanoparticles containing 18 wt%, 29 wt % and 43 wt% drug composition was 2-, 3-, and 6-fold, respectively. Therefore the polymer CMCAB was effective in forming amorphous nanoparticles which increased the solution concentration of the drug.

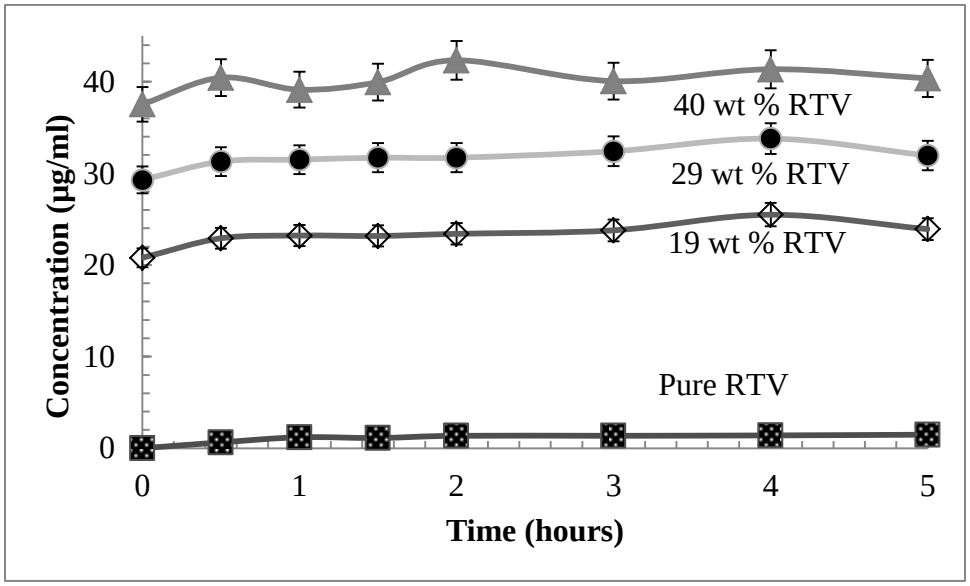

Figure 9a. Dissolution profile of CMCAB-RTV nanoparticles from 3 batches

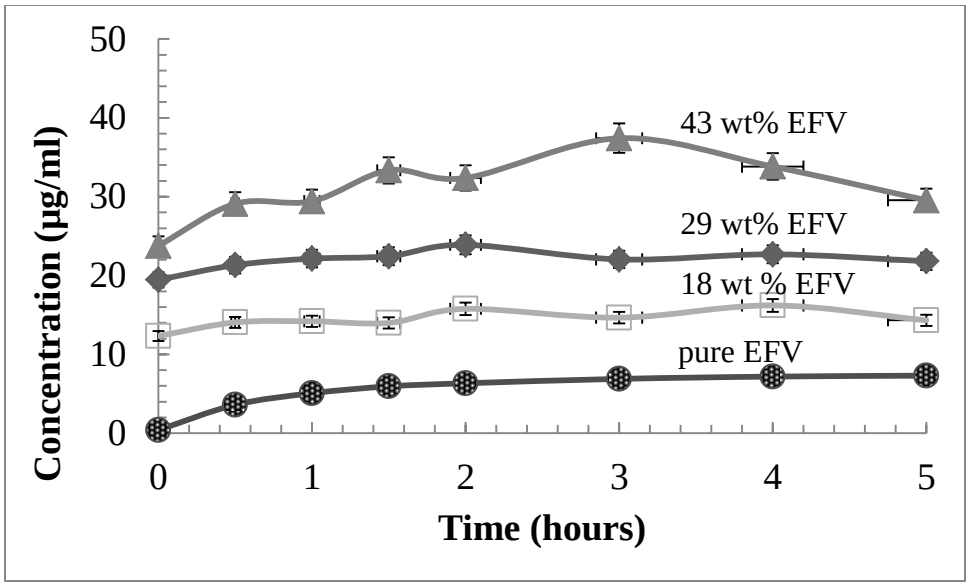

Figure 9b. Dissolution profile of CMCAB-EFV nanoparticles from 3 batches

The results from the dissolution experiment showed good enhancement of drug solubility from the amorphous solid dispersions. ASDs with CMCAB significantly increased the solubilities of both RTV and EFV and the supersaturated solutions remained stable with respect to drug re-precipitation over the course of the experiment. This suggests that the polymer not only stabilized the amorphous drug in the solid state, but also helped stabilize dissolved drug in solution. There are several possible mechanisms for drug stabilization in the solid state. It is generally accepted that drug–polymer intermolecular interactions are important for the stabilization of the solid dispersion and that this stabilization generally requires that the drug and polymer be mixed homogeneously at the molecular level. Secondly, the molecular mobility of the drug required for crystallization can be inhibited by its forming an amorphous solid solution with the high-T_g CMCAB polymer. Another factor that favors stabilization is that an amorphous drug has a lower chemical potential when mixed with a polymer which decreases the driving force for crystallization.

The mechanisms by which solid dispersions can stabilize amorphous drugs also in solution are not yet fully understood but one hypothesis is that soluble polymer at very low concentrations may associate with the drug in solution, thus suppressing drug precipitation[71,72].

The percent drug release calculated from equation 2 for RTV and EFV from the nanoparticles is shown in Figures 10a and 10b.

$$\%\, drug\ release\ =\ \frac{C_{experimental}}{C_{theoritical}} \qquad [2]$$

$C_{experimental}$ values were calculated from HPLC and values of $C_{theoretical}$ were calculated from the known values of volume of the buffer solution, amount of particles and drug composition.

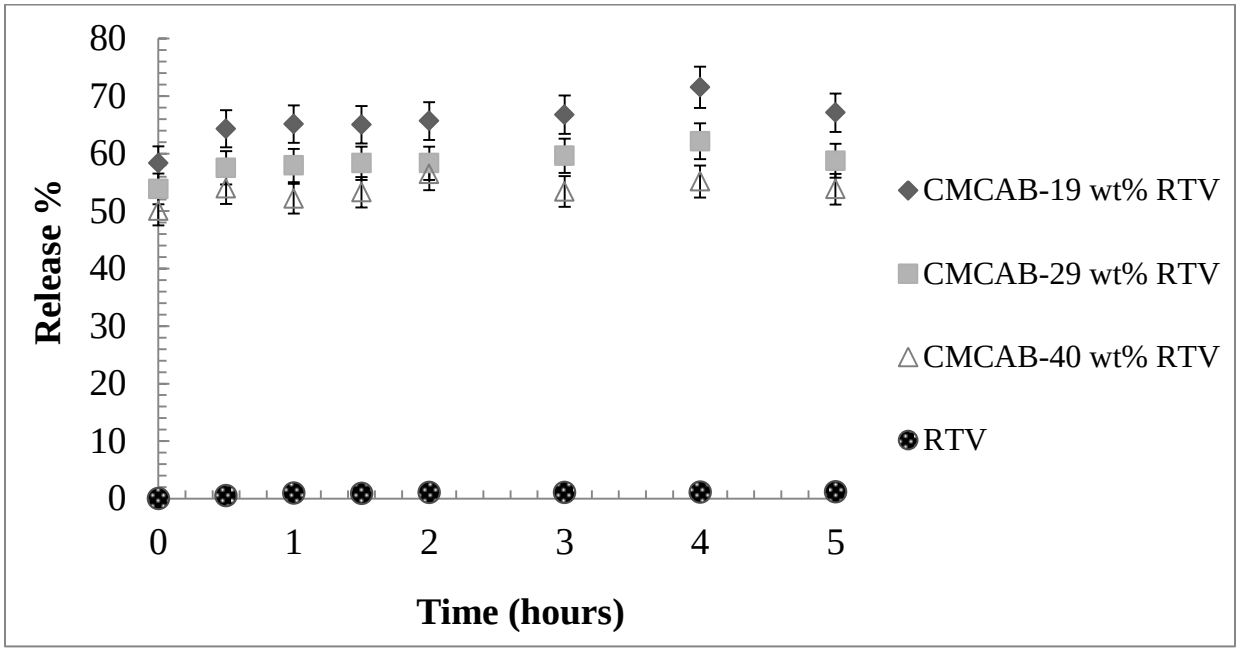

Figure 10a. Drug release profile of RTV. Approximately 70% (for drug composition 19 wt %), 60% (for drug composition of 29 wt %) and 55% (for drug composition 40 wt %) of RTV present in the amorphous matrix of CMCAB was dissolved in 5 hours

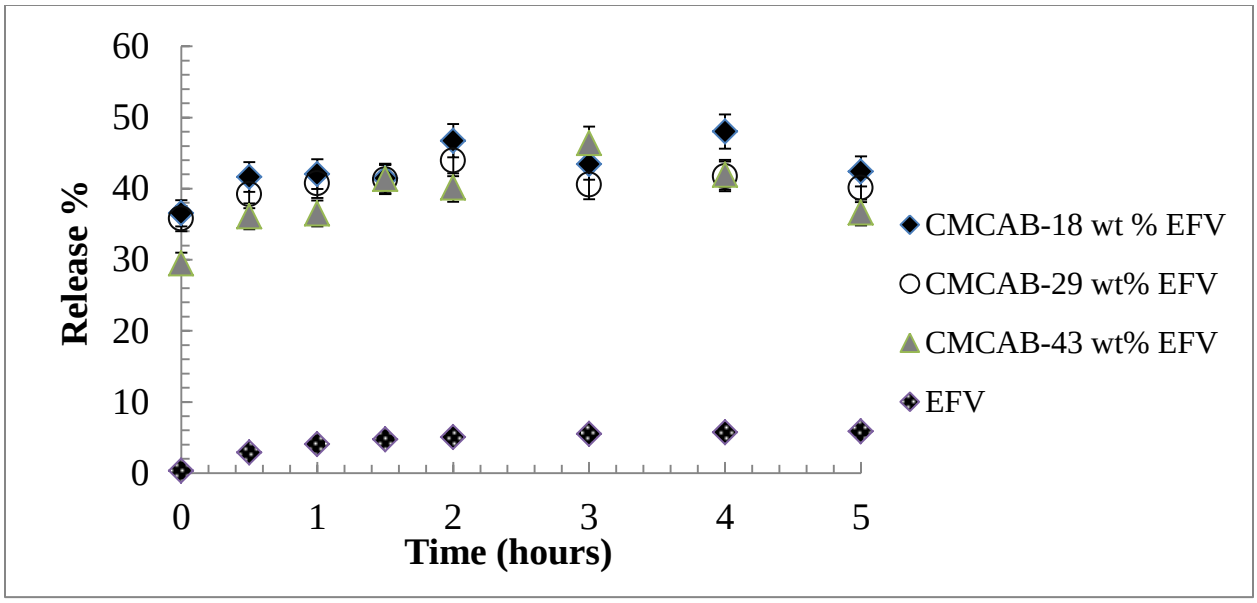

Figure 10b. Drug release profile of EFV/CMCAB nanoparticles vs pure EFV

About 50-70 % of RTV and 35-40 % of EFV was released from CMCAB nanoparticles in 5 hours in contrast to the values of < 1% and ~ 4% for the as-received crystalline RTV and EFV, respectively. The drug release decreased with increasing drug composition in the nanoparticles approximately 60 % of drug was released from nanoparticles containing 19 wt % of RTV whereas 50 % of drug was released from nanoparticles containing 40 wt% of RTV. For RTV for a given drug loading, there was essentially no change in release % after the first 30 minutes.

Previous work has shown, however, that increasing the drug loading in a polymer carrier particle can, at high drug loadings, lead to phase separation within the solid dispersion which can lead to undesirable, time-dependent re-crystallization of the drug[10,11]. Drug-release profiles can also change upon increasing the drug loading. Several studies have shown increasing the drug loading results in a reduction of the drug dissolution rate from solid dispersions[12,13,14,15,16,17,18,19,19b]. This decrease in dissolution rate was due to a reduction in the fraction of drug in the molecularly dispersed form since increasing the drug loading reduces the

average distance between drug molecules and the quantity of stabilizing polymer, both of which favor phase separation of amorphous/crystalline particulate drug in the carrier[11,20, ,7c,71]

In all of the nanoparticles we studied, there was no indication of drug crystallinity even at the highest drug loadings and so the release percentage varied by only 10% between the drug loadings of 19 wt% and 40 wt%. Thus, the flash nanoprecipitation method was an effective approach for decreasing particle size to enhance the solution concentration of poorly soluble drugs using CMCAB dispersions. CMCAB was effective in entrapping the drug in amorphous form to enhance drug release. It was shown that the polymers are effective in inhibiting crystal growth at low supersaturation, but only marginally at supersaturations corresponding to the amorphous ‘‘solubility’’. At higher supersaturation, the crystal growth mechanism is fast and continuous which makes it difficult for adsorbed polymer to block all the active growth sites[73].

The increase in the solution concentration of the drugs was observed for both nanoparticles and microparticles (Figure 11) compared to the as-received crystalline drugs. Reducing the particle size of the RTV and EFV from that of the as-received powder greatly increases the specific surface area, which provides an additional method to enhance the dissolution of RTV and EFV. There was no significant difference in the solution concentration of EFV from microparticles and nanoparticles. A slightly higher concentration of RTV was observed in the case of microparticles compared to nanoparticles.

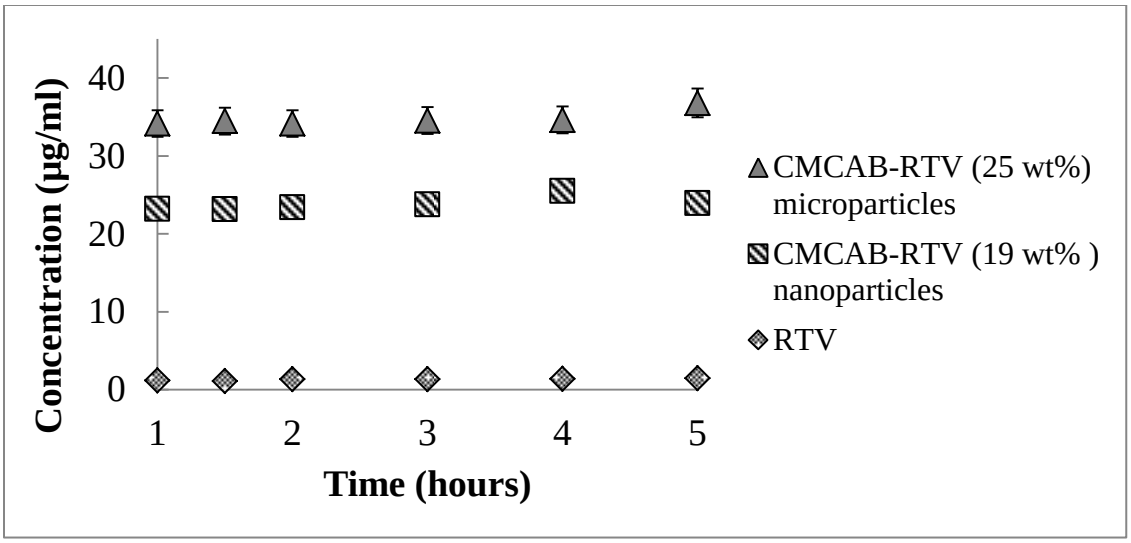

Figure 11a. Solution concentration of RTV from nanoparticle and microparticle ASDs vs pure RTV (potassium phosphate buffer, pH 6.8)

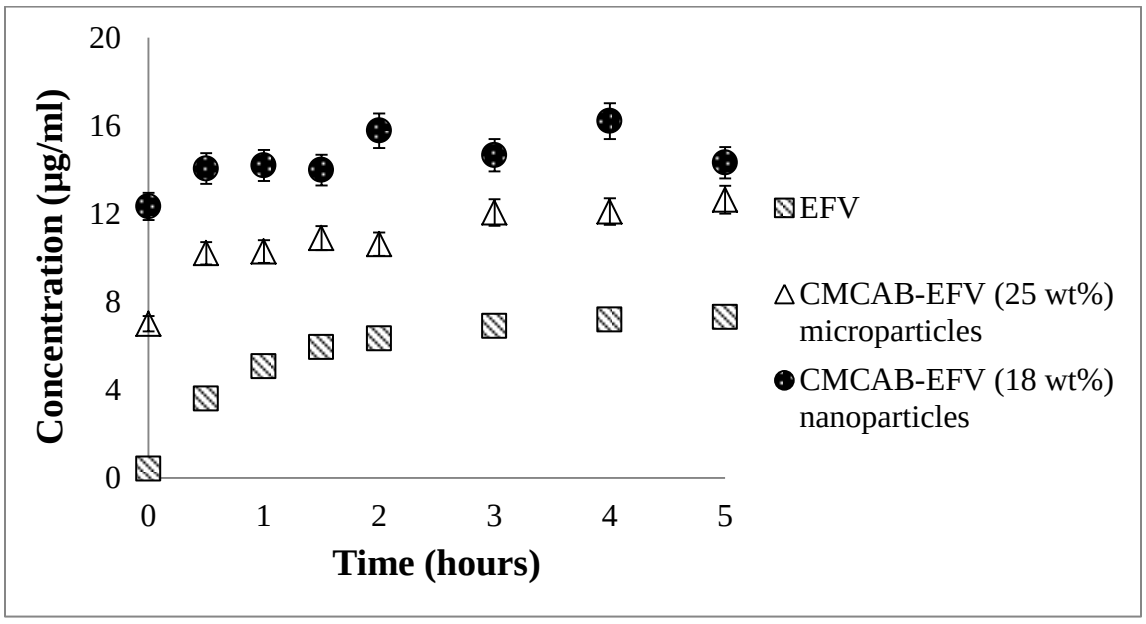

Figure 11b. Solution concentration of EFV from nanoparticle and microparticle ASDs vs pure EFV (potassium phosphate buffer, pH 6.8)

The percent drug release of RTV and EFV from nanoparticles and microparticles is compared in Figure 12. In Figure 12a, approximately 60% and 20 % of RTV was released from CMCAB nanoparticles and microparticles respectively in 5 hours. Also a higher drug release of 40 % was observed from EFV nanoparticles whereas only 6% of the drug was released from microparticles in 5 hours (Figure 12b). If the nanoparticles stabilize the drug in the amorphous form in the solution by releasing small levels of soluble polymer, this might also account for the increase in percent drug released compared to that of the microparticles.

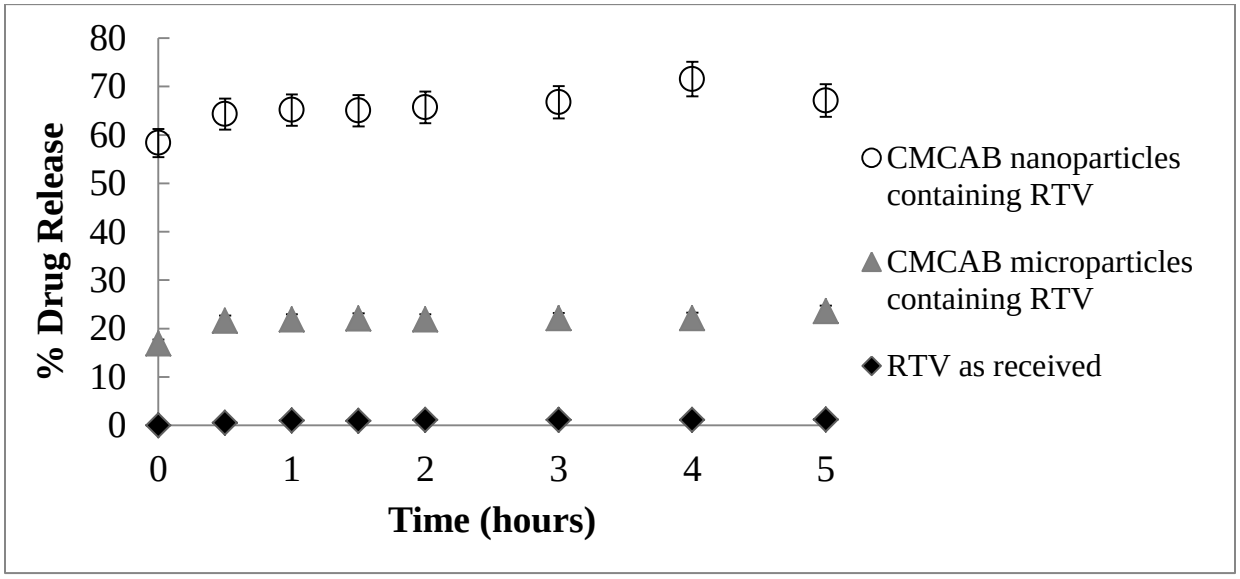

Figure 12a. Comparison of percentage drug release from CMCAB-RTV microparticles and nanoparticles (results from 3 batches).

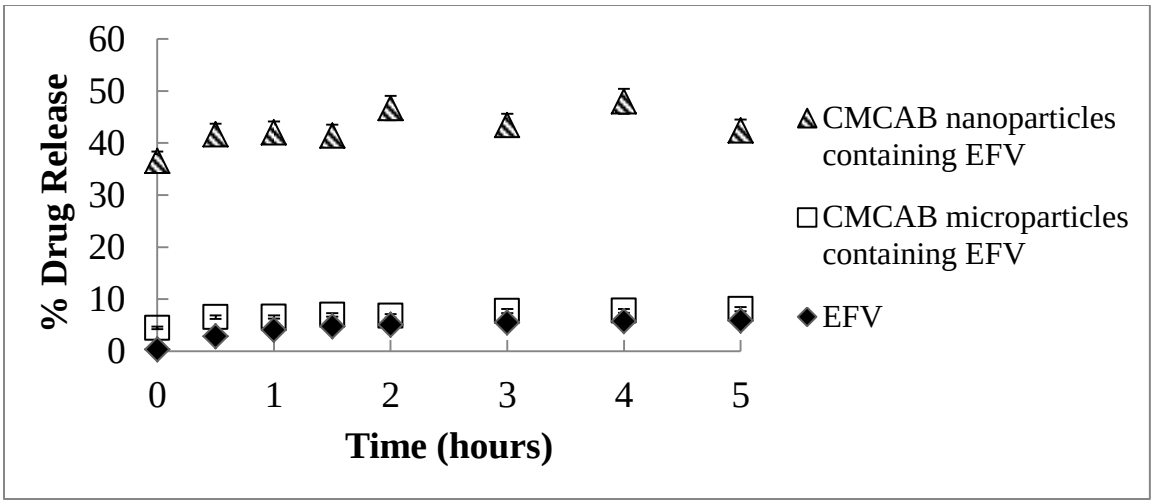

Figure 12b. Comparison of percentage drug release from CMCAB-EFV microparticles and nanoparticles (results from 3 batches).

4.4. CONCLUSIONS

This study demonstrates a method for producing CMCAB-RTV and CMCAB-EFV nanoparticles with well-defined sizes (200-300 nm) and drug loadings in the range 18-43 wt%. A multi-inlet vortex mixer was used to form the particles by a rapid precipitation step. The drug loading efficiencies in the final particles ranged from 72 % – 86 %. CMCAB polymer was effective in entrapping the drug in its amorphous state in the particle and this increased the solubility of the drugs in buffer solution. Higher drug composition in the particles showed low miscibility. However, there was no detectable crystallinity or phase separation observed for higher drug containing particles. Solution concentration and drug release from the nanoparticles and microparticles were significantly enhanced compared to those of the as received crystalline drug. Drug release decreased with increasing drug content in the particles.

The release characteristics of amorphous nanoparticles were contrasted with those of comparable amorphous microparticles. The final drug loading efficiency was 72-86 % in the nanoparticles, and 100% in the microparticles (as there was no drug loss due to processing

steps). The percentage release of drugs from nanoparticles was higher than from the microparticles. The nanosized RTV and EFV had greatly increased specific surface area compared to micron-sized particles, which greatly enhanced dissolution of RTV and EFV. There was only a slight difference of solution concentration of microparticles and nanoparticles, solution concentration of microparticles somewhat higher.

However, these are the first experiments on the effectiveness of these CMCAB-drug nanoparticles and so more complete and statistically valid tests need to be performed. More investigation is needed to characterize the very long storage stability of these particles. The enhancement of release of drugs from polymer nanoparticles for effective drug delivery of low solubility anti-viral drugs is an attractive area for additional research.

ACKNOWLEDGEMENT

The authors gratefully acknowledge funding and support from the Macromolecules and Interface Institute, Institute of Critical Technology and Applied Sciences and the National Science Foundation, (under Contract # DMR 0909065). The authors also thank Rick Caudill, Research Specialist, Department of Sustainable Biomaterials, Virginia Tech for his assistance with the PXRD analysis and Mr. Steve McCartney of the Institute for Critical Technology and Applied Science-Nanoscale Characterization and Fabrication Laboratory (ICTAS-NCFL) at Virginia Tech for help with the FESEM images.

4.5. REFERENCES

1. Lavelle, E. C.; Sharif, S.; Thomas, N. W.; Holland, J.; Davis, S. S., The importance of gastrointestinal uptake of particles in the design of oral delivery systems. *Advanced Drug Delivery Reviews* **1995,** *18* (1), 5-22.

2. Huang, J.; Wigent, R. J.; Schwartz, J. B., Drug–polymer interaction and its significance on the physical stability of nifedipine amorphous dispersion in microparticles of an ammonio methacrylate copolymer and ethylcellulose binary blend. *Journal of Pharmaceutical Sciences* **2008,** *97* (1), 251-262.

3. Kanaujia, P.; Lau, G.; Ng, W. K.; Widjaja, E.; Hanefeld, A.; Fischbach, M.; Maio, M.; Tan, R. B. H., Nanoparticle formation and growth during in vitro dissolution of ketoconazole solid dispersion. *Journal of Pharmaceutical Sciences* **2011,** *100* (7), 2876-2885.

4. Merisko-Liversidge, E.; Liversidge, G. G., Nanosizing for oral and parenteral drug delivery: A perspective on formulating poorly-water soluble compounds using wet media milling technology. *Advanced Drug Delivery Reviews* **2011,** *63* (6), 427-440.

5. Pranjali B. Gawali, S. J. K., Mangesh R. Bhalekar, Ashwini R. Madgulkar, Preparation and Characterization of Amorphous Nanoparticles for Solubility Enhancement of Ritonavir. *International Journal of Pharmaceutical Invention* **2012,** *2* (6), 27.

6. Petros, R. A.; Desimone, J. M., Strategies in the design of nanoparticles for therapeutic applications. *Nat Rev Drug Discov* **2010,** *9* (8), 615-627.

7. (a) Curatolo, W.; Nightingale, J.; Herbig, S., Utility of Hydroxypropylmethylcellulose Acetate Succinate (HPMCAS) for Initiation and Maintenance of Drug Supersaturation in the GI Milieu. *Pharmaceutical Research* **2009,** *26* (6), 1419-1431; (b) Warren, D. B.; Benameur, H.; Porter, C. J. H.; Pouton, C. W., Using polymeric precipitation inhibitors to improve the absorption of poorly water-soluble drugs: A mechanistic basis for utility. *Journal of Drug Targeting* **2010,** *18* (10), 704-731; (c) Craig, D. Q. M., The mechanisms of drug release from solid dispersions in water-soluble polymers. *International Journal of Pharmaceutics* **2002,** *231* (2), 131-144; (d) Kennedy, M.; Hu, J.; Gao, P.; Li, L.; Ali-Reynolds, A.; Chal, B.; Gupta, V.; Ma, C.; Mahajan, N.; Akrami, A.; Surapaneni, S., Enhanced Bioavailability of a Poorly Soluble VR1 Antagonist Using an Amorphous Solid Dispersion Approach: A Case Study. *Molecular Pharmaceutics* **2008,** *5* (6), 981-993; (e) Miller, D. A.; Dinunzio, J. C.; Yang, W.; Mcginity, J. W.; Williams, R. O., Enhanced In Vivo Absorption of Itraconazole via Stabilization of

Supersaturation Following Acidic-to-Neutral pH Transition. *Drug Development and Industrial Pharmacy* **2008,** *34* (8), 890-902.

8. Lindfors, L.; Forssén, S.; Westergren, J.; Olsson, U., Nucleation and crystal growth in supersaturated solutions of a model drug. *Journal of Colloid and Interface Science* **2008,** *325* (2), 404-413.

9. Esnaashari, S.; Javadzadeh, Y.; Batchelor, H. K.; Conway, B. R., The use of microviscometry to study polymer dissolution from solid dispersion drug delivery systems. *International Journal of Pharmaceutics* **2005,** *292* (1–2), 227-230.

10. Marsac, P.; Li, T.; Taylor, L., Estimation of Drug–Polymer Miscibility and Solubility in Amorphous Solid Dispersions Using Experimentally Determined Interaction Parameters. *Pharmaceutical Research* **2009,** *26* (1), 139-151.

11. Qian, F.; Huang, J.; Hussain, M. A., Drug–polymer solubility and miscibility: Stability consideration and practical challenges in amorphous solid dispersion development. *Journal of Pharmaceutical Sciences* **2010,** *99* (7), 2941-2947.

12. Six, K.; Berghmans, H.; Leuner, C.; Dressman, J.; Van Werde, K.; Mullens, J.; Benoist, L.; Thimon, M.; Meublat, L.; Verreck, G.; Peeters, J.; Brewster, M.; Van Den Mooter, G., Characterization of Solid Dispersions of Itraconazole and Hydroxypropylmethylcellulose Prepared by Melt Extrusion, Part II. *Pharmaceutical Research* **2003,** *20* (7), 1047-1054.

13. Law, D.; Schmitt, E. A.; Marsh, K. C.; Everitt, E. A.; Wang, W.; Fort, J. J.; Krill, S. L.; Qiu, Y., Ritonavir–PEG 8000 amorphous solid dispersions: In vitro and in vivo evaluations. *Journal of Pharmaceutical Sciences* **2004,** *93* (3), 563-570.

14. Kapsi, S. G.; Ayres, J. W., Processing factors in development of solid solution formulation of itraconazole for enhancement of drug dissolution and bioavailability. *International Journal of Pharmaceutics* **2001,** *229* (1–2), 193-203.

15. Janssens, S.; Nagels, S.; Armas, H. N. D.; D'autry, W.; Van Schepdael, A.; Van Den Mooter, G., Formulation and characterization of ternary solid dispersions made up of Itraconazole and two excipients, TPGS 1000 and PVPVA 64, that were selected based on a supersaturation screening study. *European Journal of Pharmaceutics and Biopharmaceutics* **2008,** *69* (1), 158-166.

16. Lakshman, J. P.; Cao, Y.; Kowalski, J.; Serajuddin, A. T. M., Application of Melt Extrusion in the Development of a Physically and Chemically Stable High-Energy Amorphous Solid Dispersion of a Poorly Water-Soluble Drug. *Molecular Pharmaceutics* **2008,** *5* (6), 994-1002.
17. (a) Konno, H.; Handa, T.; Alonzo, D. E.; Taylor, L. S., Effect of polymer type on the dissolution profile of amorphous solid dispersions containing felodipine. *European Journal of Pharmaceutics and Biopharmaceutics* **2008,** *70* (2), 493-499; (b) Abu-Diak, O. A.; Jones, D. S.; Andrews, G. P., An Investigation into the Dissolution Properties of Celecoxib Melt Extrudates: Understanding the Role of Polymer Type and Concentration in Stabilizing Supersaturated Drug Concentrations. *Molecular Pharmaceutics* **2011,** *8* (4), 1362-1371.
18. Yoshioka, M.; Hancock, B. C.; Zografi, G., Inhibition of indomethacin crystallization in poly(vinylpyrrolidone) coprecipitates. *Journal of Pharmaceutical Sciences* **1995,** *84* (8), 983-986.
19. (a) Dontireddy, R.; Crean, A. M., A comparative study of spray-dried and freeze-dried hydrocortisone/polyvinyl pyrrolidone solid dispersions. *Drug Development and Industrial Pharmacy* **2011,** *37* (10), 1141-1149; (b) Ghosh, I.; Snyder, J.; Vippagunta, R.; Alvine, M.; Vakil, R.; Tong, W.-Q.; Vippagunta, S., Comparison of HPMC based polymers performance as carriers for manufacture of solid dispersions using the melt extruder. *International Journal of Pharmaceutics* **2011,** *419* (1–2), 12-19.
20. Vasanthavada, M.; Tong, W.-Q.; Joshi, Y.; Kislalioglu, M. S., Phase Behavior of Amorphous Molecular Dispersions II: Role of Hydrogen Bonding in Solid Solubility and Phase Separation Kinetics. *Pharmaceutical Research* **2005,** *22* (3), 440-448.
21. Six, K.; Verreck, G.; Peeters, J.; Brewster, M.; Mooter, G. V. D., Increased physical stability and improved dissolution properties of itraconazole, a class II drug, by solid dispersions that combine fast- and slow-dissolving polymers. *Journal of Pharmaceutical Sciences* **2004,** *93* (1), 124-131.
22. Marsac, P.; Shamblin, S.; Taylor, L., Theoretical and Practical Approaches for Prediction of Drug–Polymer Miscibility and Solubility. *Pharmaceutical Research* **2006,** *23* (10), 2417-2426.
23. Rumondor, A. C. F.; Taylor, L. S., Effect of Polymer Hygroscopicity on the Phase Behavior of Amorphous Solid Dispersions in the Presence of Moisture. *Molecular Pharmaceutics* **2009,** *7* (2), 477-490.

24. Chan, K. L. A.; Kazarian, S. G., FTIR Spectroscopic Imaging of Dissolution of a Solid Dispersion of Nifedipine in Poly(ethylene glycol). *Molecular Pharmaceutics* **2004,** *1* (4), 331-335.

25. Van Drooge, D. J.; Hinrichs, W. L. J.; Visser, M. R.; Frijlink, H. W., Characterization of the molecular distribution of drugs in glassy solid dispersions at the nano-meter scale, using differential scanning calorimetry and gravimetric water vapour sorption techniques. *International Journal of Pharmaceutics* **2006,** *310* (1–2), 220-229.

26. Friesen, D. T.; Shanker, R.; Crew, M.; Smithey, D. T.; Curatolo, W. J.; Nightingale, J. a. S., Hydroxypropyl Methylcellulose Acetate Succinate-Based Spray-Dried Dispersions: An Overview. *Molecular Pharmaceutics* **2008,** *5* (6), 1003-1019.

27. Padden B, M. J., Robbins T, Zocharski Pd, Prasad L, Spence Jk, Lafountaine J, Amorphous solid dispersions as enabling formulations for discovery and early development. *Am Pharm Rev* **2011,** *1*, 66-73.

28. Dembri, A.; Montisci, M.-J.; Gantier, J.; Chacun, H.; Ponchel, G., Targeting of 3′-Azido 3′-deoxythymidine (AZT)-loaded poly(isohexylcyanoacrylate) nanospheres to the gastrointestinal mucosa and associated lymphoid tissues. *Pharm Res* **2001,** *18* (4), 467-473.

29. Löbenberg, R.; Maas, J.; Kreuter, J., Improved body distribution of 14C-labelled AZT bound to nanoparticles in rats determined by radioluminography. *Journal of Drug Targeting* **1998,** *5* (3), 171-179.

30. Destache, C.; Belgum, T.; Christensen, K.; Shibata, A.; Sharma, A.; Dash, A., Combination antiretroviral drugs in PLGA nanoparticle for HIV-1. *BMC Infectious Diseases* **2009,** *9* (1), 198.

31. Mainardes, R. M.; Gremião, M. P. D.; Brunetti, I. L.; Da Fonseca, L. M.; Khalil, N. M., Zidovudine-loaded PLA and PLA–PEG blend nanoparticles: Influence of polymer type on phagocytic uptake by polymorphonuclear cells. *Journal of Pharmaceutical Sciences* **2009,** *98* (1), 257-267.

32. Sharma, P.; Garg, S., Pure drug and polymer based nanotechnologies for the improved solubility, stability, bioavailability and targeting of anti-HIV drugs. *Advanced Drug Delivery Reviews* **2010,** *62* (4-5), 491-502.

33. Duan, J.; Zhang, Y.; Han, S.; Chen, Y.; Li, B.; Liao, M.; Chen, W.; Deng, X.; Zhao, J.; Huang, B., Synthesis and in vitro/in vivo anti-cancer evaluation of curcumin-loaded

chitosan/poly(butyl cyanoacrylate) nanoparticles. *International Journal of Pharmaceutics* **2010,** *400* (1–2), 211-220.

34. Posey-Dowty, J.; Watterson, T.; Wilson, A.; Edgar, K.; Shelton, M.; Lingerfelt, L., Zero-order release formulations using a novel cellulose ester. *Cellulose* **2007,** *14* (1), 73-83-83.

35. Shelton Michael, C.; Posey-Dowty Jessica, D.; Lingerfelt, L.; Kirk Shane, K.; Klein, S.; Edgar Kevin, J., Enhanced dissolution of poorly soluble drugs from solid dispersions in carboxymethylcellulose acetate butyrate matrices. In *Polysaccharide Materials: Performance by Design, American Chemical Society* **2009,** 1017, 93-113.

36. Sandra, K., Polysaccharides in Oral Drug Delivery ? Recent Applications and Future Perspectives. In *Polysaccharide Materials: Performance by Design, American Chemical Society*: **2009,** 1017, 13-30.

37. Raval, J. P.; Naik, D. R.; Amin, K. A.; Patel, P. S., Controlled-release and antibacterial studies of doxycycline-loaded poly(ε-caprolactone) microspheres. *Journal of Saudi Chemical Society* **2011,** (in press).

38. Mainardes, R. M.; Evangelista, R. C., PLGA nanoparticles containing praziquantel: effect of formulation variables on size distribution. *International Journal of Pharmaceutics* **2005,** *290* (1–2), 137-144.

39. Hariharan, S.; Bala, I.; Kumar, M. N. V. R., PLGA Nanoparticles in Drug Delivery: The State of the Art. **2004,** *21* (5), 36.

40. Johnson, B. K.; Prud; #39; Homme, R. K., Flash NanoPrecipitation of organic actives and block copolymers using a confined impinging jets mixer. *Australian Journal of Chemistry* **2003,** *56* (10), 1021-1024.

41. Johnson, B. K.; Prud'homme, R. K., Chemical processing and micromixing in confined impinging jets. *AIChE Journal* **2003,** *49* (9), 2264-2282.

42. Johnson, B. K.; Prud'homme, R. K., Mechanism for rapid self-assembly of block copolymer nanoparticles. *Physical Review Letters* **2003,** *91* (11), 118302.

43. Ungun, B.; Prud'homme, R. K.; Budijon, S. J.; Shan, J.; Lim, S. F.; Ju, Y.; Austin, R., Nanofabricated upconversion nanoparticles for photodynamic therapy. *Opt. Express* **2009,** *17* (1), 80-86.

44. Kumar, V.; Hong, S. Y.; Maciag, A. E.; Saavedra, J. E.; Adamson, D. H.; Prud'homme, R. K.; Keefer, L. K.; Chakrapani, H., Stabilization of the Nitric Oxide (NO) prodrugs and

anticancer leads, PABA/NO and double JS-K, through Incorporation into PEG-protected nanoparticles. *Molecular Pharmaceutics* **2009,** *7* (1), 291-298.

45. Chen, T.; D'addio, S. M.; Kennedy, M. T.; Swietlow, A.; Kevrekidis, I. G.; Panagiotopoulos, A. Z.; Prud'homme, R. K., Protected peptide nanoparticles: Experiments and brownian dynamics simulations of the energetics of assembly. *Nano Letters* **2009,** *9* (6), 2218-2222.

46. Ansell, S. M.; Johnstone, S. A.; Tardi, P. G.; Lo, L.; Xie, S.; Shu, Y.; Harasym, T. O.; Harasym, N. L.; Williams, L.; Bermudes, D.; Liboiron, B. D.; Saad, W.; Prud'homme, R. K.; Mayer, L. D., Modulating the therapeutic activity of nanoparticle delivered paclitaxel by manipulating the hydrophobicity of prodrug conjugates. *Journal of Medicinal Chemistry* **2008,** *51* (11), 3288-3296.

47. D'addio, S. M.; Prud'homme, R. K., Controlling drug nanoparticle formation by rapid precipitation. *Advanced Drug Delivery Reviews* **2011,** *63* (6), 417-426.

48. Liu, Y.; Cheng, C.; Prud'homme, R. K.; Fox, R. O., Mixing in a multi-inlet vortex mixer (MIVM) for flash nano-precipitation. *Chemical Engineering Science* **2008,** *63* (11), 2829-2842.

49. Gindy, M., Composite block copolymer stabilized nanoparticles: Simultaneous encapsulation of organic actives and inorganic nanostructures. *Langumir* **2008,** *24*, 83-90.

50. Hesse, L. M.; Von Moltke, L. L.; Shader, R. I.; Greenblatt, D. J., Ritonavir, Efavirenz, and Nelfinavir Inhibit CYP2B6 Activity in Vitro: Potential Drug Interactions with Bupropion. *Drug Metabolism and Disposition* **2001,** *29* (2), 100-102.

51. Ariza, R. M. Design, Synthesis, and Characterization of Magnetite Clusters using a Multi Inlet Vortex Mixer. Virginia Polytechnic Institute and State University, Blacksburg, Virginia, 2010.

52. Abdelwahed, W.; Degobert, G.; Fessi, H., Investigation of nanocapsules stabilization by amorphous excipients during freeze-drying and storage. *European Journal of Pharmaceutics and Biopharmaceutics* **2006,** *63* (2), 87-94.

53. Abdelwahed, W.; Degobert, G.; Fessi, H., A pilot study of freeze drying of poly(epsilon-caprolactone) nanocapsules stabilized by poly(vinyl alcohol): Formulation and process optimization. *International Journal of Pharmaceutics* **2006,** *309* (1–2), 178-188.

54. Kohane, D. S., Microparticles and nanoparticles for drug delivery. *Biotechnology and Bioengineering* **2007,** *96* (2), 203-209.

55. Plakkot, S.; De Matas, M.; York, P.; Saunders, M.; Sulaiman, B., Comminution of ibuprofen to produce nano-particles for rapid dissolution. *International Journal of Pharmaceutics* **2011,** *415* (1–2), 307-314.

56. Liu, P.; Rong, X.; Laru, J.; Van Veen, B.; Kiesvaara, J.; Hirvonen, J.; Laaksonen, T.; Peltonen, L., Nanosuspensions of poorly soluble drugs: Preparation and development by wet milling. *International Journal of Pharmaceutics* **2011,** *411* (1–2), 215-222.

57. Niwa, T.; Miura, S.; Danjo, K., Design of dry nanosuspension with highly spontaneous dispersible characteristics to develop solubilized formulation for poorly water-soluble drugs. *Pharmaceutical Research* **2011,** *28* (9), 2339-2349.

58. Sun, W.; Mao, S.; Shi, Y.; Li, L. C.; Fang, L., Nanonization of itraconazole by high pressure homogenization: Stabilizer optimization and effect of particle size on oral absorption. *Journal of Pharmaceutical Sciences* **2011,** *100* (8), 3365-3373.

59. Rabinow, B. E., Nanosuspensions in drug delivery. *Nature Reviews Drug Discovery* **2004,** *3*, 785-796.

60. Keck, C. M.; Müller, R. H., Drug nanocrystals of poorly soluble drugs produced by high pressure homogenisation. *European Journal of Pharmaceutics and Biopharmaceutics* **2006,** *62* (1), 3-16.

61. Rh, J. J. a. M., Nanocrystal technology, drug delivery and clinical applications. *Int J Nanomedicine* **2008,** *3*, 295-309.

62. Merisko-Liversidge, E. M.; Liversidge, G. G., Drug nanoparticles: Formulating poorly water-soluble compounds. *Toxicologic Pathology* **2008,** *36* (1), 43-48.

63. Williams, H. D.; Trevaskis, N. L.; Charman, S. A.; Shanker, R. M.; Charman, W. N.; Pouton, C. W.; Porter, C. J. H., Strategies to address low drug solubility in discovery and development. *Pharmacological Reviews* **2013,** *65* (1), 315-499.

64. Wu, L.; Zhang, J.; Watanabe, W., Physical and chemical stability of drug nanoparticles. *Advanced Drug Delivery Reviews* **2011,** *63* (6), 456-469.

65. Vogt, M.; Kunath, K.; Dressman, J. B., Dissolution enhancement of fenofibrate by micronization, cogrinding and spray-drying: Comparison with commercial preparations. *European Journal of Pharmaceutics and Biopharmaceutics* **2008,** *68* (2), 283-288.

66. Hargrove Jt, M. W., And Wentz Ac, Absorption of oral progesterone is influenced by vehicle and particle size. *Am J Obstet Gynecol* **1989,** *161*, 948-951.

67. J, N. F. a. R., Dependence of area under the curve on proquazone particle size and in vitro dissolution rate. *J Pharm Sci* **1980,** *69*, 605-607.

68. Watari, N.; Funaki, T.; Aizawa, K.; Kaneniwa, N., Nonlinear assessment of nitrofurantoin bioavailability in rabbits. *Journal of Pharmacokinetics and Biopharmaceutics* **1983,** *11* (5), 529-545.

69. Guimes Rodrigues, F.; Ricardo Chagas Da, S.; Carla Da Silva, M.; Rosana Maria Nascimento De, A.; Harumi, O., Water flux through blends from waste materials: Cellulose acetate (from sugar cane bagasse) with polystyrene (from plastic cups). *J Appl Polym Sci* **2005,** *96* (2), 516-522.

70. Rumondor, A. C. F.; Marsac, P. J.; Stanford, L. A.; Taylor, L. S., Phase behavior of poly(vinylpyrrolidone) containing amorphous solid dispersions in the presence of moisture. *Molecular Pharmaceutics* **2009,** *6* (5), 1492-1505.

71. Alonzo, D. E.; Gao, Y.; Zhou, D.; Mo, H.; Zhang, G. G. Z.; Taylor, L. S., Dissolution and precipitation behavior of amorphous solid dispersions. *Journal of Pharmaceutical Sciences* **2011,** *100* (8), 3316-3331.

72. Hancock, B. C.; Zografi, G., Characteristics and significance of the amorphous state in pharmaceutical systems. *Journal of Pharmaceutical Sciences* **1997,** *86* (1), 1-12.

73. Ilevbare, G. A.; Liu, H.; Edgar, K. J.; Taylor, L. S., Understanding polymer properties important for crystal growth inhibition—impact of chemically diverse polymers on solution crystal growth of ritonavir. *Crystal Growth & Design* **2012,** *12* (6), 3133-3143.

4.6. Supporting Information

Calculation of Drug Loading

Construction of calibration curve

In order to measure the RTV and EFV loading of the CMCAB nanoparticles, a calibration curve (**Figure S.1**) for the RTV dissolved in acetonitrile and (**Figure S.2**) for the EFV dissolved in acetonitrile was developed using a HPLC (Agilent 1200) at a wavelength of 240 nm where the absorbance was a maximum. In a typical experiment, 10 mgs of RTV (or EFV) were dissolved in a 10 mL volumetric flask containing 2 mL acetonitrile. More acetonitrile was added up to the 10 mL mark to prepare the stock solution of rifampicin in acetonitrile. This solution was serially diluted with acetonitrile to make solutions with rifampicin concentrations of 10, 20, 30, 40, 50, 60, 70 µg/mL. The equation for the calibration curve of Ritonavir in acetonitrile is

Area under curve (AUC) at 240 nm = $2352.6C_{RTV}$ where $R^2 = 0.9999$

[S.8]

The equation for the calibration curve of Efavirenz in acetonitrile is

Area under curve (AUC) at 240 nm = $7222.2C_{EFV}$ where $R^2 = 0.9999$

[S.9]

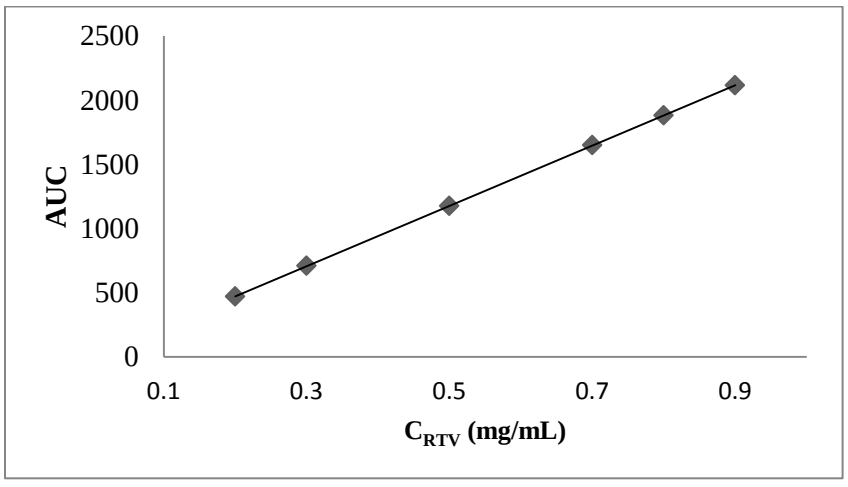

Fig S.1 Calibration curve of ritonavir dissolved in acetonitrile at 240 nm

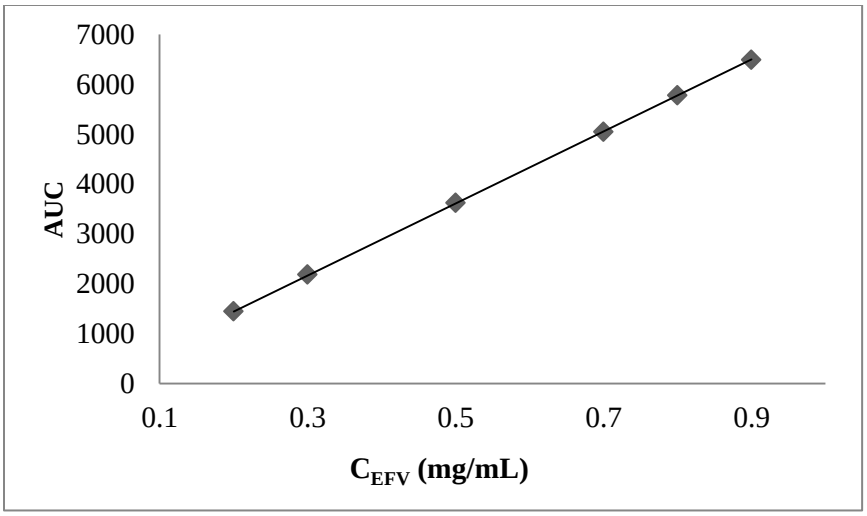

Fig S.2 Calibration curve of Efavirenz dissolved in acetonitrile at 240 nm

The dry powders (concentration of 1 mg/mL i.e. 15 mgs of powder dissolved in 15 mL of acetonitrile) of RTV/EFV-CMCAB were dissolved in acetonitrile and sonicated for 15 minutes in a bath sonicator. The sample was filtered with a 0.2 µm filter before injecting into the HPLC column.

The drug loading W_{druf} for the dried particles (after dissolving them in acetonitrile) is given by:

$$W_{drug} = \frac{Final\ concentration\ of\ the\ RTV\ or\ EFV\ in\ the\ solvent}{Initial\ concentration\ of\ particles\ in\ the\ solvent}\ x\ 100 = \frac{C_{drug}}{C_{part}} \text{ x } 100 \qquad [S.10]$$

C_{drug} = Concentration of the drug calculated from calibration curve equation S.8 and S.9.

C_{part}= Concentration of the particles dissolved in acetonitrile.

The standard deviation of the drug loading σ_{Wdrug} of the drug (RTV/RFV)-CMCAB nanoparticles is given by:

$$\sigma_{Xdrug}^2 = \sigma_{Cdrug}^2\left(\frac{m_{Ace}}{\rho_{Ace}\, m_{comp}}\right)^2 + \sigma_{mAce}^2\left(\frac{C_{drug}}{\rho_{Ace} m_{comp}}\right)^2 + \sigma_{mcomp}^2\left(\left(\frac{C_{drug} m_{Ace}}{\rho_{Ace}}\right)\left(\frac{1}{m_{comp}^2}\right)\right)^2$$

$$\sigma_{W_{drug}} = \sigma_{X_{drug}} \times 100 \qquad [S.11]$$

where:

σ_{Xdrug} = standard deviation of mass fraction of drug in the particles

σ_{wdrug} = standard deviation of weight fraction of drug in the particles

m_{Ace} = mass of acetonitrile which is used to make samples. For example, the mass of 5 mLs of acetonitrile that were typically used in the experiments would be used here.

m_{comp} = mass of the complex used in the drug loading measurements.

σ_{mAce} = standard deviation of the mass of acetonitrile used to make sample. For example, 5 mLs of acetonitrile were measured into a pre-weighed bottle and the mass was measured. This was done 5 times and the information was used to calculate σ_{mAce} = 0.1649 grams.

σ_{mcomp} = standard deviation of the mass of the dried complexes. For example, a typical mass of complex was weighed on the balance and the balance readout was observed over a period of 1 minute, recording the magnitude of the fluctuation in the measurement, Δm_{fluct}, (the maximum-to-minimum value of the mass). Here σ_{mcomp} = 0.0001 gms.

σ^2_{Cdrug}= standard deviation of the drug concentration measured with HPLC is given by:

$$\sigma^2_{Cdrug} = \sigma^2_{Abs}(\frac{1}{b})^2 + \sigma^2_a \left(\frac{1}{b}\right)^2 + \sigma^2_b \left(\frac{Abs - a}{b^2}\right)^2 \qquad [S.12]$$

where:

σ_{AUC} = standard deviation of the AUC measurement. This can be estimated from information about the typical uncertainty of the instrumental measurement of the absorbance. In this work, $\sigma_{AUC} \approx 0.004$ based on information from the manual of the HPLC (Agilent 1200).

a = y- intercept of the absorbance-calibration curve = 1.541864

b = slope of the absorbance-calibration curve = 2.350308

σ^2_a = variance of the y intercept = 3.462233

σ^2_b = variance of the slope = 8.95405*10^-6

When, for example, the concentration of a RTV is 0.17 µg/ml and the AUC is 391.5

We can write from equation S.12,

$$\sigma_{CRTV}^2 = 0.004^2 \times \left(\frac{1}{2.350508}\right)^2 + (3.462232606) \times \left(\frac{1}{2.350308475}\right)^2 + (8.95405 * 10^{-6}) \times \left(\frac{391.5 - 1.541864407}{2.350308475^2}\right)^2$$

σ_{CRTV}^2 = 0.67

Now putting the value of σ_{Crif}^2 in equation S.11, and substituting the following

σ_{mAce} = 16491 µg

ρ_{Ace} = 787000 µg/ml

m_{comp} = 1500 µg

m_{Ace}/ρ_{Ace} = V_{Ace} = volume of acetonitrile = 5 mls

We can write equation S.11 as,

$$\sigma_{Xrif}^2 = (0.67)\left(\frac{5}{5000}\right)^2 + (16491)^2\left(\frac{0.17}{78700 \times 5000}\right)^2 + 100^2\left((0.17 \times 1)\left(\frac{1}{5000^2}\right)\right)^2$$

σ_{Xrif}^2 = 6.71*10^{-7}

$or\ \sigma_{Xrif}$ = 0.000819

$\sigma_{wrif} = \sigma_{Xrif} \times 100 = 0.08$

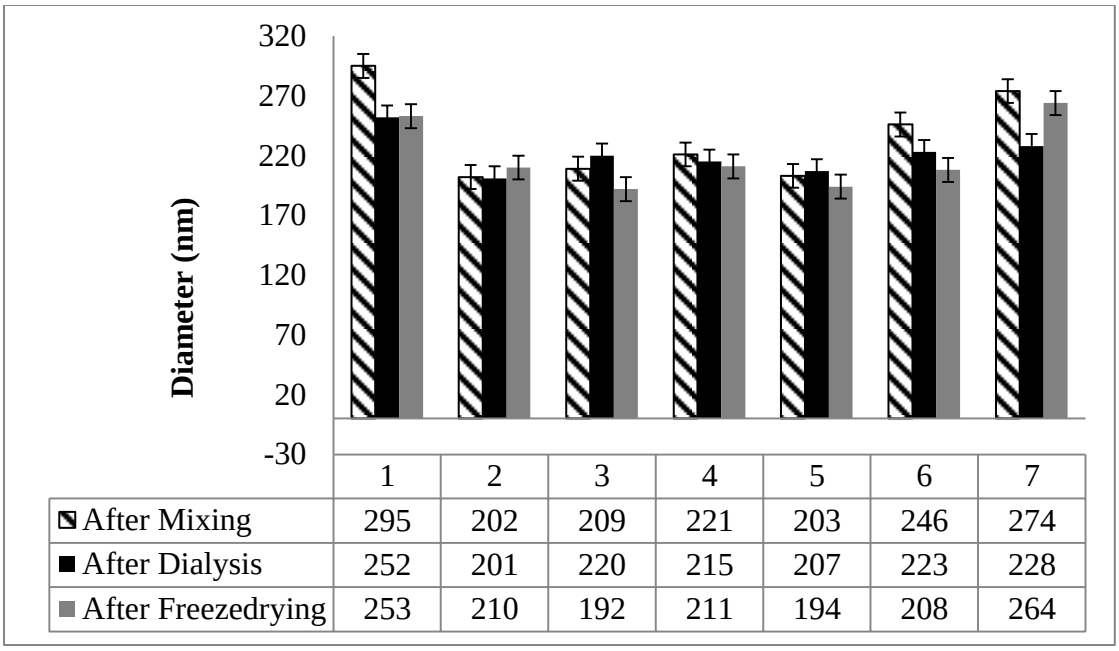

	1	2	3	4	5	6	7
After Mixing	295	202	209	221	203	246	274
After Dialysis	252	201	220	215	207	223	228
After Freezedrying	253	210	192	211	194	208	264

Fig. S.3 Particle Size Analysis of CMCAB, CMCAB-RTV and CMCAB-EFV nanoparticles after mixing, dialysis and freeze drying.

The particle size range between 200-300 nm. The error bars shows standard deviation from 3 different batches of particles. Here the numbers 1-7 represents the following:

1- CMCAB NPs
2- CMCAB- 19 wt % RTV
3- CMCAB- 29 wt % RTV
4- CMCAB-40 wt % RTV
5- CMCAB-18 wt % EFV
6- CMCAB-29 wt % EFV
7- CMCAB-43 wt % EFV

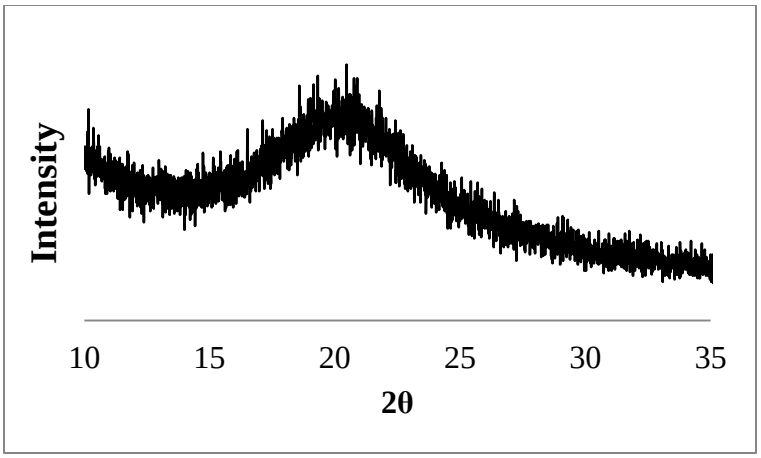

Fig. S.4 X-ray diffractograms of pure CMCAB as received

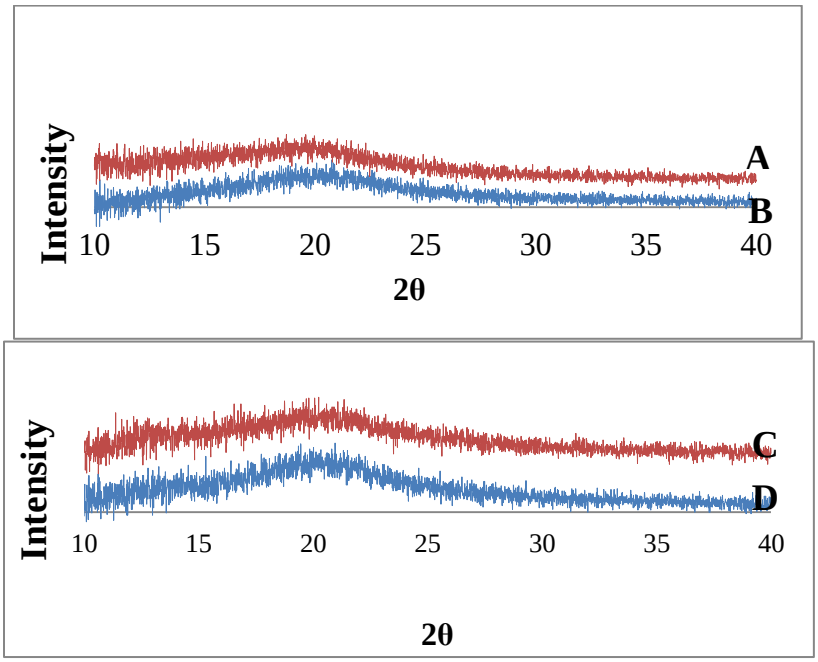

Fig. S.5 X-ray diffractograms of (A) CMCAB-RTV (actual drug loading is 29 wt%), (B) CMCAB-RTV (actual drug loading is 40 wt%), (C) CMCAB-EFV (actual drug loading is 18 wt%), (D) CMCAB-EFV (actual drug loading is 43 wt%)

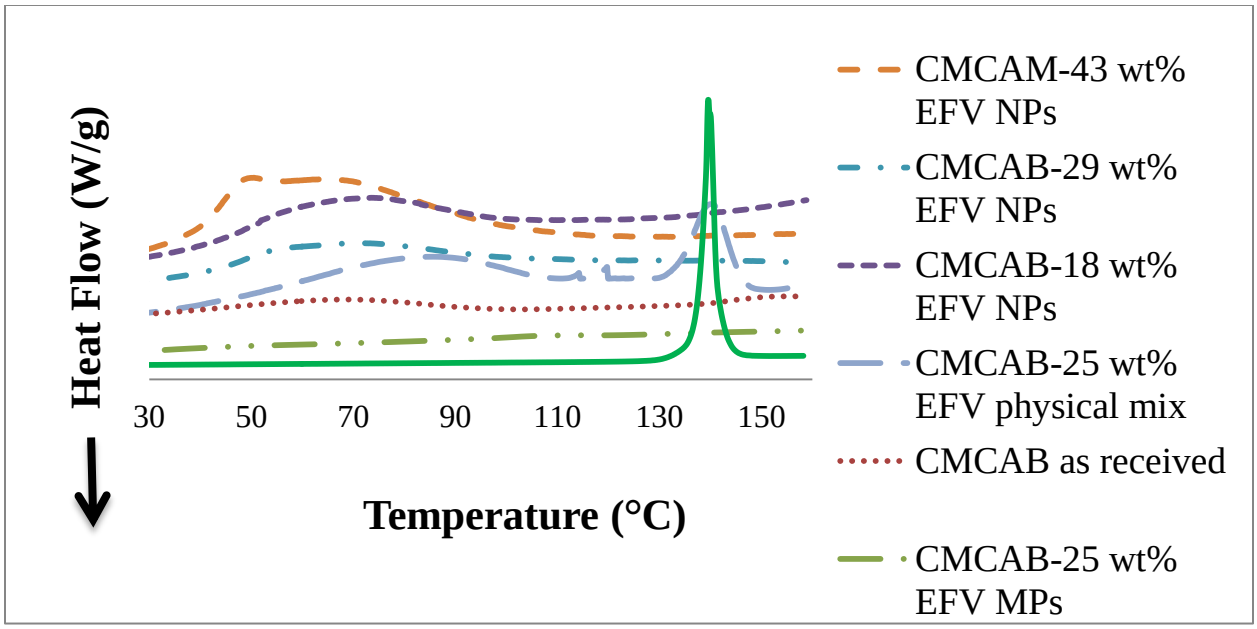

Fig. S.6. First DSC scan showing melting peak of EFV at 140° C. No such peak is observed in the any of the CMCAB-EFV nanoparticles.

Chapter 5: Preparation and Properties of Nanoparticles of Complexes of Polysaccharides and Antiviral Drugs: Effect of Polysaccharide Chemistry

Sonal Mazumder[a], Haoyu Liu[a], Junia M. Pereira[a] , Kevin J. Edgar[b], E. Bruce Orler[c], Robert B. Moore III[c] and Richey M Davis[*d]

[a]Macromolecules and Interfaces Institute, [b]Department of Sustainable Biomaterials, [c] Department of Chemistry, [d]Department of Chemical Engineering

Virginia Polytechnic Institute and State University, Blacksburg, VA 24061, USA

*Corresponding author:

Richey M. Davis
Department of Chemical Engineering, VirginiaTech, Blacksburg, VA - 24061
Tel: 001+ 540-231-4578 ; Fax : 001+ 540-231-5022
E-mail address: rmdavis@vt.edu

ABSTRACT

Nanoparticles of amorphous dispersions of antiviral drugs, ritonavir (RTV) and efavirenz (EFV) with several novel polysaccharides (cellulose esters and a pullulan derivative) were produced by a rapid precipitation process. Particles were purified by dialysis and dried powders were recovered after freeze drying. Particle diameters as measured by dynamic light scattering were in the range 100-200 nm. The nanoparticles showed significant aggregation after freeze drying but this was reduced by using trehalose as a cryoprotectant. The target drug loading in the particles was 25 wt % and the drug loading efficiencies for the cellulose ester nanoparticles ranged from 72-96% while the drug loading efficiency for the pullulan derivative nanoparticles were approximately 62%. All the nanoparticles afforded increased solution concentration and faster release compared to the pure drugs.

Keywords: Ritonavir, Efavirenz, cellulose ester, pullulan, nanoparticles, flash nanoprecipitation, multi-inlet vortex mixer, drug release

5.1. INTRODUCTION

The Human Immunodeficiency Virus (HIV) affects the immune system and is responsible for causing acquired immunodeficiency syndrome (AIDS). Currently, more than 33 million people are HIV-positive[1]. Ritonavir (RTV) and efavirenz (EFV) are two important drugs for the treatment of HIV. RTV (Figure 1(a)) is an inhibitor of the HIV protease enzyme and also a selective, competitive inhibitor of the liver enzyme Cytochrome P450 (CYP3A)[2] which helps to increase the bioavailability of other protease inhibitors like atazanavir or lopinavir that are CYP3A substrates in dual protease therapy. It has a low solubility (1.2 µg/ml) and high dosage (10 mg/kg, or 600 mg for a 60 kg person) and thus a very low oral bioavailability. A relatively high dose of the drug is required to maintain therapeutic concentrations for longer periods, this lead to several side effects (asthenia, malaise, diarrhea, nausea and vomiting, abdominal pain, dizziness, insomnia, sweating, taste abonormality).

Efavirenz (Figure 1(b)) is a non-nucleoside reverse transcriptase inhibitor (NNRTI) which has been approved by the FDA and is a first line drug of choice in Highly Active Anti-Retroviral Therapy (HAART) for treatment of HIV and AIDS. It has low water solubility (8.85 µg/ml) with 40-45% of oral bioavailability and is typically administered in doses of 600-800 mg/day. Both RTV and EFV are highly crystalline and poorly soluble in the gastrointestinal tract leading to poor bioavailability.

Oral administration of therapeutic agents is the easiest and frequently preferable mode of drug delivery, as there is no requirement for hospitalization which requires medical infrastructure, a critical issue in underdeveloped countries. In addition, patient compliance in taking oral medications is greater than with injected formulations [3]. However, it is important and challenging to attain the desired pharmacokinetic profile for a given drug, especially one with

poor aqueous solubility [4]. There are several factors in the GI tract which can limit the bioavailability of drugs such as tissue barriers (mucosa, microvilli) and physiological factors (varying pH, enzymes, transporter mechanisms).

For the purposes of drug delivery, nanoparticles are typically defined as a particulate phase consisting of an active pharmaceutical ingredient having physical dimensions less than 1 micron and are dispersed in an external phase. The large surface area per unit mass enhances the interaction of the particles with the epithelial lining and mucus. Nanoparticles with well-defined size distributions have the potential to release large fractions of their drug load in the first few hours in the small intestine. We hypothesize that effect of synergy between ASD and particle size reduction will lead to high release rate in the small intestine could lead to improved solution concentration, bioavailability and hence to a reduced required dose.

Controlling drug release kinetics from the nanocarrier can be difficult. A challenge in designing nanocarrier drug delivery systems is finding the optimized particle size that will result in desired release characteristics. Drug diffuses out of smaller nanocarriers faster, resulting in burst effects instead of sustained or controlled drug delivery over prolonged periods of time [5]. The drug release kinetics can be improved by increasing the size of the nanocarriers, which results in lower drug loss and prolonged drug release with a lower burst effect [6]. However, increasing the polymer-drug particle size may hinder their transport across membranes.

Recently, polysaccharides have been shown to be very promising for oral drug delivery due to their affinity for complexing with a variety of drugs which can suppress crystallization of the drugs, their relatively high glass transition temperatures, and their biocompatibility [7,8,9]. Though several studies have concerned the formulation of polymer-antiviral drug nanoparticles with synthetic or semisynthetic polymers (polymers prepared by chemical modification of

natural occurring polymers[10,11,12,13,14,15]), natural polysaccharides have not been explored as anti-HIV nanocarrier systems. Some of the studies with synthetic polymers are discussed in Chapter 4.

Amorphous solid dispersions (ASDs) have attracted great interest due to their utility in formulating poorly soluble active pharmaceutical ingredients (APIs) to attain effective solubility[16,17,17b] and bioavailability[18,19,20] . Although solid dispersions are well known for enhancing dissolution properties of drugs, there are several issues to consider when evaluating the dissolution behavior of solid dispersions including the drug–polymer ratio, the relative dissolution rates of the two components, and the crystallization behavior of the drug during the dissolution process[21]. Some of these issues were discussed in detail in Chapter 3.

Miscibility between the polymer and drug is an important factor in the preparation of amorphous solid dispersions of polymer-drug systems and is a measure of the ability of the polymer to dissolve the crystalline drug. Stronger interactions between the polymer and drug increase the miscibility and the ability of the polymer to form an amorphous solid dispersion with the drug which can make it more soluble[22,22b,23]. Phase separation and fast recrystallization of the amorphous form can occur as the polymer-drug interactions become weaker[24,25]. It is important to measure and, when possible, to predict polymer-drug miscibility to determine the minimum amount of polymer required to keep the drug in its amorphous form[26,27].

Many prior studies of drug-polymer nanoparticles focused on controlling drug loading and characterizing drug release but, in many cases, the method of producing the particles was not rapid and scalable. Also there are relatively few studies that focus on understanding structure-property relationships such as dissolution behavior and the stability and miscibility of amorphous solid dispersions of polymer-drug nanoparticles.

In this chapter, we focus on made RTV and EFV-containing amorphous nanoparticles, selecting from three novel cellulose derivatives and one novel pullulan derivative. All contain pendant carboxyl groups, so are pH-sensitive and water-swellable when partially ionized at pH 6-7 but insoluble at pH ~ 3-4. There is no previous study reported where these drugs were complexed these polysaccharides to form nanoparticles. We investigated the effect of processing conditions on the particle size and drug loading of nanoparticles of RTV and EFV, made with these polysaccharides using the flash nano-precipitation method [28,29,30] in a multi-inlet vortex mixer (MIVM) [31,32,33,34,35]. In this method, nanoparticles form very rapidly by controlled nucleation and growth of particles which allows for the production of nanoparticles of controlled size in a continuous manner.[36] This is achieved by controlling the Reynolds numbers and the liquid phase composition, allowing for rapid and complete mixing.[29, 36a, 37]

The work reported in this chapter focuses on establishing a methodology for preparing well-defined drug-polymer complexes relatively rapidly and in a manner that can produce particles with high drug loadings. We study particle sizes and drug loading to test control and reproducibility of the particle formation process. The suppression of drug crystallinity and miscibility with polymers is to determine the ability of polymers to stabilize against crystallization in nanoparticles. Drug release and solution concentration are studied to determine impact of polymer structure and particle size on these key parameters and to test the main hypothesis.

5.2. MATERIALS AND METHODS

5.2.1 Materials

Tetrahydrofuran (anhydrous, ACS reagent, ≥99.0% inhibitor free) was used as received. Acetonitrile (HPLC grade, >95 %) was used for HPLC analysis without further purification. RTV and EFV (Attix Pharmaceuticals, Canada) were used without further purification. (Figure 1a and Figure 1b). The pKa of RTV is 14.23 and that of EFV is 10.2. Millipore water (18.2 MΩ•cm at 25 °C ultrapure water, Synergy Ultrapure Water Systems, USA) was used for DLS measurements and in the formation of polymer/drug nanoparticles. Dialysis tubing (Spectropore, cellulose ester) which was used for solvent removal had a molecular weight cut off (MWCO) of 25K. D-(+)-Trehalose dehydrate (Sigma Aldrich, CAS 6138-23-4, molecular weight – 378.33 g/mole) was used as a cryoprotectant against aggregation during freeze drying. The abbreviations used in this paper for novel cellulose and pullulan derivatives used in this work along with some of their properties are presented in Table 1.

The general synthetic methods for the novel cellulose esters polymers and the 6 carboxypullulan ethers are described elsewhere [38,39,40] . Adipate and other ω-carboxyalkanoate (e.g., suberate and sebacate) esters of the renewable natural polysaccharide cellulose have shown potential for forming amorphous solid dispersions with hydrophobic drugs [39]. Figure 2 shows the structure of three of the cellulose esters and the 6-butyl pullulan carboxylate polymers which formed well-defined particles by the flash nanoprecipitation process.

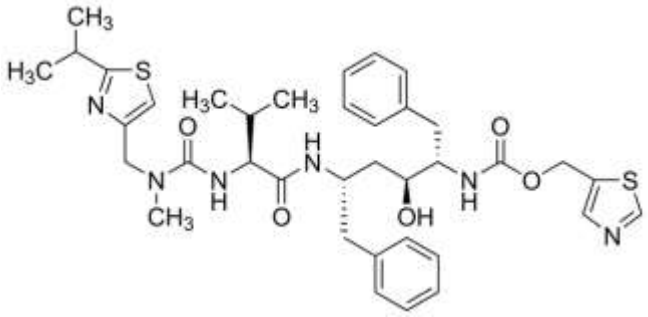

(a)

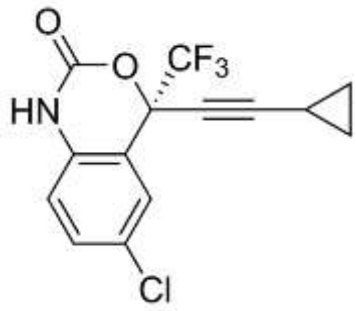

(b)

Figure 1. (a) Structure of Ritonavir (RTV)[41] , solubility ~1.2 µg/ml at pH 6.8

(b) Structure of Efavirenz (EFV)[41], solubility ~ 8.85 µg/ml at pH 6.8

Table 1. Abbreviation and properties of Novel Synthesized Cellulose and Pullulan Derivatives

Polymer	Polymer Abbreviation	DS (CO_2H)	DS (Other)	DS (Total)	Solubility Parameter ($MPa^{1/2}$)	Molecular weight ($x10^3$)	T_g (°C)
Cellulose Acetate Propionate 504-0.2 Adipate 0.33	CAP Adp 0.33	0.33	Ac 0.04; Pr 2.09	2.46	20.56	12.0	125
Cellulose Acetate Propionate Adipate 0.85	CAP Adp 0.85	0.85	Ac 0.04; Pr 2.09	2.98	21.27	9.7	110
Cellulose Acetate 320S sebacate	CA 320S Seb	0.57	Ac 1.82	2.39	22.36	25	117
6-butyl pullulan carboxylate	BPC	0.53			28	x	Above 200

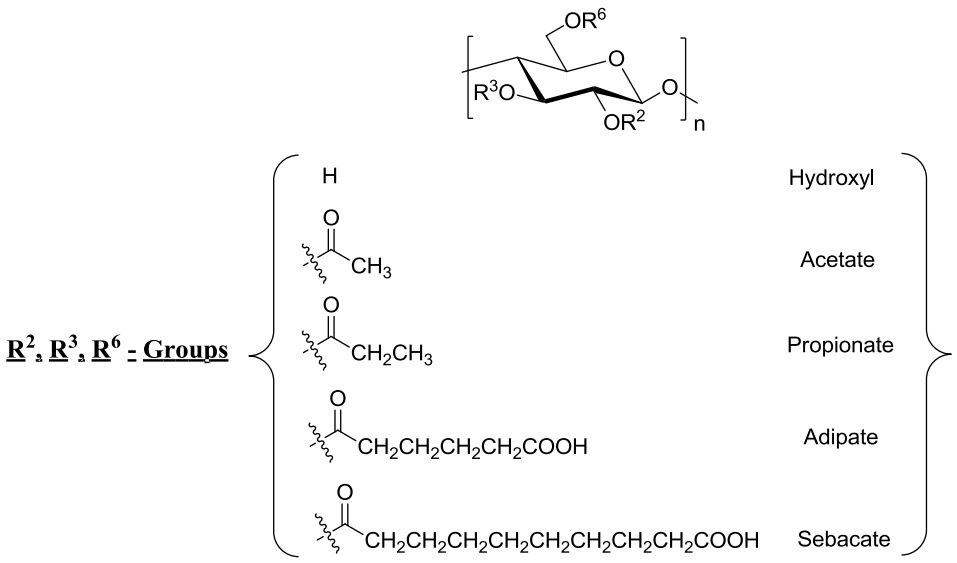

(a)

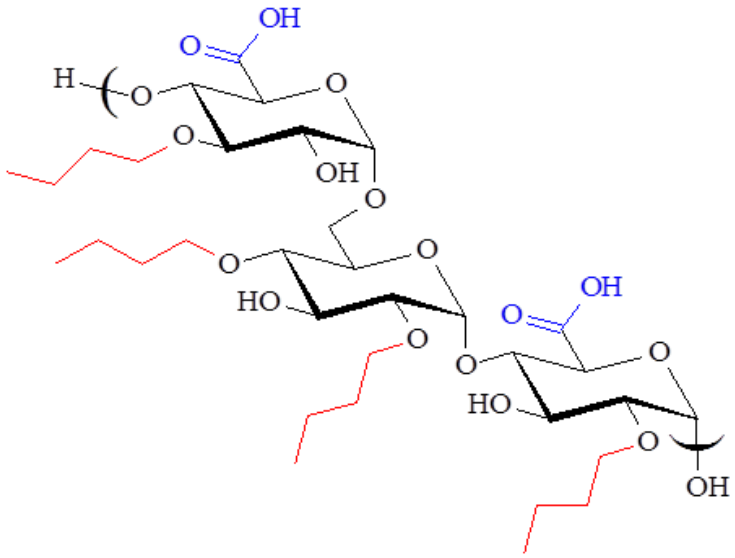

(b)

Figure 2. (a) Molecular structures of the novel cellulose derivatives. These cellulose derivatives are not regioselectively substituted, (b) Butyl pullulan-6-carboxylate (BPC)

(The following methodologies (5.2.2-5.2.8) in this section follow very closely procedures in Chapter 4: "Preparation and characterization of nanoparticles of carboxymethyl cellulose acetate butyrate containing anti-viral drugs for oral drug delivery" and are shown here for completeness.)

5.2.2 Nanoparticle preparation by rapid precipitation in the Multi Inlet Vortex Mixer

Each of the powdered polymers shown in Table 1 and drug (RTV or EFV) and THF were weighed in to a glass vial that was then sealed with a screw cap and bath sonicated (Cole Parmer model 8890) for 45 minutes. Flash nanoprecipitation of polymer-drug complexes was carried out in a four-jet Multi-Inlet Vortex Mixer that accommodates four streams.[36a,42] Polymer and drug (RTV/EFV) were dissolved in THF (organic stream) which was injected into the mixer with three other water streams. The temperature of the streams was adjusted to 25°C prior to injection into the mixer by immersing the syringes containing the organic solution and the water in a temperature controlled bath. The four inlet streams are tangential to the mixing chamber and the the exit stream comes from the center of the chamber. The nanoparticles were formed at a nominal Reynolds number of ~ 3900. The Reynolds number is a dimensionless number that is a measure of turbulence and, in this case, of mixing time. It depends upon the inlet stream velocities, viscosities, and densities[36a,29]. Calculations for the Reynolds number are shown in the Supporting Information in Chapter 3.

A New Era 4000 double syringe pump (for the organic stream) and a Harvard Apparatus Remote Infuse/Withdraw PHD 4000 Hpsi Programmable syringe pump (for the three water streams) controlled inlet flow rates. The New Era pump was controlled by the software, Syringe Pump Pro version 1.53. The injected volume ratio of THF to Millipore water was 1:9 v/v. The

polymer concentration in THF was 10 mg/mL. The target loading of the RTV and EFV was 25 wt% of the total solids on a dry basis.

5.2.3 Microparticle formation

CAP Adp 0.33 or CAP Adp 0.85 (150 mg) in 40 mL acetone were stirred at room temperature until the polymer was completely dissolved (approximately 2 hours). Ritonavir (50 mg) was added to this solution and stirred for 10 min. The acetone solution containing the dissolved polymer and drug was added dropwise to 150 mL of water. The organic solvent was removed from the resulting suspension using a rotary evaporator. The resulting aqueous solution was then freeze-dried to yield microparticles of amorphous solid dispersions of ritonavir/ polymers.

5.2.4 Nanoparticles recovery, solvent removal and drying

Since the particles exit from the MIVM in a mixed organic-water phase, it was necessary to remove the solvent and any unincorporated drug from the particles. Thus, particles were processed by dialysis followed by freeze drying. Polymer-RTV/EFV suspensions were recovered from the mixer and dialyzed to remove THF, free drug, and dissolved polymer molecules. Particle suspensions (40 mL) was added to dialysis tubing, which was placed in 4 L of DI water. The water was changed 4 times over a period of 24 hours. The dialyzed particles were dried in a LABCONCO freeze dryer at 0.018 mbar for 2 days.

5.2.5 Drug composition by HPLC

Drug loading and drug release were measured using an Agilent 1200 Series HPLC system which consisted of a quaternary pump, online degasser, manual injector with a 20-μL sample loop and Agilent chemstation LC 3D software. Chromatography was conducted in reverse mode using acetonitrile and phosphate buffer (0.05M, pH 5.65). Gradient at 40% for 1

min, raised to 60% in 14 min, was reduced to 40% in 1 min, held at 40% for 4 min. Total analysis time was 20 min. Mobile phase was flow rate 1.5 mL/min, column temperature at 30^{o}C. Sample injection volume 5 µL. Detection was performed by a diode array detector at a wavelength of 240 nm for ritonavir and efavirenz. Calibration curves for RTV and EFV dissolved in acetonitrile were developed and are shown in Figures S.1 and Figure S.2, respectively, in the Supporting Information in Chapter 4.

5.2.6 Particle size – Dynamic light scattering and Scanning Electron Microscopy

Dynamic light scattering (DLS) measurements of the nanoparticle sizes were performed before and after dialysis using a Malvern Zetasizer Nano-ZS (Malvern Instruments Ltd, Malvern, UK) at a wavelength of 633 nm and with a scattering angle of 173˚ at 25 ± 0.1 ºC. Intensity average diameters were obtained by calculations using Malvern's Zetasizer nano 6.12, software that utilizes an algorithm based upon Mie theory with the assumption that the scattering particles are hard spheres. For DLS analysis of the complexes, typically 200 µL of the nanoparticle suspension obtained from the mixer were diluted with 2 mL of deionized water. The dialyzed suspensions (1 mL) were diluted with 3 mL of deionized water and the freeze dried powders were diluted with deionized water to make a concentration of 0.1 mg/mL. Trehalose was added before freezing (as a cryoprotectant) at various values of the ratio of nanoparticles: trehalose ranging from 1:1 to 1:10 to control the redispersibility of the particles. Trehalose forms hydrogen bonds with nanoparticles during freeze drying and is preferably to many other cryoprotectants since it has a high T_g, and is not very chemically reactive [43]. Trehalose was added in nanoparticles of the cellulose derivatives but not added in BPC nanoparticles. The suspensions were sonicated with a bath sonicator (Cole Parmer model 8890) for 10 minutes before measuring the particle size by dynamic light scattering. Field emission scanning electron

microscope (FESEM) images of the microparticles were obtained using a LEO (Zeiss) 1550 instrument at a 5 kV accelerating voltage in the conventional high vacuum mode. The microparticles were sonicated at 0.01 mg/ml in DI water. Approximately 100 µl of the prepared samples was placed on imaging tape and allowed to dry at room temperature. Samples for SEM were mounted on metal stubs and coated with gold prior to analysis.

5.2.7 Characterization of crystallinity

Crystallinity of nanoparticles and microparticles was evaluated by powder X-ray diffraction (PXRD) and differential scanning calorimeter (DSC). Particles were stored for 2-3 weeks before analyzing with PXRD and DSC. The particles were kept in glass vials covered tightly with screw caps and stored in refrigerator (~-20°C).

PXRD patterns were obtained using Bruker D8 Discover X-ray Diffraction system (Madison, Wisconsin). The X-ray tube consists of a target material made of copper, which emits a Kα radiation (λ = 1.54 Aº) using a power rating of 2200 watts and an accelerating potential of 60 kV. The divergence and scattering slits were set at 1.0° and the receiving slit was at 0.1 mm. The experiment was conducted with a scan range from 10° - 40° 2θ, while the scanning speed was 4°/min.

Morphology was investigated using a TA Instruments differential scanning calorimeter (Q2000) equipped with a RCA90 refrigerated cooling accessory. Samples (1.5-3.5 mg) in aluminum Tzero pans were heated at a scanning rate of 10° C/min from a temperature of -85°C to 180°C, quenched and then heated again. Dry N_2 was used as the purge gas at 50 ml/min. The instrument was equilibrated at -85°C. The calibration of the temperature and cell constant was carried out with indium. T_g was recorded as the mid-point of the endothermic step transition

from the 2nd heat scan. Thermal transitions were viewed and analyzed using the analysis software Universal Analysis 2000.

5.2.8 Dissolution studies

Typically, RTV/EFV (10 mgs) or nanoparticles (15 mg) were dispersed in potassium phosphate buffer (80 mL, pH 6.8) at 37°C for 5 h. The apparatus used in the release experiments consisted of 250-mL jacketed flasks with circulating ethylene glycol/water (1:1) to control the temperature. The mixture was constantly stirred at 200 rpm with a magnetic stirr bar. Aliquots (0.8 mL) were withdrawn from the suspensions every 0.5 hour (during the first 2 hours), then every hour for 5 h. Phosphate buffer (pH 6.8, 0.8 mL) was added to maintain constant volume after each aliquot was withdrawn. Samples were ultracentrifuged at 13,000 rpm (equivalent of 16060 g's) in an accuSpin Micro (Fisher Scientific) for 10 minutes. The supernatant was recovered, and the solution concentration was determined by HPLC. CAP adipate microparticles with equivalent amount of drug as nanoparticles were used to compare the solubility and release of drugs from both kinds of particles. The solubility studies were done approximately 2-3 weeks after the preparation of the particles. During that period, the particles were kept in glass vials covered tightly with screw caps and stored in a refrigerator at 4 C.

5.3. RESULTS AND DISCUSSION

We investigated the drug composition, size, crystallinity and solubility of the nanoparticles, comparing with equivalent microparticles formed by a co-precipitation method. The role of polymers in enhancing solubility and inhibiting drug crystallinity in the particles is also discussed.

5.3.1 Drug incorporation in particles

Nanoparticle RTV and EFV drug loadings are shown in **Table 2.** The calculations for wt % of drug (W_{drug}) and standard deviation of drug loading (σ_{wdrug}) were made using equations [S.9] and [S.10] in Supplementary Information.

Table 2. RTV and EFV composition in polysaccharide nanoparticles measured by HPLC at 240 nm. Averages from three batches are shown.

	Drug composition (wt%) in CAP Adp 0.33 (standard deviation = σ_{wdrug})	**Drug composition (wt%) in CAP Adp 0.85 (standard deviation = σ_{wdrug})**	**Drug composition (wt%) in CAP 320S Seb (standard deviation = σ_{wdrug})**	**Drug composition (wt%) in BPC (standard deviation = σ_{wdrug})**
RTV	24 (0.02)	22 (0.02)	20 (0.01)	15 (0.03)
EFV	20 (0.01)	19 (0.01)	21 (0.01)	16 (0.01)

For all of these samples, the relative standard deviation (RSD) of drug loading in wt% defined by $RSD_{Wdrug} = \sigma_{Wdrug}/ X_{drug} *100$ % was 0.3-0.4% for all samples which showed good batch-to-batch reproducibility. There was some loss of free drug during the dialysis step. The nanoparticle drug loading efficiency was comparable (88-96 %) for all cellulosic polymers. By comparison, the BPC nanoparticles showed a lower drug loading efficiency of about 62%. The cellulose derivatives are hydrophobic in nature and therefore able to retain more hydrophobic drug after processing. BPC on the other hand is more hydrophilic and releases drug upon interaction with an aqueous environment. There were no significant differences between the trends of RTV and EFV loading in the particles.

The RTV content of the microparticles of CAP Adp 0.33 and CAP Adp 0.85 prepared for comparison experiments was 24 wt%, which corresponded to a 96% drug loading efficiency.

5.3.2 Particle size analysis

Particle size analysis of nanoparticles by dynamic light scattering

Figure 3 shows particle sizes for polysaccharide nanoparticles with RTV and EFV after each processing step including after mixing in the MIVM, after dialysis, and after freeze drying. The particle sizes were compared after each processing step to observe any significant change in the size due to the effect of processing step.

The particle sizes from all three processing steps for all the drug compositions were found to be between 100-200 nm with a polydispersity index approximately 0.2. The particle sizes were comparable after mixing and dialysis with a standard deviation of approximately ±30 nm. However, significant aggregation was observed after freeze drying. The addition of trehalose before freezing at a weight ratio trehalose:nanoparticles of 1:9 resulted in a significant reduction in particle size and polydispersity index. Table 3 shows that particles made with CAP Adp 0.33 and CAP Adp 0.85 were more effectively redispersed upon the addition of trehalose and that higher concentrations of trehalose resulted in smaller values of the polydispersity index (PDI). It is important to note that trehalose was only used for particle size experiments and not for the drug dissolution experiments.

The particle sizes of BPC did not show narrow particle size distributions upon redispersion after freeze drying. Due to the hydrophilic nature of the polymer, there was a tendency to absorb moisture and agglomerate rather than re-dispersing on suspension in DI water. The texture of the cellulose nanoparticles obtained after freeze drying was fluffy which readily formed powder-like particles whereas the BPC nanoparticles were sticky in nature and

did not form powders. The batch-to-batch repeatability of the particle size (after freeze drying and redispersion) was characterized by the relative standard deviation (=standard deviation/particle size x 100 %) which ranged between ~6-29 %.

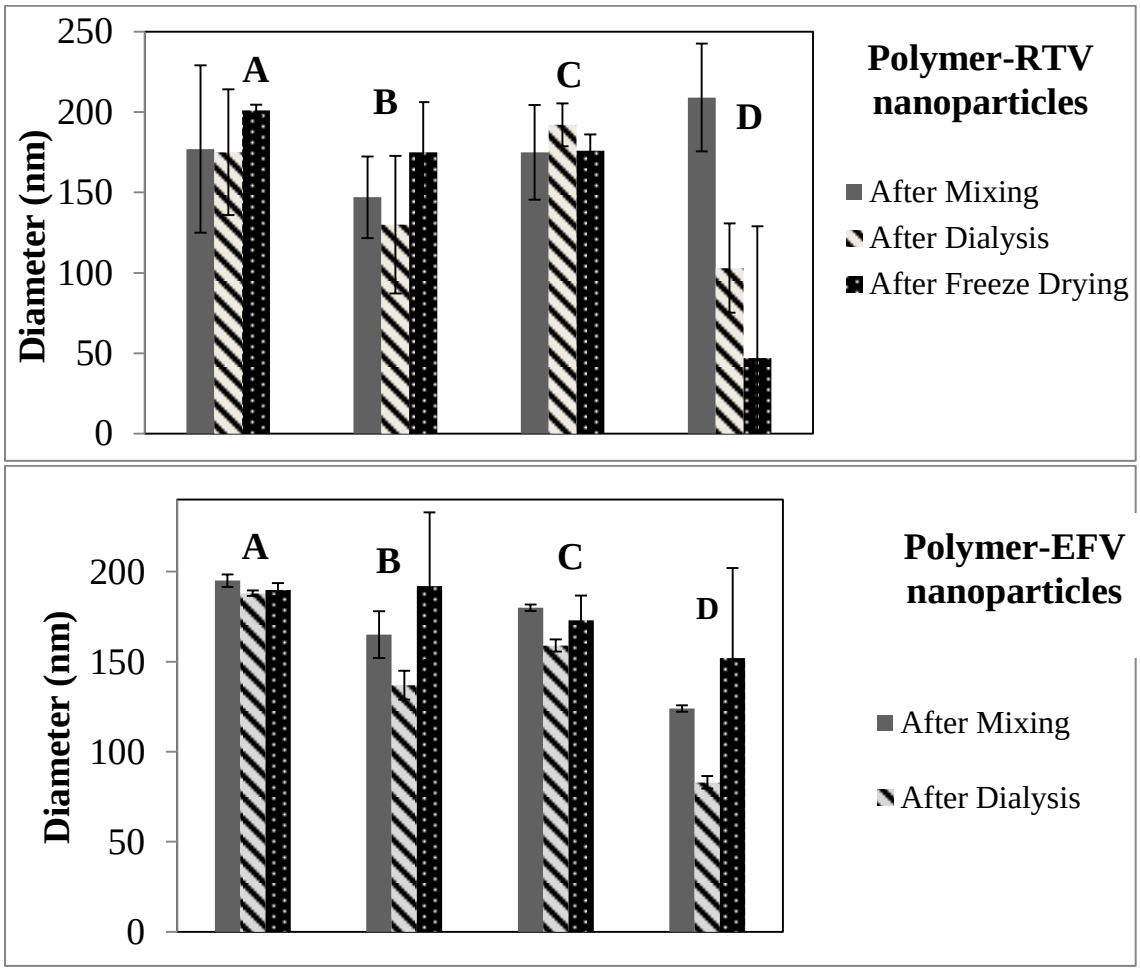

Figure 3. Particle sizes of polysaccharide-drug (RTV and EFV) nanoparticles after mixing, dialysis and freeze drying. The freeze dried powders except BPC were mixed with trehalose before freeze drying. The targeted drug composition was 25 wt% and the actual compositions of the freeze-dried particles are shown in Table 2. The error bars shows standard deviation from 3 different batches of particles. A = CAP Adp 0.33, B = CAP Adp 0.85, C= CA 320S Seb, D = BPC nanoparticles.

Table 3. Effect of trehalose on particle sizes of freeze dried nanoparticles

Polymer - RTV	Diameter of freeze dried powder without trehalose (PDI)	Diameter of freeze dried powder nanoparticle: trehalose = 1:1 (PDI)	Diameter of freeze dried powder with nanoparticle trehalose = 1:9 (PDI)
CAP Adp 0.33	2430 (1.0)	934 (0.5)	165 (0.3)
CAP Adp 0.85	1356 (0.7)	908 (0.4)	148 (0.25)

Particle size analysis of the microparticles by FESEM

The microparticles were too large and too aggregated to be measured by dynamic light scattering and so they were characterized by FESEM. The microparticles formed agglomerated subunits of nearly spherical particles ranging in size from 1-3 μm for CAP Adp 0.33-RTV microparticles and 2-8 μm for CAP Adp 0.85 microparticles.

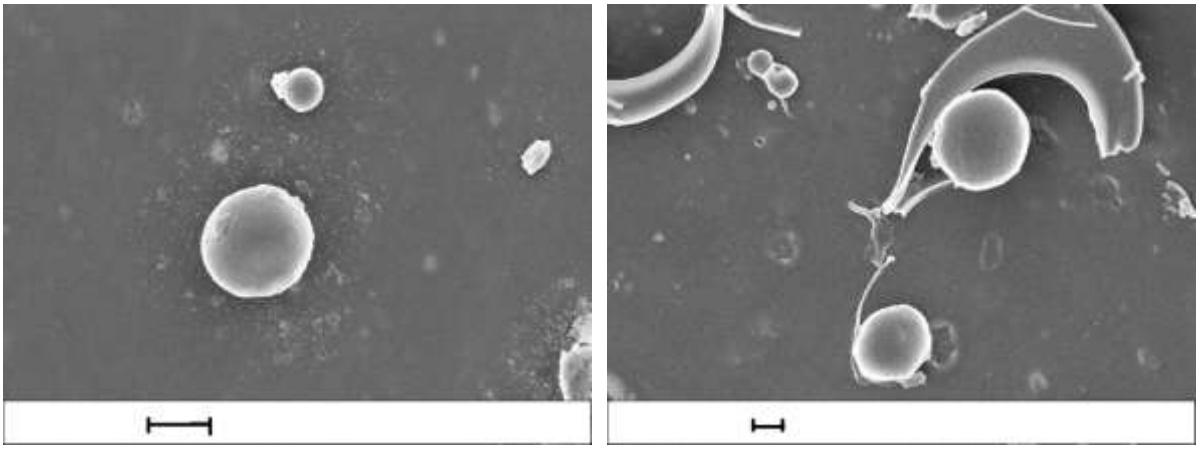

(a) (b)

Figure 4. Scanning electron microscope images for (a) CAP Adp 0.33-RTV microparticles at 15Kx magnification , (b) CAP Adp 0.85-RTV microparticles at 7Kx magnification. The bar in each image corresponds to 2 μm.

5.3.3 Crystallinity of nanoparticles and microparticles

The influence of novel polysaccharides upon possible phase transformation in polymer-RTV and polymer-EFV nanoparticles was investigated through X-ray diffraction. The PXRD pattern of the drugs as-received had distinctive peaks as shown in Figures 5a and 5b along with results for the nanoparticles (Figures 5c and 5d). The X-ray diffraction pattern for pure RTV drug showed numerous strong distinctive peaks at ~ 16°, 18°, 20°, 22° at 2θ indicating a highly crystalline nature. The X-ray diffraction pattern for pure EFV drug also showed numerous strong distinctive peaks at 10°, 12°, 20°, 22°, 25°, 28° at 2θ indicating its crystallinity. The polymers were amorphous in nature (Figure S1.A in Supporting Information). Finally, the PXRD of solid dispersions of the nanoparticles and microparticles (Figure S1.B) showed no diffraction peaks, indicating that they contained amorphous drug.

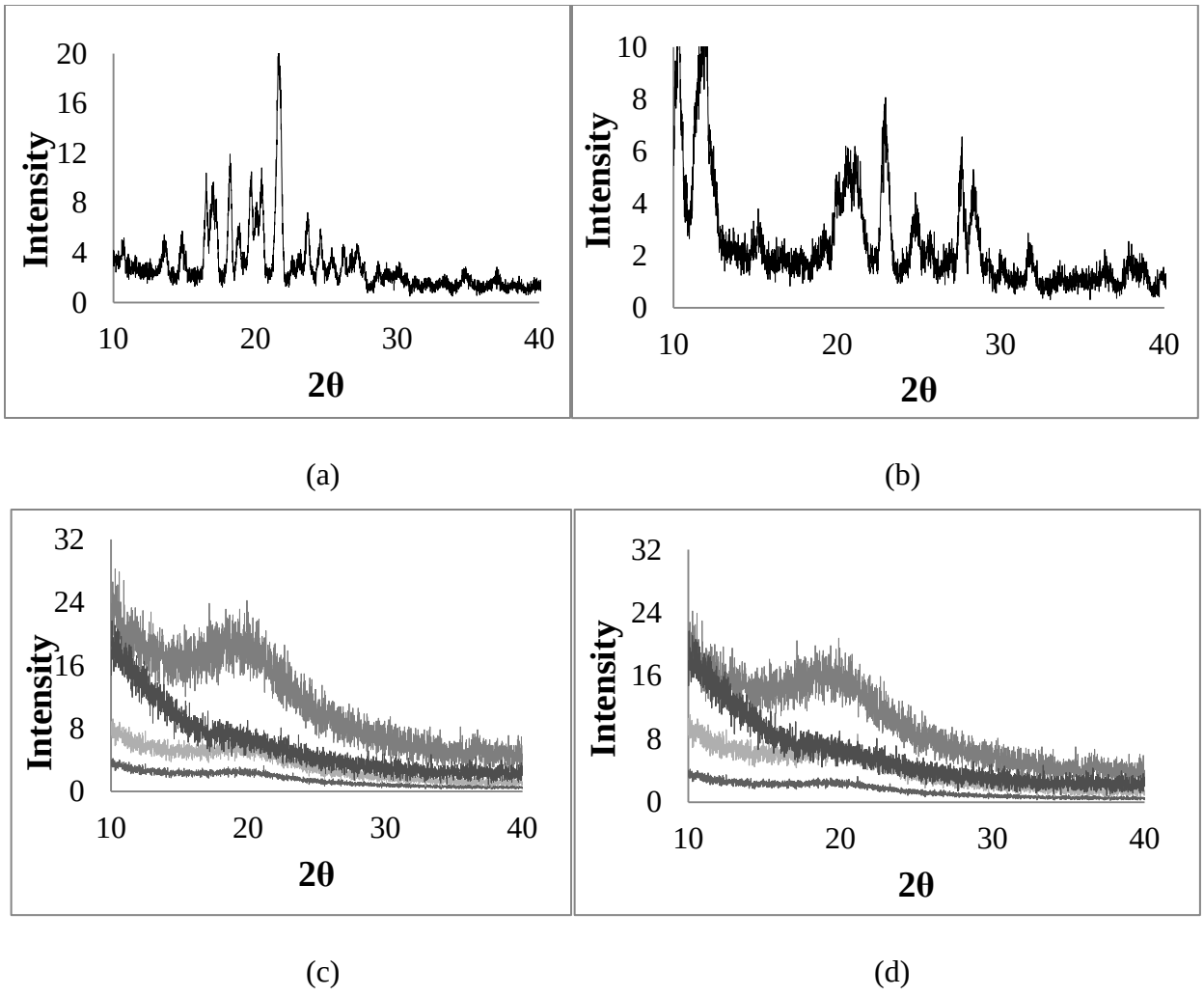

Figure 5. X-ray diffractograms of (a) Crystalline RTV (as received), (b) Crystalline EFV (as received) and polyssacharide nanoparticles (c) ascending order: CAP Adp 0.33-RTV, CAP Adp 0.85-RTV, CA 320S Seb-RTV, BPC-RTV, (d) ascending order : CAP Adp 0.33-EFV, CAP Adp 0.85-EFV, CA 320S Seb-EFV, BPC-EFV showed no diffraction peaks implying the drugs were mostly amorphous

5.3.4 Differential Scanning Calorimetry

DSC scans for RTV, polymers, and polymer-drug nanoparticles are shown in Figure 6. Ritonavir showed a sharp melting peak at 126° C. During the scanning of RTV-containing nanoparticles, no endotherm was observed around the melting point of ritonavir indicating that

ritonavir was present in its amorphous state. Similar results were obtained for polymer-EFV particles as shown in Figure S.2 of the Supplemental Information.

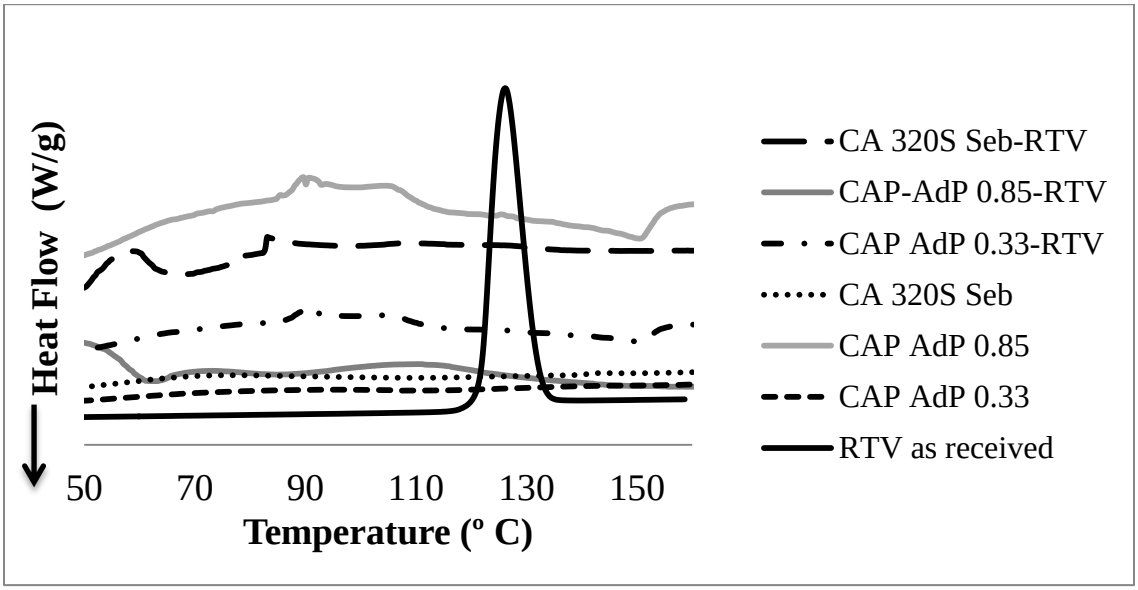

Figure 6. First DSC scan showing melting peak of RTV at 126° C. No such peak is observed in any of the polymer-drug nanoparticles.

The T_g values of RTV and EFV nanoparticles and the pure components are shown in Table 4. Glass transitions of the nanoparticles were between those of the polymers (between 105°C -122°C) and pure RTV (50° C) or EFV (34°C). The intermediate T_g suggested that the drugs were homogeneously and molecularly dispersed in the amorphous polymer matrix. The glass transitions of BPC polymers and BPC-drug nanoparticles were not measured as the temperatures were above the decomposition temperatures of the drug. This is consistent with the hypothesis that BPC can form blends with RTV and EFV that could be stable during storage.

Table 4. Glass transitions of polymer, drugs and polymer-drug nanoparticles (2nd DSC scans) and Fox ideal mixing equation

Samples	No drugs	RTV (Drug loading)	RTV	EFV (Drug loading)	EFV
	Tg (°C)	Tg (°C) (wt %)	T_g (°C) Fox ideal	Tg (°C) (wt %)	T_g (°C) Fox ideal
CAP Adp 0.33	**122**	64 (24)	102	51 (20)	101
CAP Adp 0.85	**105**	55 (22)	90	42 (19)	89
CA-320S Seb	**111**	52 (20)	97	47 (21)	92
BPC	*	*		*	
RTV as received	**-**	**51**		**-**	
EFV as received	**-**	**-**		**35**	

*The glass transitions of BPC polymers and BPC containing drug nanoparticles were not measured as the temperatures are above the decomposition temperatures of the drug. The DSC scan up to a temperature of 200ºC did not show any T_g of BPC showing that the polymer has a high T_g and can form stable blends with drug molecules.

It is helpful to study the amorphous form of the drugs (RTV and EFV) in the solid dispersions by measuring the glass transition temperature of the solid dispersion. Such measurements can establish whether or not the drug and the polymer form one miscible phase (i.e. a single T_g value, solid dispersion) or immiscible phases (i.e. multiple T_g values, glassy suspension) [44,45]. All results in Table 4 show the presence of a single glass transition temperature, suggesting that the drug and the polymer formed one miscible amorphous phase. However, the glass transition temperatures of the drug-containing nanoparticles are similar to those of the drugs. This can pose storage problems as it is known that the storage temperature of 50°C below the T_g reduces the mobility sufficiently to allow acceptable physical stability[46,47]. For example, a previous study has shown that in the absence of polymer, the drug indomethacin recrystallized in less than 6 weeks at storage temperatures 20°C below the Tg. However, when the drug was

molecularly dispersed in PVP solid dispersions, the difference between the T_g of indomethacin in the formulations and the storage temperature increased to 40–50°C and recrystallization of indomethacin was suppressed[48]. Such low glass transitions may not be suitable for storage.

The glass transition temperatures for the polymer-drug solid dispersions obtained from the DSC experiment were compared with those predicted from the Fox equation (1) which assumes ideal mixing:

$$\frac{1}{T_g} = \frac{w_{Polymer}}{T_g^{Polymer}} + \frac{w_{RTV(or\ EFV)}}{T_g^{RTV\ (or\ EFV)}} \qquad (1)$$

where $W_{(\text{RTV or EFV})}$ and $W_{(\text{POLYMER})}$ are the weight fractions of RTV (or EFV) and polymer, respectively, and $T_g^{(\text{RTV or EFV})}$ and $T_g^{(\text{Polymer})}$ are the glass transition temperatures of RTV (or EFV) (i.e. 51ºC or 35 ºC) and polymer, respectively. The assumption of ideal mixing results in a linear extrapolation between the T_g values obtained for drugs (RTV and EFV) and polymer. Thus, any deviation from the predicted values is taken to indicate the presence of molecular interactions.

The extent of deviations of the T_g values from the Fox equation is shown in Figure 7. It can be seen that the experimentally determined values of T_g for the nanoparticles (NP) were approximately 2 times lower than the values predicted from the Fox equation.

Even though the nanoparticles did not show a significant increase in T_g compared to that of the pure drug, they did not show phase separation in the solid state or drug re-crystallization upon storage for few weeks (3 weeks) before the characterizations involving DSC and XRD were performed. DSC curves of the microparticles (CAP Adp 0.33 and CAP Adp 0.85) are shown in Figure S2 of the supporting information. The T_g values of microparticles couldn't be determined.

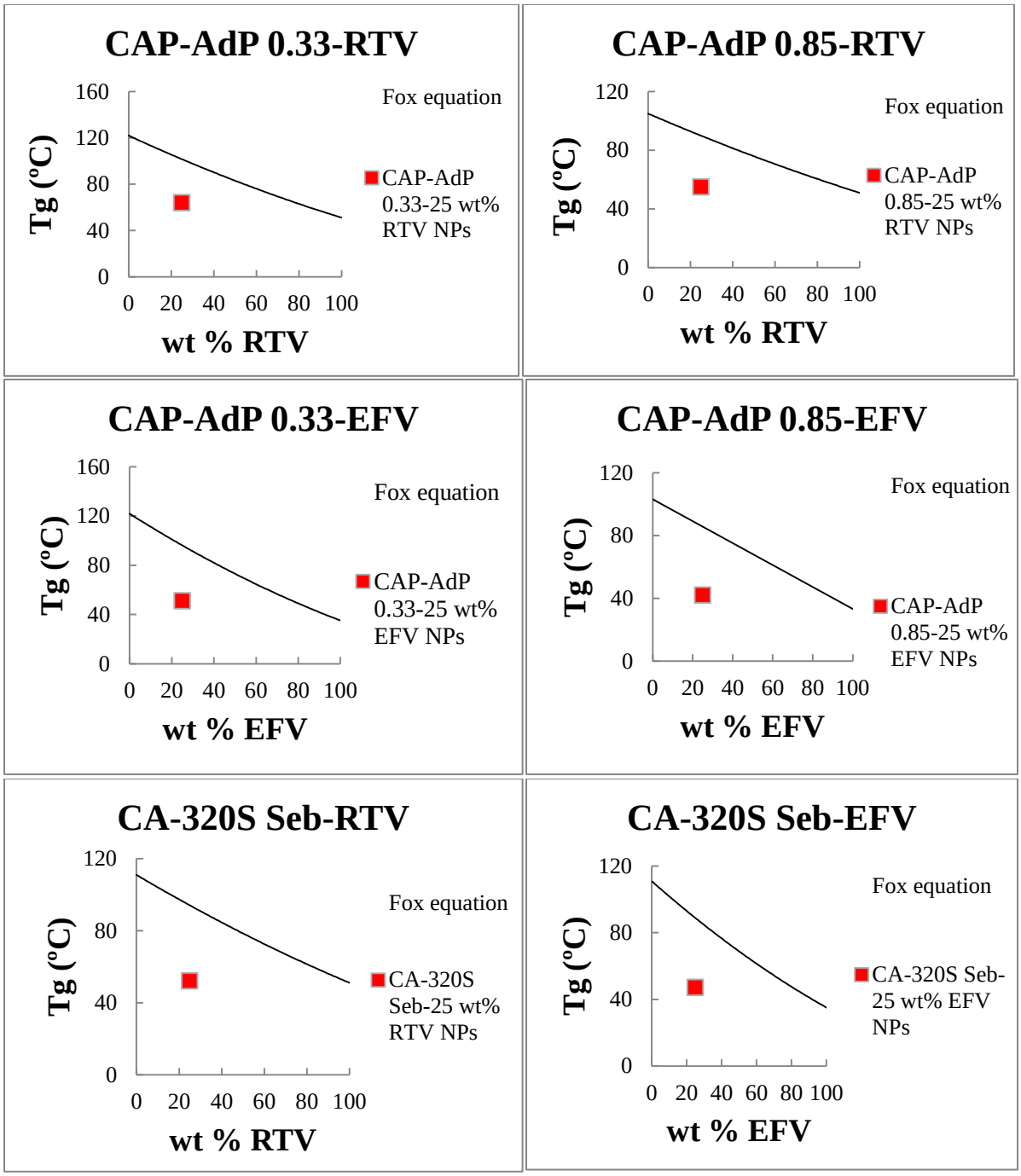

Figure 7. Comparison between experimental T_g and theoretical predictions (Fox ideal T_g) of nanoparticles

5.3.5. Dissolution studies

The results from the dissolution experiment showed good enhancement of drug solution concentration from the ASD (Figure 8). There was an almost 10-fold and 25-fold increase in solubility of RTV from thecellulose derivatives and BPC, respectively, compared to the crystalline drug as-received. The increase in the solution concentration of EFV was comparatively less, 1-fold and 4-fold from cellulose derivatives and BPC, respectively, compared to EFV as-received. Among the cellulose derivatives, the CAP Adp 0.33 showed lesser increase in solubility compared to the others with respect to the free drug. However, there was not much difference in the solubility concentration among the cellulose derivatives.

The significant increase of solution concentration of drug in the case of BPC might be due to the hydrophilic nature of the BPC polymer. The solubility parameters shown in Table 1 characterize the relative hydrophobicities of the novel polymers. The method proposed by Fedors was used to estimate the SP [49]. The SP provides a numerical estimate of magnitude of the intermolecular forces within a material and can be a good indication of solubility[39]. The higher the SP, the more hydrophilic the material. For example the SP of BPC which is the most hydrophilic, is 28 $MPa^{1/2}$, whereas, the for comparatively hydrophobic polymers (CAP Adp 0.33, CAP Adp 0.85 and CA 320S Seb), the SP lies between 20.56-22.36 $MPa^{1/2}$.

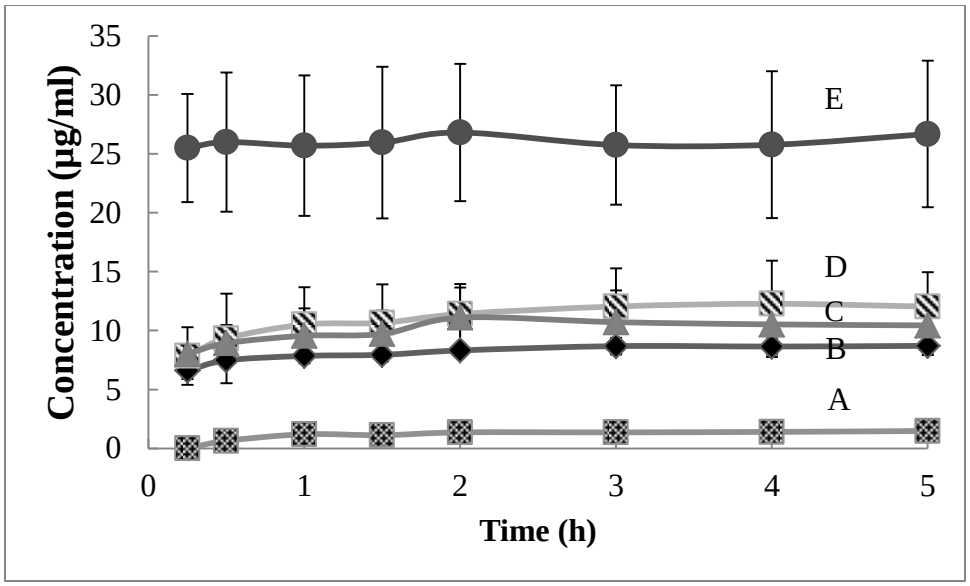

Figure 8a. Concentration profile of RTV (A) as received, (B) from CAP Adp 0.33, (C) from CA 320S Seb, (D) from CAP Adp 0.85, (E) from BPC. The error bars represents standard deviation of results from 3 batches.

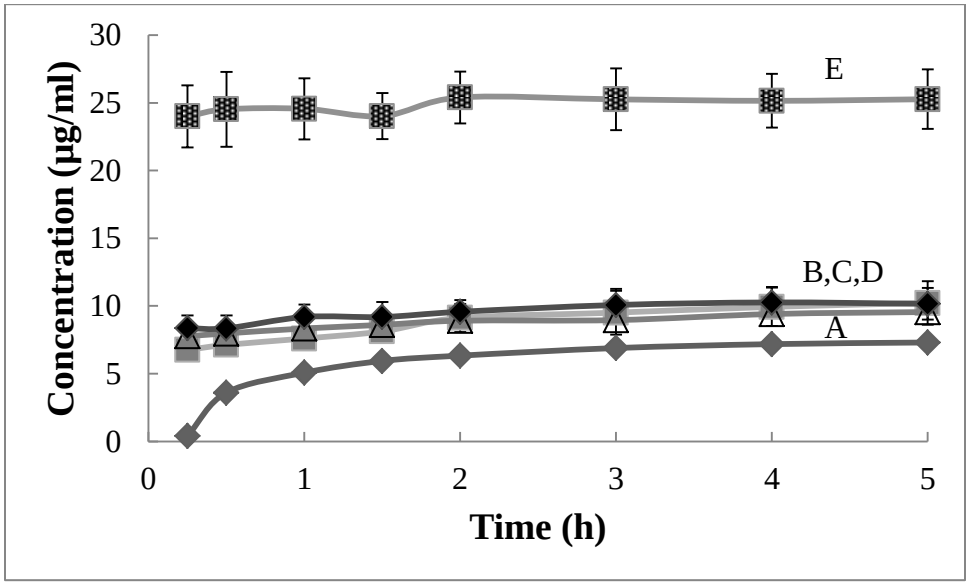

Figure 8b. Concentration profile of EFV (A) as received, (B) from CAP Adp 0.33, (C) from CAP Adp 0.85, (D) from CA 320S Seb, (E) from BPC. The error bars represent standard deviation from 3 batches.

The amorphous blends with cellulose derivatives and the pullulan derivative significantly increased the solubility of both RTV and EFV, more significantly in the case of BPC, and the supersaturated solutions remained stable with respect to drug re-precipitation over the course of the experiment. This suggests that the polymers not only stabilized the amorphous drugs in the solid state, but also helped stabilize the dissolved drugs in solution.

There are several possible mechanisms for drug stabilization in the solid state. It is generally accepted that drug–polymer intermolecular interactions are important for the stabilization of solid dispersions. An important assumption is that the two components (drug and polymer) are mixed homogeneously at the molecular level. Secondly, the molecular mobility of the drugs required for crystallization can be inhibited due to its forming an amorphous solid solution with the high-T_g (glass transition temperature) polymers.

The mechanisms by which polymers can stabilize amorphous drugs also in solution are not yet fully understood but one hypothesis is that soluble polymer at very low concentrations may associate with the drug in solution, thus suppressing drug precipitation [50,46].

The percent drug release from the particles was calculated from equation 2 for RTV and EFV and is shown in Figure 9a and Figure 9b.

$$\%\ drug\ release\ =\ \frac{C_{experimental}}{C_{theoritical}} \qquad (2)$$

$C_{experimental}$ was obtained from HPLC and $C_{theoretical}$ was calculated from the known values of volume of the buffer solution, the mass of particles, and drug composition. Drug release was studied up to 5 hours. CAP Adp 0.33 released about 20 % of RTV, CAP Adp 0.85 which released 27 % of RTV and CA 320S Seb released 30 % of RTV within 5 hours.

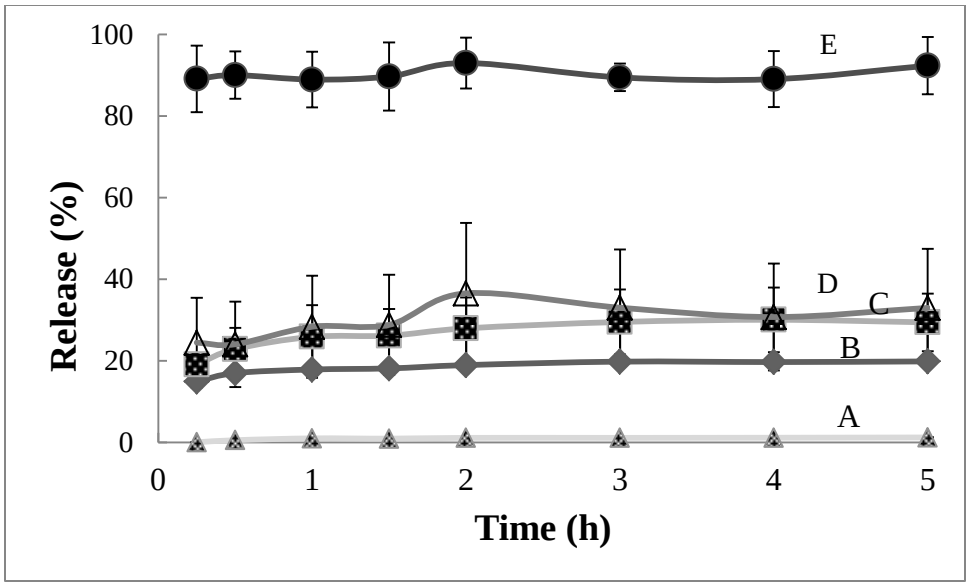

Figure 9a. Release profile of RTV (A) as received, (B) from CAP Adp 0.33, (C) from CAP Adp 0.85, (D) from CA 320S Seb, (E) from BPC. The error bars represent standard deviation of results from 3 batches.

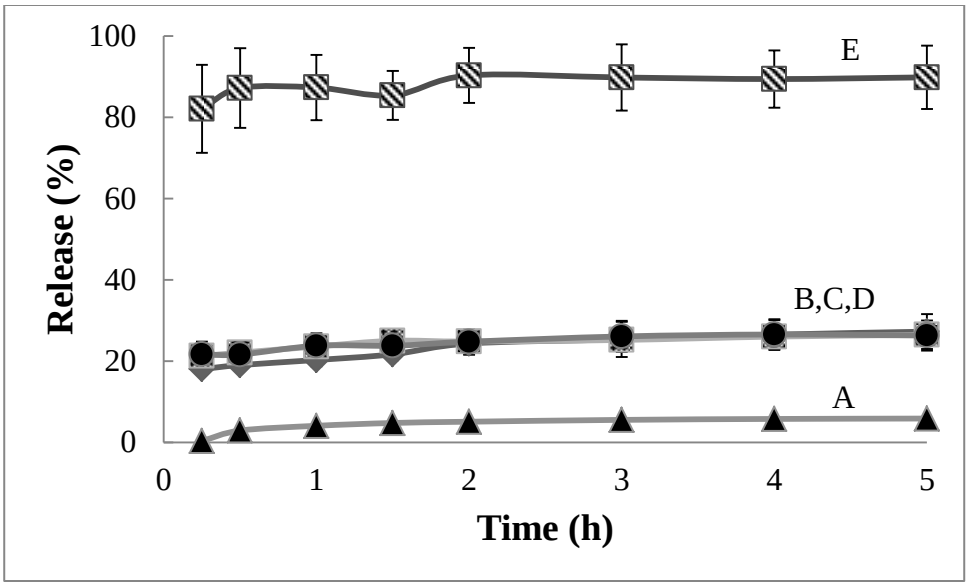

(a)

Figure 9b. Release profile of EFV (A) as received, (B) from CAP Adp 0.33, (C) from CAP Adp 0.85, (D) from CA 320S Seb, (E) from BPC. The error bars represent standard deviation of results from 3 batches.

Drug release can be correlated with the polymer solubility parameter. CAP Adp 0.33 has the lowest solubility parameter among the three cellulose derivatives studied and therefore is more hydrophobic, whereas CA 320S Seb is comparatively more hydrophilic as it has a higher solubility parameter and provides higher RTV solution concentration. All these polymers have been shown to be effective in inhibiting RTV recrystallization[39]. Polymers with solubility parameters between 20-23 $MPa^{1/2}$ could inhibit crystal growth in solution whereas any polymers with a solubility parameter less than 20 were mostly ineffective. Hydrophobicity is likely to affect the extent of adsorption of polymer to the crystal surface which in turn influences the effectiveness. If the polymer is very hydrophobic, it would be expected to interact more favorably with other monomer units to form a more condensed globule which either may not adsorb on the crystal, or, if it adsorbs, may not have high surface coverage. If the polymer is very hydrophilic, it can interact more with the water and comparatively less with the drug. Therefore

an optimal hydrophobicity could exist for inhibiting crystallization. Previous work has shown that ionizable carboxylic acids are effective inhibitors of RTV crystallization[39]. Moderate hydrophobicity leads to inhibition of crystal growth. The degree of carboxyl substitution (DS) may also influence the crystallization inhibitory ability of the various polymers with a higher DS resulting in more inhibition. Extremely hydrophobic polymer segments may strongly interact with hydrophobic drugs, leading to reduced drug release[39]. The BPC derivative is extremely hydrophilic in nature, enhancing drug release. Therefore, our findings were in accord with those of previous studies [39,].

Comparison of Drug Solubility and Release from Nanoparticles and Microparticles

The solubility characteristics and percentage drug release of RTV from nanoparticles and microparticles (prepared by co-precipitation) of both cellulose adipate derivatives (CAP Adp 0.33 and CAP Adp 0.85) are compared in Figure 10. In Figure 11a, the solution concentration of the drug was enhanced approximately 6-fold and 8-fold for CAP Adp 0.33 and CAP Adp 0.85, respectively, compared to crystalline RTV. The solution concentration of RTV from nanoparticles was slightly higher than from corresponding microparticles but within the margin of error.

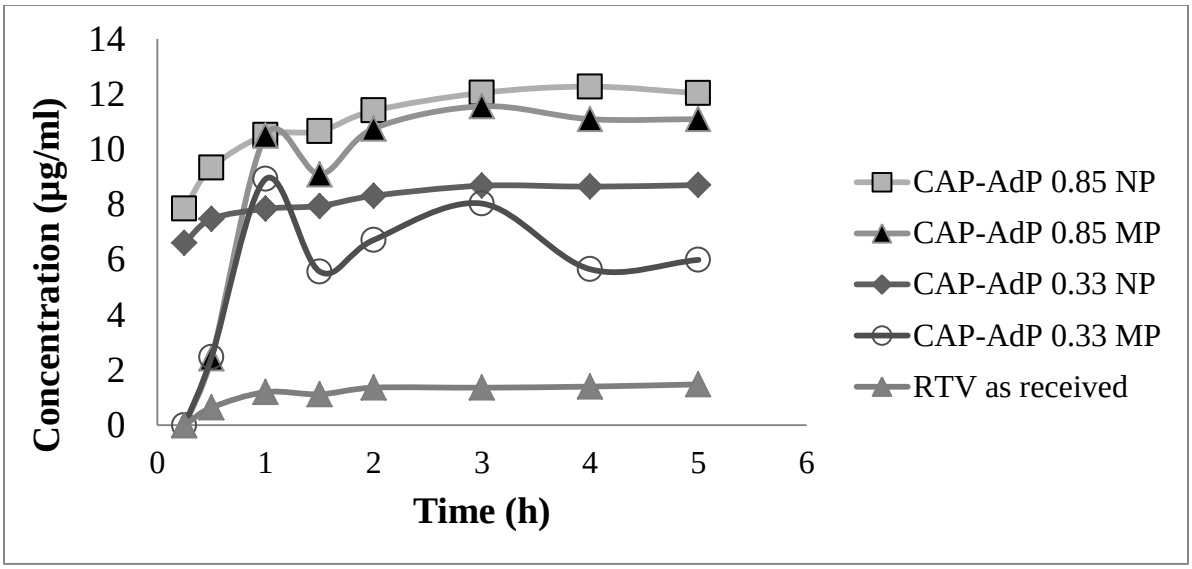

Figure 10a. Comparison of solubility of RTV from CAP Adp 0.33 and CAP Adp 0.85 microparticles (MP) and nanoparticles (NP) and crystalline RTV as received (result from 1 batch). RTV compositions are listed in Table 2.

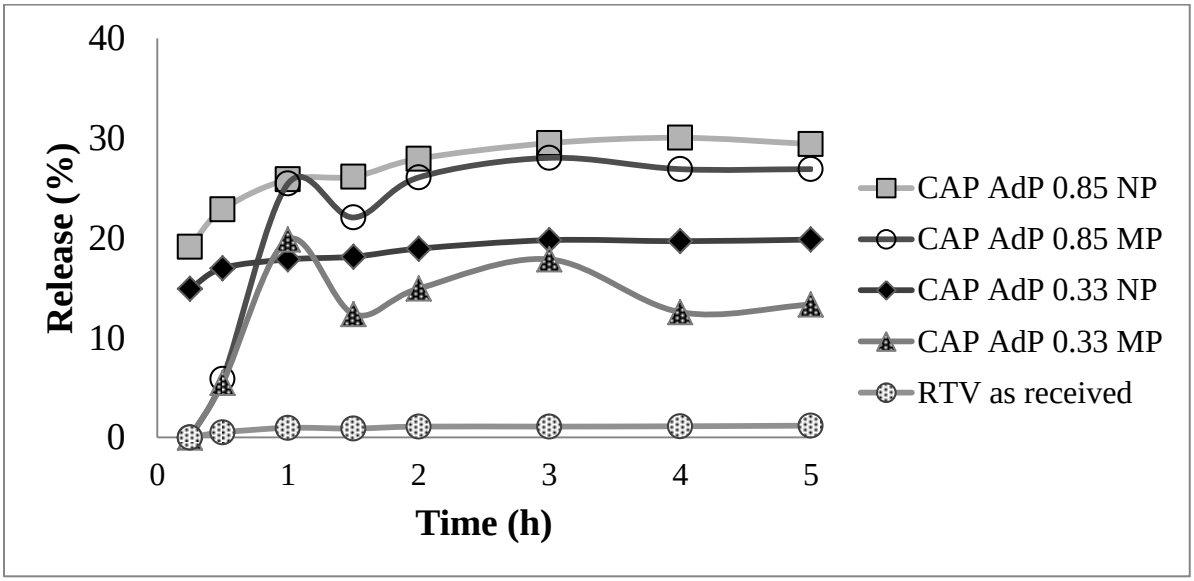

Figure 10b. Comparison of RTV release from CAP Adp 0.33 and CAP Adp 0.85 microparticles (MP) and nanoparticles (NP), vs crystalline RTV (result from 1 batch). RTV compositions are listed in Table 2.

There was an increase in release of drugs from both nanoparticles and microparticles. There was release of RTV (approximately 15% from CAP Adp 0.33 and 19 % from CAP Adp 0.85) from nanoparticles within first 15 minutes after the particles were dispersed in the buffer but no drug was released from the microparticles during that time. The drug release from microparticles was only observed after half an hour. The much higher specific surface area of the nanoparticles resulted in enhancing the early time dissolution rate of RTV compared to the microparticles. Around 19 % and 30 % of RTV was released from CAP Adp 0.33 and CAP Adp 0.85 after 5 hours.

5.4. CONCLUSIONS

This study demonstrates a method for producing cellulose derivative and BPC amorphous nanoparticles containing RTV and EFV, with well-defined sizes (100 nm – 200 nm). The multi-inlet vortex mixer was used to control particle size and nucleation rate, and flash nanoprecipitation was shown to be an effective method for making these nanoparticles. The particles were processed by dialysis followed by freeze drying; a suitable cryoprotectant trehalose was used for inhibiting particle aggregation during freeze drying. The drug loading efficiency in the final particles was 88-96 % except BPC where the drug loading efficiency was 62%. The polymers were effective in entrapping the drug in its amorphous state in the particle. This increased the solubility of the drugs in buffer solution. There was an increase in percentage drug release from the nanoparticles compared to the pure crystalline drug. The microparticles containing RTV and EFV showed peak/trough fluctuations in solubility and drug release values compared to nanoparticles which showed a comparatively steady pattern Therefore, nanoparticles of polysaccharides-drug complexes showed potential for enhancing the solubility

and sustained release of poorly soluble drugs (RTV and EFV). The dissolution behavior was dependent on both the properties of the polymer (solubility parameter, degree of substitution, hyphobocity) as well the drug (solubility parameter, solubility, presence of hydrophobic groups). The polymers with solubility parameter between 20-23 $MPa^{1/2}$ could inhibit crystal growth in solution, anything less than 20 were mostly ineffective. However, BPC with a higher solubility parameter (28 $MPa^{1/2}$) showed very high concentration and release compared to the crystalline drugs but did not show well defined drug composition and particle size.

Future studies of polysaccharides for the preparation of amorphous solid dispersions will focus on whether the polymer hydrophobicity is likely to affect the extent of adsorption of the polymer to the crystal surface of the drug. If the polymer is very hydrophobic, it could interact more favorably with other, similar polymer chains to form a more condensed globule which either may not adsorb on the crystal or if it adsorbs may not have high surface coverage. If the polymer is very hydrophilic, it can interact more with the water and comparatively less with the drug. Therefore an optimal hydrophobicity could exist for inhibiting crystallization. Future studies will also probe whether a higher degree of carboxyl substitution (DS) shows more effective inhibition of crystallization as suggested by the pullulan derivative results. There can be differences in the particle shape, size, polydispersity and morphology depending on the preparation method so care must be taken to use the synthesis method and purification (separation, drying) techniques to obtain well-defined particles. The use of excipients such as cryoprotectants (or excipients) to control particle size would be an additional and useful step.

ACKNOWLEDGEMENTS

The authors gratefully acknowledge funding and support from the Macromolecules and Interface Institute and the National Science Foundation under Contract # DMR 0909065. The authors also thank Rick Caudill, Research Specialist, Department of Sustainable Biomaterials for his assistance with the PXRD analysis and Mr. Steve McCartney, of the Institute for Critical Technology and Applied Science-Nanoscale Characterization and Fabrication Laboratory (ICTAS-NCFL) at Virginia Tech for help with the FESEM images.

5.5. REFERENCES

1. World Helath Organization, AIDS epidemic update **2009**, Retrieved from http://data.unaids.org/pub/report/2009/jc1700_epi_update_2009_en.pdf

2. Yekkala, R. S.; Ashenafi, D.; Mariën, I.; Xin, H.; Haghedooren, E.; Hoogmartens, J.; Adams, E., Evaluation of an International Pharmacopoeia method for the analysis of ritonavir by liquid chromatography. *Journal of Pharmaceutical and Biomedical Analysis* **2008,** *48* (3), 1050-1054.

3. Lavelle, E. C.; Sharif, S.; Thomas, N. W.; Holland, J.; Davis, S. S., The importance of gastrointestinal uptake of particles in the design of oral delivery systems. *Advanced Drug Delivery Reviews* **1995,** *18* (1), 5-22.

4. Daugherty, A. L.; Mrsny, R. J., Regulation of the intestinal epithelial paracellular barrier. *Pharmaceutical Science & Technology Today* **1999,** *2* (7), 281-287.

5. (a) Gref, R.; Minamitake, Y.; Peracchia, M.; Trubetskoy, V.; Torchilin, V.; Langer, R., Biodegradable long-circulating polymeric nanospheres. *Science* **1994,** *263* (5153), 1600-1603; (b) Fu, K.; Harrell, R.; Zinski, K.; Um, C.; Jaklenec, A.; Frazier, J.; Lotan, N.; Burke, P.; Klibanov, A. M.; Langer, R., A potential approach for decreasing the burst effect of protein from PLGA microspheres. *Journal of Pharmaceutical Sciences* **2003,** *92* (8), 1582-1591.

6. (a) Yoo, H. S.; Oh, J. E.; Lee, K. H.; Park, T. G., Biodegradable nanoparticles containing doxorubicin-plga conjugate for sustained release. *Pharm Res* **1999,** *16* (7), 1114-1118; (b) Langer, R., Drug delivery and targeting. *Nature* **1998,** *392* (6679 Suppl), 5-10.

7. Posey-Dowty, J.; Watterson, T.; Wilson, A.; Edgar, K.; Shelton, M.; Lingerfelt, L., Zero-order release formulations using a novel cellulose ester. *Cellulose* **2007,** *14* (1), 73-83-83.

8. Shelton Michael, C.; Posey-Dowty Jessica, D.; Lingerfelt, L.; Kirk Shane, K.; Klein, S.; Edgar Kevin, J., Enhanced dissolution of poorly soluble drugs from solid dispersions in carboxymethylcellulose acetate butyrate matrices. In *Polysaccharide Materials: Performance by Design*, American Chemical Society **2009**, 1017, 93-113.

9. Sandra, K., Polysaccharides in oral drug delivery? Recent applications and future perspectives. In *Polysaccharide Materials: Performance by Design*, *American Chemical Society* **2009**, 1017, 13-30.

10. Dembri, A.; Montisci, M.-J.; Gantier, J.; Chacun, H.; Ponchel, G., Targeting of 3′-Azido 3′-deoxythymidine (AZT)-loaded poly(isohexylcyanoacrylate) nanospheres to the gastrointestinal mucosa and associated lymphoid tissues. *Pharm Res* **2001,** *18* (4), 467-473.

11. Löbenberg, R.; Maas, J.; Kreuter, J., Improved body distribution of 14C-labelled AZT bound to nanoparticles in rats determined by radioluminography. *Journal of Drug Targeting* **1998,** *5* (3), 171-179.

12. Destache, C.; Belgum, T.; Christensen, K.; Shibata, A.; Sharma, A.; Dash, A., Combination antiretroviral drugs in PLGA nanoparticle for HIV-1. *BMC Infectious Diseases* **2009,** *9* (1), 198.

13. Mainardes, R. M.; Gremião, M. P. D.; Brunetti, I. L.; Da Fonseca, L. M.; Khalil, N. M., Zidovudine-loaded PLA and PLA–PEG blend nanoparticles: Influence of polymer type on phagocytic uptake by polymorphonuclear cells. *Journal of Pharmaceutical Sciences* **2009,** *98* (1), 257-267.

14. Sharma, P.; Garg, S., Pure drug and polymer based nanotechnologies for the improved solubility, stability, bioavailability and targeting of anti-HIV drugs. *Advanced Drug Delivery Reviews* **2010,** *62* (4-5), 491-502.

15. Ranjit Mondol, S. P., Somasree Ray, Sabyasachi Maiti, Polymeric Nanocarriers: A promising research avenue for the delivery of antihiv drugs. *International Journal of Applied Pharmaceutics* **2010,** *2* (2), 1-5.

16. Hancock, B.; Parks, M., What is the true solubility advantage for amorphous pharmaceuticals? *Pharmaceutical Research* **2000,** *17* (4), 397-404.

17. (a) Konno, H.; Handa, T.; Alonzo, D. E.; Taylor, L. S., Effect of polymer type on the dissolution profile of amorphous solid dispersions containing felodipine. *European Journal of*

Pharmaceutics and Biopharmaceutics **2008,** *70* (2), 493-499; (b) Leuner, C.; Dressman, J., Improving drug solubility for oral delivery using solid dispersions. *European Journal of Pharmaceutics and Biopharmaceutics* **2000,** *50* (1), 47-60.

18. Chen, Y.; Zhang, G. G. Z.; Neilly, J.; Marsh, K.; Mawhinney, D.; Sanzgiri, Y. D., Enhancing the bioavailability of ABT-963 using solid dispersion containing Pluronic F-68. *International Journal of Pharmaceutics* **2004,** *286* (1–2), 69-80.

19. Dinunzio, J. C.; Miller, D. A.; Yang, W.; Mcginity, J. W.; Williams, R. O., Amorphous compositions using concentration enhancing polymers for improved bioavailability of itraconazole. *Molecular Pharmaceutics* **2008,** *5* (6), 968-980.

20. Kennedy, M.; Hu, J.; Gao, P.; Li, L.; Ali-Reynolds, A.; Chal, B.; Gupta, V.; Ma, C.; Mahajan, N.; Akrami, A.; Surapaneni, S., Enhanced bioavailability of a poorly soluble vr1 antagonist using an amorphous solid dispersion approach: A case study. *Molecular Pharmaceutics* **2008,** *5* (6), 981-993.

21. A.P. Simonelli, S. C. M., W.I. Highuchi, Dissolution rates of high energy sulfathiazole-provideone coprecipitates ii : characterization of form of drug controlling its dissolution rate via solubility studies. *Jounral of Pharamaceutical Sciences* **1976,** *65* (3), 355-361.

22. (a) Weuts, I.; Van Dycke, F.; Voorspoels, J.; De Cort, S.; Stokbroekx, S.; Leemans, R.; Brewster, M. E.; Xu, D.; Segmuller, B.; Turner, Y. T. A.; Roberts, C. J.; Davies, M. C.; Qi, S.; Craig, D. Q. M.; Reading, M., Physicochemical properties of the amorphous drug, cast films, and spray dried powders to predict formulation probability of success for solid dispersions: Etravirine. *Journal of Pharmaceutical Sciences* **2011,** *100* (1), 260-274; (b) Wiranidchapong, C.; Tucker, I. G.; Rades, T.; Kulvanich, P., Miscibility and interactions between 17β-estradiol and Eudragit® RS in solid dispersion. *Journal of Pharmaceutical Sciences* **2008,** *97* (11), 4879-4888.

23. Yoo, S.-U.; Krill, S. L.; Wang, Z.; Telang, C., Miscibility/stability considerations in binary solid dispersion systems composed of functional excipients towards the design of multi-component amorphous systems. *Journal of Pharmaceutical Sciences* **2009,** *98* (12), 4711-4723.

24. Tobyn, M.; Brown, J.; Dennis, A. B.; Fakes, M.; Gao, Q.; Gamble, J.; Khimyak, Y. Z.; Mcgeorge, G.; Patel, C.; Sinclair, W.; Timmins, P.; Yin, S., Amorphous drug–PVP dispersions: Application of theoretical, thermal and spectroscopic analytical techniques to the study of a molecule with intermolecular bonds in both the crystalline and pure amorphous state. *Journal of Pharmaceutical Sciences* **2009,** *98* (9), 3456-3468.

25. Zhu, Q.; Taylor, L. S.; Harris, M. T., Evaluation of the microstructure of semicrystalline solid dispersions. *Molecular Pharmaceutics* **2010,** *7* (4), 1291-1300.

26. Rumondor, A. F.; Ivanisevic, I.; Bates, S.; Alonzo, D.; Taylor, L., Evaluation of drug-polymer miscibility in amorphous solid dispersion systems. *Pharmaceutical Research* **2009,** *26* (11), 2523-2534.

27. Al-Obaidi, H.; Lawrence, M. J.; Al-Saden, N.; Ke, P., Investigation of griseofulvin and hydroxypropylmethyl cellulose acetate succinate miscibility in ball milled solid dispersions. *International Journal of Pharmaceutics* **2013,** *443* (1–2), 95-102.

28. Johnson, B. K.; Prud; #39; Homme, R. K., Flash nanoprecipitation of organic actives and block copolymers using a confined impinging jets mixer. *Australian Journal of Chemistry* **2003,** *56* (10), 1021-1024.

29. Johnson, B. K.; Prud'homme, R. K., Chemical processing and micromixing in confined impinging jets. *AIChE Journal* **2003,** *49* (9), 2264-2282.

30. Johnson, B. K.; Prud'homme, R. K., Mechanism for rapid self-assembly of block copolymer nanoparticles. *Physical Review Letters* **2003,** *91* (11), 118302.

31. Ungun, B.; Prud'homme, R. K.; Budijon, S. J.; Shan, J.; Lim, S. F.; Ju, Y.; Austin, R., Nanofabricated upconversion nanoparticles for photodynamic therapy. *Opt. Express* **2009,** *17* (1), 80-86.

32. Kumar, V.; Hong, S. Y.; Maciag, A. E.; Saavedra, J. E.; Adamson, D. H.; Prud'homme, R. K.; Keefer, L. K.; Chakrapani, H., Stabilization of the Nitric Oxide (NO) prodrugs and anticancer leads, PABA/NO and double JS-K, through incorporation into PEG-protected nanoparticles. *Molecular Pharmaceutics* **2009,** *7* (1), 291-298.

33. Chen, T.; D'addio, S. M.; Kennedy, M. T.; Swietlow, A.; Kevrekidis, I. G.; Panagiotopoulos, A. Z.; Prud'homme, R. K., Protected peptide nanoparticles: Experiments and brownian dynamics simulations of the energetics of assembly. *Nano Letters* **2009,** *9* (6), 2218-2222.

34. Ansell, S. M.; Johnstone, S. A.; Tardi, P. G.; Lo, L.; Xie, S.; Shu, Y.; Harasym, T. O.; Harasym, N. L.; Williams, L.; Bermudes, D.; Liboiron, B. D.; Saad, W.; Prud'homme, R. K.; Mayer, L. D., Modulating the therapeutic activity of nanoparticle delivered paclitaxel by manipulating the hydrophobicity of prodrug conjugates. *Journal of Medicinal Chemistry* **2008,** *51* (11), 3288-3296.

35. D'addio, S. M.; Prud'homme, R. K., Controlling drug nanoparticle formation by rapid precipitation. *Advanced Drug Delivery Reviews* **2011,** *63* (6), 417-426.

36. (a) Liu, Y.; Cheng, C.; Prud'homme, R. K.; Fox, R. O., Mixing in a multi-inlet vortex mixer (MIVM) for flash nano-precipitation. *Chemical Engineering Science* **2008,** *63* (11), 2829-2842; (b) http://www.avert.org/worldstats.htm.

37. Gindy, M., Composite block copolymer stabilized nanoparticles: Simultaneous encapsulation of organic actives and inorganic nanostructures. *Langumir* **2008,** *24*, 83-90.

38. Kar, N.; Liu, H.; Edgar, K. J., Synthesis of cellulose adipate derivatives. *Biomacromolecules* **2011,** *12* (4), 1106-1115.

39. Ilevbare, G. A.; Liu, H.; Edgar, K. J.; Taylor, L. S., Understanding polymer properties important for crystal growth inhibition—impact of chemically diverse polymers on solution crystal growth of ritonavir. *Crystal Growth & Design* **2012,** *12* (6), 3133-3143.

40. Pereira, J. M., Mahoney M., Edgar, K. J., Synthesis of amphiphilic 6-carboxypullulan ethers. *Carbohydrate Polymers* **2013,** http://dx.doi.org/10.1016/j.carbpol.2012.12.029

41. Hesse, L. M.; Von Moltke, L. L.; Shader, R. I.; Greenblatt, D. J., Ritonavir, efavirenz, and nelfinavir inhibit CYP2B6 activity in vitro: Potential drug interactions with bupropion. *Drug Metabolism and Disposition* **2001,** *29* (2), 100-102.

42. Ariza, R. M. Design, Synthesis, and characterization of magnetite clusters using a multi inlet vortex mixer. Virginia Polytechnic Institute and State University, Blacksburg, Virginia, **2010**.

43. Andronis, V.; Zografi, G., The Molecular mobility of supercooled amorphous indomethacin as a function of temperature and relative humidity. *Pharmaceutical Research* **1998,** *15* (6), 835-842.

44. Huang, J.; Wigent, R. J.; Schwartz, J. B., Drug–polymer interaction and its significance on the physical stability of nifedipine amorphous dispersion in microparticles of an ammonio methacrylate copolymer and ethylcellulose binary blend. *Journal of Pharmaceutical Sciences* **2008,** *97* (1), 251-262.

45. Rumondor, A. C. F.; Marsac, P. J.; Stanford, L. A.; Taylor, L. S., Phase behavior of poly(vinylpyrrolidone) containing amorphous solid dispersions in the presence of moisture. *Molecular Pharmaceutics* **2009,** *6* (5), 1492-1505.

46. Hancock, B. C.; Zografi, G., Characteristics and significance of the amorphous state in pharmaceutical systems. *Journal of Pharmaceutical Sciences* **1997,** *86* (1), 1-12.

47. Hancock, B.; Shamblin, S.; Zografi, G., Molecular mobility of amorphous pharmaceutical solids below their glass transition temperatures. *Pharmaceutical Research* **1995,** *12* (6), 799-806.
48. Yoshioka, M.; Hancock, B. C.; Zografi, G., Inhibition of indomethacin crystallization in poly(vinylpyrrolidone) coprecipitates. *Journal of Pharmaceutical Sciences* **1995,** *84* (8), 983-986.
49. Fedors, R. F., A method for estimating both the solubility parameters and molar volumes of liquids. *Polymer Engineering & Science* **1974,** *14* (2), 147-154.
50. Alonzo, D. E.; Gao, Y.; Zhou, D.; Mo, H.; Zhang, G. G. Z.; Taylor, L. S., Dissolution and precipitation behavior of amorphous solid dispersions. *Journal of Pharmaceutical Sciences* **2011,** *100* (8), 3316-3331.
51. Liu, H.; Ilevbare, G. A.; Cherniawski, B. P.; Ritchie, E. T.; Taylor, L. S.; Edgar, K. J., Synthesis and structure-property evaluation of cellulose ω-carboxyesters for amorphous solid dispersions. *Carbohydrate Polymers* **2012**, http://dx.doi.org/10.1016/j.carbpol.2012.11.049

5.6. Supporting Information

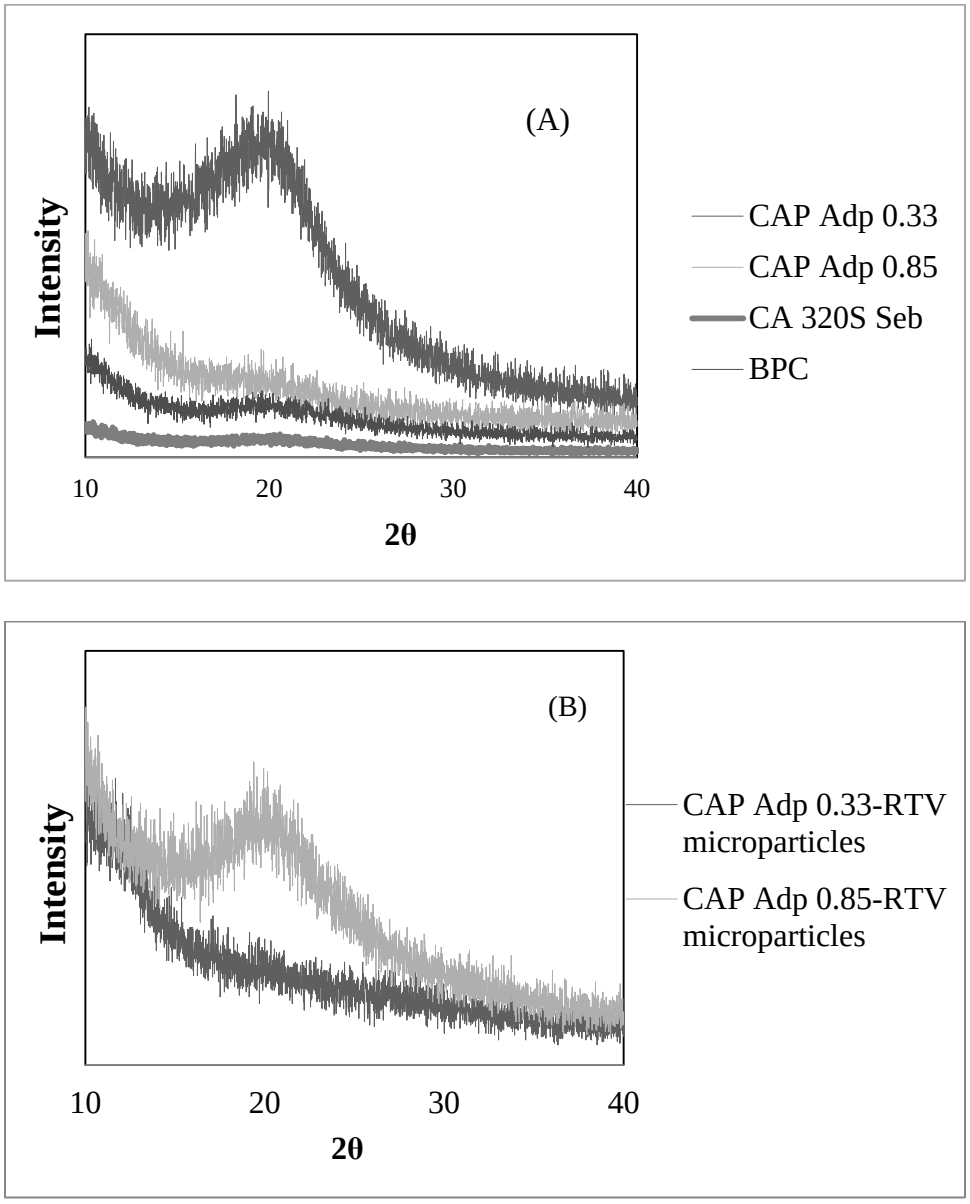

Fig. S.1 X-ray diffractograms of (A) polymers as received (B) CAP adipates 0.33 and 0.85 microparticles containing RTV

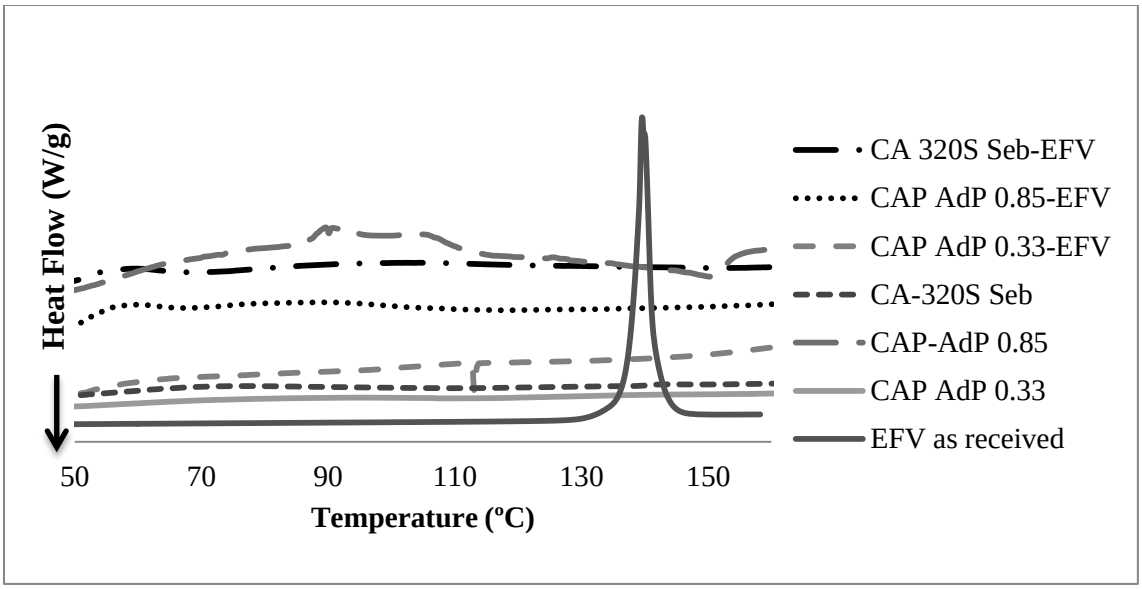

Fig. S.2 First DSC scan showing melting peak of EFV at 140° C. No such peak is observed in the any of the polymer-EFV nanoparticles.

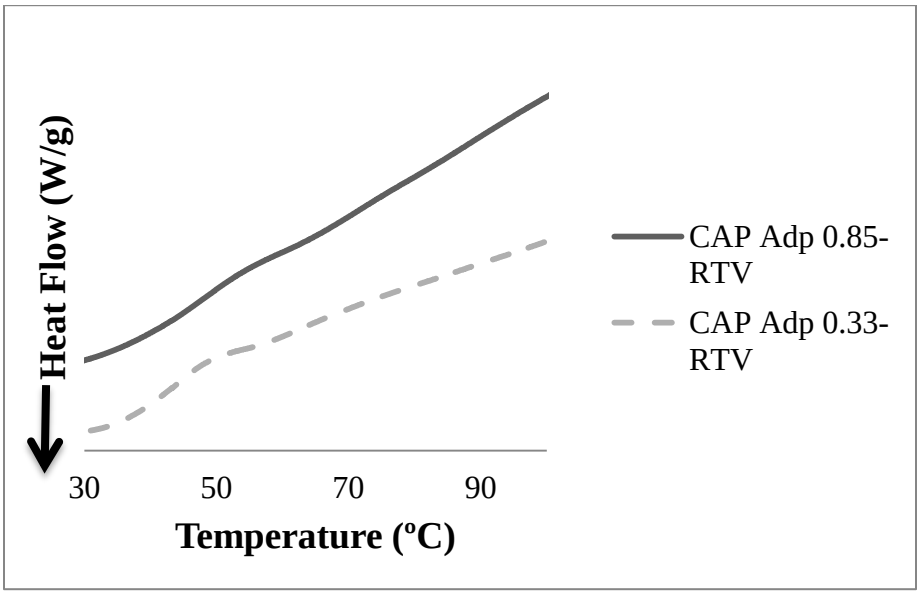

Fig. S.3 DSC scan of RTV containing CAP Adp 0.33 and CAP Adp 0.85

Chapter 6. Conclusions and Future Work

The work in this thesis focused on the synthesis and characterization of amorphous solid dispersions of drug-containing polymer nanoparticle complexes. The knowledge gained from this work is intended to aid in the design of well-defined nanoparticles that could be applied in oral drug delivery. These amorphous solid dispersion nanoparticles have been shown to have the potential to enhance drug bioavailability and stability. The first half of this chapter presents these conclusions in sequence. The second half of this chapter outlines work that at this time is not complete, but shows considerable promise for future work.

6.1 Conclusions

Amorphous solid dispersion formulations containing amorphous drugs physically dispersed within an inert polymer matrix have shown significant solution concentration advantages and, ultimately, enhanced oral bioavailability. Enhancement of the rate of dissolution of solid drug product will be necessary to maximize the release of drug. Also it will be important to protect some drugs from stomach acid degradation so that most of it is released in the small intestine for further absorption. Rapid nanoparticle production is critical ultimately for practical applications. With that in mind, the main goals of this work have been to develop methods to aid in the design of well-defined (particle size and drug composition) polysaccharide-nanoparticle systems that will protect the drug at lower pH values and increase the release and solution concentration at higher pH. This research has involved the development of processing methods to prepare, separate, purify, and dry nanoparticles as well as the ability to redisperse for further characterization.

In **Chapter 3,** a methodology to produce amorphous solid dispersions (ASDs) of an antibacterial drug rifampicin and the high T_g polysaccharide CMCAB was presented. The

nanoparticle suspensions were prepared with the multi-inlet vortex mixer. Two different particle purification and recovery methods were investigated – flocculation with acids and dialysis followed by freeze drying. Intensity-average hydrodynamic diameters ranged from 100-400 nm. Flocculation followed by vacuum filtration proved to be a useful particle isolation technique. Both citric acid and dilute hydrochloric acid gave comparable results, inducing flocculation in almost the same times. There was a significant difference in the flocculation time of samples subjected first to rotary evaporation to remove THF (30 seconds) compared to samples not subjected to rotary evaporation (30-45 minutes). The flocculation/vacuum filtration process is significantly faster than the dialysis/freeze drying process in purifying rifampicin-CMCAB nanoparticles.

The particles processed by acid flocculation were not easily dispersible so probe sonication was used to redisperse the particles in DI water. However, particles processed by dialysis/freeze drying were much easily redispersed. Particles processed by the flocculation/vacuum filtration process also had higher rifampicin loadings than did particles processed by dialysis/freeze drying. It was shown that rifampicin-containing nanoparticles at 500 μg/ml were non-toxic to murine macrophage cell line J774A.1 *in vitro*. The biologic activity of rifampicin was well preserved after CMCAB nanoparticle formation. The nanoparticles processed by dialysis and freeze drying were compared to microparticles (particle size 2-10 μm) of rifampicin-CMCAB prepared by spray drying. The rifampicin in both the nanoparticles and microparticles was amorphous. The release studies of the drug showed that the % release from nanoparticles was higher than that from microparticles at pH 6.8. However, at pH 1.2, rifampicin release from the nanoparticles was essentially the same as that from the free drug and was subject to acid degradation. By comparison, the microparticles showed no drug release at pH 1.2,

indicating that these particles could protect the rifampicin under stomach acid conditions. Therefore, nanoparticles of CMCAB without any further steps to protect the nanoparticles are not suitable for oral delivery of rifampicin. It is important to complex the rifampicin or the polymer with another compound which can slow down the drug release in stomach and yet give significant release in the small intestine. A very important example, as mentioned earlier, is in the work where rifampicin has been incorporated into poly(ε-caprolactone) nanoparticles in the size range 100-200 nm using flash nanoprecipitation. Due to rifampicin's solubility in water, it was necessary to first make an insoluble pro-drug form by conjugating it with Vitamin E succinate and with poly(ε-caprolactone) which is biodegradable. The resulting pro-drugs were then co-precipitated with diblock copolymers of poly(ethylene oxide-b-ε-caprolactone) at loadings of 14.5 wt % of rifampicin. Hydrolytic cleavage of the linking group provided a mechanism for the sustained release of rifampicin[1].

In **Chapter 4,** two poorly soluble antiviral drugs ritonavir (RTV) and efavirenz (EFV) were used to prepare CMCAB ASD nanoparticles. The multi-inlet vortex mixer was used to form the particles by a rapid precipitation step. Here the target drug loading was varied between 25-50 wt % and the particle size, final drug loading and dissolution studies of the nanoparticles were evaluated. Final drug loadings were in the range 18-43 wt% with well-defined sizes (200-300 nm). Drug loading efficiencies in the final particles ranged from 72 % – 86 %. CMCAB was effective in entrapping the drug in its amorphous state in the particle and this increased drug solution concentration in pH 6.8 buffer. There was no detectable crystallinity or phase separation observed for any of the drug-containing particles. The nanoparticles were compared to microparticles produced by a co-precipitation method. The final loading was 72-86 % in the nanoparticles, and 100% in the microparticles as there was no drug loss due to processing steps.

Solution concentration and drug release from the nanoparticles and microparticles significantly enhanced compared to those of crystalline drug. Drug release decreased with increasing amount of drug in the particles.

Amorphous nanoparticle release characteristics were compared with those of amorphous microparticles of the same polymer and drug. The percentage release of drugs from nanoparticles was higher than that from microparticles. The particle size of the nanosized RTV and EFV resulted in greatly increasing the specific surface area compared to the micron-sized particles, which enhanced the dissolution rate of RTV and EFV. There was only a slight difference of solution concentration enhancement between microparticles and nanoparticles.

In **Chapter 5,** we demonstrated the method to produce cellulose ω-carboxyalkanoates and BPC nanoparticles with RTV and EFV, with well-defined sizes (100-200 nm). The Multi-Inlet Vortex Mixer was used to control particle size and nucleation rate. The particles were processed by dialysis followed by freeze drying. A cryoprotectant trehalose was used for inhibiting particle aggregation during freeze drying. The drug loading efficiency in the final particles was 88-96 % except BPC where the drug loading efficiency was 62%. The nanoparticles made with cellulose derivatives used in this work did not show an intermediate T_g, but rather showed a low T_g very near to the T_g of the drug itself. However, there was no phase separation or appearance of crystalline peak when measured by DSC and XRD. This increased the solution concentrations of the drugs in a pH 6.8 buffer. There was an increase in percentage drug release from the nanoparticles compared to the pure crystalline drug. Polysaccharide nanoparticles showed potential for enhancing the solution concentration and sustained release of poorly soluble drugs (RTV and EFV). Previous studies showed dissolution behavior was dependent on both the properties of the polymer (solubility parameter, degree of substitution,

hydrophobicity) as well the drug (solubility parameter, solubility, presence of hydrophobic groups)[2]. The polymers with solubility parameters between 20-23 $MPa^{1/2}$ could inhibit crystal growth in solution, anything less than 20 $MPa^{1/2}$ were mostly ineffective. However, 6-butyl pullulan carboxylate with a higher solubility parameter (as high as 28 $MPa^{1/2}$) showed very high concentration and release compared to the crystalline drugs but did not show well defined drug compositions and particle sizes. In future work on the preparation or selection of polysaccharides for use in nanoparticulate drug polymer amorphous solid dispersions, one should take into account the polymer's hydrophobicity which is likely to affect the extent of adsorption of polymer to the crystal surface of the drug. If the polymer is very hydrophobic, it would be expected to interact more favorably with other monomer units to form a more condensed globule which either may not adsorb on the crystal or if it adsorbs may not have high surface coverage. If the polymer is very hydrophilic, it can interact more with the water and comparatively less with the drug. Therefore an optimal hydrophobicity could exist for inhibiting crystallization. A higher degree of carboxylic acid substitution (DS) shows more effective inhibition of crystallization. There can be differences in the particle shape, size, polydispersity and morphology depending on the preparation method so care must be taken to use the synthesis method and purification (separation, drying) techniques to obtain well defined particles. The use of excipients such as cryoprotectants (or excipients) to control particle size would be an additional and useful step.

6.2 Future Work

6.2.1 Calculation of Reynolds number, supersaturation and mixing time specific to polymer-drug in solvent

The Reynolds number for CMCAB-drug systems (or any polymer-drug system) made in the multi inlet vortex mixer (MIVM) must be calculated more precisely than was done in this

work. Secondly, the effect of Reynolds number on the diameter of the particles formed in the MIVM should be studied such as in the Reynolds number range 50-10,000. The Reynolds number at which the particle diameter is constant is where the mixing time is equal to the nucleation time. At a higher Reynolds number, the particle size will be constant and only vary with supersaturation. So, calculation of supersaturation and mixing time is also essential [3,4].

6.2.2 Analyzing content of Tetrahydrofuran (THF) in the final particles-alternative solvents

It is important to remove THF from the nanoparticle suspensions obtained from MIVM. It is not desirable to have THF in the final nanoparticles made for oral delivery. Though dialysis and rotary evaporation are effective ways of removing THF, the residual amount can be quantified by analytical techniques like gas chromatograph (GC). Alternative solvents like acetone, ethanol, and methanol can be explored.

6.2.3 Using high speed ultracentrifuge to separate nanoparticles during dissolution studies

The presence of polymer-drug nano-assemblies complicates analysis since small aggregates do not easily separate from free drug by traditional centrifuge or filtration based separation techniques. Some initial work was done to understand the best way to separate free drug from nanoparticles. CMCAB-RTV nanoparticles were dispersed in potassium phosphate buffer at pH 6.8 and 1 ml of the suspension was collected after 1.5 hours. The suspension was either filtered, centrifuged at different speeds, or ultra-centrifuged to investigate the best method to isolate free drug in the supernatant[5]. Simple filtration of the nanosuspension by 20 nm Anotop filter was not possible due to clogging of the filter. The nanosuspension was centrifuged at different g-forces (16,060 and 22,789) and ultracentrifuged at very high g-force (144,794). One

of the samples was centrifuged at 16,060 g's and filtered by 20 nm filter (Figure 1). Most of the drug-polymer nanoparticles were removed from the samples processed with the ultracentrifuge and by centrifuging at 16,060 g's followed by filtration. Therefore, centrifugation at 16,060 g's followed by filtration can be a very good technique to separate free drug from drug-polymer nanoparticles. However, while using filters, the drug particles may adsorb to the surface of the filters, thus reducing the utility of this method.

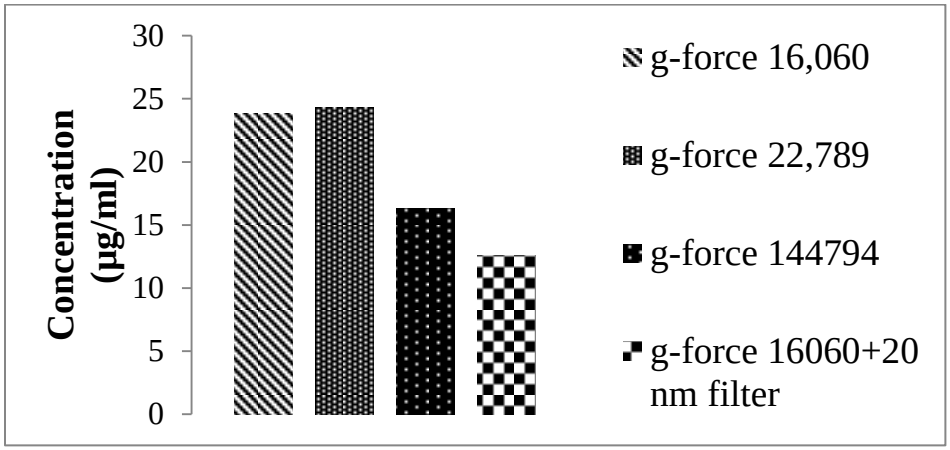

Figure 1. Drug concentration using different separation based approaches

6.2.4 In-vivo studies of all the nanoparticles

One of the most important studies which need attention in future is the in vivo performance of the nanoparticles. Drug degradation, solubility and release in animals can be studied. The pharmacokinetics (PK) and tissue distribution of the nanoparticles can also be studied to define therapeutic effect and toxicity. Biodegradable polymers can be explored. The size, surface charge and surface chemistry can be investigated for studying PK and biodistribution.

6.2.5 Synthesis of polysaccharides suitable for production of nanoparticles by rapid precipitation method

More polysaccharides, especially biodegradable polysaccharides, which are suitable for rapid precipitation should be explored. We studied several polysaccharides such hydroxypropylmethyl cellulose acetate succinate (HPMCAS), cellulose acetate suberate (CA-320S Sub), cellulose acetate propionate sebacate (CAP-Seb) and sodium alginate which did not form well-defined particles when prepared in the MIVM but are very important for oral drug delivery applications. Additional studies are needed with these and other polysaccharides to define mixer conditions that would lead to well-defined particle sizes and drug compositions. This could involve the use of solvents other than THF for making particles which are suitable for the mixer. In addition, mixtures of polymers should be studied to learn if it is possible to optimize the hydrophobic-hydrophilic ratio and form well-defined particles.

6.2.6 Combination of two or more drugs in the same polymer matrix (or blends of polymers)

This thesis studied one drug at a time in various polymer matrixes. Most of the formulations used to treat diseases like tuberculosis and HIV require combination of two or more drugs. Therefore, efforts should be made to form nanoparticles of two or more drugs to learn whether the drugs form amorphous solid dispersions. Measurements of the size, drug compositions, morphology, and drug release should be done. The work will be challenging, yet rewarding.

6.3 References

1. (a) D'addio, S. M. Tuberculosis therapeutics: engineering of nanomedicinal systems for local delivery of targeted drug cocktails. princeton university, 2012; (b) Ying, L. Formulating nanoparticles by flash nanoprecipitation for drug delivery and sustained release. Princeton University, 2007.

2. Ilevbare, G. A.; Liu, H.; Edgar, K. J.; Taylor, L. S., Understanding polymer properties important for crystal growth inhibition—impact of chemically diverse polymers on solution crystal growth of ritonavir. *Crystal Growth & Design* **2012,** *12* (6), 3133-3143.

3. Kumar, V.; Prud'homme, R. K., Thermodynamic limits on drug loading in nanoparticle cores. *Journal of Pharmaceutical Sciences* **2008,** *97* (11), 4904-4914.

4. Johnson, B. K.; Prud'homme, R. K., Chemical processing and micromixing in confined impinging jets. *AIChE Journal* **2003,** *49* (9), 2264-2282.

5. Van Eerdenbrugh, B.; Vermant, J.; Martens, J. A.; Froyen, L.; Humbeeck, J. V.; Van Den Mooter, G.; Augustijns, P., Solubility increases associated with crystalline drug nanoparticles: methodologies and significance. *Molecular Pharmaceutics* **2010,** *7* (5), 1858-1870.